

Synthesis & Applications of Biochar-based Nanocomposites for Removal of Contaminants of Emerging Concerns in Aqueous Solution

A thesis submitted to the
UPES

For the award of
Doctor of Philosophy
in
Chemistry

By
Prakash Bobde

September 2024

Supervisor(s)
Dr. Shikha Wadhwa
Dr. Jitendra Kumar Pandey
Dr. Ranjit Kumar



Applied Science Cluster
School of Advanced Engineering (SoAE)
UPES
Dehradun-248007, Uttarakhand

Synthesis & Applications of Biochar-based Nanocomposites for Removal of Contaminants of Emerging Concerns in Aqueous Solution

A thesis submitted to the
UPES

For the award of
Doctor of Philosophy
in
Chemistry

By
Prakash Bobde
(SAP ID: 500087078)

September 2024

Supervisor

Dr. Shikha Wadhwa

Associate Professor, Applied Science
Cluster, School of Engineering, UPES

Supervisor

Dr. Jitendra Kumar Pandey

Professor
UPES

External Supervisor

Dr. Ranjit Kumar

Associate Professor
Shiv Nadar University



Applied Science Cluster
School of Advanced Engineering (SoAE)
UPES
Dehradun-248007, Uttarakhand

DECLARATION

I declare that the thesis entitled, “**Synthesis & Applications of Biochar-based Nanocomposites for Removal of Contaminants of Emerging Concerns in Aqueous Solution**” has been prepared by me under the guidance of Dr. Shikha Wadhwa, Associate Professor of Applied Science Cluster, School of Advanced Engineering, UPES, Dehradun, Dr. Jitendra Kumar Pandey, Professor, UPES, Dehradun and Dr. Ranjeet Kumar, Department of Chemical Engineering, Shiv Nadar Institution of Eminence, Delhi-NCR. No part of this thesis has formed the basis for the award of any degree or fellowship previously.



Mr. Prakash Bobde

Date : 15/04/2024



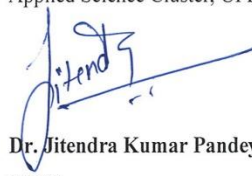
CERTIFICATE

I certify that **Prakash Bobde** has prepared his thesis entitled “**Synthesis & Applications of Biochar-based Nanocomposites for Removal of Contaminants of Emerging Concerns in Aqueous Solution**”, for the awards of PhD degree of the UPES, under my guidance. He has carried out the work at the Applied Science Cluster, UPES.

Dr Shikha Wadhwa
Associate Professor
Applied Science Cluster
School of Advanced Engineering
UPES, Dehradun – 248007
Uttarakhand
Date: 06-09-2024

CERTIFICATE

I certify that Prakash Bobde has prepared his thesis entitled “**Synthesis & Applications of Biochar-based Nanocomposites for Removal of Contaminants of Emerging Concerns in Aqueous Solution**”, for the award of PhD degree of the UPES, under my guidance. He has carried out the work at the Applied Science Cluster, UPES.



Dr. Jitendra Kumar Pandey
UPES,
Dehradun-248007, Uttarakhand
Date: 15-04-2024

CERTIFICATE

I certify that Mr. Prakash Bobde has prepared his thesis entitled “**Synthesis & Applications of Biochar-based Nanocomposites for Removal of Contaminants of Emerging Concerns in Aqueous Solution**”, for the award of PhD degree of the UPES, under my guidance. He has carried out the work at the Applied Science Cluster, UPES, Dehradun.

Ranjit Kumar

Dr. Ranjit Kumar
Senior Scientist
Department of Chemical Engineering,
Shiv Nadar Institution of Eminence,
Delhi-NCR-201314
Date: 15-04-2024

ABSTRACT

This thesis investigates the synthesis and application of biochar-based nanocomposites for the removal of contaminants of emerging concerns (CECs) from aqueous solutions. Biochar, a carbon-rich material derived from biomass, serves as the foundational material for the development of nanocomposites. Various modification techniques, including the incorporation of metal oxides and layered double hydroxides, are explored to enhance the adsorption capacity and efficiency of biochar for targeted contaminants.

The research encompasses comprehensive characterization techniques such as Fourier Transform Infrared Spectroscopy (FTIR), X-ray Diffraction (XRD), Scanning Electron Microscopy (SEM), CHNS analysis, and BET nitrogen adsorption-desorption isotherm. These analyses provide insights into the structural, morphological, and surface properties of the developed nanocomposites, essential for understanding their adsorption mechanisms and performance.

The adsorption efficiency of the synthesized biochar-based nanocomposites is evaluated for various contaminants of emerging concerns, including antibiotics and pharmaceuticals. Response Surface Methodology (RSM) is employed to optimize the adsorption process by investigating the influence of key parameters such as pH, adsorbent dosage, initial concentration of contaminants, and temperature.

Kinetic, isotherm, and thermodynamic studies are conducted to elucidate the adsorption mechanisms and thermodynamic feasibility of the process. The results highlight the significance of chemisorption, electrostatic interactions, and surface functional groups in enhancing the adsorption capacity of the developed nanocomposites.

Furthermore, the regeneration potential of the biochar-based nanocomposites is investigated to assess their reusability and sustainability for repeated adsorption-

desorption cycles. The findings contribute to the understanding of the feasibility and efficacy of biochar-based nanocomposites as environmentally friendly adsorbents for the removal of contaminants of emerging concerns from aqueous solutions.

Overall, this research provides valuable insights into the synthesis, characterization, optimization, and application of biochar-based nanocomposites for addressing water pollution challenges posed by contaminants of emerging concerns. This work explores the application of pine cone biomass generated from pine trees which is a main cause for the forest fires, for the removal of CECs thereby contributing to the development of sustainable solutions for water treatment and environmental remediation.

ACKNOWLEDGEMENT

I am profoundly grateful to the UPES for providing me with the platform and resources to pursue my doctoral studies. Under the visionary leadership of the Vice-Chancellor, Dr. Ram Sharma, and the guidance of the Dean of Research and Development, Prof. D K Avasthi, and the Associate Dean of Research and Development, Prof. S M Tauseef, & Prof. Pankaj Kumar, Prof. Ashish Mathur and R&D, UPES has fostered an environment of academic excellence, innovation, and research.

I extend my deepest gratitude to my supervisor, Dr. Shikha Wadhwa, Dr. Jitendra Kumar Pandey, and Dr. Ranjit Kumar, whose expertise, guidance, and unwavering support have been instrumental in shaping my research journey. Their mentorship, constructive feedback, and encouragement have played a pivotal role in the development and completion of this thesis. I am immensely grateful for the opportunity to work under their supervision.

To my friends and colleagues, I express my sincere appreciation for their camaraderie, support, and intellectual companionship throughout this doctoral odyssey. Their diverse perspectives, stimulating discussions, and unwavering encouragement have not only enriched my research but have also made the journey enjoyable and memorable.

My heartfelt gratitude goes to my family for their unconditional love, unwavering encouragement, and sacrifices. Their unwavering belief in my abilities has been a constant source of motivation and inspiration. I am deeply indebted to them for their endless support and understanding throughout this journey.

I would also like to acknowledge Dr. Amit Sharma, Dr. Sukdeb pal, Mr. Charu Pant, Mr. Umamaheshwara Rao who have contributed to my academic and personal growth during my tenure at UPES. Their guidance, encouragement, and support have been invaluable.

Finally, I extend my gratitude to all the participants, research collaborators, and individuals who have contributed to my research in any capacity. Their willingness to share knowledge, resources, and insights has enriched my work and contributed to its success.

Thank you.

A handwritten signature in blue ink, appearing to read 'Prakash Bobde', with a stylized flourish at the end.

Mr. Prakash Bobde

TABLE OF CONTENTS

Abstract	i
Acknowledgement	iii
List of figures	x
List of tables	xiv
List of abbreviations	xvii
Chapter 1	1
INTRODUCTION	2
1.1 Water pollution	2
1.2 Contaminants of Emerging Concerns (CECs): an overview	2
1.3 Classification of CECs	4
1.4 Sources of CECs in the water environment	6
1.5 Ecotoxicological effects of CECs	8
1.6 Conventional treatment methods for removal of CECs	12
1.6.1 Sand filtration	12
1.6.2 Coagulation-flocculation	12
1.6.3 Activated sludge treatment	13
1.7 Advanced treatment methods for removal of CECs	14
1.7.1 Membrane technology	14
1.7.2 Adsorption	15
1.7.3 Advanced oxidation process	16
1.7.4 Solvent extraction	16
1.7.5 Electrochemical method	17
1.8 Nanomaterials for water treatment	17
Chapter 2	19
LITERATURE REVIEW	20
2.1 Adsorption	20
2.2 Adsorbents used for the adsorption of CECs	21
2.2.1 Activated carbon	22
2.2.2 Zeolites	22

2.2.3 Clays	23
2.2.4 Chitosan	23
2.2.5 Agricultural/Agro-industrial biomass	24
2.2.6 Biochar	24
2.2.7 Industrial waste	25
2.2.8 Polymers	25
2.2.9 Nanomaterials	26
2.3 Biochar as greener/sustainable adsorbent	27
2.4 Chemical modification of biochar	28
2.5 Mechanism of adsorption of CECs	29
2.5.1 Adsorptive mechanism for tetracycline	29
2.5.2 Adsorptive mechanism for oxytetracycline	33
2.5.3 Adsorptive mechanism for diclofenac sodium	39
2.5.4 Adsorptive mechanism for bisphenol A	39
2.5.5 Adsorptive mechanism for atrazine	40
2.5.6 Adsorptive mechanism for ciprofloxacin and sparfloxacin	41
2.5.7 Adsorptive mechanism for metformin and diazinon	44
2.5.8 Adsorptive mechanism for triclosan and norfloxacin	45
2.5.9 Adsorptive mechanism for ibuprofen and ketamine	46
2.5.10 Adsorptive mechanism for doxycycline & salicylic acid	47
2.6 Research gaps	47
2.7 Objectives	48
Chapter 3	49
MATERIALS & METHODS	50
3.1 Materials	50
3.2 Methods	50
3.2.1 Synthesis	50
3.2.1.1 Synthesis of pine cone biochar (PCBC)	50
3.2.1.2 Synthesis of manganese oxide/PCBC	50
3.2.1.3 Synthesis of LDH/PCBC	51

3.2.1.4 Synthesis of Fe ₃ O ₄ /PCBC	52
3.2.2 Selection of adsorbent	52
3.2.3 Adsorbent characterization	53
3.2.4 Effect of time on the adsorption of CECs	54
3.2.5 Effect of initial CECs concentration of the adsorption	54
3.2.6 Response Surface Methodology (RSM) study	55
3.2.7 Adsorption kinetics	56
3.2.8 Adsorption isotherm	57
3.2.9 Thermodynamic parameter	57
3.2.10 Regeneration study	58
Chapter 4	59
ADSORPTION OF OXYTETRACYCLINE ONTO	60
MANGANESE OXIDE MODIFIED PINE CONE BIOCHAR	
4.1 Introduction	60
4.2 Results & Discussion	63
4.2.1 Selection of the best adsorbent	63
4.2.2 Characterization of the adsorbent	63
4.2.3 Effect of contact time on the adsorption of OTC	67
4.2.4 RSM study	67
4.2.5 Fitting the model	72
4.2.6 Optimization of the adsorption of OTC	74
4.2.7 Kinetic, Isotherm & Thermodynamic study	75
4.2.8 Regeneration study	82
4.2.9 Adsorption mechanism	82
4.3 Conclusion	85
Chapter 5	86
ADSORPTION OF TETRACYCLINE BY MANGANESE	87
OXIDE-MODIFIED PINE CONE BIOCHAR	
5.1 Introduction	87
5.2 Results & Discussion	89

5.2.1 Selection of the best adsorbent	89
5.2.2 Effect of contact time on the adsorption of TC	90
5.2.3 RSM study	90
5.2.4 Optimization of the adsorption of TC	96
5.2.5 Kinetic, isotherm & thermodynamic study	96
5.2.6 Regeneration study	102
5.2.7 Adsorption mechanism	103
5.3 Conclusion	106
Chapter 6	107
ADSORPTION OF CIPROFLOXACIN BY LAYERED	108
DOUBLE HYDROXIDE-MODIFIED PINE CONE BIOCHAR	
6.1 Introduction	108
6.2 Results & Discussion	111
6.2.1 Selection of adsorbent	111
6.2.2 Adsorbent characterization	112
6.2.3 Influence of contact duration on the adsorption of CPF	115
6.2.4 Model of fitting and Analysis of Variance using CCD	116
6.2.5 Interaction effects of different experimental factors	119
6.2.6 Process parameter optimization	122
6.2.7 Adsorption kinetic, isotherm & thermodynamic study	123
6.2.8 Regeneration study of LDH/PCBC	130
6.2.9 Adsorption mechanism of CPF on LDH/PCBC	131
6.3 Conclusion	134
Chapter 7	135
ADSORPTION OF TRICLOSAN BY PINE CONE BIOCHAR	136
7.1 Introduction	136
7.2 Results & Discussion	138
7.2.1 Selection of the best adsorbent	138
7.2.2 Characterization of the adsorbent	139
7.2.3 Effect of contact time on the adsorption of TS	141

7.2.4 RSM study	141
7.2.5 Optimization of the adsorption of TS	146
7.2.6 Kinetic, isotherm and thermodynamic study	147
7.2.7 Regeneration study	152
7.2.8 Adsorption mechanism	153
7.3 Conclusion	155
Chapter 8	156
CONCLUSION	157
8.1 Summary	157
8.2 Conclusion	158
8.3 Future prospects	160

LIST OF FIGURES

Figure 1.1:	Classification of CEC	4
Figure 1.2:	Sources of CECs	7
Figure 2.1:	The probable regulating mechanisms of TC adsorption	31
Figure 2.2:	The proposed adsorption mechanisms for CPF on g-MoS ₂ -BC composites	41
Figure 2.3:	Schematic for the adsorption of CPF & SPF onto Fe ₃ O ₄ /Graphene oxide citrus peel biochar	43
Figure 2.4:	Possible adsorption mechanism of metformin onto alkaline biochar	44
Figure 4.1:	Comparison of different synthesized adsorbent	63
Figure 4.2:	(a)XRD, (b)FTIR of PCBC and MnO ₂ /PCBC	64
Figure 4.3:	BET adsorption-desorption isotherm of (a) PCBC and (b) MnO ₂ /PCBC	65
Figure 4.4:	SEM images of (a) PCBC and (b) MnO ₂ /PCBC	66
Figure 4.5:	Effect of the amount of OTC adsorbed (mg/g) against contact time onto adsorbent MnO ₂ /PCBC	67
Figure 4.6:	pH point of zero charge (pH _{PZC}) of MnO ₂ /PCBC	70
Figure 4.7:	3D surface graphs of percent removal efficiency of OTC by using MnO ₂ /PCBC	72
Figure 4.8:	Optimization of adsorption process of OTC onto MnO ₂ /PCBC	74
Figure 4.9:	(a) PFO and (b) PSO (c) Elovich and (c) ID plots for the adsorption of OTC on MnO ₂ /PCBC.	76
Figure 4.10:	(a) Langmuir (b) Freundlich (c) Temkin and (d) Dubinin-Radushkevich plots for the adsorption of OTC on MnO ₂ /PCBC.	78
Figure 4.11:	Plot of $R\ln K_{eq}$ versus $(1/T) \times 10^3(K^{-1})$ for estimation of thermodynamic parameters.	80
Figure 4.12:	Regeneration of MnO ₂ /PCBC for OTC adsorption	82

Figure 4.13:	(a) Effect of EDTA on the adsorption of OTC, (b) FTIR spectra of MnO ₂ /PCBC before and after adsorption of OTC (MnO ₂ /PCBC-OTC), (c) Possible adsorption mechanism of MnO ₂ /PCBC for OTC	83
Figure 5.1:	Comparison of different adsorbent for the removal of TC	89
Figure 5.2:	Effect of the amount of TC adsorbed (mg/g) against contact time onto adsorbent MnO ₂ /PCBC	90
Figure 5.3:	3D surface graphs of percent removal efficiency of TC by using MnO ₂ /PCBC	94
Figure 5.4:	Optimization of adsorption process of TC onto MnO ₂ /PCBC	96
Figure 5.5:	(a) PFO and (b) PSO (c) Elovich and (c) ID plots for the adsorption of TC on MnO ₂ /PCBC.	97
Figure 5.6:	(a) Langmuir (b) Freundlich (c) Temkin and (d) Dubinin-Radushkevich plots for the adsorption of TC on MnO ₂ /PCBC.	99
Figure 5.7:	Plot of $R\ln K_{eq}$ versus $(1/T) \times 10^3 (K^{-1})$ for estimation of thermodynamic parameters.	100
Figure 5.8:	Regeneration of MnO ₂ /PCBC for TC adsorption	103
Figure 5.9:	(a) Effect of EDTA on the adsorption of TC onto MnO ₂ /PCBC, (b) FTIR spectra of MnO ₂ /PCBC before and after adsorption of TC (MnO ₂ /PCBC -TC), (c) Proposed adsorption mechanism of TC adsorption on MnO ₂ /PCBC.	104
Figure 6.1:	Comparison of different adsorbent for the removal of CPF	111
Figure 6.2:	(a)XRD, (b)FTIR of PCBC and LDH/PCBC	113
Figure 6.3:	BET adsorption-desorption isotherm of LDH/PCBC	113
Figure 6.4:	FESEM images of (a)PCBC (magnification x2000) and (b)LDH/PCBC (magnification x100000)	114
Figure 6.5:	Influence of the quantity of CPF adsorbed (mg/g) versus contact duration onto the adsorbents	115
Figure 6.6:	Plot of initial pH versus ΔpH for LDH/PCBC	120

Figure 6.7:	3D surface graphs for % removal efficiency of CPF by LDH/PCBC	122
Figure 6.8:	Optimization of adsorption process of CPF onto LDH/PCBC	123
Figure 6.9:	(a) PFO, (b) PSO (c) Elovich and (d) ID plots for the adsorption of CPF on LDH/PCBC.	124
Figure 6.10:	(a)Langmuir, (b)Freundlich, (c)Temkin and (d)Dubinin-Radushkevich plots for the adsorption of CPF on LDH/PCBC.	127
Figure 6.11:	Plot of $R\ln K_d$ versus $(1/T) \times 10^3(K^{-1})$ for estimation of thermodynamic parameters.	129
Figure 6.12:	Adsorbent regeneration study	131
Figure 6.13:	(a) Effect of EDTA on adsorption of CPF, (b) FTIR spectra of LDH/PCBC before and after adsorption of CPF (LDH/PCBC-CPF), (c) Proposed adsorption mechanism of CPF adsorption on LDH/PCBC.	133
Figure 7.1:	Comparison of different synthesized adsorbent	139
Figure 7.2:	(a) XRD pattern and (b) FTIR spectra of PCBC	139
Figure 7.3:	SEM images of PCBC	140
Figure 7.4:	Effect of the amount of TS adsorbed (mg/g) against contact time onto adsorbent PCBC	141
Figure 7.5:	3D surface graphs of percent removal efficiency of TS by using PCBC	145
Figure 7.6:	Optimization of adsorption process of TS onto PCBC	146
Figure 7.7:	(a) PFO and (b) PSO (c) Elovich and (c) ID plots for the adsorption of TS on PCBC.	148
Figure 7.8:	(a) Langmuir (b) Freundlich (c) Temkin and (d) Dubinin-Radushkevich plots for the adsorption of TS on PCBC.	150
Figure 7.9:	Plot of $R\ln K_d$ versus $(1/T) \times 10^3(K^{-1})$ for estimation of thermodynamic parameters.	151
Figure 7.10:	(a) Regeneration of PCBC for TS adsorption, (b) FTIR spectra of PCBC before and after adsorption of TS	154

(PCBC-TS), (c) Possible adsorption mechanism of PCBC for TS

LIST OF TABLES

Table 1.1:	Ecotoxicological effects of CECs	9
Table 2.1:	Experimental conditions and adsorption capacities of different bio-based adsorbent reported for the removal of CECs	36
Table 3.1:	Experimental ranges and levels in CCD of the independent variables	56
Table 4.1:	Physicochemical properties of PCBC and MnO ₂ /PCBC	66
Table 4.2:	Elemental composition of PCBC and MnO ₂ /PCBC	66
Table 4.3:	Experimental and predicted values for adsorption of OTC on adsorbent MnO ₂ /PCBC obtained through CCD and RSM	68
Table 4.4:	Analysis of variance for % removal efficiency of OTC by using MnO ₂ /PCBC	69
Table 4.5:	Optimum values for adsorption of OTC onto MnO ₂ /PCBC	74
Table 4.6:	Kinetic parameters for the adsorption of OTC onto MnO ₂ /PCBC	77
Table 4.7:	Isotherm parameters for the adsorption of OTC onto MnO ₂ /PCBC	79
Table 4.8:	Thermodynamic parameters for the adsorption of OTC onto MnO ₂ /PCBC	80
Table 4.9:	Comparison of OTC adsorption onto different adsorbents reported in literature.	81
Table 5.1:	Experimental and predicted values for adsorption of TC on adsorbent MnO ₂ /PCBC obtained through CCD and RSM	91
Table 5.2:	Analysis of variance for adsorption capacity of TC by using MnO ₂ /PCBC	92
Table 5.3:	Optimum values for adsorption of TC onto MnO ₂ /PCBC	96
Table 5.4:	Kinetic parameters for the adsorption of TC onto MnO ₂ /PCBC	98
Table 5.5:	Isotherm parameters for the adsorption of TC onto	100

	MnO ₂ /PCBC	
Table 5.6:	Thermodynamic parameters for the adsorption of TC onto MnO ₂ /PCBC	101
Table 5.7:	Comparison of TC adsorption onto different adsorbents reported in literature.	102
Table 5.8:	Physicochemical properties of MnO ₂ /PCBC before and after TC adsorption	105
Table 6.1:	Microstructural properties and elemental composition of the adsorbents	115
Table 6.2:	Elemental composition of PCBC and MnO ₂ /PCBC	115
Table 6.3:	Adsorption capacity values for the adsorption of CPF on LDH/PCBC obtained using CCD and RSM	118
Table 6.4:	ANOVA results for adsorption capacity of CPF by using LDH/PCBC	119
Table 6.5:	Optimum values for adsorption of CPF by LDH/PCBC	123
Table 6.6:	Kinetic parameters for the adsorption of CPF onto LDH/PCBC	126
Table 6.7:	Isotherm parameters for the adsorption of CPF onto LDH/PCBC	128
Table 6.8:	Thermodynamic parameters for the adsorption of OTC onto MnO ₂ /PCBC	129
Table 6.9:	Adsorption of CPF onto numerous adsorbents reported in literature.	130
Table 7.1:	Physicochemical properties of PCBC	140
Table 7.2:	Experimental and predicted values for adsorption of TS on adsorbent PCBC obtained through CCD and RSM	142
Table 7.3:	Analysis of variance for adsorption capacity of TS by using PCBC	144
Table 7.4:	Optimum values for adsorption of TS onto PCBC	147
Table 7.5:	Kinetic parameters for the adsorption of TS onto PCBC	149

Table 7.6:	Isotherm parameters for the adsorption of TS onto PCBC	150
Table 7.7:	Thermodynamic parameters for the adsorption of TS onto PCBC	152
Table 7.8:	Comparison of TS adsorption onto different adsorbents reported in literature.	153
Table 8.1:	Summary of removal efficiencies of various CECs from water using different biochar-based adsorbents	160

LIST OF ABBREVIATIONS

AC	Activated Carbon
AOP	Advanced Oxidation Process
ARE	Average Relative Error
ASWs	Artificial Sweeteners
AZ	Atrazine
BPA	Bisphenol A
CEC	Contaminants of Emerging Concern
CFN	Caffeine
CLB	Cauliflower Leaves Biochar
CPF	Ciprofloxacin
DC	Doxycycline
DEET	N,N-Diethyl-meta-toluamide
DS	Diclofenc Sodium
DWTP	Drinking Water Treatment Plant
DZ	Diazinon
ED	Electrodialysis
EDCs	Endocrine Disrupting Chemicals
EU	European Union
FO	Forward Osmosis
FRs	Fire Retardants
GO	Graphene Oxide
IBF	Ibuprofen
KM	Ketamine
KP	Ketoprofen
LDH	Layered Double Hydroxide
MD	Membrane Distillation

MEPBAC	Magnetic Palm Biomass Activated Carbon
MF	Metformin
MMBC	Magnetic MMT-biochar composite
MMT	Montmorillonite
MWWTP	Municipal Waste Water Treatment
NF	Nanofiltration
NOR	Norfloxacin
NP	Naproxen
OTC	Oxytetracycline
PBDEs	Polybrominated Diphenyl Ethers
PCBC	Pine Cone Biochar
PPCPs	Pharmaceutical and Personal Care Products
RO	Reverse Osmosis
SA	Salicylic acid
SF	Sand Filtration
SMX	Sulphamethoxazole
TC	Tetracycline
TPs	Transformation Products
TS	Triclosan
US EPA	United States Environmental Protection Agency
VOCs	Volatile Organic Compounds
WWTP	Waste Water Treatment Plant

Chapter 1
INTRODUCTION

Chapter 1

INTRODUCTION

1.1. Water Pollution

Reiterating the critical importance of water for all living organisms, it is evident that water resources are increasingly strained due to factors such as a growing global population, industrialization, and agricultural expansion (Dey et al., 2019; Jurado et al., 2012). As a result, the demand for clean and potable water has surged. This has put significant pressure on water bodies, as they are continually impacted by the discharge of substantial quantities of wastewater (Dey et al., 2019). Beyond the challenge of ensuring access to high-quality drinking water, several studies have indicated that nearly 50% of indigenous freshwater fish and about one-third of the global frog population are on the brink of extinction (Dey et al., 2019). This represents a significant global concern that calls for urgent monitoring, quality management, and remediation efforts. National and international environmental agencies have, for the most part, established discharge standards for complex organic substances, heavy metals, and a few trace compounds (Dey et al., 2019; Geissen et al., 2015; Rodriguez-Narvaez et al., 2017).

1.2. Contaminants of Emerging Concerns (CECs): an Overview

In the recent decades, population growth and modern life styles have led to synthesis of numerous compounds in agrochemicals, cosmetics, chemicals, and pharmaceutical industries which are consumed and disposed in aquatic environment on a daily basis by millions of people around the world (Ahmed et al., 2016; P. Shukla et al., 2021). However, the concentration of these compounds in water bodies are often identified in ng to μg per litre, it is reported that these compounds, even at low concentration, pose huge risks to the ecosystems and human health, due to bioaccumulation and biomagnification, endocrine disruption, antibiotic-resistant bacteria proliferation and toxicity (Oladipo et al., 2018; P. Shukla et al., 2021). The scientific and legislative community is currently referring to these chemical compounds as ‘Contaminants of Emerging Concern’

(CEC). Pharmaceuticals and personal care products (PPCPs), alkylphenols, bisphenol A (BPA), phthalates, perfluoroalkyl and polyfluoroalkyl substances (PFASs), and transformation products of these chemicals are some examples of CECs. These compounds originate from industrial, domestic, agricultural, hospital and laboratory wastewater due to limited waste-water treatment by traditional water purification methods and runoff water from non-point sources. Municipal wastewater treatment plant (MWWTP) effluent is associated with the most crucial sources of CECs in the surroundings. CEC flow to MWWTPs after being ingested by the population and collected in sewer systems, which are typically not removed (S. Kim et al., 2018). As a result, CECs flow to nearest water bodies due to discharge of MWWTP effluent into water, and depending on their physicochemical qualities, may seep into groundwater or get adsorbed on soil and sediment. Untreated sewage discharged into surface waters, as well as erroneous disposal of expired medicines/cosmetics in toilets or landfill sites, all contribute to CECs contamination of surface and ground water.

Despite the fact that CECs are present in small concentrations in water bodies, they pose a hazard to various ecosystems. CECs are known to be linked with feminization and behavioral variations in fish, neurological, reproductive, and immunological disorder in animals. Cancer, antibiotic resistant bacteria, heart diseases, obesity, and development of type II diabetes in humans, lessening of micro invertebrate diversity in rivers, and bird extinction are some of the ecotoxicological effects associated with CECs (Starling et al., 2019).

The amount of toxins in wastewater processing facilities, drinking water, and industrial discharge are also monitored by some regulatory authorities. Hence, the criteria for permissible limit of CECs in water discharge should be set at a level which does not pose any health risk. These recent findings on CECs have led to upgradation of legislation directives by environmental agencies in developed countries to promote control and/or prevention of CECs introduction into surface and ground waters, and soil.

1.3. Classification of CECs:

CECs were found in water samples from Waste Water Treatment Plants (WWTPs)(Deblonde et al., 2011), Drinking Water Treatment Plants (DWTPs) (Furlong et al., 2017), surface water (Clara et al., 2010), and groundwater (Lapworth et al., 2012) through many investigations. There has been a plethora of investigations devoted to the detection of specific kinds of developing environmental pollutants (Clarke & Smith, 2011). PPCPs, pesticides, endocrine disrupting chemicals (EDCs), artificial sweeteners (ASWs) and fire retardants (FRs) are among the substances which consists of CECs (Houtman, 2010). Figure 1.1 shows the classification of CECs.

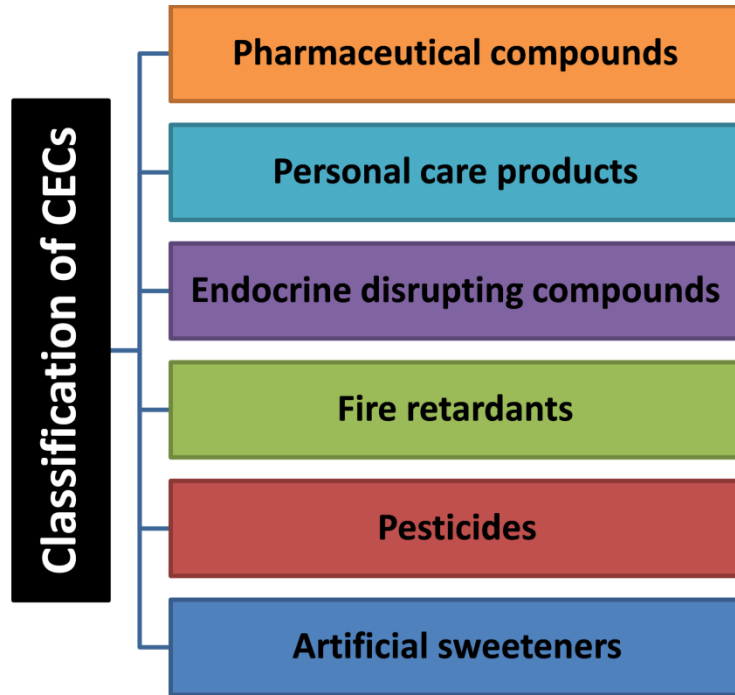


Figure 1.1: Classification of CECs(Prakash Bobde, Sharma, Kumar, Pandey, et al., 2023)

Pharmaceuticals and their associated metabolites undergo natural transformation and removal processes within the environment. These processes, including dilution, degradation, and sorption, are influenced by factors such as the compounds hydrophobicity, biodegradability, and prevailing environmental conditions. Consequently, these factors account for the presence of these

substances at minimal, trace-level concentrations in water sources and drinking water (Stefanakis & Becker, 2019). Pharmaceutical compounds, like many other chemicals, undergo various biotic and abiotic processes that can alter their structure when released into the environment (Stefanakis & Becker, 2019).

A prominent category of CECs resulting from personal care product is UV filters. These UV filters are available in a wide array of products, including sunscreens, shampoos, cosmetics, and hair dyes, designed to shield the skin and hair from the harmful effects of sun radiation (Nawaz & Sengupta, 2019; Richardson & Ternes, 2018). UV filters primarily fall into two categories: organic and inorganic. UV filters have frequently been detected in environmental water bodies, introduced through activities such as swimming or indirectly through the discharge of treated wastewater, with concentrations typically in the microgram per liter ($\mu\text{g/L}$) range (Nawaz & Sengupta, 2019; Richardson & Ternes, 2018).

Substances, whether of synthetic or natural origin, have the capacity to imitate hormones and thereby interfere with or disrupt the regular hormonal processes. Endocrine-disrupting compounds (EDCs) raise significant ecological and health-related apprehensions due to their ability to affect the endocrine system. These substances, whether occurring naturally or being artificially synthesized, are recognized or anticipated to have an impact on the endocrine system (Nawaz & Sengupta, 2019).

Fire retardants are employed in plastics, textiles, and foam furnishings to decrease their susceptibility to combustion by disrupting the polymer burning process. These flame retardants can come in the form of halogenated or brominated compounds. Polybrominated diphenyl ethers (PBDEs) are bioaccumulative flame retardants and are categorized as endocrine-disrupting chemicals (EDCs) (Rahman et al., 2001; Stefanakis & Becker, 2019).

Pesticides have been consistently identified in groundwater at minimal concentrations over an extended period. These pesticides encompass both synthetic chemicals and naturally occurring compounds. They find application in agriculture for the purpose of managing weed, pest, and crop disease issues. In

recent years, substances like atrazine, once deemed environmentally hazardous, have been discontinued. However, the replacements, such as diuron, may also carry adverse consequences. Presently, one of the notable pesticides under scrutiny is metaldehyde, which, in certain instances, has been found to exceed the EU's prescribed drinking water threshold for pesticides, as reported by the Environmental Agency in 2010 (Stefanakis & Becker, 2019).

Concerns regarding the toxicity of artificial sweeteners have emerged in the context of aquatic organisms. Recent research has revealed the toxicity of their transformation products (TPs). There is no evidence of sucralose bioaccumulation, but signs of oxidative damage in lipids and proteins are evident (Saucedo-Vence et al., 2017). Acesulfame photolysis products exhibited toxic effects on zebrafish embryos, with the photolysis process occurring naturally in sunlight. This study also identified six new transformation products of acesulfame (A. J. Li et al., 2016; C. Li et al., 2016; D. Li et al., 2016; Nawaz & Sengupta, 2019).

1.4. Sources of CECs in the water environment

Households are significant sources of various CECs, particularly pharmaceuticals and Personal Care Products (PCPs) like natural hormones and synthetic steroids. In the UK, the predominant method for disposing off unused or expired pharmaceuticals is through household waste or down the sink/toilet (Stefanakis & Becker, 2019).

Hospital waste adds to CECs with pharmaceuticals, medical supplies, and potentially hazardous materials, posing risks if improperly disposed. Certain substances found in hospital wastewater, such as iopromide, iopamidol, and diatrizoate, exhibit considerable persistence in aquatic environments and have also been identified in groundwater (Sacher et al., 2001; Schulz et al., 2008; Stefanakis & Becker, 2019; Ternes & Hirsch, 2000).

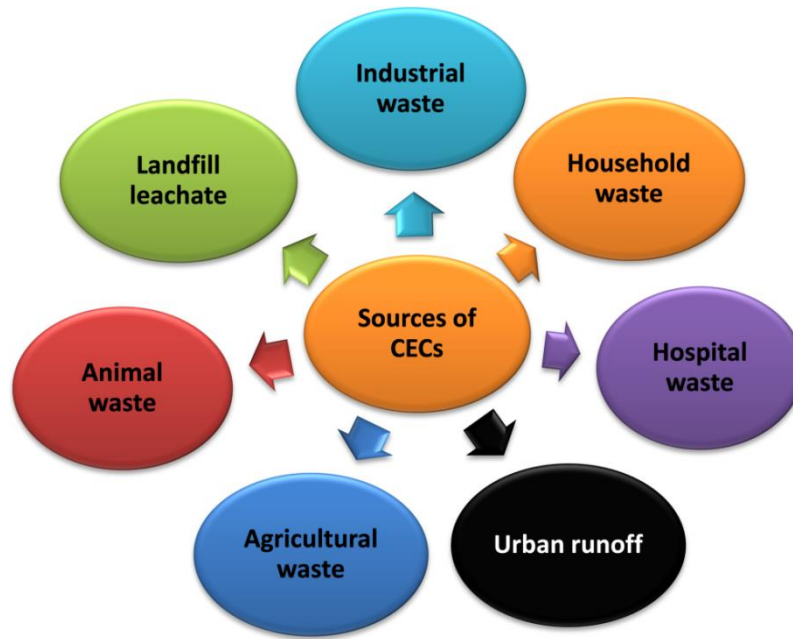


Figure 1.2: Sources of CECs (Prakash Bobde, Sharma, Kumar, Pandey, et al., 2023)

Agricultural pesticide usage stands out as a primary source of contamination. Agricultural waste releases CECs such as pesticides, fertilizers, and veterinary drugs into the environment, threatening soil and water quality (Stefanakis & Becker, 2019). Urban runoff introduces pollutants like heavy metals, pesticides, and hydrocarbons from roads, industrial zones, and urban landscapes into water bodies. Animal waste, particularly in intensive farming, contributes pathogens, antibiotics, and hormones to ecosystems through runoff and leaching, affecting water and soil health (Stefanakis & Becker, 2019).

Landfills serve as the ultimate resting place for a diverse mix of municipal solid and liquid waste, comprising discarded materials from residential, commercial, and industrial origins. The utilization of landfills for waste disposal is expected to rise with the global population's growth and the development of nations (Z. Lu et al., 2012; Masoner et al., 2014; Mouser et al., 2005). In the United States, despite a decrease in the number of active landfills from around 7,900 in 1988 to 1,900 in 2009, the average size of landfills has expanded (Masoner et al., 2014).

1.5. Ecotoxicological effect of CECs

A variety of nations have tracked the prevalence of PPCPs in the ecosystem and identified them as pollutants (Xiaoning Wang et al., 2016). Germany conducted a worldwide evaluation of PPCPs in the ecosystem in 2014, and 631 out of 713 PPCPs examined were confirmed to be above respective diagnostic thresholds. These PPCPs were discovered in surface waterways such as lakes and rivers, as well as in groundwater, compost, soil, and potable water (aus der Beek et al., 2016). Cattle were given high dosages of diclofenac sodium (DS) to alleviate fever and discomfort. Predators feasted on the livestock that were not retrieved. As predators of the species Gyps are susceptible to DS, 10–40 million predators perished of renal disease, pushing the bird to death (aus der Beek et al., 2016). It is known that a lot of fish populations have declined dramatically in the previous 10–15 years, possibly as a result of ethinylestradiol and similar potentially harmful contaminants. Certain depressant medications, such as oxazepam, can affect the behaviour and eating of fish like European perch at concentrations as low as 1.8 µg/L, resulting in food chain pattern disruption (Brodin et al., 2013). Table 1.1 summarizes the ecological effects of CECs.

Table 1.1: Ecotoxicological effects of CECs

Classifications of CECs	Frequently detected compounds	Ecotoxicological effects	References
Pharmaceutical compounds	<p>Antibiotics - Sulfamethoxazole, Amoxicillin, Ciprofloxacin, Ofloxacin, Erythromycin, Trimethoprim, Ampicillin, Tylosin, Enoxacin, Difloxacin, Doxycycline, Mecillinum, Tetracycline, Cefaclor, Sulfapyridine, Cefalexin</p> <p>Anticonvulsants - Dilantin, Cabapentin, Primidone, Phenobarbital, Carbamazepine</p> <p>Antidepressants - Diazepam, Fluoxetine, Oxazepam, Imipramine, Doxepin, Thioridazine, Meprobamate</p> <p>Antineoplastics - Tamoxifen, Methotrexate, Epirubicin, Ifosfamide, Cyclophosphamide</p> <p>Beta-blockers - Propranolol, Pindolol, Metoprolol, Nadolol, Atenolol, Sotalol, Acebutolol</p> <p>Hormones - Testosterone, Estrone, Androstenedione, Mestranol, Estriol, 17-β Estradiol</p> <p>Lipid regulators - Furosemide, Gemfibrozil, Clofibrate, Bezafibrate, Clorfibric acid, Simvastatin</p> <p>Nonsteroidal anti-inflammatory drugs - Salicylic acid, Phenazone, Nimesulide, Paracetamol, Naproxen, Ketoprofen, Acetaminophen, Ibuprofen, Diclofenac, Aspirin, Indomethacin</p>	Miscarriage, pregnancy complications, feminization in fish, injurious to marine organisms, constrained polypregeneration and diminished reproduction, growth impairment in human embryonic kidney cells	(Nawaz & Sengupta, 2019)

Personal care products (PPCPs)	<p>Disinfectants - Bromoprene, Chloroprene, 2-phenylphenol, 4-chlorocresol, 4-chloroxylenol, Triclosan</p> <p>Fragrances - Musk ketone, Musk xylene</p> <p>Preservatives - Methyl paraben, 2-phenoxyethanol, derivatives of 4-hydroxybenzoate</p> <p>Sunscreen agents - Ethylhexyl methoxycinnamate, Octocrylene, Oxybenzone</p>	Ochronosis, potential mutagenicity, irritant, allergic, phototoxic, dizziness, fatigue, irritation to eyes, throat and nose, carcinogenic, neurotoxic	(A. D. Khan & Alam, 2019)
Endocrine Disrupting Compounds (EDCs)	Phthalates, phenol, bisphenol A	disrupt the endocrine and hormonal functions, create medical problems by mimicking or blocking hormones and disturbing the body's regular processes, harm human reproductive system and induce preterm, underweight newborns, metabolic disorders (heart disease, prediabetes, high blood pressure, and hyperlipidaemia), as well as other wellness impacts (thyroid hormone instability and abnormal immune operation) in humans	(Giulivo et al., 2016; James-Todd et al., 2016; Muhamad et al., 2016)
Fire Retardants (FRs)	Tetrabromobisphenol A (TBBPA), hexabromocyclododecane (HBCD), triphenyl phosphate (TPP), tricresyl phosphate (TCP), dimethyl methylphosphonate (DMMP)	Carcinogenic, affects neurodevelopment and reproductive systems	(X. Zhang et al., 2016; Y. N. Zhang et al., 2016)
Pesticides	resmethrin, cypermethrin, bifenthrin, tolylfluanid, methoxychlor and triazine	hazardous to spiders, carabid beetles, insects such as honeybees, bumble bees, fruit flies, and mammals	(Dawson et al., 2010; Fountain et al., 2007; Giglio et al., 2011; Kevan, 1999)

Consumption of more than two PPCPs at once may cause interaction issues in people (X. Wu et al., 2015), where 500 ng/day per chemical was consumed concurrently by consumption of vegetable crops cultivated with PPCPs polluted water. Regular consumption to PPCPs, particularly antibiotics, results in antimicrobial tolerance in people, potentially increasing the chance of mortality. Stuart et al. 2012 demonstrated that parabens conquered estrogenic task and triggered virologically facilitated instant systemic hyper acuity responses whereas N,N-diethyl-meta-toluamide (DEET) hindered the enzyme accountable for central nervous system function (Stuart et al., 2012). Verslycke et al. discovered a significant level of protection for triclosan (TS) consumption across all pathways, such as bio solids – soil-plant – human, and concluded that the pollutant might represent a low danger to human health (Verslycke et al., 2016).

A case of endocrine disruption in snails induced by tributyltin consumption was generalized to vertebrates, particularly fish, which were shown to be just as susceptible to this substance as snails and experienced endocrine impacts at ecological quantities (Lagadic et al., 2018). CECs are present in the environment at extremely low doses for longer time (Daughton, 2002). Low-dose CEC consumption may not produce explicit harm, but instead modest alterations in the individuals' health and physiology (e.g. behaviour). These minor adjustments demonstrate the ability to have adverse environmental consequences in terms of population and biodiversity. The drug, venlafaxine, which affects brain tissue, has also been linked to neurotoxicity (Bidel et al., 2016).

Antibiotics have a number of detrimental effects on agro-environment, according to Du and Liu (Du & Liu, 2012), such as: (1) germinating seeds and crop growth reduction; (2) soil microbial action suppression; (3) antibiotic deposition in plant biomass; and (4) syphoning diffusion into underground water. Antibiotics and their breakdown by-products were studied for their environmental effects, and microbial communities impervious to antibiotics were discovered after long-term vulnerability due to biological diversity and transmission (Du & Liu, 2012). Girardi et al.(Girardi et al., 2011) also confirmed that ciprofloxacin (CPF) (at

doses of 0.2, 2, and 20 mg/kg) significantly reduces micro flora in soil. They also discovered that this antibiotic was still bioactive after a longer duration (29 days).

1.6. Conventional treatment methods for removal of CECs

The presence of contaminants of emerging concern (CECs) in the environment has wide-ranging impacts, affecting public health, marine ecosystems, and contributing to the emergence of antibiotic-resistant bacteria, neurotoxic effects, disruption of endocrine systems, and the development of tumors (Mahmood et al., 2022). To remove CECs from water, a variety of conventional treatment methods have been explored, including sand filtration, coagulation/flocculation, activated sludge treatment, among others. These methods are discussed below in detail.

1.6.1. Sand filtration

For systems that are smaller, one of the easiest and best methods for treating drinking water is sand filtration (SF). Many contemporary infections and pollutants can now be effectively treated because of modifications and adaptations made to this technology (Jobb et al., 2007). SF, which includes physico-chemical and biological removal methods for various target pollutants, is a crucial treatment step in drinking water treatment plants for the production of drinking water (Bai et al., 2016; Jinsong Wang et al., 2021). SF normally has a bed that is 1.5–2.5 metres tall and is run at a downward filtration velocity of 3–8 metres per hour (Jinsong Wang et al., 2021). Furthermore, to avoid blockage by residual materials such as excess biomass and precipitated metal oxides, the filters must be backwashed on a regular basis (Albers et al., 2015; Jinsong Wang et al., 2021).

1.6.2. Coagulation-flocculation

The coagulation-flocculation process is a commonly employed technique for the filtration of industrial and urban wastewaters (Pavón-Silva et al., 2009; Rodrigues et al., 2008; Teh et al., 2016). As early as 1500 BC, it was documented that the Egyptians were using aluminium sulphate, known as alum, to induce particles that were suspended to settle in water (Parsons & Jefferson, 2009; Teh et al., 2016). These days, turbidity, natural organic matter, and other soluble organic and inorganic contaminants in wastewater are reduced by agglomerating tiny particles

and colloids into bigger particles by the process of coagulation-flocculation (Parsons & Jefferson, 2009; Teh et al., 2016). This procedure consists of two separate steps: (1) flocculation, which involves using mild agitation to agglomerate tiny particles into well-defined flocs, and (2) quick mixing of a dispersed coagulant into water or wastewater to be treated (Spellman, 2023; Teh et al., 2016). Ultimately, the wastewater/treated water (supernatant) is shifted to a different treatment process or released into a watercourse, and the flocs are let to settle and ultimately be collected as sludge. Coagulation flocculation has been effectively used in many types of water treatment because of its simple design, low energy consumption, and ease of operation (AlMubaddal et al., 2009; Teh et al., 2016; Torres et al., 2009).

1.6.3. Activated sludge treatment

Aeration and sludge settling are the two distinct stages that make up the activated sludge treatment. Typically, this unit operates without allowing any settling in the aeration tank (Scholz, 2016). As a result, it operates after the aeration tank using a totally different settlement tank that continuously removes and returns sludge to it (Scholz, 2016). In addition to supplying the microorganisms with a sufficient amount of food, the continual mixing activity is necessary to maintain a maximal oxygen concentration gradient, which facilitates mass transfer and aids in the dispersal of metabolic waste products from inside the flocs (Scholz, 2016).

The mixed liquor, or wastewater and microbiological mass combined, is displaced into a sedimentation tank by the settled wastewater when it reaches the aeration tank (Scholz, 2016). The cleared effluent, which is almost entirely solid-free, is released as the final effluent in this second step, where the flocculated biomass quickly drops out of suspension to create sludge. For every kilograms of BOD₅ eliminated, 0.5 to 0.8 kg of dry weight of sludge is created in the traditional AS process (Scholz, 2016). The sludge may be readily pumped since it resembles weak slurry with 0.5% to 2.0% dry solids. Although it is challenging to concentrate AS to >4% dry particles by gravity alone under typical working conditions, the viscosity increases quickly as the solids content rises (Scholz,

2016). In order to guarantee that, there is sufficient microbial population to completely oxidize the wastewater throughout its retention time inside the aeration tank, the majority of the AS is returned to the aeration tank to serve as an inoculum of microorganisms. Prior to disposal, the extra sludge (8–10% of the daily production) has to be treated (Scholz, 2016).

1.7. Advanced treatment methods for removal of CECs

The removal of developing pollutants cannot be performed by conventional wastewater treatment techniques, which is why they were mostly ineffectual (Nghiem & Fujioka, 2016). Because of this, the waste water treatment need to be developed by involving advanced treatment techniques, including membrane separation, advanced oxidation, ozonation, and activated carbon adsorption (Nghiem & Fujioka, 2016). The advanced treatment processes are discussed below.

1.7.1. Membrane technology

Reverse osmosis (RO) and nanofiltration (NF), in particular, are high pressure membrane techniques that are often used to remove developing pollutants (Nghiem & Fujioka, 2016). In fact, potable water recycling applications and the generation of drinking water from polluted surface water are the main uses for full-scale NF or RO systems nowadays, with the aim of eliminating new pollutants (Beyer et al., 2014; Fujioka et al., 2012; Nghiem & Fujioka, 2016; Ventresque et al., 2000). Other notable membrane technologies that have not yet been used on a large scale but have the potential to remove developing trace organic pollutants include membrane electrodialysis (ED), membrane distillation (MD), and forward osmosis (FO) (Nghiem & Fujioka, 2016). This chapter will not give a full examination of FO, MD, and ED due to their still-emerging character. Rather, only essential elements related to eliminating emerging trace organic pollutants will be covered (Nghiem & Fujioka, 2016).

The majority of contaminants in water may be eliminated using high pressure membrane filtration (Nghiem & Fujioka, 2016). Recent decades have seen a decrease in the cost of water treatment systems that use high pressure membrane

processes, such as RO and NF, due to technical advancements in the manufacture of materials and modules (Nghiem & Fujioka, 2016). The capacity of RO and NF membranes to separate mono- and divalent ions sets them apart from one another. For instance, RO membranes are often used in the semiconductor industry, for wastewater recycling, and for saltwater desalination, where a high level of salt and other dissolved pollutant removal including CECs—is necessary (Nghiem & Fujioka, 2016). Conversely, NF membranes have been used in drinking water treatment facilities in situations when the source (surface or ground water, for example) has been contaminated with volatile organic compounds (VOCs) or includes divalent ions (calcium and manganese) (Nghiem & Fujioka, 2016).

1.7.2. Adsorption

Adsorption processes appear to be better than other separation techniques for removing pollutants from water environments because they minimize biological sludge, are highly efficient, simple to use even in large-scale applications, and require inexpensive adsorbent materials (Varjani et al., 2020; Yaashikaa et al., 2019). One of the most efficient advanced wastewater treatment technologies is adsorption, which is widely used by academic and industrial researchers to remove different types of contaminants. One of the adsorbents in the water treatment process that has been studied the most is activated carbon (Rajan et al., 2016; Rao et al., 2009). It is a surface-based technique where Vander Waals forces hold the adsorbate onto the adsorbent surface (Rajan et al., 2016). Chemical bonding and electrostatic attraction are some possible mechanisms of adsorption of adsorbates (Rajan et al., 2016). It is a well-known technique for eliminating dangerous substances from contaminated waterways (Vinod K. Gupta & Ali, 2001; Vinod K. Gupta et al., 2002; Rajan et al., 2016; Sheha & Metwally, 2007). However, as the high bed loading is involved, it is too costly for concentrated waste water; in these situations, a big bed would need to be installed, which would require a huge capital investment, or frequent regeneration, which would require a high running cost (Rajan et al., 2016).

1.7.3. Advanced oxidation process

The oxidation process, sometimes referred to as the advanced oxidation process (AOP), is one of the most widely used chemical procedures for spent water (Deng & Zhao, 2015; Donkadokula et al., 2020). An appropriate number of hydroxyl radicals (OH^\bullet) are produced in this method for purifying water, and this idea was subsequently extended to sulphate radicals ($\text{SO}_4^{\bullet-}$) oxidative reactions (Deng & Zhao, 2015; Donkadokula et al., 2020). AOPs have been investigated for their potential to inactivate pathogens and pathogenic markers, in addition to their ability to degrade organic and inorganic contaminants (Deng & Zhao, 2015; Donkadokula et al., 2020). Strong oxidants have the ability to quickly break down any substances in wastewater, which is why AOPs are regarded as the finest solutions for treating wastewater (Deng & Zhao, 2015; Donkadokula et al., 2020). Although alternative materials, including ferryl ions, are suggested, hydroxyl radicals are the conventionally accepted name for the reactive species generated (Deng & Zhao, 2015; Pignatello et al., 2006). A detailed discussion of the Fenton-related chemistry for treating water and wastewater has already been covered elsewhere (Deng & Zhao, 2015; Pignatello et al., 2006).

1.7.4. Solvent extraction

Three main processes could be involved in the solvent extraction process. The process of moving the solute from water into the solvent is called extraction (Kiezyk & Mackay, 1971; Rajan et al., 2016). The second step is called "solute removal," during which the solvent is recycled back into the extractor and the solute is extracted (Kiezyk & Mackay, 1971; Rajan et al., 2016). The third step is solvent recovery, where the wastewater raffinate can be used to extract the solvent (Kiezyk & Mackay, 1971; Rajan et al., 2016). The primary purpose of solvent extraction is to remove phenols, creosols, and other phenolic acids from polluted water that contains small amounts of solutes from petroleum refineries and coke-oven plants in the steel and plastics industries (Mahmood et al., 2022; Rajan et al., 2016).

1.7.5. Electrochemical method

A low-level direct current is applied through two electrodes to initiate the electrochemical (EC) process (Dionísio et al., 2021). Because the electric potential accelerates the oxidation of CECs and concurrently fosters the production of OH[•], this mechanism can break down contaminants from polluted matrices (Dionísio et al., 2021; Ferreira et al., 2018; Magro et al., 2020). In order to remove CECs from wastewater matrices, the EC procedure has also been researched in the field of wastewater treatment (Dionísio et al., 2021; Gadipelly et al., 2014; Lima Morais et al., 2019; Zaied et al., 2020).

1.8. Nanomaterials for water treatment

Materials with at least one dimension less than 100 nm are referred to as nanomaterials (Mahmood et al., 2022). The greater surface area and density of nanomaterials lead to an increase in resolution mobility, surface reactivity, and adsorption efficiency (Mahmood et al., 2022). Utilizing nanoparticles for wastewater treatment through adsorption, adsorption-oriented polymers, and filtration has been made easier by recent research into the use of nanomaterials (Mahmood et al., 2022). It has been revealed that CECs can be efficiently removed from wastewater by using nanomaterials. Numerous nanomaterials, including carbon nanomaterials, metal-oxide nanoparticles, zerovalent metal nanoparticles, and nanocomposites, have been described for the treatment of wastewater (Mahmood et al., 2022).

Due to its tiny size and large surface area, zerovalent metal is an important nanomaterial for wastewater treatment that is also highly reactive (Borrego et al., 2016; Mahmood et al., 2022). Researchers have recently focused their attention on a number of zerovalent metal nanoparticles, such as nickel, zinc, iron, aluminium, and silver, with the purpose of eliminating contaminants (Borrego et al., 2016; Mahmood et al., 2022). Because of their possible antibacterial qualities, silver nanoparticles are typically employed as disinfectants to get rid of a lot of bacteria, viruses, and fungus (Borrego et al., 2016; Mahmood et al., 2022). Photocatalytic degradation has gained significant interest as a promising and

developing technology (H. Lu et al., 2016). The breakdown of contaminants in water and wastewater has been effectively achieved by the use of photocatalytic degradation technology in recent times (H. Lu et al., 2016).

Due to the accessibility and ease of usage, iron oxide nanoparticles have garnered increasing attention in recent years as a means of eliminating heavy metals (H. Lu et al., 2016). As nanoadsorbents, Fe_3O_4 , $\gamma\text{-Fe}_2\text{O}_4$, and $\alpha\text{-Fe}_2\text{O}_3$ are frequently utilized (H. Lu et al., 2016). The separation and recovery of nanosorbent compounds from polluted water often provide significant obstacles for water treatment because of their tiny size (H. Lu et al., 2016). Fe_3O_4 and $\gamma\text{-Fe}_2\text{O}_4$ have been effectively employed as sorbent materials to remove different heavy metals from water systems (Lei et al., 2014; Ngomsik et al., 2012; Tan et al., 2014).

Graphene and carbon nanotubes are examples of carbon-based nanomaterials that come in both functionalized and non-functionalized forms (Smith & Rodrigues, 2015). Metal or metal oxides can also be used to functionalize these nanomaterials. Fe/ Fe_3O_4 , Al/ Al_2O_3 , TiO_2 , and Ag are the most often utilized metals and metal oxides in carbon-based nanocomposites for water treatment applications (Guo et al., 2012; V. K. Gupta et al., 2011; J. D. Kim et al., 2013; Pyrzyńska & Bystrzejewski, 2010; Shaari et al., 2012; Smith & Rodrigues, 2015). It has been demonstrated that adding metal or metal oxides to nanocomposites enhances the adsorption and disinfection capabilities of carbon-based nanomaterials (Smith & Rodrigues, 2015).

Chapter 2
LITERATURE REVIEW

Chapter 2

LITERATURE REVIEW

2.1. Adsorption process

The adsorption process using solid adsorbents is considered as one of the most effective ways to treat and remove organic pollutants in wastewater treatment among the several strategies for treating water (Crini, 2005; Rashed, 2013). Adsorption has an advantage over the other techniques due to its straightforward design and potential for minimal cost and land requirements (Crini, 2005; Rashed, 2013). The adsorbate accumulates at the adsorbent surface during the adsorption process, which is a surface phenomenon. The method is predicated on the idea that adsorption reduces the energy of the interface, which can be between a liquid and a solid, solid and gas, solid and liquid, or liquid and gas (Dąbrowski, 2001). Adsorption may be conceptually separated from absorption, which includes bulk material, since it is restricted to the contact. The **species** of the adsorbent and adsorbate that are involved to determine the specific form of contact and bonding that occurs. Both chemisorption and physical adsorption are common classifications for the adsorption process. When there is physical adsorption, also known as physisorption, the adsorbate attaches itself to the surface by electrostatic attraction, hydrogen bonding, or weak van der Waals forces. It is thought that physisorption has low interaction energy—less than 15–30 kJ/mol—and is reversible. Adsorbate and surface sites react chemically through covalent bonding to create chemisorption. Between the adsorbates and the adsorbents, new, very energetic chemical bonds are created that are irreversible and can range from tens to hundreds of kJ/mol. Adsorption and desorption are linked processes that demonstrate the movement of sorbate ions from the surface of the sorbent into solution. The quantity of sorbate that has been desorbed from the solid determines how much the sorbent regenerates; as desorption grows, so does the sorbent renewal process, according to the experimental conditions that are used (Sahoo & Prelot, 2020).

The following are the fundamental needs for a good adsorbent in order to achieve excellent performance and sorption efficiency (Ali, 2012; Hristovski & Markovski, 2017; Sadegh et al., 2017). To remove the greatest quantity of contaminants, it is first important to develop sorbents with high sorption capacities. Additionally, it must have great selectivity for certain contaminants, particularly those that are present in water at low concentrations or in situations when several components are competing with one another. It also has to be recyclable and reusable. This implies that in order to renew the adsorbent, the contaminants that have been adsorbed must be readily removed from its surface. Quick mass transfer of pollutants requires quick kinetics and adequate accessibility to the sorption sites, which are provided by the sorbent. This needs to be true in a variety of operational and water matrix scenarios. In addition, it must be low-cost and easy to manufacture in large quantities—especially when compared to alternative water treatment methods. When used in large-scale applications, this also entails minimizing the need for maintenance and operation. Naturally, it should also be benign and favorable to the environment (Sahoo & Prelot, 2020).

The creation of modified and novel qualities or the fusion of several features is the source of this expanding interest in materials for the adsorption of a wide range of pollutants. All sorption phenomena are dependent on the material's interfacial qualities since adsorption takes place at the interface. Adsorption rises when the adsorbent's accessible surface area is expanded. Materials with a high surface to volume ratio or those with varying porosity levels have high specific surface area values. The quantity of exposed active sites is necessary for the high chemical and surface reactivity, and the presence of certain functional groups on the adsorbent increases this reactivity (Sahoo & Prelot, 2020).

2.2. Adsorbents used for the adsorption of CECs

Because of its high effectiveness, wide specific surface area, and hydrophobic interactions, activated carbon is the most often utilized adsorbent in the removal of CECs (Almeida-Naranjo et al., 2023; Grassi et al., 2012; Sophia A. & Lima,

2018). There have also been reports on the utilization of clays, alumina, nanoparticles, zeolites, composites, soil, and metal-organic frameworks (such as graphene, magnetic nanoparticles, and carbon nanotubes) (Ahmad et al., 2019; Almeida-Naranjo et al., 2023; Rout et al., 2021). However, the high cost of activated carbon and other adsorbents prevents their widespread usage (Almeida-Naranjo et al., 2023; Grassi et al., 2012; Sophia A. & Lima, 2018). This has accelerated the demand for low-cost, broadly accessible, little processed, and ecologically benign substitute materials (Almeida-Naranjo et al., 2023; Quesada et al., 2019). The most popular materials for CECs removal are covered in this section.

2.2.1. Activated carbon

The most common adsorbent material utilized in wastewater treatment plant is activated Carbon (AC), which was utilized in 3311 thousand metric tons in 2021 and at a rate of between 5.5 and 8.1% year between 2008 and 2018 (Pallarés et al., 2018). For the elimination of CECs, AC has been shown to be the most effective adsorbent (Almeida-Naranjo et al., 2023; Grassi et al., 2012; Sophia A. & Lima, 2018). Acetaminophen, testosterone, androstenedione, progesterone (Grassi et al., 2012), paracetamol (García-Mateos et al., 2015), , metronidazole (Forouzesh et al., 2019), nimesulide (Raupp et al., 2021) were removed using AC. However, AC is an expensive adsorbent with high recovery costs, and its renewal reduces its effectiveness (<40%) (Almeida-Naranjo et al., 2023; Sophia A. & Lima, 2018).

2.2.2. Zeolites

Zeolite is a hydrated aluminosilicate mineral that occurs naturally. It has a three-dimensional tetrahedral structure made up of connected SiO_4 and AlO_4 units. Its structure is porous and is made up of chambers and channels (Solińska & Bajda, 2022)(Ozin et al., 1989). Additionally, the zeolite has a permanent negative charge, which are mostly found in zeolitic channels and on the exterior surfaces. This is due to the replacement of Al^{3+} ions for Si^{4+} ions in the tetrahedral units (Solińska & Bajda, 2022). The elimination of phenol, dichlorophenol (S. H. Lin & Juang, 2009), nicotine, carbamazepine, erythromycin, nitrosamines nitrobenzene

(N. Jiang et al., 2018), tetracycline, oxytetracycline (Lye et al., 2017), and 2,4,6-trichlorophenol (N. Jiang et al., 2020) was effectively achieved by zeolites. They achieved removal efficiencies ranging from 45% to 90% (de Sousa et al., 2018; N. Jiang et al., 2018; S. H. Lin & Juang, 2009; Lye et al., 2017; Pukcothanung et al., 2018).

2.2.3. Clays

Clays and clay minerals are one type of readily accessible adsorbent that has been used in water remediation applications. They are naturally occurring, non-toxic, and affordable (Ewis et al., 2022; Lazaratou et al., 2020). According to Chen et al. (L. Chen et al., 2016), the family of phyllosilicates that contains clay minerals like montmorillonite and kaolinite include both planar hydrous and non-planar hydrous phyllosilicates. The physiochemical features of clays and clay minerals, such as swelling and ion exchange capacity, along with their unique two-dimensional (2D) layer structure allow them to effectively adsorb a wide range of organic and inorganic water contaminants (L. Chen et al., 2016; Ewis & Hameed, 2021; Ewis et al., 2022). Clays were utilized in the removal of CECs like ciprofloxacin (H. Chen et al., 2015; C. J. Wang et al., 2011), carbamazepine (W. Zhang et al., 2010), triclosan (Cardona et al., 2023), tetracycline and bisphenol A (Adesina et al., 2023), and oxytetracycline (Ashiq et al., 2021), etc.

2.2.4. Chitosan

The organic polysaccharide chitosan is plentiful and has been extensively studied for its potential to remediate wastewater contaminated by CECs (R. Huang et al., 2023). Many reactive amino and hydroxyl groups found in chitosan have the ability to bind and exchange ions with heavy metal ions through chelation, electrostatic attraction, and other means (Q. Jiang et al., 2022). Furthermore, chitosan's high functionality allows for a variety of chemical changes by grafting or crosslinking with other reactive groups like phosphate and sulphate (Abdel-Raouf et al., 2023). CECs such as ciprofloxacin (R. Huang et al., 2023), tetracycline (da Silva Bruckmann et al., 2022; Rizzi et al., 2019), triclosan

(Matolia et al., 2019; Rasheed et al., 2022), methyl paraben and propyl paraben (Mashile et al., 2020) were removed by using chitosan.

2.2.5. Agricultural/Agro-industrial biomass

Comparing with different adsorbents, using biomass or agricultural waste offers the advantages of being more affordable, biodegradable, and environmentally friendly. Consequently, certain biomass materials have been used to adsorb CECs, including *Dialium guineense* (Eze et al., 2021; Ezekoye et al., 2020), banana peel (Farias et al., 2023), rice husk (Triwiswara et al., 2020), yam peel (Akpomie et al., 2023), jackfruit peel (Qureshi et al., 2020), tamarind shell (N et al., 2022), corn cob (Ajala et al., 2023), grapefruit peel (Prakash Bobde, Sharma, Kumar, Pandey, et al., 2023), and rice peel (Akpomie et al., 2023). These types of biomass was used for the removal of ciprofloxacin (Akpomie et al., 2023), ketoprofen (Huan Wang et al., 2023), sulfanilamide (Gámiz et al., 2022), triclosan (Cho et al., 2021), etc.

2.2.6. Biochar

Because it is a biowaste-based, economical, and sustainable adsorbent, biochar is seen as a potential option. It is a stable, carbon-rich, pyrolytic or anaerobic material that is produced from organic material as a raw material and has undergone thermal treatment (Mahdi et al., 2019)(Jha et al., 2023). Biochar is mostly made from waste products, either lignin- or non-lignin-containing, from the wood, fibre processing, agriculture, and aquaculture sectors, among others. Hydrophobicity, long-term stability, chemical composition, high porosity, huge surface area, and other characteristics are some of the unique qualities of biochar. This means that it might be a good fit for a number of uses, including the removal of hazardous pollutants, the sequestration of carbon, the adsorption of greenhouse gases, etc (Jha et al., 2023). Various types of biochar were utilized for the removal of tetracycline (Z. Fan et al., 2022; Hoslett et al., 2021; R. Li et al., 2020; S. Luo et al., 2022; Premarathna et al., 2019; Sun et al., 2021; Q. Wang et al., 2023; Yu et al., 2020), bisphenol A (Katibi et al., 2021; Jinpeng Wang & Zhang, 2020), oxytetracycline (Feng et al., 2021a; G. Liang et al., 2019; Ramanayaka, Kumar, et

al., 2020; Ramanayaka, Tsang, et al., 2020; Solmaz et al., 2023; Z. Wei et al., 2023), diclofenac sodium (Al-Qahtani et al., 2023; de Souza dos Santos et al., 2020; Lins et al., 2020; Nguyen et al., 2021), atrazine (Y. Wang et al., 2020), ciprofloxacin (Hamadeen & Elkhatib, 2022; Özer & İmamoğlu, 2022; Wakejo et al., 2022; Z. Yang et al., 2020; Yue Zhou et al., 2019), sparfloxacin (Yue Zhou et al., 2019), triclosan (Cho et al., 2021), ibuprofen (Nguyen et al., 2021), etc.

2.2.7. Industrial waste

Because of its affordability, ease of production, and accessibility to low-cost precursor components, the usage of zeolites (adsorbent) derived directly from coal fly-ash (CFA), a byproduct of burnt coal, has garnered a lot of scientific interest (Ahmaruzzaman, 2010; Aigbe et al., 2021; N. Jiang et al., 2018). Zeolites are frequently taken into consideration in the fields of gas separation, water purification, and remediation due to their high adsorption capacity, huge surface area, exceptionally high porosity, and thermal stability (Aigbe et al., 2021). Red mud is a highly alkaline byproduct that is created during the Bayer process, which turns bauxite ore into alumina for the manufacture of aluminium (Aydin et al., 2019). The need for aluminium is rising in tandem with population growth and urbanisation, and one of the biggest issues facing aluminium production facilities is how to store and dispose of red mud. The globe produces 120 million tons of red mud a year, according to estimates. According to Grafe et al. (2011) (Gräfe et al., 2011), red mud comprises silica, aluminium, iron, calcium, titanium, sodium, and trace levels of potassium. Because of its structural characteristics and chemical and mechanical stability, it has the potential to be an excellent adsorbent for treating water (Aydin et al., 2019).

2.2.8. Polymers

Activated carbon and mesoporous sorbents have higher adsorption capacities than polymeric sorbents, but they also have certain benefits. Because of their high surface area and mechanical robustness, polymeric materials have prospective uses in the water treatment industry as an alternative to activated carbon (Akhtar et al., 2016; Pan et al., 2009). Polymeric sorbents are characterized by their

excellent mechanical strength, homogeneous pore size distribution, and facile regeneration in moderate environments. Unlike activated carbon, which needs to be regenerated often, polymeric sorbents are long-lasting and fouling-resistant, lasting up to 2,000 regeneration cycles (Akhtar et al., 2016; Xu et al., 2003).

2.2.9. Nanomaterials

The remarkable qualities of carbon nanotubes (CNTs) point to a number of beneficial uses for them as adsorbents in the removal of CECs from residential and commercial wastewaters (de Azevedo et al., 2023; El-Sheikh et al., 2019; Ncibi & Sillanpää, 2015). CNT have large surface area as well as a distribution of pores that are ideal for adsorption processes (de Azevedo et al., 2023; Gil et al., 2018; Machado et al., 2011; Pires et al., 2019). These materials are appropriate for effective adsorption procedures due to their electronic characteristics and dimensionality, which is comparable to the scale of many pollutants' molecules (Abo El Naga et al., 2019; de Azevedo et al., 2023).

The cylindrical graphite sheets found inside CNTs have an extremely high van der Waals index. High polarizability carbon atoms that are sp^2 -hybridized are present in the benzenoid rings of graphite sheets. CNTs have been utilized for the removal of ciprofloxacin (Elamin et al., 2022; H. Li et al., 2018; J. Yao et al., 2023), triclosan (S. Zhou et al., 2013), oxytetracycline (Y. Fan et al., 2023), sulfamethazine (Ameen et al., 2020), norfloxacin (Ohale et al., 2023), sulfamethoxazole, sulfapyridine (Tian et al., 2013), caffeine (Quintero-Jaramillo et al., 2021) and diclofenac (Gil et al., 2018).

A two-dimensional (2D) monolayer of sp^2 hybridised carbon atoms organised in a honeycomb pattern and joined by functional groups that include oxygen, such as hydroxyl, carboxyl, and epoxy groups, is known as graphene oxide (GO) (Hiew et al., 2019). With its distinct qualities, including a relatively high specific surface area, a wide range of surface functional groups, and strong colloidal stability, GO has emerged as a promising adsorbent for the treatment of wastewater (Hiew et al., 2019). According to reports, GO's high adsorption capacity is facilitated by a number of adsorption mechanisms, including hydrophobic, electrostatic, and

hydrogen bonding between GO's functional groups and the pollutants' active ingredient (Hiew et al., 2019; Kyzas et al., 2015; Y. L. Zhang et al., 2014). For this reason, highly polar and soluble contaminants might be effectively removed using GO as an adsorbent (Hiew et al., 2019). GO has been utilized for the removal of caffeine (M. B. Andrade et al., 2022; Xueyu Wang et al., 2022), diclofenac (Hiew et al., 2019; Mahmoodi et al., 2021), ciprofloxacin (F. Wang et al., 2016), triclosan (Yuanyuan Zhou et al., 2023), tetracycline (Y. Gao et al., 2012), oxytetracycline (El Hadki et al., 2021), etc.

The short intraparticle diffusion distance, cheap cost, and high effectiveness of pollutant removal are the distinguishing features of metal-based nano adsorbents. In addition, their surface area remains unchanged upon compression, and they exhibit resistance against abrasion, magnetic fields, and photocatalysis (Almeida-Naranjo et al., 2023). Maghemite ($\gamma\text{-Fe}_2\text{O}_3$), spinel ferrites ($\text{M}^{2+}\text{Fe}_2\text{O}_4$, where M: iron, cadmium, copper, nickel, cobalt, manganese, zinc, magnesium) and hematite ($\alpha\text{-Fe}_2\text{O}_3$) are examples of magnetic nanoadsorbents that are excellent adsorbing materials for the collection and removal of harmful components from polluted water (Kundururu et al., 2017). Metal-based nanoadsorbents have been utilized for the removal of carbamazepine (Gabet et al., 2023), ciprofloxacin (Rakshit et al., 2013), triclosan (So et al., 2019)(Y. Wu et al., 2018), tetracycline (Xiangyu Wang et al., 2023), caffeine (Abdel-Aziz et al., 2020) and sulfamethoxazole (Song et al., 2021).

2.3. Biochar as greener/sustainable adsorbent

Biochar became the new promising adsorbent when compared to different adsorbents. The sustainable production of various biochars from a variety of waste materials such as pine cone, rice husk, coconut shell, etc. makes it stand out among other adsorbents. Biochar, derived from lignocellulosic biomass, has been effective in the removal of CECs from aquatic environment. However, the pure biochar's ability to selectively adsorb high concentration pollutants has several limitations (Ma et al., 2014).

2.4. Chemical modification of biochar

Numerous techniques were used to alter the characteristics of biochar in order to overcome its limitations for environmental applications. The two primary physical modifications are gas and steam purging (Jianlong Wang & Wang, 2019). Removing contaminants like metals and adding acid functional groups to the surface of biochar is the primary goal of acid modification (Jianlong Wang & Wang, 2019). Phosphoric acid (Özer & İmamoğlu, 2022), sulfuric acid (V. Shukla et al., 2023), nitric acid (Fernando et al., 2021), hydrochloric acid (Han et al., 2022) are commonly used acid for the activation of biochar. Sayin et al. (Sayin et al., 2021) reported that, the biochar's H_3PO_4 modification enhanced its adsorption ability for CPF by a factor of 17 to 39. The adsorption capacity of methyl paraben, carbamazepine, ibuprofen and triclosan was increased after the sulfuric acid modification (Choudhary & Philip, 2022).

Increasing the surface area and the functional groups that contain oxygen is the primary goal of alkaline modification (Jianlong Wang & Wang, 2019). Sodium hydroxide (NaOH) and potassium hydroxide (KOH) are mostly used bases for the modification of biochar. When compared to pristine biochar, KOH-modified biochar improved tetracycline removal by up to 3.50 times (cassava stalk), 4.99 times (rubber wood), and 2.14 times (sugarcane bagasse), respectively (Q. Wang et al., 2023). Oxidizing chemicals can be used to modify the biochar to enhance the amount of oxygen-containing functional groups (Jianlong Wang & Wang, 2019). By altering biochar with potassium permanganate, its surface area rose from 101 to 205 m^2/g . Potassium permanganate treatment of biochar increased its adsorption capability (Hongyu Wang et al., 2015).

Adsorption, catalysis, and magnetic properties of biochar may all be altered by using metal salts or metal oxides. This type of modification can be carried out by two ways: (1) feedstock initially mixed with the metal salts or metal oxides, and then pyrolyzed at particular temperature to synthesize biochar, (2) feedstock is initially pyrolyzed at particular temperature to synthesize biochar, and then biochar is mixed with the metal salts or metal oxides under specific

circumstances. Following MnO₂ coating, MnO₂/biochar's adsorption capacity for both tetracycline and doxycycline was noticeably greater than that of pure biochar (Jiang Li et al., 2020). Pristine poplar wood biochar has a slightly greater Brunauer-Emmett-Teller (BET) specific surface area of 431.6 m²/g than Fe₂O₃ modified poplar wood biochar (422.1 m²/g) (H. Liang et al., 2022). Fe₂O₃ modified grapefruit peel biochar's specific surface area grew from 1.71 m²/g to 20.73 m²/g—a considerable increase as compared to pristine grapefruit peel biochar. This could be because the loaded iron oxide nanoparticles have a large specific surface area, which greatly increases the surface area of modified biochar (Jinpeng Wang & Zhang, 2020). The bisphenol A removal efficiency of biochar was substantially increased from 85.97% to 94.2% after modification of biochar with Fe₃O₄ (Katibi et al., 2021). The specific surface area of MnO₂ modified bamboo willow biochar was found to be increased after modification of pristine bamboo willow biochar (Feng et al., 2021b).

2.5. Mechanism of adsorption of CECs

In general, the adsorption mechanism of CECs on biochar-based materials could be the hydrophobic interaction, pore filling, π - π electron donor acceptor (EDA) interaction, hydrogen bonding, ion exchange and electrostatic interactions. The adsorption mechanism depends on the initial pH of aqueous CEC solution, pyrolysis temperature of the biomass and adsorbent dose. In the next sections, adsorptive mechanisms for CECs removal using biochar & biochar-based composites is reviewed.

2.5.1. Adsorptive mechanism for Tetracycline (TC)

Fourier Transformation Infra-red (FTIR) spectral analysis and Raman spectral analysis manifested the existence of aromatic sp² groups & π -electron donors in the food scraps & trimmings biochar. TC structure also contains aromatic ring & C=C bond, leading to π - π EDA interaction in the adsorption of TC by food scraps & trimmings biochar. The hydrogen bonding could be possible among the biochar and TC due to the proximity of hydrogen & oxygen carrying functional groups in the TC structure (Hoslett et al., 2021).

At the pH levels used in the experiments, the adsorption of TC on the ball-milled magnetic nanobiochar through electrostatic attraction was relatively restricted. As the ionic strength rose, the adsorbed concentrations of TC decreased slightly, indicating that electrostatic attractions played a relatively little part in the adsorption mechanism. Furthermore, adsorption kinetic investigations demonstrated that chemisorption regulated the adsorption of TC, with the rate-controlling adsorption phases being external mass transfer and intra-particle diffusion. The FTIR & XPS spectrum of ball-milled magnetic biochar following TC adsorption revealed that TC was obligated on the exterior of ball-milled magnetic nanobiochar via $-OH$, $C=C$, $O-C=O$ and $HO-C=O$ functional groups (R. Li et al., 2020). TC was adsorbed onto ball-milled magnetic nanobiochar through π - π assembled relationship among aromatic carbon pattern of the ball-milled magnetic nanobiochar and the 4 aromatic rings in the structural composition of TC as revealed in Fig. 2.1(Zeng et al., 2019). Additionally, the molecular composition of TC accommodates various components that play the role of H^+ acceptors or pair H^+ acceptors and as well as donors which could form hydrogen bond with biochar (W. Yang et al., 2011). Hence, it is inferred that coupled electrostatic forces, hydrogen bonds, and $C\pi - C\pi$ bonding are primary determinants of TC adsorption (R. Li et al., 2020).

To check the mechanism of the adsorption of TC onto the Fe_3O_4 modified waste sludge biochar, XPS analysis was carried out before and after the adsorption. Carbon, oxygen, and nitrogen mostly exist in the biochar in the form of aldehydes, CO, and NH_3 . The change in the values of area, and specific gravity of the carbon, oxygen, and iron confirmed that the aldehydes, Fe-O-Fe, C-O-Fe, C=O/C-O, Fe^{2+} , Fe^{3+} , Fe_3O_4 , and FeOOH played a part in the adsorption of TC onto the Fe_3O_4 modified waste sludge biochar implying π - π interaction, hydrogen bonding, cation π -interaction and metal ion complexation (Sun et al., 2021). The kinetic study revealed that the adsorption of TC onto Fe_3O_4 /biochar follows pseudo second order (PSO) equation. This confirmed that the adsorption of TC was carried out through the chemical mechanism (S. Luo et al., 2022).

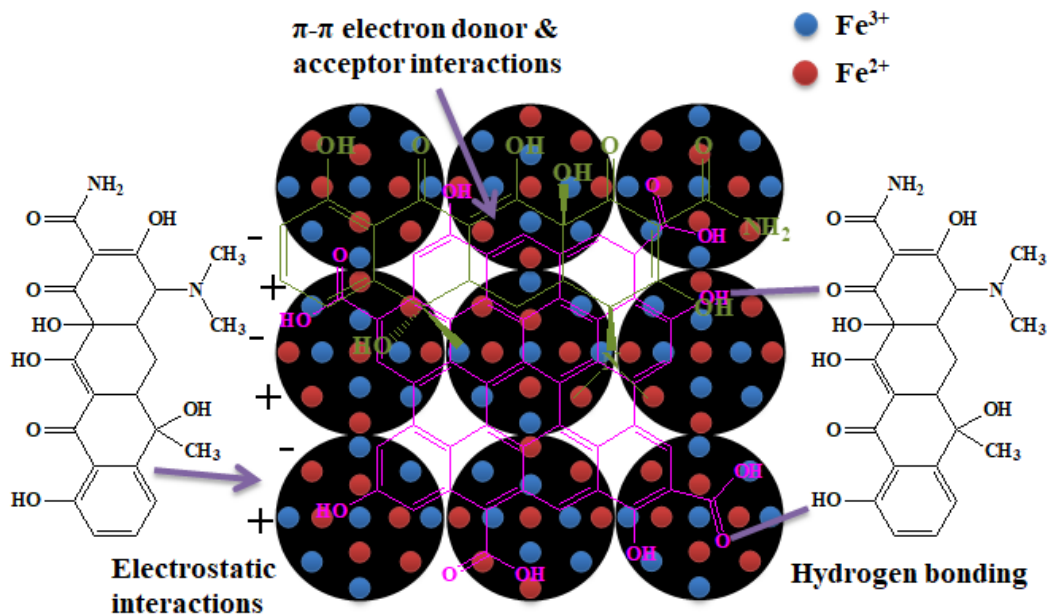


Figure 2.1: The probable regulating mechanisms of TC adsorption (Prakash Bobde, Sharma, Kumar, Pandey, et al., 2023)

Specific surface area, pore size, and pore volume of grapefruit biochar reduced following the adsorption of TC, suggesting that pore filling might be the mechanism for the adsorption of TC. In the pH range of 3.3 – 6.8, the presiding species in the TC solution H_2^0 , which resulted in the enhanced adsorption efficiency of the positively charged grapefruit biochar for TC. When the pH of the TC solution was enhanced from 7.7 to 8.5, the presiding category in the solution of TC was H^- , which resulted in the reduced adsorption efficiency of the negatively charged grapefruit biochar for TC. The pH of TC solution being more than 7 caused electrostatic repulsion resulting in the reduced adsorption efficiency of grapefruit biochar. At pH equal to 6.2, grapefruit biochar was positively charged, revealing that the electrostatic interaction might be another mechanism for the adsorption of TC onto grapefruit biochar. The peak of the hydroxyl group in the FTIR spectra became broad and moved to the higher wavelength range, influencing the hydrogen bonding during TC adsorption onto grapefruit biochar. The shifting of the carbonyl group towards lower wavelength range revealed π - π EDA interaction or π - π conjugate effects (Yu et al., 2020).

TC adsorption onto municipal solid waste-montmorillonite biochar (MSW-MMT) happened through both physisorption and chemisorption. Furthermore, the study demonstrated physisorption to be the major contributor to MSW-high MMT's TC adsorption efficiency. Biochar could physically act together with TC during physisorption via a pore-filling process and intercalation contact. Positively charged TC is prevalent at $\text{pH} < 4.0$, and it can approach the interlayer gap of clay minerals by swapping with hydrated cations such as Na^+ , Ca^{2+} in the interlayer space. The zwitterion variant of TC is the dominating constituent in the pH between 4 – 8, and it can also enter the interlayer gap among two t-to-t sheets of the clay material. The principal representation of MMT in the XRD signal was moved to $2\theta = 4.03^\circ$, which correlated well to $d_{(001)}$ of 2.19 nm. This could be due to TC complexation into the inter-layer gap of MMT clay mineral, which results in TC removal on the clay-biochar compound. The main component of TC at $\text{pH} > 8$ is anionic, therefore would electrostatically resist negatively charged clay sites, causing a reduction in adsorption efficiency at pH 8. Despite physisorption being the dominant mode of adsorption, chemisorption via chemical bonding and an increase in accessible interaction area caused by the accumulation of MMT on biochar substrates also aided adsorption (Premarathna et al., 2019).

TC adsorption on the adsorbent surface was previously governed by both its functional groups and physical structure. The effect of different pH levels on TC adsorption in KBC (potassium hydroxide-activated biochar) was investigated, and it was discovered that the electrostatic effect had only a little influence. This demonstrated that TC adsorption did not occur largely via an electrostatic process. Instead, TC adsorption by KBC was thought to utilize a mixture of three distinct routes. The first phase was pore adsorption, in which the carbonized, high-temperature KOH-activated KBC's well-developed micro- and meso-porous structures encouraged physical diffusion and pore-filling, allowing TC molecules to be removed in the past. Historically, hydrogen bonding was the second route for TC adsorption. The analysis of the FTIR spectra revealed that the 3427 cm^{-1} peak of KBC expanded after adsorption, whereas the position of the CH peak at

882 cm^{-1} changed. These changes showed the formation of hydrogen bonds between KBC and functional groups in TC molecules, resulting in TC elimination. The third contributing mechanism was the EDA stacking interaction. KBC's graphitized structure, which is rich in electrons, enabled it to connect with the aromatic and amino structures of TC molecules via EDA stacking interactions, as demonstrated by XRD tests (Z. Fan et al., 2022).

2.5.2. Adsorptive mechanism for Oxytetracycline (OTC)

Oxytetracycline (OTC) has a high pH reactivity and exhibits chemical discrimination beyond a broad pH range. OTC occurs in the anionic form at $\text{pH} > 7.5$, whereas the cationic form predominates at $\text{pH} < 3.5$. It exists in a polyanionic form within the pH range of 3.5-7.5. A physical adsorption pathway is demonstrated by the effective Elovich model for biochar. Negatively charged OTC molecules can create weak bonds, permitting for multilayer adsorption, which is the development of layers one by one. Physical adsorption is governed by pore-filling and film diffusion, in addition to the weak Van der Waals interactions, dipolar interactions and hydrogen bonding (Ramanayaka, Kumar, et al., 2020; Ramanayaka, Sarkar, et al., 2020). It is shown that OTC removal by colloidal biochar & nanobiochar occurs by physisorption. Additionally, the adsorption of OTC onto colloidal biochar happened through both chemisorption and physisorption processes (Ahmed et al., 2015). Nevertheless, in the case of colloidal biochar, both processes can occur simultaneously or independently, which is impossible to describe. The isotherm depicts a two-step mechanism, with the Langmuir model governing the first stage and Hills model governing the second. Because there are two different phases, one after the other, we may deduce that monolayers are generated by binding interactions and multilayers are produced by weak bonds among OTC molecules on the base of the monolayer. The dominating adsorption process, on the other hand, differed depending on a variety of component like medium pH, adsorbent material, adsorbate species, and so on (Ramanayaka, Kumar, et al., 2020).

Higher correlation coefficients (R^2) and mean average relative error (ARE) were obtained for the pseudo-first order (PFO) representation as contrasted to PSO model at lower concentration suggesting that contact time data fitted well with the PFO model. But at higher concentration, lower determination constant and higher relative error were obtained for the PFO model as contrasted to PSO model suggesting that contact time data fitted the latter. Consequently, when utilizing this material (composite), the kinetics become more complicated, implying that adsorption may not occur spontaneously and that some parameters had to be changed to get the highest adsorption potential (Azizian, 2004; W. Wang & Wang, 2018). Chemical adsorption being a sluggish reaction, is the limiting mechanism, requiring 6 hours to attain equilibrium (Ho & McKay, 2000; Ramanayaka, Kumar, et al., 2020).

Dendro wood nanobiochar was recovered from a dendro thermal power plant in Thirappane, Sri Lanka, as a residue of *Gliricidia sepium* gasification. Using a double-disc mill, dendro wood biochar was transformed into dendro wood nanobiochar. The adsorption of OTC was achieved using the synthetic dendro wood nanobiochar. The S-type isotherm curve, among the many various types of isotherms, showed a lot of difficulties, which could be owing to connections among the surface and already adsorbed molecules till the binding influence decreases with intensity. The Hill isotherm model is a three-parameter model that explains how multiple interaction types work together on homogeneous surfaces. OTC have $pH > 1$, indicating that OTC and dendro wood nanobiochar formed a positive cooperative bond. High initial isotherm slope and a high sorptive index in the isotherm curve represents strong affinity (k_f), with the Hills model showing a closer behaviour than the Freundlich model (Saadi et al., 2015). According to the Freundlich model, dendro wood nanobiochar is heterogeneous; the active sites and energies of which are dispersed epidemically. The formerly engaged binding areas are comparably powerful until the adsorption process is completed, at which point the energy declines epidemically. This model implies multilayer adsorption and hence can be used as a variant of the Langmuir model, which can be used to

represent multilayer adsorption as well. The adsorption capacity of the OTC onto dendro wood nanobiochar, or the variability of the dendro wood nanobiochar exterior, is represented by 'n' in the Freundlich isotherm. As a result, $n > 1$ shows that the OTC is adsorbing well on dendro wood nanobiochar. With $n > 1$, the Freundlich model was fairly suited to OTC in this investigation, demonstrating that OTC has a preferential binding to dendro wood nanobiochar. The heterogeneity rises as the value of n approaches 0, and the adsorption isotherm gets progressively nonlinear. Additionally, if $1/n < 0.1$, the sorption is permanent. The $1/n$ value for OTC in observational proof modelling showed that the adsorption process is changeable. As a result, desorption may be a viable option for recovering dendro wood nanobiochar (Ramanayaka, Tsang, et al., 2020). MnO_2 modified bamboo willow biochar showed higher adsorption capacity for oxytetracycline (OTC) at pH 5, revealing that the π - π EDA interactions among OTC and MnO_2 modified bamboo willow biochar may be one of the adsorption mechanisms.

Table 2.1: Experimental conditions and adsorption capacities of different bio-based adsorbent reported for the removal of CECs

Feedstock	Biochar type	Surface Area (m ² /g)	Pollutant Name	Adsorption Condition			Adsorption Capacity (mg/g)	References
				pH	Time (min.)	Concentration (mg/L)		
Food scrap & plant trimming	Biochar	-	TC	7	360	100	15.52	(Hoslett et al., 2021)
Wheat Straw	Ball-milled magnetic nanobiochar	-	TC	-	1440	40	268.30	(R. Li et al., 2020)
Waste activated sludge	Fe ₃ O ₄ modified waste sludge biochar		TC	7	1440	100	141.63	(Sun et al., 2021)
Activated sludge	Fe ₃ O ₄ modified activated sludge biochar	75.34	TC	5.5	1200	200	184.50	(S. Luo et al., 2022)
Grapefruit	Grapefruit biochar	130.83	TC	6.2	30	50	37.92	(Yu et al., 2020) (Jinpeng Wang & Zhang, 2020)
	Fe ₂ O ₃ modified grapefruit peel biochar	70.732	BPA	-	180	8-200	342.46	
Municipal solid waste	Montmorillonite municipal solid waste biochar	8.72	TC	7-8	360	0.25-250	77.96	(Premarathna et al., 2019)
caulis spatholobi residue	Potassium modified caulis spatholobi residue biochar	1336.31	TC	-	-	-	830.78	(Z. Fan et al., 2022)
Dendro wood	Macro biochar	260.83	OTC	9	300	50	129.34	(Ramanayaka, Kumar, et al., 2020)
	colloidal biochar	284.28					136.70	
	nanobiochar	28.56		4.8	720	10-500	113.20	
	Dendro wood nanobiochar	28					519.95	

								(Ramanayaka, Tsang, et al., 2020)
Bamboo Willow	MnO ₂ modified bamboo willow biochar	278.6	OTC	-	1440	10-300	383.39	(Feng et al., 2021a)
Cauliflower leaves	Magnetic montmorillonite cauliflower leave biochar composite	67.77	OTC	6.5	1440	10-150	58.85	(G. Liang et al., 2019)
Poplar leaf	KHCO ₃ modified poplar leaf biochar	1769.7	OTC	-	180	-	1850.5	(Z. Wei et al., 2023)
Lemon pulp	KOH activated lemon pulp biochar	1333.1	OTC	2-8	75	10-150	104.22	(Solmaz et al., 2023)
Bovine bone	MgAl-LDH modified bovine bone biochar	-	DS	-	1440	30	2114.43	(Lins et al., 2020)
Syagrus Coronata	MgAl-LDH modified syagrus coronata biochar	168.02	DS	-	-	-	116.52	(de Souza dos Santos et al., 2020)
Tea	Fe ₃ O ₄ @TAC@SA polymer	228	DS	3	90	-	2.669 mmol/g	(Al-Qahtani et al., 2023)
Palm Kernel Shell	Fe ₃ O ₄ modified palm kernel shell biochar	362.06	BPA	-	240	8-150	4.73	(Katibi et al., 2021)
Corn Stalks	NiFeZn-LDH modified corn stalks biochar	17.76	AZ	-	720	20-90	123.10	(Y. Wang et al., 2020)
Rice straw	g-MoS ₂ modified rice straw biochar	-	CPF	5.6	7200	-	37.90	(Z. Yang et al., 2020)
Pumpkin peel	H ₃ PO ₄ activated pumpkin peel biochar	689.9	CPF	8	1440	-	153.9	(Özer & İmamoğlu, 2022)
Pomegranate peel	Nanostructured activated biochar	142.86	CPF	-	-	-	89.94%	(Hamadeen & Elkhatib,

								2022)
Bamboo sawdust	FeCl ₃ and KOH modified biochar		CPF	-	-	-	78.43	(Wakejo et al., 2022)
Citrus peel	Fe ₃ O ₄ /Graphene oxide citrus peel biochar	1556	SPF CPF	-	4320	360 160	502.37 283.44	(Yue Zhou et al., 2019)
Artichoke leaves	Alkaline biochar	8.8274	MF	-	45	10-100	30.30	(Mahmoud et al., 2020)
Coconut shell	Coconut shell biochar	508.072	DZ	7	120	0.2-10	10.33	(Baharum et al., 2020)
Peat based biomass	Magnetically engineered sulphurized peat-based activated carbon	724	SMX	11	60	1-15	1.29	(V. Shukla et al., 2023)
Kenaf	Kenaf-derived biochar	268.9	TS		1440	5-200	77.40	(Cho et al., 2021)
Poplar wood chips	Fe ₂ O ₃ modified biochar	431.6	NOR	6	1440	20	38.77	(H. Liang et al., 2022)
Peanut shell	K ₂ FeO ₄ modified peanut shell biochar	374	DS IBF	-	1200	20-60 10-25	128.30 66.30	(Nguyen et al., 2021)
Pomelo peels	ZIF-8 modified pomelo peels biochar	508.82	KM	-	1440	0-6	32.50	(Liu et al., 2021)
Rice Husk	MnO ₂ modified biochar	64.32	TC DC	6	1440	5-100	24.69 27.29	(Jiang Li et al., 2020)
Walnut shell	Fe ₂ O ₃ modified walnut shell biochar	786	SA NP KP	-	120	100-500	683 533 444	(Anfar et al., 2020)

OTC acted as electron acceptor attributed to the electron-withdrawing potential of ketone group (Feng et al., 2021a). Table 2.1 highlights a review on the experimental conditions reported for the removal of CECs by bio-based adsorbent.

2.5.3. Adsorption mechanism for Diclofenac Sodium (DS)

The R^2 values of PSO kinetic model were found to be higher than the PFO kinetic model values affirming that the former kinetic model best fitted for the adsorption of DS onto MgAl-LDH modified bovine bone biochar and follow the physical adsorption mechanism. According to the thermodynamic study, the adsorption process of DS onto MgAl-LDH modified bovine bone biochar was found to be spontaneous, exothermic, and increased entropy (Lins et al., 2020).

The adsorption of DS onto MgAl-LDH modified syagrus coronata biochar happened spontaneously indicated by the negative values of Gibb's free energy ΔG° at all temperatures. Negative values of ΔH° suggested the exothermic adsorption process where the magnitude of ΔH° indicated chemisorption process (Piccin et al., 2017). The gain in overall entropy, as shown by the positive value of ΔS° , implied that a modification in the adsorbent composition had occurred. Additionally, adsorbate immobilization at active areas on the adsorbent surface is thought to have occurred at random. Several studies verified these findings (de Souza dos Santos et al., 2020; Dotto et al., 2013; Lonappan et al., 2018; Santos et al., 2020; Suriyanon et al., 2013).

2.5.4. Adsorption mechanism for Bisphenol A (BPA)

Katibi et al. and Wang et al. observed the average pore size of the biochar below 50 nm which established the mesoporous structure of the biochar. Pore filling might be one of the adsorption mechanisms as BPA can pierce pores of the biochar. In acidic pH of the BPA solution, the $-OH$ group in the structure of the BPA are protonated which results in the electrostatic repulsion with the positively charged surface of biochar, Fe_3O_4 modified palm kernel shell biochar and Fe_2O_3

modified grapefruit peel biochar. The presence of carbonyl and carboxyl group on the biochar surface responsible for the π - π EDA interaction with the $-\text{OH}$ group of the BPA. Hydrogen bonding may be one of the adsorption mechanisms for the adsorption of BPA onto biochar, Fe_3O_4 modified palm kernel shell biochar and Fe_2O_3 modified grapefruit peel biochar due to the presence of $-\text{OH}$ group of the BPA and $-\text{OH}$ & $-\text{COO}$ group of the BC surface. In basic pH of the BPA solution, BPA^{2-} and HBPA^- results in the electrostatic repulsion with the negatively charged surface of the Fe_3O_4 modified palm kernel shell biochar and Fe_2O_3 modified grapefruit peel biochar. The hydrophobic location of the BC could be mixed with BPA attributed to its strong hydrophobicity. Thus, hydrophobic interaction may be one of the adsorption mechanisms (Katibi et al., 2021) (Jinpeng Wang & Zhang, 2020).

2.5.5. Adsorption mechanism for Atrazine (AZ)

Findings of XPS examination of AZ adsorption on corn stalks biochar, NiFeZn-LDH modified corn stalks biochar (NiFeZn-LDH/BC), and NiFeZn-LDH modified corn stalks biochar after heating at 600°C (NiFeZn-LDH/BC-P) are reported (Y. Wang et al., 2020). The XPS examination reveals that the maxima shifted slightly post adsorption. After adsorption, the CO_3^{2-} peaks of the NiFeZn-LDH/BC and NiFeZn-LDH/BC-P are significantly distinct, showing that carbonates play fundamental role in the adsorption process. Furthermore, π - π electron correlations among the biochar surface and AZ are possible. Changes in adsorbent shown might be due to the interchanging mode of carbon and oxygen-bearing functional groups. One of the most noticeable shifts in C1s in the entire array of all adsorbents is the difference in carbon-bearing functional groups. Upon NiFeZn-LDH/BC adsorption, the oxygen-containing functional groups in AZ are altered. The XPS spectrum revealed three LDH metal components (Ni, Fe, and Zn), showing that the material is stable in the real experimental investigation (Alekseeva et al., 2011). The XPS spectra of the sample before and after adsorption showed that C1s and O1s peaks are attenuated as a result of the sorption process. The C-O bond somewhat weakens upon AZ adsorption, which

could be produced by AZ adsorption triggered by metal ions. The reduction in C–O in NiFeZn-LDH/BC-P seems to be more compatible with the conclusions of the experimental investigation, implying that NiFeZn-LDH/BC-P has improved adsorption ability. Furthermore, AZ degrades and lowers the C–O structure, resulting in a higher M–O–M (Jin et al., 2016). As a result, the CO_3^{2-} comprising additional C–O bonds and π - π bond relationship with AZ are the contributing factors to AZ elimination in the adsorption mechanism (Y. Wang et al., 2020).

2.5.6. Adsorption mechanism for Ciprofloxacin and Sparfloxacin

The result from the impact of pH of CPF solution indicated that the electrostatic interactions might be one of the mechanisms for the adsorption of CPF onto the g-MoS₂ modified rice straw biochar. The stretching peak at 1396 cm⁻¹ obtained in FTIR spectra due to the aromatic ring in g-MoS₂ modified rice straw biochar was

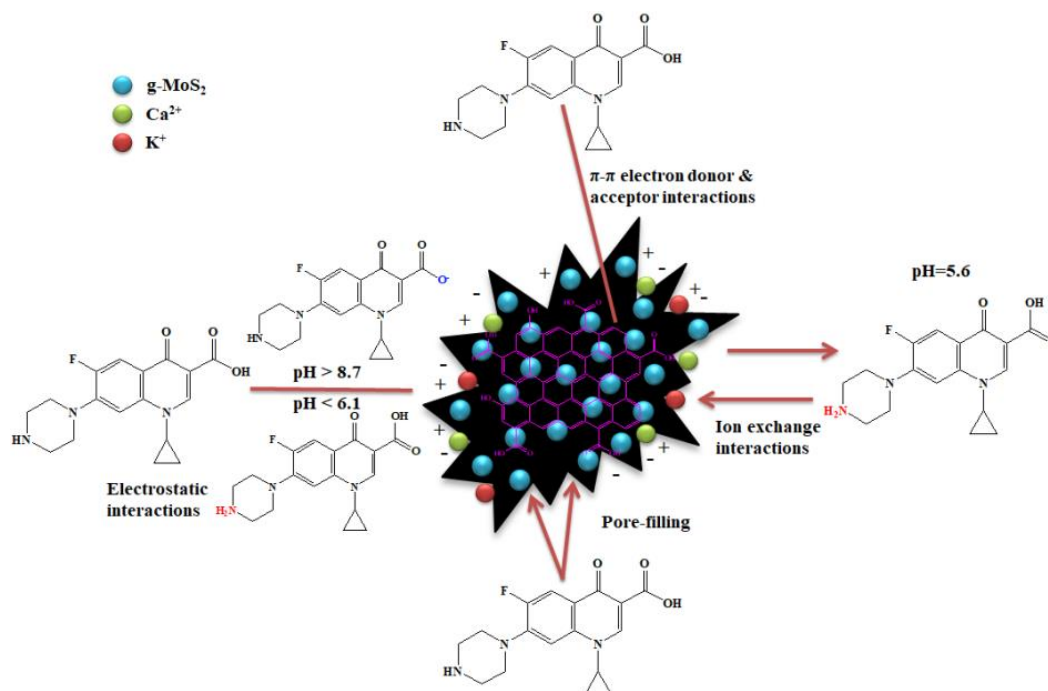


Figure 2.2: The proposed adsorption mechanisms for CPF on g-MoS₂-BC composites (Prakash Bobde, Sharma, Kumar, Pandey, et al., 2023)

moved to the 1402 cm⁻¹ following adsorption of CPF, encouraging the π - π EDA interaction among the g-MoS₂ modified rice straw biochar and CPF. The hydroxyl group on the surface of g-MoS₂ modified rice straw biochar could act as a π -

electron donor and CPF could act as a π electron acceptor due to the presence of most electronegative element F in the aromatic structure, signifying that the π - π EDA interaction may be the adsorption mechanism. The decreased pore size of the g-MoS₂ modified rice straw biochar after the adsorption indicated that the pore filling is the chief way for the adsorption of CPF. The atomic percentage of sodium and potassium elements decreased after the adsorption indicating that the ion exchange may be one of the processes for the adsorption of CPF onto g-MoS₂ modified rice straw biochar (Fig. 2.2) (Z. Yang et al., 2020).

The surface area analysis outcome revealed the porosity of Fe₃O₄/Graphene oxide citrus peel biochar which promoted the physical adsorption of SPF and CPF onto the Fe₃O₄/Graphene oxide citrus peel biochar. The structure of the graphite on the Fe₃O₄/Graphene oxide citrus peel biochar was authenticated through Raman & XPS spectra. The graphite surface of the Fe₃O₄/Graphene oxide citrus peel biochar could act as a π -electron donor and SPF and CPF could act as a π electron acceptor due to the presence of most electronegative element in the aromatic structure. CPF is less electron deficient than SPF, as SPF structure contains two fluorine atoms. It resulted that SPF was easy to be adsorbed onto Fe₃O₄/Graphene oxide citrus peel biochar by π - π EDA interaction. The hydrogen bonding could be a possible mechanism among the Fe₃O₄/Graphene oxide citrus peel biochar and SPF/CPF facilitated by the existence of oxygen containing functional groups in the SPF/CPF structure.

The greater hydrophobicity could conclude in a highly beneficial emendation among SPF/CPF and Fe₃O₄/Graphene oxide citrus peel biochar resulting in additional adsorption (Fig. 2.3) (Yue Zhou et al., 2019).

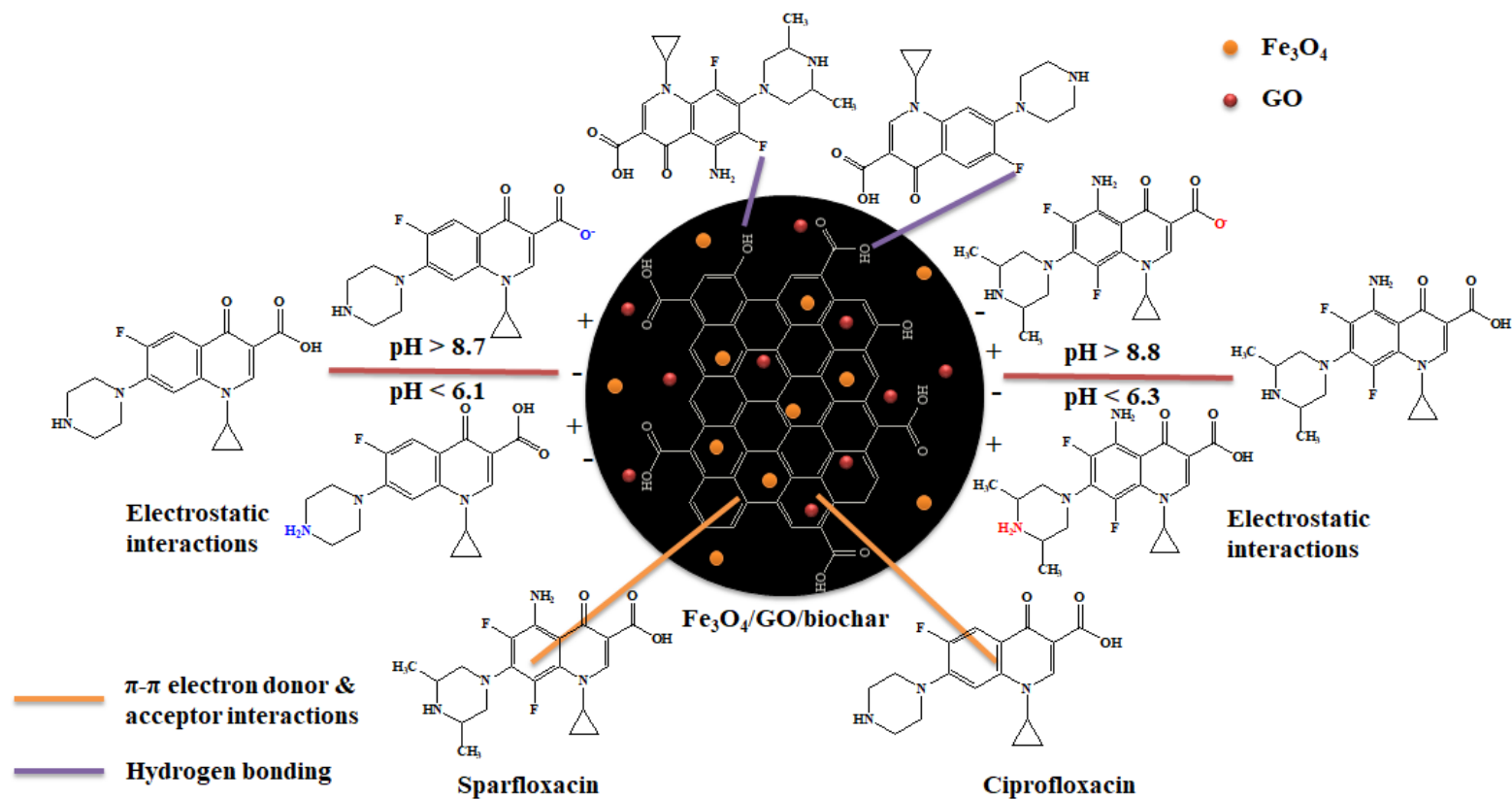


Figure 2.3: Schematic for the adsorption of CPF & SPF onto Fe₃O₄/Graphene oxide citrus peel biochar (Prakash Bobde, Sharma, Kumar, Pandey, et al., 2023)

2.5.7. Adsorption mechanism for Metformin (MF) and Diazinon (DZ)

Mahmoud et al. (Mahmoud et al., 2020) synthesized alkaline biochar using artichoke leaves as feedstock. Scanning Electron Micrographs (SEM) of alkaline biochar depicts a homogeneous binding, with the prominent involvement of NaOH in pore structure and pore diameter of alkaline biochar. The calculated R^2 values of PFO, intraparticle diffusion (ID) model, and Elovich model were found to be smaller than the PSO model which was thought to be the prime depiction of the adsorption mechanism of Metformin (MF) onto alkaline biochar. The $-OH$ group interacts with the amine group of the MF on the exterior of alkaline biochar through hydrogen bonding to promote the adsorption activity as shown in Fig. 2.4.

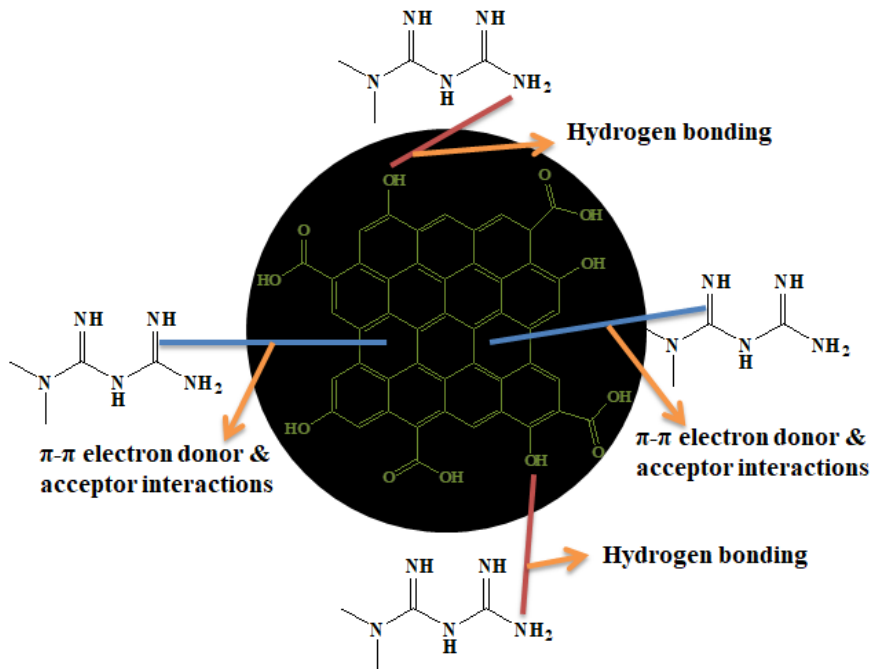


Figure 2.4: Possible adsorption mechanism of metformin onto alkaline biochar (Prakash Bobde, Sharma, Kumar, Pandey, et al., 2023)

The adsorption of MF onto the alkaline biochar may have occurred due to π - π interaction. The thermodynamic study, the adsorption process of MF onto alkaline biochar was found to be spontaneous, exothermic with increased entropy and follow the physical adsorption mechanism (Mahmoud et al., 2020). The adsorption of diazinon (DZ) onto the coconut shell biochar is thought to be due to

the electrostatic attraction as the biochar and DZ acquired different charges. The anionic DZ form adsorbed on the cationic surface of the coconut shell biochar. This mechanism could be active primarily for the removal of DZ (Baharum et al., 2020).

2.5.8. Adsorption mechanism for Triclosan (TS) and Norfloxacin (NOR)

Cho et al. explained the adsorption mechanism of triclosan (TS) onto Kenaf derived biochar using kinetic and isotherm equation. According to the values of correlation coefficient and sum of squared error, PSO best fitted the adsorption process of TS onto biochar than that of PFO equation. This confirmed that the TS is chemisorbed onto biochar. The obtained value of model parameter of the Dubinin-Radushkevich isotherm model also suggested that the chemical adsorption was the presiding mechanism (Cho et al., 2021).

To boost the adsorption capacity of the biochar, most of the researchers modify biochar by doping different composites onto the surface of biochar. This section evaluates the adsorption mechanisms of various CECs on several biochar composites. To clarify the adsorption mechanism of norfloxacin (NOR) onto Fe₂O₃ modified biochar, FTIR analysis before and after adsorption of Fe₂O₃ modified biochar was investigated. Some functional group stretching vibrations were moved slowly before & after the adsorption, which revealed the participation in the adsorption process. The intensity of the hydroxyl group was weakened after the adsorption revealing that the adsorption of NOR onto Fe₂O₃ modified biochar might have been due to hydrogen bonding. Slight shifting of C=C band and the falling of intensity of the O-C=O bond revealed that π - π interaction plays a crucial role in the adsorption process. The presence of high-electronegative element F in the structure of norfloxacin decreased the electron density on the benzene ring which further act as a π -electron acceptor while the existence of the aromatic groups on the surface of the Fe₂O₃ modified biochar which could be utilized as a π -electron donor to participate in the π - π EDA interaction with NOR, which could be another adsorption mechanism. The

microstructure analysis of Fe₂O₃ modified biochar following the adsorption of NOR, suggested that pore filling may be the process for the adsorption of NOR. The adsorption capacity was determined to be maximum at the pH nearly equal to neutral which was due to the hydrophobicity among the NOR & Fe₂O₃ modified biochar (H. Liang et al., 2022).

2.5.9. Adsorption mechanism for Ibuprofen (IBF) and Ketamine (KM)

K₂FeO₄ modified peanut shell biochar comprised of carboxylic (-C=O) functional group which could act as a π -electron acceptor for the interaction with the -OH group of the Diclofenac Sodium (DS) and ibuprofen (IBF) causing π - π EDA interaction. FTIR spectrum of K₂FeO₄ modified peanut shell biochar before and after the adsorption of DS and IBF exhibited shifting of C=C vibrational band. This confirmed π - π EDA interaction between pollutant and adsorbent. FTIR spectra also revealed the peak shift of vibration of -OH and -CO stretching; vanished peak of Fe-O and some new peaks appeared after adsorption. This shifting of peaks after adsorption confirmed the hydrogen bond formation among the oxygen containing functional group of DS/IBF and K₂FeO₄ modified peanut shell biochar (Nguyen et al., 2021).

In another finding, the adsorption of ketamine (KM) on ZIF-8 modified pameo peels biochar is investigated (Liu et al., 2021). The binding energy of Zn²⁺ was moved after the adsorption as shown in XPS characterization suggesting that zinc reacted with KM. A new peak of Cl 2p confirmed the adsorption of KM onto the ZIF-8 modified pameo peels biochar. The peaks for C-C/C=C, C-O/C-N, O-C=O, and π - π^* were moved from their original position suggesting the adsorption of KM onto the ZIF-8 modified pameo peels biochar through π - π -EDA interaction. The binding energy of O was found to be increased, indicating that hydrogen bonding contact has occurred. In summary, it was suggested that the ZIF-8 modified pameo peels biochar adsorbed KM through π - π EDA interaction, hydrogen bonding & chelation, and pore filling (Liu et al., 2021).

2.5.10. Adsorption mechanism for Doxycycline (DC), Salicylic acid (SA), Naproxen (NP) and Ketoprofen (KP)

Freundlich model revealed a strong correlation for the adsorption of TC and doxycycline (DC) onto the MnO₂ modified biochar, stipulating that the Freundlich model is well fitted to the adsorption of TC and DC. The findings of constructing a PSO kinetic model demonstrate that the proposed method governing TC and DC adsorption could be chemisorption. According to the thermodynamic study, the adsorption process of TC & DC onto MnO₂ modified biochar was found to be spontaneous, endothermic, and increased entropy of adsorbate and adsorbent interface (Jiang Li et al., 2020).

However, to explain the exact mechanism for the adsorption of CECs onto the surface of biochar is very difficult, researchers had suggested that the adsorption of CECs onto biochar may be due to the pore diffusion, electrostatic interaction, hydrophobic interaction, π - π EDA interaction, ion exchange and hydrogen bonding.

2.6. Research Gaps:

- Despite numerous exhaustive scientific studies on environmental pollutants like hydrocarbons and heavy metals in wastewater, there has been a noticeable lack of in-depth systematic investigations into the presence of Contaminants of Emerging Concern (CECs) and the documentation of appropriate remediation technology. As a result, achieving sustainable treatment of water contaminated with CECs remains an ongoing challenge.
- While Biochar and biochar-based nanocomposites have been utilized by researchers for removing Contaminants of Emerging Concern (CECs), their adsorption capacity has often been found to be insufficient. To enhance biochar modification methods, the primary focus should be on tailoring different modified biochar formulations to suit specific application requirements. Firstly, there's a need to develop modified biochar with enhanced adsorption capacity to effectively capture pollutants while maintaining its adsorptive efficacy. Secondly, the development of modified

biochar with selective adsorption capabilities is essential to target specific pollutants.

- Further in-depth research is required to understand how pollutants are adsorbed onto modified biochar. While numerous studies have explored this phenomenon, the complexity of several interacting mechanisms remains a challenge. The predominant mechanism and its relative contribution are still unclear, underscoring the importance of clarifying these issues. Such clarification is vital for enhancing the adsorption capacity and expanding the environmental applications of modified biochar. Addressing the effective desorption of pollutants from biochar for subsequent safe treatment and optimizing the recycling of the adsorbed biochar are important considerations that need to be taken into account.

2.7. Objectives:

- Synthesis & Characterization of biochar-based nanocomposites.
- Isotherm, Kinetic, Thermodynamic & Regeneration study of biochar-based nanocomposites for removal of Diclofenac, Ketoprofen, Oxytetracycline & Ciprofloxacin, etc.
- Optimization of reaction conditions to develop a sustainable method for removal of CECs.

Chapter 3
MATERIALS & METHODS

Chapter 3

MATERIALS & METHODS

3.1. Materials:

The pine-cone biomass was collected from the forest area of Dehradun, Uttarakhand, India. Chemicals used were of laboratory grade. KMnO_4 , $\text{Mg}(\text{NO}_3)_2 \cdot 6\text{H}_2\text{O}$, $\text{Al}(\text{NO}_3)_3 \cdot 9\text{H}_2\text{O}$, FeCl_3 , $\text{FeSO}_4 \cdot 7\text{H}_2\text{O}$, HNO_3 , urea, NH_4OH and HCl were purchased from Merck, India. H_2O_2 was purchased from Loba Chemie Limited. NaOH was procured from Sisco Research Laboratories and NaCl (99%) was purchased from Fine Chem India. The analytical grade Oxytetracycline (OTC), Ciprofloxacin (CPF), Triclosan (TS) and Tetracycline (TC) were purchased from Tokyo Chemical Industry.

3.2. Methods:

3.2.1. Synthesis:

3.2.1.1. Synthesis of pine-cone biochar (PCBC)

After cleaning to eliminate any dirt attached to the pine-cone biomass, the collected pine-cone biomass was dried at 120°C overnight in the oven. It was then processed to a particle size of under $150\ \mu\text{m}$. The pine-cone biomass was carbonized in tubular furnace at 700°C for 2 hours at a heating ramp rate of $7^\circ\text{C}/\text{min}$ in the presence of nitrogen. The carbonized product that we get is denoted as pine-cone biochar (PCBC).

3.2.1.2. Synthesis of MnO_2/PCBC

In the synthesis of 25:75 MnO_2/PCBC , a process was followed as follows: Initially, 0.79 g of KMnO_4 and 2.25 g of as-prepared PCBC were dissolved in 150 mL of distilled water, and the mixture was stirred for 60 minutes at room temperature. During this time, KMnO_4 and PCBC were thoroughly mixed. Hydrogen peroxide (H_2O_2) was then added drop-wise to the solution until the pink color of KMnO_4 disappeared. The solution was stirred for an additional 60 minutes. To reach a pH of 7, 0.1 M HNO_3 was used for pH adjustment before subjecting the solution to centrifugation and washing with distilled water. The

solid obtained after filtration was subsequently dried for 12 hours in an oven at 105°C. The dry residue was crushed using a mortar and pestle to obtain the final product, 25:75 MnO₂/PCBC.

For the synthesis of 5:95 MnO₂/PCBC and 15:85 MnO₂/PCBC, the same method was applied with varying quantities of reagents. Specifically, 0.16 g KMnO₄ and 2.85 g PCBC were used for 5:95 MnO₂/PCBC, while 0.47 g KMnO₄ and 2.55 g PCBC were used for 15:85 MnO₂/PCBC. These adjustments in reagent quantities allowed for the successful synthesis of the desired manganese dioxide (MnO₂) to PCBC ratios, following the same procedural steps as in the synthesis of 25:75 MnO₂/PCBC.

3.2.1.3.Synthesis of LDH/PCBC

The synthesis of 25:75 LDH/PCBC involved a hydrothermal method conducted under autogenous pressure. Initially, a mixed solution was prepared, labeled as solution A, by dissolving 0.84 g of Mg(NO₃)₂.6H₂O, 0.25 g of Al(NO₃)₃.9H₂O, 0.48 g of urea, and 0.75 g of PCBC in 150 mL of distilled water. To this, a solution labeled as solution B was created, consisting of 2N sodium hydroxide. Gradually, solution B was added dropwise to solution A while maintaining continuous agitation until the pH of the mixture reached 10. The resulting solution was subjected to hydrothermal treatment in a Teflon-lined stainless-steel autoclave, maintaining a temperature of 120°C. After 12 hours of heating, the precipitate was collected through centrifugation, and the collected precipitate was subsequently washed multiple times with distilled water and ethanol. Finally, the 25:75 LDH/PCBC product obtained was dried at 105°C for 24 hours.

For the synthesis of 5:95 LDH/PCBC and 15:85 LDH/PCBC, a parallel procedure was implemented while adjusting the quantities of reagents used. Specifically, 0.17 g and 0.50 g of Mg(NO₃)₂.6H₂O, 0.05 g and 0.15 g of Al(NO₃)₃.9H₂O, 0.10 g and 0.29 g of urea, and 0.95 g and 0.85 g of PCBC were used for the respective compositions. These adaptations in reagent quantities facilitated the successful synthesis of LDH/PCBC composites with the desired 5:95 and 15:85 ratios while

adhering to the same hydrothermal methodology as employed for the 25:75 LDH/PCBC.

3.2.1.4. Synthesis of Fe₃O₄/PCBC

In the synthesis of 25:75 Fe₃O₄/PCBC, a co-precipitation method was employed. Initially, a mixed solution, labeled as solution A, was prepared by dissolving 2.43 g of FeCl₃, 0.45 g of urea, and 2.25 g of PCBC in 150 mL of distilled water. A separate solution, labeled as solution B, was created by dissolving 1.04 g of FeSO₄·7H₂O. Solution B was then added dropwise to solution A, and the resulting mixture was stirred for an additional 15 minutes. The pH of the mixture was carefully adjusted to the range of 10.5-11 by slowly adding NH₄OH while agitating. After 30 more minutes of stirring, the mixture was left undisturbed overnight. The following day, the precipitate was collected through centrifugation and thoroughly washed with both distilled water and ethanol. The final step involved drying the product, 25:75 Fe₃O₄/PCBC, at 105°C for 24 hours.

To synthesize 5:95 Fe₃O₄/PCBC and 15:85 Fe₃O₄/PCBC, the same co-precipitation method was utilized with varying quantities of reagents. Specifically, 5:95 Fe₃O₄/PCBC was produced using 0.81 g FeCl₃, 0.15 g urea, 2.85 g PCBC, and 0.21 g FeSO₄·7H₂O. For the 15:85 Fe₃O₄/PCBC variant, the quantities of reagents were adjusted to 1.62 g FeCl₃, 0.30 g urea, 2.55 g PCBC, and 0.63 g FeSO₄·7H₂O. These variations in reagent quantities allowed for the successful synthesis of 5:95 and 15:85 Fe₃O₄/PCBC, following the same procedural steps as in the synthesis of 25:75 Fe₃O₄/PCBC.

3.2.2. Selection of adsorbent:

This experiment's goal was to examine the adsorption of pollutants using a 200 mg/L CEC solution and several adsorbents. 20 mL of the CEC solution were used in a 100 mL conical flask for the experiment. The chosen adsorbent was added to the flask at a dosage of 0.5 g/L. A neutral pH of 7 was achieved for the solution, and 298K (25°C) was kept as the constant temperature. The adsorbent was given an extended time to interact with the pollutants by placing the flask shaking incubator for 1440 minutes.

The shaking incubator was turned off after 1440 minutes of shaking, and the mixture was thoroughly filtered to remove the pollutant and adsorbent. The amount of pollutant removal was then ascertained by measuring the concentration of the pollutant in the filtered solution. By calculating the percentage of pollutant removal using equation 3.1, it was possible to determine the adsorption effectiveness of the selected adsorbent under the given circumstances. This experiment provided useful data for further investigation and attempted to evaluate how well the adsorbent removed the contaminant from the solution.

$$\% \text{ Removal} = \frac{(c_o - c_e)}{c_o} \times 100 \quad (3.1)$$

With, c_o (mg/L) being the initial pollutant concentration, c_e (mg/L), the equilibrium concentration of pollutant,

3.2.3. Adsorbent characterization:

XRD (Bruker D8-Advance Eco) patterns were taken to identify the crystalline phases present in synthesized adsorbent. An FTIR spectrophotometer (Perkin Elmer Frontier FT-IR/FIR) was used to investigate functional groups present in the composite. The spectral range considered was 4000-400 cm^{-1} . Surface area, pore size and pore volume of the adsorbents were investigated by BET Nitrogen adsorption technique (Quantachrome, Autosorb). Physicochemical properties were also investigated using CHNS analyzer (Thermo Scientific) and Inductively Coupled Plasma-Optical Emission Spectroscopy (ICP-OES) (AnalytikJena). The Scanning Electron Microscope (SEM) was used to examine the surface morphology of adsorbents. The pH point of zero charge (pH_{PZC}) of adsorbent was investigated as mentioned in the latest study (Jang et al., 2018). 0.01 M 50 mL NaCl solution was taken in different conical flasks. With the use of 0.1 M HCl or 0.1 M NaOH, the pH of the NaCl solution was fixed in the range 3 - 11. 10 mg of adsorbent was added to all the conical flasks and flasks were kept in the orbital shaking incubator (REMI TFT 24 Plus) at 20°C at 150 rpm. The final pH of NaCl solution was determined after 24 hours of shaking. The pH_{PZC} from all NaCl solutions containing adsorbent was calculated using the formula ΔpH (final pH – initial pH) = 0.

3.2.4. Effect of time on the adsorption of CECs

Adsorption of CECs on adsorbent was observed at different time intervals. A fixed amount of adsorbent (10 mg) was added into different conical flasks, and the CECs solution (20 mL, 200 mg/L) was added into each conical flask. The pH of the CECs solution was fixed to 7 by using 0.1 M NaOH or 0.1 M HCl before adding to the conical flasks. All the flasks were kept in the orbital shaking incubator at 25⁰C for 24 h for shaking at 200 rpm. Conical flasks were taken out from the incubator at the time intervals of 5, 15, 30, 60, 120, 240, 480, 960, and 1440 min. The concentration of the CECs remaining in the aqueous solution was assessed using HPLC (LC 2030C 3D Plus). The amount of CECs adsorbed by the adsorbent was computed by using equation 3.1 and 3.2:

$$q_t = \frac{(c_o - c_e)V}{m} \quad (3.2)$$

With, c_o (mg/L) being the initial OTC concentration, c_e (mg/L), the equilibrium concentration of OTC, V (L), the volume of the OTC solution, m (g), the weight of the MnO₂/PCBC, and q_t (mg/g) is the adsorption capacity. The data obtained from the kinetic plots are fitted to different kinetic models to ascertain the model that fits best and describes the adsorption characteristics of CECs adsorption onto the adsorbent.

3.2.5. Effect of initial CECs concentration on the adsorption

Adsorption experiments were performed using constant optimized dose of adsorbent. In separate conical flasks varying concentrations (50, 75, 100, 125, 150, 175, 200 mg/L) of 20 mL CECs were added. The pH of all the CECs solutions was fixed to optimized pH by using 1M NaOH or HCl prior to addition of adsorbent into each conical flask. All the conical flasks were kept in the orbital shaking incubator for shaking at optimized temperature for 24 h at 200 rpm speed. After shaking, the final concentration of the CECs was determined using HPLC. To determine the adsorption capacity of the adsorbent and the isotherm fitting, the adsorption isotherm was obtained for Langmuir, Freundlich, Temkin and Dubinin-Radushkevich models.

3.2.6. Response Surface Methodology (RSM) study:

Ideal requirements for effective adsorption of CECs onto adsorbent were calculated using Central Composite Design (CCD) beneath RSM, a helpful synchronized simulation methodology (S. Dehghan et al., 2018; Dolatabadi, Naidu, et al., 2022; Jokandan et al., 2019; Witek-Krowiak et al., 2014). This method includes three principal steps: experimental design, simulation and optimization. The said model provides comparatively limited factor variations for the determination of complex response functions (S. Dehghan et al., 2017; Toles et al., 1997). Four factors (A, B, C, and D) and five-levels CCD ($-\alpha$, -1 , 0 , $+1$, $+\alpha$) were used in the augmentation part, with pH, adsorbent dose, initial CEC concentration, and temperature being used with least number of investigations. The independent variables and five levels were coded for each variable.

Based on preliminary tests, the least and extreme values (Table 3.1) provided for all variables were selected. All investigations were executed doubly and the mean values of percentage removal were considered roughly suitable, and the interpretation of the results applies the second order polynomial representation with suitable approximate regression coefficients. The simplified second order polynomial framework for the response surface study is described as follows:

$$Y = \beta_0 + \sum_{i=1}^k \beta_i x_i + \sum_{i=1}^k \beta_{ii} x_i^2 + \sum_{i=1}^{k-1} \sum_{j=2}^k \beta_{ij} x_i x_j + \varepsilon \quad (3.3)$$

Where, Y is the intended outcome; x_i and x_j are the source factors impacting the outcome Y ; and β_0 , β_i , β_{ii} and β_{ij} are the regression coefficients for a potential target, sequential influence, square influence and significant impact, respectively. ε represents the stochastic error and k is the numeral of variables. In the current investigation, $k=4$.

Design-Expert scheme like ANOVA (Analysis of Variance) focused mostly on F and P -values and give quite insightful information on the key influence and associations among parameters, as well as its connection to the outcome (Noudeh et al., 2023). The quadratic representation's fit goodness was demonstrated by the coefficient of resolution R^2 , and its statistical significance was verified in the same method by the Fisher's F -test. In the current analysis, a sum of 27

experiments were developed to investigate the coefficients and the oblique mathematical representation produced was verified by following the investigations with the best response factors as anticipated by optimizing the reply. By resolving the regression equation and inspecting the response surface graphs, optimum values were obtained for selected variables. The response surface graphs are utilized to evaluate various relationships between unconventional factors during belongings and the desirability as persistent for the four variables. These three-directional plots offer correct geometrical descriptions on the system's behavior.

Table 3.1: Experimental ranges and levels in CCD of the independent variables

Independent variables	Ranges and levels				
	$-\alpha$	-1	0	+1	$+\alpha$
pH (A)	2	3	7	11	12
Adsorbent Dose (B)(g/L)	0.05	0.1	0.3	0.5	0.55
Initial concentration of CEC (C)(mg/L)	31.25	50	125	200	218.75
Temperature (D)(°K)	279.25	283	298	313	316.75

3.2.7. Adsorption Kinetics

Four kinetic models are generally expressed as below:

Lagergren's PFO kinetic model (V. Shukla et al., 2023):

$$\ln(q_e - q_t) = \ln q_e - K_1 t \quad (3.4)$$

Ho's PSO kinetic model (V. Shukla et al., 2023):

$$\frac{t}{q_t} = \frac{1}{K_2 q_e^2} + \frac{t}{q_e} \quad (3.5)$$

Elovich kinetic model (Gerente et al., 2007):

$$q_t = \frac{1}{\beta} \ln(\alpha\beta) + \frac{1}{\beta} \ln t \quad (3.6)$$

Weber & Morris ID kinetic model (V. Shukla et al., 2023):

$$q_t = K_i t^{1/2} + c \quad (3.7)$$

Where, q_e (mg/g) and q_t (mg/g) are the amounts of adsorbed adsorbate at equilibrium and at time t , respectively. K_1 (min^{-1}) is the rate constant of Lagergren PFO adsorption. K_2 (g/mg min) is the equilibrium rate constant of Ho's PSO adsorption. α (mg/g min.) denotes the initial sorption rate and β is related to the

extent of the surface coverage and the activation energy for chemisorption. K_i (mg/g min.^{1/2}) is the Weber and Morris rate constant.

3.2.8. The adsorption isotherm

Four isotherm equations are generally expressed as below:

Langmuir isotherm equation (Gerente et al., 2007; Özacar & Şengil, 2004):

$$\frac{C_e}{q_e} = \frac{1}{K_L} + \frac{a_L}{K_L} C_e \quad (3.8)$$

Freundlich isotherm equation (Özacar & Şengil, 2003):

$$\ln q_e = \ln K_f + \frac{1}{n} \ln C_e \quad (3.9)$$

Temkin isotherm equation (Özacar, 2003):

$$q_e = \frac{RT}{b} \ln A + \frac{RT}{b} \ln C_e \quad (3.10)$$

Where, $\frac{RT}{b} = B$

Dubinin-Radushkevich isotherm equation (Shahwan & Erten, 2004):

$$\ln q_e = \ln q_m - \beta \varepsilon^2 \quad (3.11)$$

Where q_e (mg/g) is the adsorption capacity and C_e (mg/L) unadsorbed pollutant concentraion. In the Langmuir model, the constant K_L (L/g) represents the Langmuir equilibrium constant, while K_L/a_L yields the theoretical monolayer saturation capacity, denoted as Q_o . The Freundlich model employs the constant K_f (L/g) and the exponent n (g/L), where K_f denotes the Freundlich constant and n signifies the Freundlich exponent. As for the Dubinin-Radushkevich model, q_m signifies the Dubinin-Radushkevich monolayer capacity (mmol/g), β is associated with sorption energy, and ε represents the Polanyi potential.

3.2.9. Thermodynamic parameter

Vont Hoff equation is as below(V. Shukla et al., 2023).

$$\Delta G^0 = -RT \ln K_{eq} \quad (3.12)$$

$$K_{eq} = \frac{q_e}{C_e} \quad (3.13)$$

$$\ln K_{eq} = \frac{\Delta S^0}{R} - \frac{\Delta H^0}{RT} \quad (3.14)$$

Where K_{eq} is the distribution coefficient for the adsorption, T is the absolute temperature, R is gas constant, ΔG° , ΔH° and ΔS° are Gibbs free energy change, enthalpy change and entropy change, respectively.

3.2.10. Regeneration study:

In water and wastewater treatment systems, the adsorbent's reusability is a crucial economic consideration (Abu Rumman et al., 2021; Wakejo et al., 2022). In order to evaluate this, the research used previously established ideal operating conditions to examine the potential of various adsorbents throughout five consecutive cycles of adsorption and desorption. The most efficient desorbing solution for pollutant desorption was found by testing a range of solutions, including methanol, 0.3M NaOH, 0.3M HCl, and a mixture of 3% NaOH and methanol (Wakejo et al., 2022). These solutions have been used to desorption of pollutants from various adsorbents in earlier investigations. The adsorbent's reusability test was then conducted using the desorbing solution that performed the best (Wakejo et al., 2022). Adsorbent was put through many cycles in the process; after each adsorption-desorption cycle, the adsorbent was carefully cleaned with ultrapure water, filtered, and oven-dried to prepare it for use in the next adsorption cycle. Equation (3.1) was used to calculate the adsorption efficiency of the adsorbents after each cycle.

Chapter 4
ADSORPTION OF OXYTETRACYCLINE ONTO
MANGANESE OXIDE MODIFIED PINE CONE BIOCHAR

Chapter 4

ADSORPTION OF OXYTETRACYCLINE ONTO MANGANESE OXIDE MODIFIED PINE CONE BIOCHAR

4.1. Introduction

Contaminants of emerging concern (CECs) encompass a diverse array of chemical compounds, including pharmaceuticals, personal care products, pesticides, and industrial chemicals, which have gained recognition due to their presence in aquatic environments at varying concentrations (Abdoallahzadeh et al., 2023; Dolatabadi et al., 2023; Dolatabadi, Kheirieh, et al., 2022; Y. Fan et al., 2023; Kiani et al., 2021; Mansouri et al., 2018; Singh et al., 2023). The adverse effects associated with CECs are a subject of growing concern in both environmental and human health contexts (Dolatabadi, Ghorbanian, et al., 2021; Dolatabadi, Naidu, et al., 2021; Hashemi et al., 2022; B. Wang et al., 2023). Oxytetracycline hydrochloride (OTC), a broad-spectrum antibiotic, is one of the widely used antibiotics in medicine, cattle, and aquaculture which is recognized as one of the emerging pollutant (Gu et al., 2021; Z. Wei et al., 2023). Prolonged and indiscriminate use of OTC has been linked to the development of antibiotic-resistant genes, which can propagate through food, water, and natural environments. This poses a serious threat to human health and ecosystem balance (Dai et al., 2022; Solmaz et al., 2023). It is noteworthy that the proliferation of antibiotic-resistant genes has the potential to harm ecosystem and possibly endanger human health, resulting in kidney disease and cancer (Kashyap et al., 2023; Nagarajan & Chandiramouli, 2022; Hongkui Zhang et al., 2022). Hence, there is a need for a technique that can effectively remove OTC from wastewater. Conventional waste-water treatment methods are not intended to remove recalcitrant and complex molecules such as antibiotics (de Ilurdoz et al., 2022; X. Li et al., 2022). Currently, a number of advanced wastewater treatment techniques such as adsorption (Y. Fan et al., 2023; B. Wang et al., 2023), biodegradation

(Kayal & Mandal, 2022), chemical oxidation (Huo et al., 2023), and photocatalytic degradation (Regulska et al., 2022) are employed to remove OTC from water. Due to the straightforward operation, high effectiveness, and lack of harmful byproducts, adsorption is considered to be the most feasible among these techniques for removing recalcitrant pollutants from water (de Ilurdoz et al., 2022; X. Li et al., 2022). Activated carbon (Azari et al., 2020; Barjasteh-Askari et al., 2021; Hongsawat & Prarat, 2022), clay minerals (B. Wang et al., 2023), zeolites (Başkan et al., 2022), metal oxides (Das & Panda, 2022), nanomaterials (Almufarij et al., 2022), and biochar (Vievard et al., 2023) have been used by many researchers for the adsorptive removal of OTC from water. Out of numerous adsorbents, biochar has attracted attention due to its remarkable production from waste (*i.e.* efficiently converting trash into usable form) and its capability to remove several recalcitrant pollutants from water (Vievard et al., 2023). It is made by pyrolyzing waste biomass, such as coconut husk, pine needles, pine cone, agriculture waste, peanut waste, and pineapple peel etc. (Kumar et al., 2023; Vievard et al., 2023) with excellent yield.

In this work, pine-cone biochar is modified & utilized for sustainable removal of oxytetracycline from water. Due to their needles and twigs high resin content, Chir Pine trees are extremely combustible and prone to forest fires (Fulé et al., 2021). By using vast amount of pine tree biomass (organic resource) in a sustainable manner (Neelima Shah, IFS Rajiv Dhiman, 2022), we can overcome such natural disasters from harming the forest cover. Several researchers used pine cone, pine needle and pine bark as feedstock to obtain biochar for their study (Cela-Dablanca et al., 2022; Debnath et al., 2017; D. Pandey et al., 2022). Due to high porosity, unique chemical composition, surface chemistry, cost-effective and renewable & sustainable source pine cone biochar is considered as an effective adsorbent (Kumar et al., 2023). However, it often has a low ability for adsorbing antibiotics (Feng et al., 2021a) on its own. The antibiotics adsorption by biochar (BC) made from *Robinia pseudoacacia* (Xiao et al., 2020), food scrap and plant trimming (Hoslett et al., 2021), is only between 10 and 16 mg/g. Therefore, it is

essential to modify biochar for the optimization of its surface properties to enhance its capacity to effectively adsorb specific pollutants (Das & Panda, 2022). Surface modification of biochar is known to increase its surface area for improved affinity towards target contaminants for adsorption (X. Wei et al., 2022). Manganese oxide (MnO_2) nanoparticles have received more attention as a promising and most efficient adsorbent due to high specific surface area and excellent adsorption capability (Feng et al., 2021a). Modifying biochar with MnO_2 enhances its adsorption capacity by introducing several key advantages (Feng et al., 2021a). MnO_2 significantly increases the available surface area for adsorption due to its porous structure, providing more active sites for pollutant attachment (Jiang Li et al., 2020). Moreover, MnO_2 can chemically react with certain contaminants, facilitating their removal through precipitation or degradation (MnO_2 is a well-known catalyst) (Jiang Li et al., 2020). Additionally, MnO_2 promotes selective adsorption and surface functionalization, allowing for targeted capture of specific pollutants and enhancing the affinity between biochar and contaminants, ultimately resulting in a more effective adsorption process (Feng et al., 2021a).

Hence, this study is aimed at the evaluation of the performance of MnO_2/PCBC for OTC removal from water as influenced by experimental parameters such as pH, initial OTC concentration, MnO_2/PCBC dose & temperature. XRD, SEM, FTIR, CHNS, ICP-OES, surface area and pore size measurements were used to examine the attributes of the prepared MnO_2/PCBC composites. The adsorption kinetics, isotherms, thermodynamics, mechanism and regeneration of MnO_2/PCBC with respect to OTC adsorptive removal are also studied. This is the first study on the application of MnO_2/PCBC for OTC removal which demonstrates high adsorption capacity and regeneration of the adsorbent. The results indicate comparable performance of MnO_2/PCBC with the reported adsorbents for OTC removal from water. This work presents MnO_2/PCBC as a sustainable adsorbent derived from waste pine-cone biochar for large scale

adsorptive removal of OTC from water in comparison to many reported adsorbents.

4.2. Results & Discussion

4.2.1. Selection of the best adsorbent

Figure 4.1a displays the percentage removal efficiency of oxytetracycline (OTC) pollutant for a variety of materials, including PCBC, MnO_2 , Fe_3O_4 , LDH, $\text{Fe}_3\text{O}_4/\text{PCBC}$ composite, MnO_2/PCBC composite, and LDH/PCBC composite. The MnO_2/PCBC composite had the highest OTC removal effectiveness of all the adsorbents tested, at 89.90%. Because of its improved OTC removal capability, the MnO_2/PCBC composite is chosen for further research.

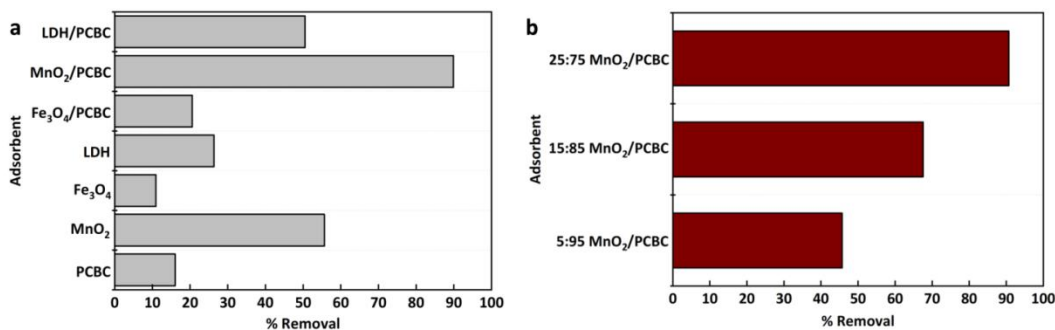


Figure 4.1: Comparison of different synthesized adsorbent (Prakash Bobde, Sharma, Kumar, Pal, et al., 2023)

Figure 4.1b displayed the percentage removal efficiency of the pollutant OTC for three distinct composite materials: 5:95 MnO_2/PCBC , 15:85 MnO_2/PCBC , and 25:75 MnO_2/PCBC . With an OTC removal effectiveness of 90.68%, the 25:75 MnO_2/PCBC composite outperformed the other composite materials. Because of its better efficacy in OTC elimination, the 25:75 MnO_2/PCBC composite is selected for detailed research.

4.2.2. Characterization of the adsorbent

The crystalline structures of PCBC and MnO_2/PCBC were examined using XRD analysis (in the 2θ range $10\text{-}80^\circ$) (figure 4.2a). The crystalline planes of calcite were identified as the source of the diffraction peaks at 23.4° and 43.6° for PCBC. The prominent peak at 23.4° is attributed to the crystal plane index C(002), which correlates with the alignment and azimuthal orientation of the aromatic and

carbonized structure (Yan et al., 2021). Another notable peak appears at 43.6° , attributed to C(100) diffractions originating from graphitic and hexagonal carbons, indicative of the size of the aromatic lamina. The distinct C(100) peak suggests a significant presence of aromatic lamina, highlighting its high degree of alignment (Yan et al., 2021). Following MnO_2 deposition, MnO_2/PCBC displayed an amorphous nature demonstrated by lower intensity peaks at 26.6° (310) and 36.7° (211) (Haipeng Zhang et al., 2020).

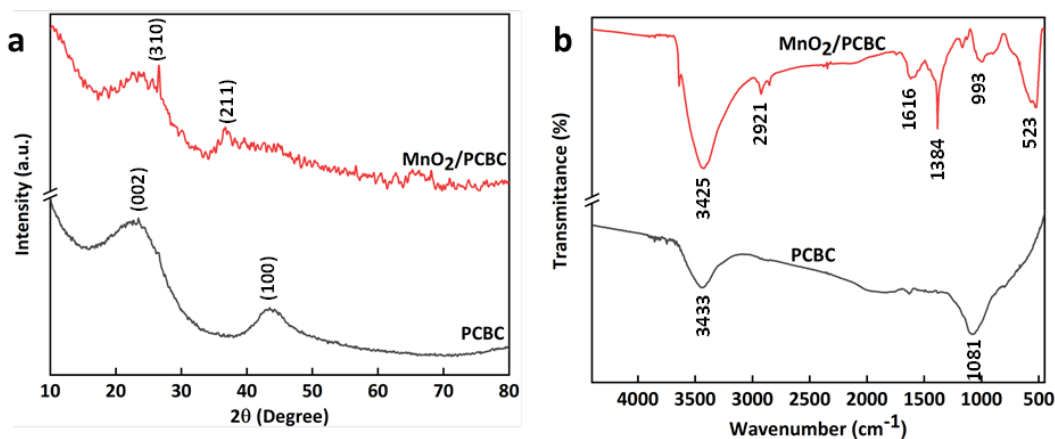


Figure 4.2: (a)XRD, (b)FTIR of PCBC and MnO_2/PCBC (Prakash Bobde, Sharma, Kumar, Pal, et al., 2023)

The FTIR spectra of a PCBC and MnO_2/PCBC composites are given in figure 4.2b. The spectra demonstrated a significant peak around 3425 cm^{-1} for MnO_2/PCBC and 3433 cm^{-1} for PCBC due to stretching vibration of O-H bonds in hydroxyl groups (P. Bobde et al., 2022; Prakash Bobde et al., 2021), whereas the spectral band at 2921 cm^{-1} in MnO_2/PCBC is assigned to C-H stretching and deformation vibration (B. Zhang et al., 2017). A spectral band at about 1616 cm^{-1} indicated C=C bonds stretching vibration (Al-Musawi, Rajiv, et al., 2021; Ramanayaka, Kumar, et al., 2020). Two peaks at around 1384 and 993 cm^{-1} were found to be corresponding to bending vibrations of C-H (Ramanayaka, Kumar, et al., 2020) and C=C bonds, respectively. The peaks around 1081 cm^{-1} in PCBC is most likely caused by the -OH bending and C-O-C bending in the cellulose and lignin structures of the PCBC (B. Zhang et al., 2017). Furthermore, a peak at 523

cm^{-1} was also observed in the spectra of the MnO_2/PCBC composite, confirming the formation of Mn-O bonds (Feng et al., 2021a).

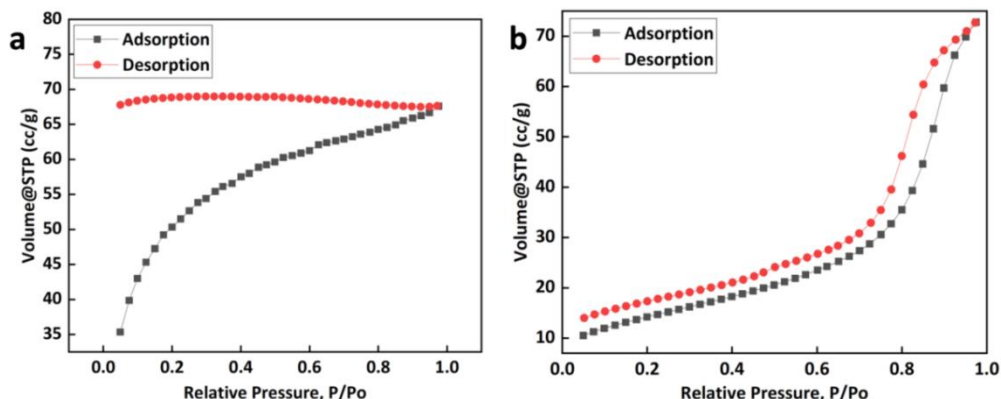


Figure 4.3: BET adsorption-desorption isotherm of (a) PCBC and (b) MnO_2/PCBC (Prakash Bobde, Sharma, Kumar, Pal, et al., 2023)

The N_2 adsorption-desorption isotherm of PCBC and MnO_2/PCBC were measured at 77.35 K and displayed in figure 4.3a and 4.3b, respectively. As can be observed from figure 4.3b, when the value of P/P_o was low, the amount of N_2 adsorbed rose significantly, indicating the presence of micropores on the surface of MnO_2/PCBC . The adsorption capacity then gradually rose as the relative pressure increased. The BET equation was used to compute the specific surface area (SSA). BET results indicate that MnO_2/PCBC has slightly more total pore volume and average pore size than PCBC (table 4.1). However, modification of PCBC by MnO_2 into MnO_2/PCBC may result in a SSA reduction of around one order of magnitude. This could be attributed to the creation of surface-bonded species during the modification of PCBC by MnO_2 . The IUPAC defines PCBC as a Type I isotherm, while the Type III isotherm was observed for MnO_2/PCBC . A process of uncontrolled multilayer development is likewise indicated by Type III isotherm. Type III isotherms develop as a result of significant lateral contacts among adsorbed molecules as opposed to interactions between the adsorbent surface and adsorbate. Due to the non-rigid aggregation of the bio-based adsorbent particles, the N_2 adsorption isotherm of MnO_2/PCBC does not flatten at the greatest recorded relative pressure.

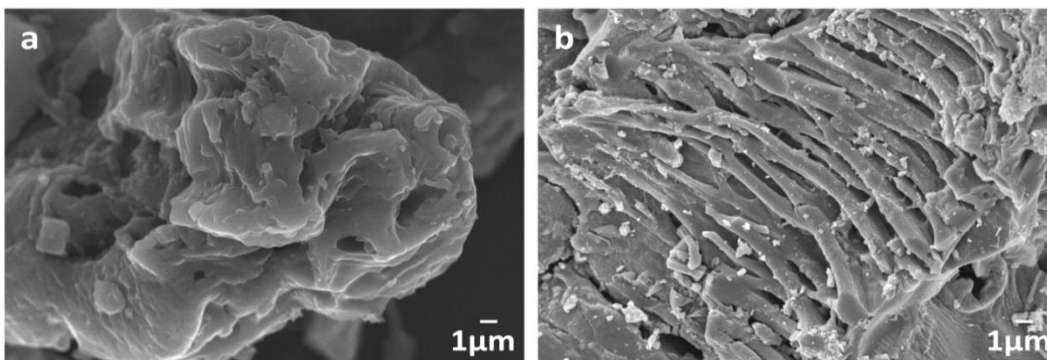


Figure 4.4: SEM images of (a) PCBC and (b) MnO₂/PCBC (Prakash Bobde, Sharma, Kumar, Pal, et al., 2023)

SEM was used to examine the PCBC and MnO₂/PCBC morphology and structure; the resulting images are displayed in figure 4.4a and 4.4b. The SEM of PCBC (figure 4.4a) displayed an uneven and smooth surface on a porous structure. MnO₂/PCBC's agglomerated structure didn't change significantly (figure 4.4b), although the modification left the surface a little rough. MnO₂ was deposited on the MnO₂/PCBC's surface and in its pores, and some of the MnO₂ molecules formed agglomerates. SEM images revealed that manganese oxides had successfully covered the PCBC surface, which is in line with the conclusions made by Gao et al. (M. Gao et al., 2018).

Table 4.1: Physicochemical properties of PCBC and MnO₂/PCBC

Adsorbent	Specific Surface Area (SSA) (m ² /g)	Total pore volume (cm ³ /g)	Average pore size (nm)
PCBC	172.19	0.1046	1.2144
MnO ₂ /PCBC	50.760	0.1126	4.4349
MnO ₂ /PCBC after OTC adsorption	11.505	0.0226	3.9316

Table 4.2: Elemental composition of PCBC and MnO₂/PCBC

Adsorbent	Elemental Composition (Weight %)					
	C (%)	H (%)	O (%)	N (%)	Mn (%)	K (%)
PCBC	82.97	1.10	14.42	1.31	0.02	0.18
MnO ₂ /PCBC	67.62	0.94	22.48	1.77	6.01	1.18
MnO ₂ /PCBC after OTC adsorption	-	-	-	-	-	-

The physical and chemical properties of PCBC and MnO₂/PCBC are listed in table 4.1 and 4.2. The elemental analysis reveals that the addition of MnO₂ causes manganese to emerge on the surface of MnO₂/PCBC in comparison to PCBC, and that this decreases the carbon content of the PCBC while increasing the oxygen content.

4.2.3. Effect of contact time on the adsorption of OTC

Figure 4.5 reveals the plot of the amount of OTC adsorbed (mg/g) as a function of contact time for 200 mg/L OTC onto the adsorbent MnO₂/PCBC. Figure 4.5 indicated that the quantity of OTC adsorption, q_e (mg/g), is increased with contact time from 0 min to 1440 min. For the first 480 min, the adsorption amount increased from 79.71 to 326.28 mg/g and further increased to 365.62 mg/g before reaching the equilibrium at 1440 min in case of adsorbent MnO₂/PCBC. Thus, the adsorption capacity increased exponentially within 480 min reaching equilibrium at 1440 min.

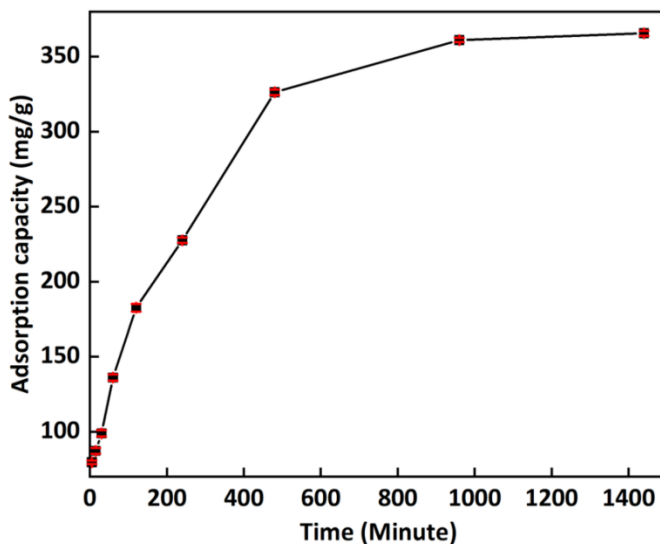


Figure 4.5: Effect of the amount of OTC adsorbed (mg/g) against contact time onto adsorbent MnO₂/PCBC (Prakash Bobde, Sharma, Kumar, Pal, et al., 2023)

4.2.4. RSM Study

To evaluate the entity, interaction and quadratic effects of the variables affecting the adsorption efficiency of OTC on MnO₂/PCBC adsorbent, variance analysis

(ANOVA) is performed. The real values of four variables and percent removal values (experimental and predicted) for adsorption of OTC on adsorbent MnO₂/PCBC are given in table 4.3. The total of squares and average squares of each factor, F-values as well as P values are shown in table 4.4. ANOVA confirms the validity and adequacy of the models. By bisecting the total of the squares of various sources, the formula and the error variance by the corresponding degree of freedom give the mean square values.

Table 4.3: Experimental and predicted values for adsorption of OTC on adsorbent MnO₂/PCBC obtained through CCD and RSM

Run No.	A	B (g/L)	C (mg/L)	D (K)	Experimental	Predicted	Residual
1	3	0.1	50	283	55.62	54.52	1.10
2	11	0.1	50	283	73.28	70.52	2.76
3	3	0.5	50	283	92.74	94.90	-2.16
4	11	0.5	50	283	84.87	82.05	2.82
5	3	0.1	200	283	18.91	14.12	4.79
6	11	0.1	200	283	54.18	57.96	-3.78
7	3	0.5	200	283	57.74	59.40	-1.66
8	11	0.5	200	283	74.42	74.38	0.04
9	3	0.1	50	313	58.83	57.49	1.34
10	11	0.1	50	313	92.65	92.35	0.31
11	3	0.5	50	313	95.06	92.63	2.43
12	11	0.5	50	313	95.22	98.63	-3.41
13	3	0.1	200	313	22.71	26.88	-4.17
14	11	0.1	200	313	93.11	89.57	3.54
15	3	0.5	200	313	65.53	66.91	-1.39
16	11	0.5	200	313	98.30	100.75	-2.45
17	2	0.3	125	298	64.67	64.89	-0.22
18	12	0.3	125	298	96.19	96.03	0.15
19	7	0.05	125	298	48.45	53.14	-4.69
20	7	0.55	125	298	90.00	85.37	4.63
21	7	0.3	31.25	298	94.94	99.09	-4.15
22	7	0.3	218.75	298	79.24	75.16	4.09
23	7	0.3	125	279.25	63.73	66.85	-3.11
24	7	0.3	125	316.75	88.23	85.18	3.05
25	7	0.3	125	298	82.41	82.96	-0.55
26	7	0.3	125	298	83.46	82.96	0.51
27	7	0.3	125	298	83.16	82.96	0.20

Regression analysis of the percent elimination efficiency of OTC using MnO₂/PCBC revealed the importance of each coefficient measured using the F-test and p-value at a significance level of 0.05. The related variables would be more important if the absolute p-values were lower and the F-value was higher. It revealed that the factors with the greatest influence is the linear term of all parameters (pH, AD, IC, and temp), the quadratic term of pH (AA), the quadratic term of AD (BB), the interaction impact of pH and AD (AB) for the reduction of OTC through both the adsorbent. The rest of the variance analysis revealed a negligible influence with a p-value greater than 0.05.

Table 4.4: Analysis of variance for % removal efficiency of OTC by using MnO₂/PCBC

Source	Sum of square	DDL	Mean square	F-value	P-value
Model	11917.54	14	851.25	47.37	< 0.0001
A-pH	2969.32	1	2969.32	165.24	< 0.0001
B-MnO ₂ /PCBC dose	3177.46	1	3177.46	176.82	< 0.0001
C-OTC initial concentration	1751.47	1	1751.47	97.47	< 0.0001
D-Temperature	1028.86	1	1028.86	57.26	< 0.0001
pH*MnO ₂ /PCBC dose	832.49	1	832.49	46.33	< 0.0001
pH*OTC initial concentration	775.04	1	775.04	43.13	< 0.0001
pH*Temperature	355.5	1	355.5	19.78	0.0008
MnO ₂ /PCBC dose*OTC initial concentration	23.89	1	23.89	1.33	0.2713
MnO ₂ /PCBC dose*Temperature	27.5	1	27.5	1.53	0.2397
OTC initial concentration*Temperature	95.71	1	95.71	5.33	0.0396
(pH) ²	14.93	1	14.93	0.8311	0.3799
(MnO ₂ /PCBC dose) ²	450.52	1	450.52	25.07	0.0003
(OTC initial concentration) ²	41.71	1	41.71	2.32	0.1535
(Temperature) ²	115.67	1	115.67	6.44	0.0261
Residual	215.64	12	17.97		
Lack of Fit	215.05	10	21.5	73.02	0.0136
Pure Error	0.589	2	0.2945		
Cor Total	12133.17	26			

The point of zero charge (pH_{PZC}) of MnO₂/PCBC is revealed in figure 4.6. OTC has three different pK_a values. OTC is H₄OTC⁺ at pH < 3.27, H₃OTC at 3.27 < pH < 7.32, H₂OTC⁻ at 7.32 < pH < 9.11 and HOTC²⁻ at pH > 9.11 (G. Liang et al.,

2019). The surface of MnO₂/PCBC is positively charged at pH < pHPZC=7.3 and negatively charged at pH > pHPZC=7.3.

As shown in figure 4.7, by rising pH value of OTC solution, the removal efficiency of MnO₂/PCBC increased. MnO₂/PCBC had a positive charge, which increased electrostatic attraction, whereas the OTC molecule did not have any net charge at pH range of 3.27 to 7.32. MnO₂/PCBC showed increasing percentage removal despite the negative-negative electrostatic repulsion at pH > 7.32. These findings demonstrated that strong hydrogen bonding, π - π electron donor acceptor interaction along with electrostatic interaction affected the MnO₂/PCBC and OTC molecule interaction. A similar trend in the percentage removal is observed for OTC onto the surface of BC/MnO₂ (Jiang Li et al., 2020).

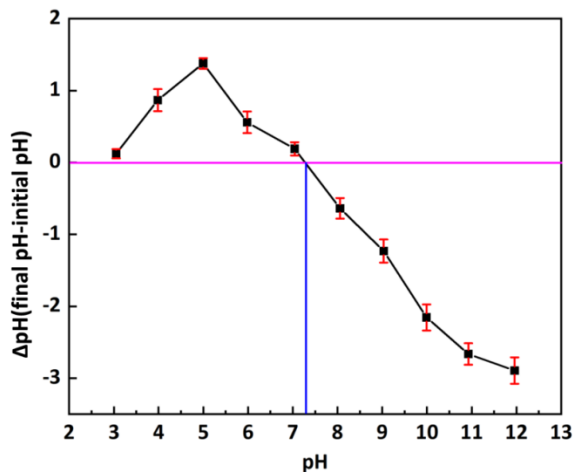


Figure 4.6: pH point of zero charge (pHPZC) of MnO₂/PCBC (Prakash Bobde, Sharma, Kumar, Pal, et al., 2023)

As shown in figure 4.7, by enhancing MnO₂/PCBC dose, OTC removal efficiency is improved and is attributed to the activated adsorbent surface having higher adsorption sites accessible to remove OTC. An increase in the adsorption of OTC with a rise in adsorbent dosage may be because of the availability of a substantial number of active adsorption sites present on the adsorbent. Finite surfaces are offered for adsorption at low dosage, resulting in minimal percentage reduction, however as the MnO₂/PCBC amount rises, high adsorption-friendly sites are

present, thereby improving the adsorption performance (Harja & Ciobanu, 2017; Q. Li et al., 2021). Also, the OTC removal efficiency is reduced with the rising preliminary concentration of OTC. Decreasing removal efficiency by rising preliminary concentration may be attributed to the presence of additional OTC ions in solution at increased concentrations and adsorption site is a restricting variable in the adsorption mechanism. By increasing the OTC concentration, adsorption sites are decreased, as additional ions are added into the process. The number of adsorption sites becomes the limiting factor as the concentration rises, resulting in lower adsorption (Harja & Ciobanu, 2017). As revealed in figure 4.7, OTC removal efficiency enhanced with rising temperature indicating that the adsorption of OTC onto MnO₂/PCBC is favored at high temperatures and the adsorption process is endothermic (G. Liang et al., 2019).

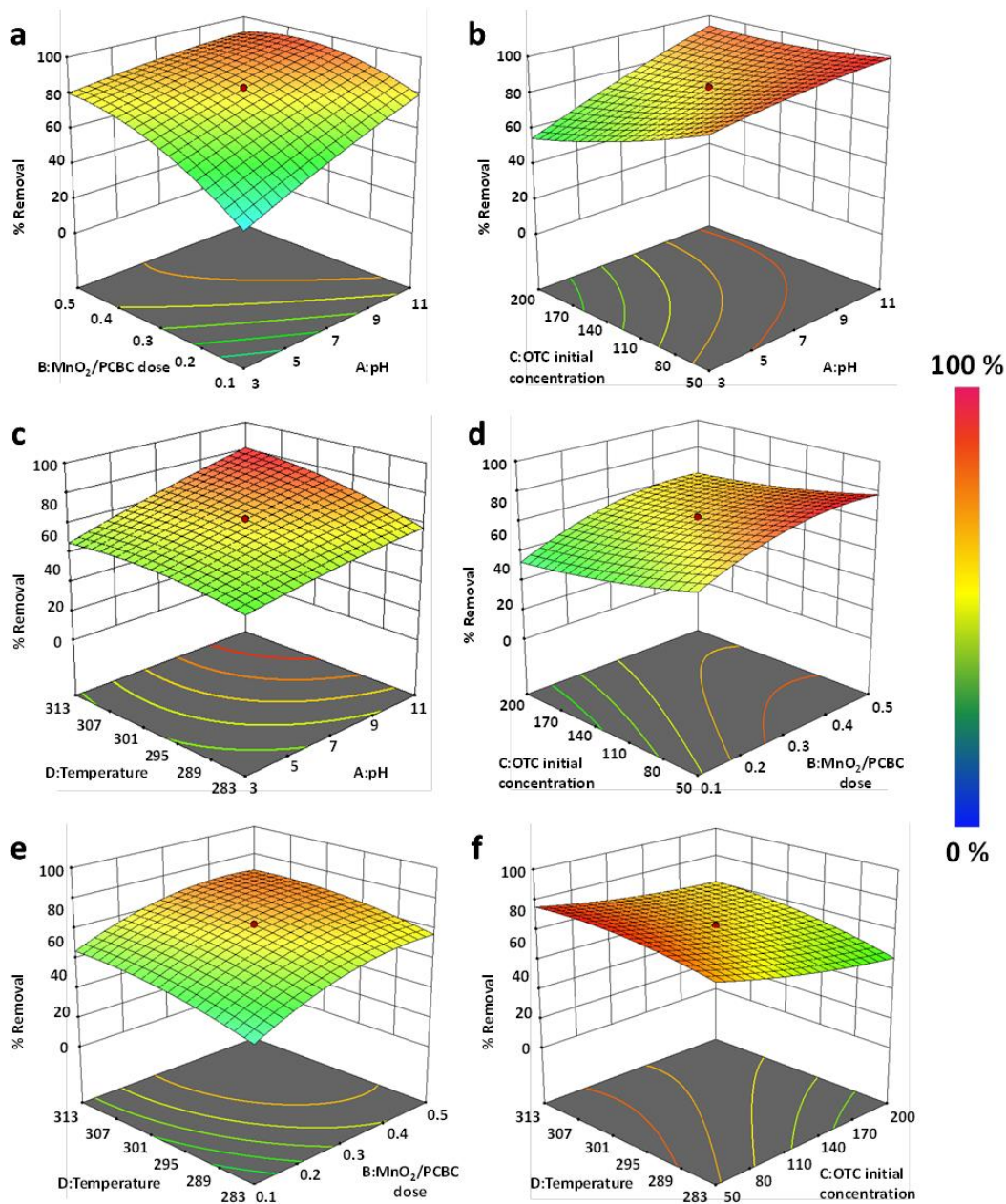


Figure 4.7: 3D surface graphs of percent removal efficiency of OTC by using $MnO_2/PCBC$ (Prakash Bobde, Sharma, Kumar, Pal, et al., 2023)

4.2.5. Fitting the model

The evaluation of the coefficient (R^2) is required to determine the model. The magnitude of the correlation coefficient is $R^2 = 98.2$ for the removal of OTC by adsorbent $MnO_2/PCBC$. This indicated that only 1.78 % of the design did not

describe the overall factor model for the adsorbent MnO₂/PCBC. The magnitude of the modified correlation coefficient for the adsorbent MnO₂/PCBC (adjusted $R^2 = 96.15\%$ respectively) is however strong, indicating greater importance of the consequence. The expected magnitude of R^2 is strong to endorse big model significance. The expected R^2 was 88.80% implying that the design would not merely clarify 11.20% of the total variations for the adsorbents. After variance analysis (ANOVA), the regression equation gave the degree of OTC removal as a function of initial solution pH (A), adsorbent dose (B), initial OTC concentration (C), and temperature (D). By following numerous regression analyses on the investigational data, the empirical values of the CCD configuration were pertinent with a complete second order mathematical model. The inferential association between the OTC reduction (Y) and the 4 different parameters in uncoded RSM units is defined by equation 4.1 for the adsorbent MnO₂/PCBC.

$$\begin{aligned} \% \text{ removal} = & -1648.2678 - 19.0945A + 379.1167B - 1.0809C + 11.5657D - 0.0998A^2 - \\ & 219.1799B^2 + 0.0005C^2 - 0.0197D^2 - 9.0165AB + 0.0232AC + 0.0786AD + 0.0815BC - \\ & 0.43706BD + 0.0022CD \end{aligned} \quad (4.1)$$

Using equation and the values for all variables, removal percentages can be determined in all cases where the concept is laid. Positive and negative signs prior in equation 4.1 reflect the synergistic and antagonistic impact of pH, primary concentration of OTC, adsorbent dosage and temperature. The existence of a particular parameter in a concept implied a benefactor influence; the two factors signify a double variable impact and a second order factor imply a quadratic effect.

Analysis of variance for % removal efficiency of OTC by using MnO₂/PCBC highlighting the importance of all coefficients as calculated by the F-values and p-values are given in Table 4.4. The significance of the related coefficient increases with increasing F-values and decreasing p-values. "Prob > F" values below 0.0500 also demonstrate a strong substantial regression at a confidence level of 95%. In this scenario, important model parameters were the first-order key effects,

square effects, and interaction effects of the initial OTC solution pH, adsorbent dosage, initial OTC concentration and temperature.

4.2.6. Optimization of the adsorption of OTC

The main objective in designing the 27 experiments using RSM is to rectify the variable (pH, primary concentration of OTC, adsorbent dosage and temperature) of the adsorption for maximum reduction efficiency of OTC onto MnO₂/PCBC. Figure 4.8 demonstrates the optimization of various factors for the adsorption of OTC onto MnO₂/PCBC. In the present work, Minitab 16.1 software was employed to determine the ideal values of the variables from the model developed by CCD. The ideal values of the factors along with the predicted and experimental percent removal for adsorption of OTC onto MnO₂/PCBC are given in table 4.5. For the confirmation of the model, experimental testing was carried out under optimal scenarios. The experimental results demonstrated OTC percentage removal to be 88.1 % using the optimum values of each parameter which is in good conformity with the predicted value (88.4 %) for adsorbent MnO₂/PCBC.

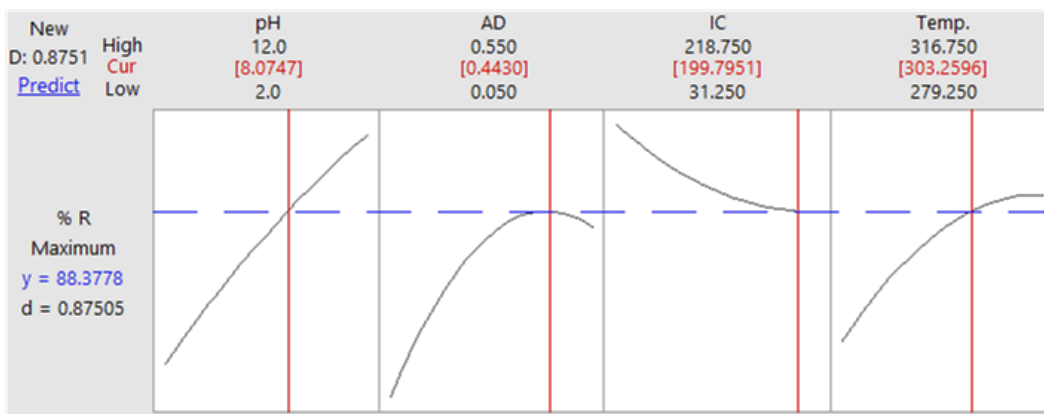


Figure 4.8: Optimization of adsorption process of OTC onto MnO₂/PCBC (Prakash Bobde, Sharma, Kumar, Pal, et al., 2023)

Table 4.5: Optimum values for adsorption of OTC onto MnO₂/PCBC

Adsorbent	A	B (g/L)	C (mg/L)	D (°K)	% Removal	
					Predicted	Experimental
MnO ₂ /PCBC	8.0	0.44	200	303	88.4	88.1

A-pH, B-MnO₂/PCBC dose, C-Initial OTC concentration, and D-Temperature

4.2.7. Kinetic, isotherm and thermodynamic study

Figure 4.9a, 4.9b, 4.9c, and 4.9d illustrates the PFO, PSO, Elovich and ID equation curve fitting and the results of PFO, PSO, Elovich and ID constants, q_e , K_1 , K_2 , α , β , K_i , c and R^2 are represented in table 4.6. The R^2 value for the linear plot of PFO, PSO, Elovich and ID equation is 0.9956, 0.9925, 0.9233 and 0.9361 respectively. In case of the OTC-MnO₂/PCBC system, a PSO equation provided theoretical q_e values that closely matched experimental values. This indicates that a PSO chemical reaction accurately describes the adsorption kinetics of OTC, and that this reaction is a crucial factor in the rate-determining step. The adsorption of OTC by KOH modified bio-based adsorbent and magnetic montmorillonite-bio-based adsorbent composite demonstrated comparable results (J. Luo et al., 2018) (G. Liang et al., 2019). Thus, the key rate-determining phase in the adsorption of OTC onto MnO₂/PCBC may be the proposed chemisorption.

The adsorption capacity relative to $t^{1/2}$ for ID of OTC by MnO₂/PCBC is shown in figure 4.9d. The findings indicated that the graphs are multilinear, implying that the process went through two or more phases. There is exterior layer adsorption, as illustrated in figure 4.9d (stage 1). Stage 1 is the shortest and ends in 30 minutes, followed by the intraparticle diffusion control phase (stage 2), which lasts 30 minutes to 480 minutes. Following 480 minutes, the equilibrium's ending adsorption (stage 3) commences. The variance of the first straight section (stage 2) represents the variable function that contributes to ID, whereas the intercept of this segment corresponds to the thickness of the boundary layer.

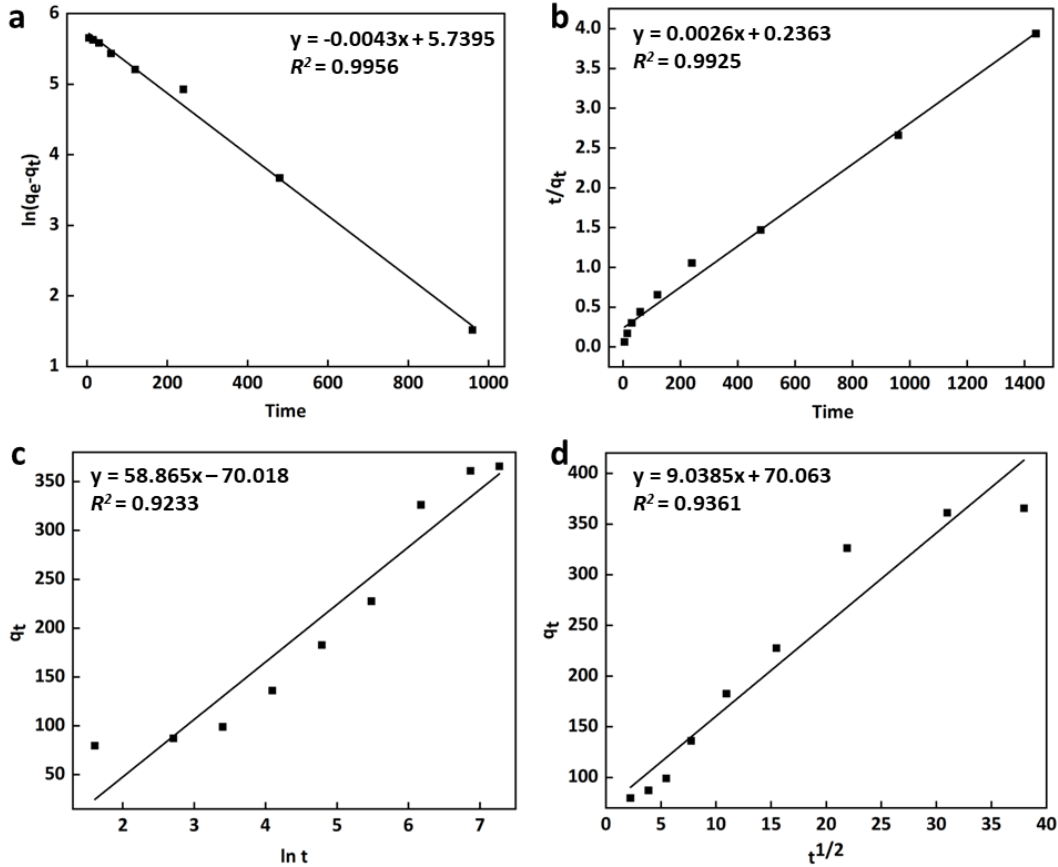


Figure 4.9: (a) PFO and (b) PSO (c) Elovich and (c) ID plots for the adsorption of OTC on MnO₂/PCBC. Experimental conditions: MnO₂/PCBC dose = 0.5 g/L, Initial concentration of OTC = 200 mg/L, Temperature = 298K, pH = 7. (Prakash Bobde, Sharma, Kumar, Pal, et al., 2023)

Table 4.6 also includes the R^2 values for the ID model, which indicate that OTC adsorption by MnO₂/PCBC can be followed by ID with regard to 480 minutes. With reference to, the lines do not cross the origin, implying that ID is involved in the adsorption system, but it is not the only method for limiting rates, and that certain other processes still play an important role in the adsorption system (Al-Musawi, Rajiv, et al., 2021; Balarak, Zafariyan, et al., 2021). Layer sorption and ID are likely to occur concurrently, influencing the kinetic model of the OTC-MnO₂/PCBC connection.

Table 4.6: Kinetic parameters for the adsorption of OTC onto MnO₂/PCBC

	C_0 (mg/L)	200
	Theoretical q_e (mg/g)	365.62
PFO	q_e (mg/g)	309.79
	K_1 (min ⁻¹)	0.0043
	R^2	0.9956
PSO	q_e (mg/g)	384.61
	K_2 (g.mg ⁻¹ .min ⁻¹)	2.86 x 10 ⁻⁵
	R^2	0.9925
Elovich	α	17.918
	β	0.0169
	R^2	0.9233
ID	K_i (mg/g.min ^{1/2})	9.0385
	c	70.063
	R^2	0.9361

Fig 4.10(a, b, c and d) displays OTC adsorption equilibrium on MnO₂/PCBC. The value of R^2 mentioned in Table 4.7 is higher in Langmuir and Freundlich isotherm for adsorption of OTC onto MnO₂/PCBC than Temkin and Dubinin-Radushkevich isotherm values. For the adsorption of OTC by MnO₂/PCBC, the Langmuir and Freundlich equation represents the most suitable experimental data than the Temkin and Dubinin-Radushkevich isotherm equations.

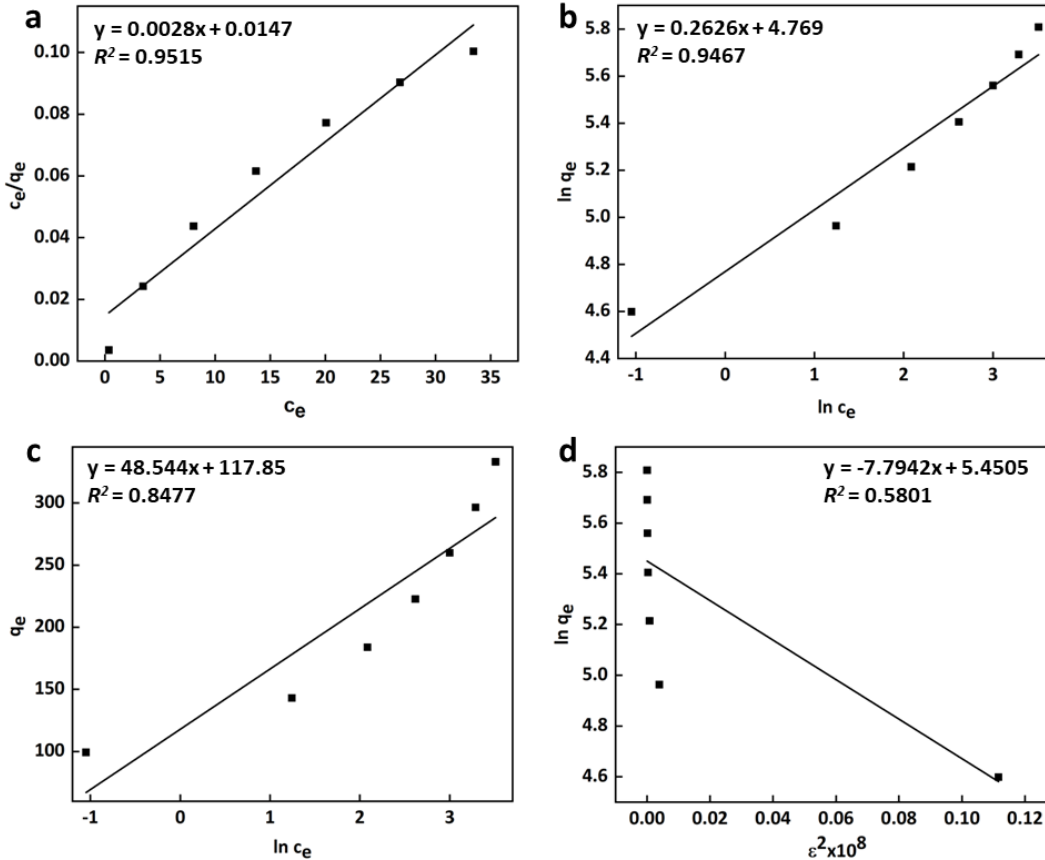


Figure 4.10: (a) Langmuir (b) Freundlich (c) Temkin and (d) Dubinin-Radushkevich plots for the adsorption of OTC on MnO₂/PCBC. Experimental Conditions: MnO₂/PCBC dose= 0.5 g/L, shaking time = 1440 min., Temperature = 298 K, pH = 8. (Prakash Bobde, Sharma, Kumar, Pal, et al., 2023)

The monolayer saturation capacity of MnO₂/PCBC, Q_0 , was found to be 357.14 mg/g. The isotherm shape can be defined by a separation factor (R_L) for a Langmuir-type adsorption mechanism. It has been noticed that the value of R_L , ~ 0.21 validates the favorable OTC uptake process. The value of Freundlich parameter $n > 1$, it indicates a favorable adsorption of OTC onto MnO₂/PCBC. It is known that if the value of $1/n < 0.1$, it indicates an irreversible process, and if $1/n > 0.1$, it indicates a reversible process (Ramanayaka, Kumar, et al., 2020; Ramanayaka, Tsang, et al., 2020). The experimental data of OTC adsorption onto MnO₂/PCBC denotes the value of $1/n$ is 0.26 which is more than 0.1, indicating

the reversible process. As a result, MnO₂/PCBC can be retrieved upon desorption for further use as adsorbent. The Temkin model's computed binding energy (B=48.54 J/mol) is found to be higher than 8 J/mol, implying that OTC is chemisorbed onto MnO₂/PCBC surface. The value of Dubinin-Radushkevich parameter adsorption energy, E, was found to 2532 kJ/mol which results the sorption of OTC onto MnO₂/PCBC found to be chemisorption process. High adsorption energies are related to chemisorption since the method includes sharing and transferring electrons among MnO₂/PCBC and OTC (Balarak, Zafariyan, et al., 2021; Bisaria et al., 2022).

Table 4.7: Isotherm parameters for the adsorption of OTC onto MnO₂/PCBC

Langmuir	K_L (L/g)	68.027
	a_L (L/mg)	0.1904
	Q_o (mg/g)	357.14
	R_L	0.2079
	R^2	0.9515
Freundlich	K_f	117.80
	n (g/L)	3.8080
	R^2	0.9467
Temkin	B	48.544
	A (L/g)	11.332
	R^2	0.8477
Dubinin-Radushkevich	q_m (mg/g)	232.87
	β (mol ² k/J ²)	7.794 x 10 ⁻⁸
	E (kJ/mol)	2532.8
	R^2	0.5801

Fig. 4.11 displays the plot of $R\ln K_d$ versus $(1/T)$. The negative values of ΔG° for the MnO₂/PCBC adsorbent at all temperatures suggested that the adsorption process is spontaneous. Additionally, an increasingly negative free energy change with rising temperature suggests that the feasibility of the process at higher temperatures. The positive values of ΔH° and ΔS° suggested that the adsorption on MnO₂/PCBC is an endothermic process and favored by increased randomness (Q. Li et al., 2021; P. Zhang et al., 2019).

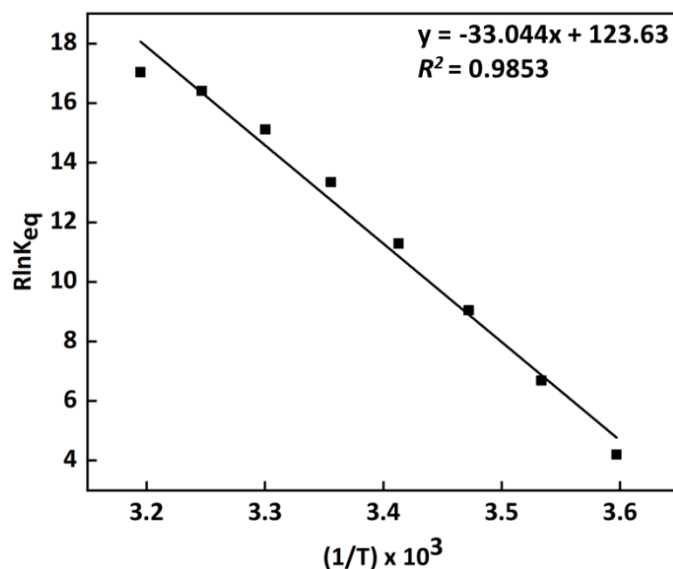


Figure 4.11: Plot of $R\ln K_{eq}$ versus $(1/T) \times 10^3 (K^{-1})$ for estimation of thermodynamic parameters. (Prakash Bobde, Sharma, Kumar, Pal, et al., 2023)

Table 4.8: Thermodynamic parameters for the adsorption of OTC onto

MnO ₂ /PCBC		
	ΔH° (kJ/mol)	33.044
	ΔS° (J/mol)	123.63
ΔG° (kJ/mol)	278 K	-1.325
	283 K	-1.943
	288 K	-2.561
	293 K	-3.180
	298 K	-3.798
	303 K	-4.416
	308 K	-5.034
	313 K	-5.652

This outcome was evaluated in relation to other research that used various adsorbents to extract OTC from water, as shown in Table 4.9. Among other adsorbents, the MnO₂/PCBC composite demonstrated a greater adsorption capability. When compared to other adsorbents, the MnO₂ supported on the pinecone bio-based adsorbent has shown satisfactory removal efficiency with a maximum capacity of adsorption. Consequently, MnO₂/PCBC is a promising material for OTC adsorption.

Table 4.9: Comparison of OTC adsorption onto different adsorbents reported in literature.

Adsorbent	c_0 (mg/L)	Dosage (g/L)	pH	Temp (K)	Time (min.)	q_e (mg/g)	Removal (%)	Reference
Magnetic bio-based adsorbent	10-200	2	3.61	298	2880	21.8	61.9	(Gu et al., 2021)
Magnetic attapulgite-bio-based adsorbent composite	10-150	2	6.5	288-308	2160	33.3	-	(Z. Wang et al., 2019)
B-cyclodextrin/carboxymethylcellulose hydrogel films	200	2	8	303	180	54.3	-	(Juengcharoonpon et al., 2019)
Magnetic montmorillonite cauliflower leave bio-based adsorbent composite	10-150	2	6.5	288-308	1440	58.8	92.5	(G. Liang et al., 2019)
Zeolite/Fe ₃ O ₄	-	-	-	298-323		83.3	-	(Başkan et al., 2022)
CTAB modified zeolite	-	-	-	318	90	108.4	99.8	(Mostafapour et al., 2022)
Colloidal dendro wood bio-based adsorbent	25-1000	1	9	303	300	136.7	-	(Ramanayaka, Kumar, et al., 2020)
KMnO ₄ modified corn stover bio-based adsorbent	10-200	6	3	288-318	1440	200.4	-	(Yue et al., 2023)
municipal solid waste-derived bio-based adsorbent and montmorillonite (MSW-BC-MMT)	10-250	2	6	298	480	233.0	-	(Weerasooriyagedara et al., 2022)
Molecularly imprinted polymer	25	0.6	5	323	60	666.5	92.04	(Khatibi et al., 2021)
MnO ₂ modified pine cone bio-based adsorbent (MnO ₂ /PCBC)	50-200	0.44	8	298	1440	357.14	88.1	This Study

4.2.8. Regeneration Study

Repeated cycles of adsorption-desorption studies were undertaken to examine the regeneration potential of MnO₂/PCBC. Figure 4.12 displays the OTC adsorption efficiency by MnO₂/PCBC following various adsorption cycles. The outcome showed that as the number of cycles increased, the percentage removal of OTC onto MnO₂/PCBC steadily reduced. The synthesized MnO₂/PCBC is reusable up to five cycles for OTC removal with a percentage removal of around 80% after the fifth cycle. Merely 8% loss in the removal efficiency was observed after 5th cycle which indicates that the adsorbent is reusable and sustainable.

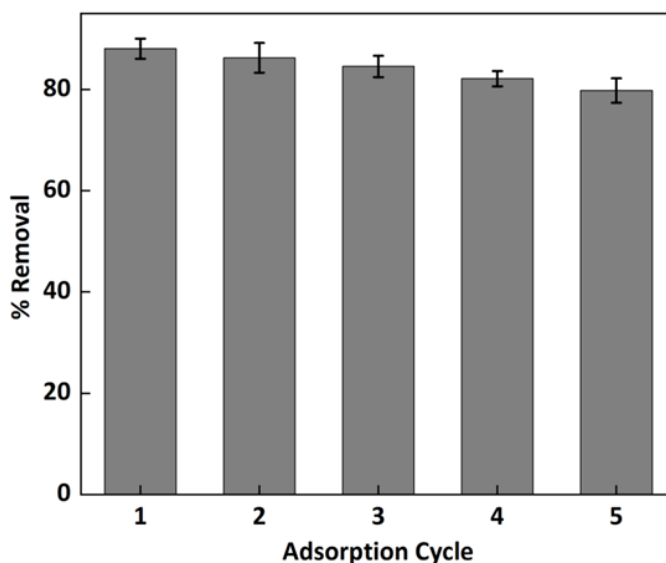


Figure 4.12: Regeneration of MnO₂/PCBC for OTC adsorption (Prakash Bobde, Sharma, Kumar, Pal, et al., 2023)

4.2.9. Adsorption Mechanism

To validate the influence of surface complexation on OTC adsorption, EDTA-2Na was introduced into the solution to assess its impact on adsorption efficiency (Fig. 4.13a). Upon the addition of 1 mM EDTA, the OTC removal rate by MnO₂/PCBC decreased by approximately 18%. This decline suggests that manganese oxide formed complexes with -NH₂ and reactive oxygen-containing functional groups within OTC molecules, facilitating efficient and selective adsorption through complexation (Xinyi Liao et al., 2023). After adsorption of

OTC, adsorbent average pore size, BET specific surface area, and total pore volume were found to

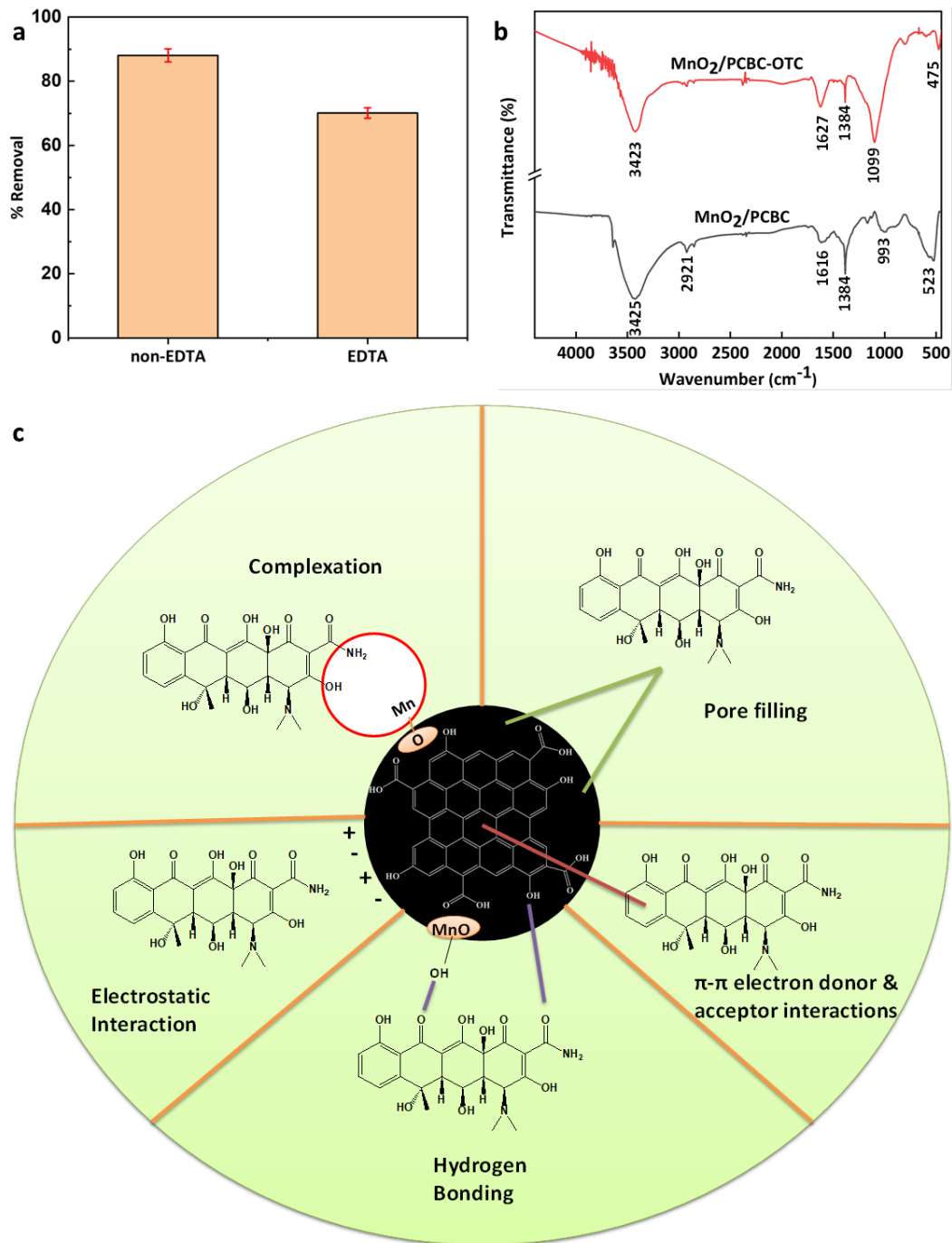


Figure 4.13: (a) Effect of EDTA on the adsorption of OTC, (b) FTIR spectra of MnO₂/PCBC before and after adsorption of OTC (MnO₂/PCBC-OTC), (c)

Possible adsorption mechanism of MnO₂/PCBC for OTC. (Prakash Bobde, Sharma, Kumar, Pal, et al., 2023)

be reduced (Table 4.1). This suggests that pore filling may play a role as one of the factors affecting the OTC adsorption onto MnO₂/PCBC. According to Liang et al. the specific surface area and pore structure are significant variables that influence the adsorption of organic pollutants on bio-based composites by a pore-filling mechanism (H. Liang et al., 2022). OTC has three different pK_a values: OTC is H₄OTC⁺ at pH < 3.27, H₃OTC at 3.27 < pH < 7.32, H₂OTC⁻ at 7.32 < pH < 9.11 and HOTC²⁻ at pH > 9.11 (G. Liang et al., 2019). The surface of MnO₂/PCBC is positively charged at pH < pH_{PZC}=7.3 and negatively charged at pH > pH_{PZC}=7.3. As shown in figure 4.7, by rising pH value of OTC solution, the removal efficiency of MnO₂/PCBC increased. MnO₂/PCBC had a positive charge, which increased electrostatic attraction, whereas the OTC molecule did not have any net charge in the pH range of 3.27 to 7.32 (Jiang Li et al., 2020). Based on the data gathered above, a proposed adsorption mechanism for OTC adsorption onto the surface of MnO₂/PCBC was made. From the study of kinetic and isotherm, it is inferred that the adsorption process of OTC onto MnO₂/PCBC involves chemisorption (Yaoyu Zhou et al., 2017). Figure 4.13b revealed the FTIR spectra of MnO₂/PCBC before and after OTC adsorption. Little shift in the peaks of FTIR was observed in OTC adsorbed MnO₂/PCBC. This may be due to the interaction of functional groups present on MnO₂/PCBC with OTC during adsorption process. The C=O (carboxylic and ketonic, 1384 cm⁻¹) and C=C (1615 cm⁻¹) peaks shift and growth indicated the vital importance of π-π interactions among OTC and MnO₂/PCBC in the adsorption processes. OTC might operate as π-electron acceptors attributed to the -NH₂ functional groups and O and/or N-hetero aromatic rings. MnO₂/PCBC surfaces have -OH, C=C, and C=O functional groups that could serve as π-electron donors. As a result, the π-π interaction may be used to modulate the adsorption of OTC onto the surface of MnO₂/PCBC (G. Liang et al., 2019; J. Luo et al., 2018). Additionally, the functional groups of the OTC and the benzene ring of the surface of MnO₂/PCBC may serve as H-bond

donors, suggesting that hydrogen bonding may have increased the sorption affinity of MnO₂/PCBC for OTC (G. Liang et al., 2019; J. Luo et al., 2018). Figure 4.13c displays the possible adsorption mechanism of MnO₂/PCBC for OTC.

4.3. Conclusion

This study explored the adsorption of oxytetracycline by MnO₂/PCBC with remarkable success. The research achieved a remarkable removal efficiency of 88.1% under optimized conditions of pH 8, adsorbent dosage 0.44 g/L, initial OTC concentration 200 mg/L, and temperature 303 K. The PSO ($R^2=0.99$) model was found to be the best fit for the adsorption kinetics. The adsorption process conformed well to both Langmuir ($R^2=0.95$) and Freundlich ($R^2=0.95$) isotherm models, with a monolayer adsorption capacity (q_m) of 357.14 mg/g. Notably, the adsorption of oxytetracycline on the adsorbent is spontaneous and endothermic. It is also worth noting that MnO₂/PCBC is recyclable and reusable as an effective adsorbent for antibiotic removal from water. The mechanism underlying OTC adsorption by MnO₂/PCBC primarily involves hydrogen bonding, π - π electron donor acceptor interactions, pore filling and electrostatic interactions. Importantly, MnO₂/PCBC demonstrated the highest maximum removal efficiency for OTC compared to most of the reported adsorbents in previous studies. These findings hold significant promise for environmental engineers, suggesting that MnO₂/PCBC can be strategically employed to effectively mitigate OTC contamination in aqueous environments simultaneously mitigating the waste management of pine cones in the forest areas of Himachal Pradesh.

Chapter 5
ADSORPTION OF TETRACYCLINE BY MANGANESE
OXIDE-MODIFIED PINE CONE BIOCHAR

Chapter 5

ADSORPTION OF TETRACYCLINE BY MANGANESE OXIDE-MODIFIED PINE CONE BIOCHAR

5.1. Introduction

Tetracycline (TC) is a widely employed antibiotic in modern medicine, serving to combat or prevent infections in both humans and animals. As a bacteriostatic agent, it is effective against a spectrum of pathogens, including gram-positive and gram-negative bacteria, mycoplasma, and certain fungi (Asgharian et al., 2020). Despite their significant contributions to human welfare, a notable proportion of antibiotics, estimated to be between 70% to 90%, are released into the environment during practical use. This is primarily due to their limited absorption and metabolism within the body (Sun et al., 2021). TC has been detected in treated waters at extremely low concentrations, typically in the range of micrograms per liter ($\mu\text{g/L}$) or nanograms per liter (ng/L). However, its levels are significantly higher, ranging from 100 to 500 milligrams per liter (mg/L), in the effluents of hospital and pharmaceutical manufacturing wastewaters (Asgharian et al., 2020).

Tetracyclines found in soil can contribute to the development of antibiotic-resistant microbial populations, posing a threat to environmental health. Furthermore, their presence in soil, as well as in underground and surface waters, can lead to the destruction of microorganisms and disruption of natural microbial communities. This disruption may further contribute to the evolution of antibiotic-resistant pathogenic microorganisms. Therefore, it is imperative to prioritize the development of efficient and sustainable methods for removing tetracycline from water. Doing so is crucial for enhancing water quality, mitigating harm to public health, and advancing the adoption of low-cost wastewater treatment technologies (Tanyol & Torğut, 2022). Various methods have been employed for the removal of TC, encompassing biodegradation (Shao et al., 2018), photocatalysis (Saadati

et al., 2016; L. Yao et al., 2021), membrane filtration (Košutić et al., 2007), ozonation (M. H. Khan et al., 2010), photolysis (Jiao et al., 2008), catalysis (Hao et al., 2021), electrochemical oxidation (Jianbing Wang et al., 2018), and adsorption (Priya & Radha, 2017).

Adsorption is regarded as the most practical method among these techniques for eliminating stubborn pollutants from water due to its simple operation, high efficiency, and absence of harmful byproducts (Prakash Bobde, Sharma, Kumar, Pal, et al., 2023). Biochar has garnered significant attention as an adsorbent owing to its efficient conversion of waste into a usable form and its ability to remove various stubborn pollutants from water (Prakash Bobde, Sharma, Kumar, Pal, et al., 2023; Vievard et al., 2023). It is produced by pyrolyzing waste biomass, including coconut husk, pine needles, pine cones, agricultural waste, peanut waste, and pineapple peel, resulting in excellent yield (Prakash Bobde, Sharma, Kumar, Pal, et al., 2023; Kumar et al., 2023; Vievard et al., 2023). Chir pine, prevalent in regions like India, is generated in vast quantities which can be utilized as an organic resource for biochar production. Through the sustainable utilization of vast quantities of pine tree biomass (Kumar et al., 2023), we can prevent forest fires taking place due to highly combustible needles and twigs (Fulé et al., 2021). Pine-cone biochar is regarded as an effective adsorbent due to its high porosity, distinctive chemical composition, surface chemistry, cost-effectiveness, and status as a renewable and sustainable resource (Kumar et al., 2023).

Because of its inherent low adsorption capacity for antibiotics (Feng et al., 2021b), modifying biochar is crucial to optimize its surface properties and improve its ability to effectively adsorb specific pollutants. Manganese oxide (MnO_2) nanoparticles have emerged as a highly promising and efficient adsorbent, garnering increased attention for their high specific surface area, catalytic effect and exceptional adsorption capability (Feng et al., 2021b). By incorporating MnO_2 into biochar, its adsorption capacity can be significantly enhanced, offering several key advantages (Feng et al., 2021b). The porous

structure of MnO_2 substantially augments the available surface area for adsorption, thereby providing a greater number of active sites for pollutant attachment (Jiang Li et al., 2020).

Therefore, this study aims to assess the efficacy of MnO_2/PCBC in removing TC from water, considering experimental variables such as pH, initial TC concentration, MnO_2/PCBC dosage, and temperature.

5.2. Results & Discussion

5.2.1. Selection of the adsorbent

The removal efficiency of many adsorbents for the contaminant Tetracycline (TC) is shown in figure 5.1a. With 79.7% TC removal effectiveness, MnO_2/PCBC demonstrated highest adsorption for TC. As a result of its greater ability to remove TC, MnO_2/PCBC is the most effective adsorbent and is chosen for the removal of TC from water.

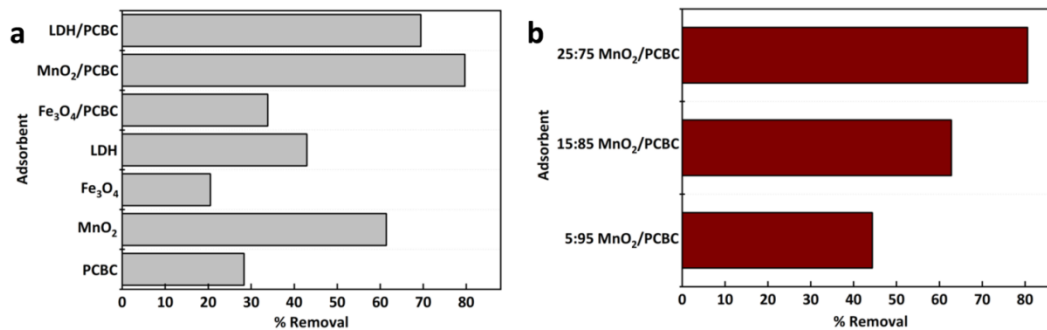
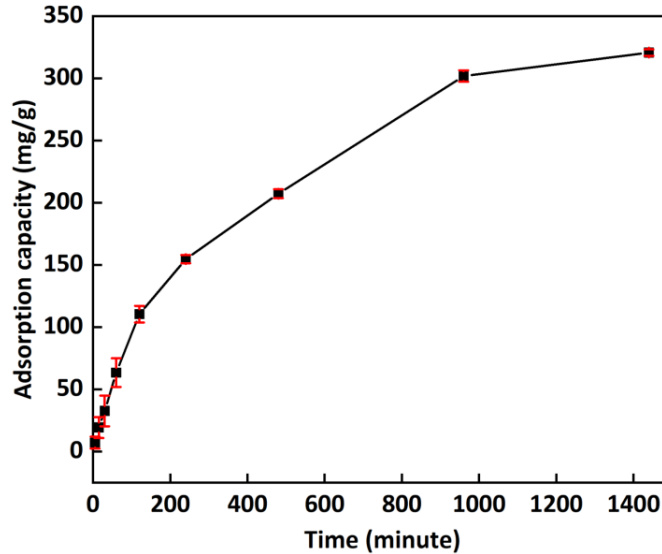


Figure 5.1: Comparison of different adsorbent for the removal of TC

The efficiencies of several MnO_2/PCBC composite materials for the removal of TC, namely 5:95 MnO_2/PCBC , 15:85 MnO_2/PCBC , and 25:75 MnO_2/PCBC , were determined and plotted in figure 5.1b. With 80.6% TC removal efficiency, the 25:75 MnO_2/PCBC composite outperformed the other adsorbents. Due to the better ability of 25:75 MnO_2/PCBC to remove TC, this composition of adsorbent is used for the optimization of parameters for the removal of TC.

5.2.2. Effect of contact time on the adsorption of TC

Tetracycline (TC)'s adsorption capability onto the MnO₂/PCBC over a range of time intervals is depicted in figure 5.2. The adsorption process is time-dependent



and continues as the length of exposure of TC to the adsorbent grows, as evidenced by the exponentially increasing trend of adsorption capacity with time. The adsorption capacity is 7.30 mg/g at 5 minutes, which is rather low at first, but it increases progressively over time. Notably, the adsorption capacity achieves its highest value of 320.66 mg/g at 1440 minutes, indicating the maximum adsorption of TC at equilibrium.

Figure 5.2: Effect of the amount of TC adsorbed (mg/g) against contact time onto MnO₂/PCBC

5.2.3. RSM study

Using a central composite design (CCD) analysis, the TC removal process for the MnO₂/PCBC was optimized. The study employed four primary independent characteristics, including pH, MnO₂/PCBC dosage, and starting TC concentration, and temperature. Table 5.1 shows the experimental and predicted values for adsorption of TC on MnO₂/PCBC obtained through CCD and RSM. According to the quadratic model, there is a relationship between response (percentage removal) and operational parameters (Al-Qahtani et al., 2023; Huihui Wang et al., 2022). The expected TC percentage removal, is represented by linear terms in

equation 5.1, and A, B, C and D stand for the coded values of pH, MnO₂/PCBC dosage, initial TC concentration, temperature, respectively. In this equation, the quadratic terms are A², B², C² and D², and the interaction terms are AB, AC, AD, BC, BD, and CD. The antagonistic and synergistic impacts of the parameters are represented by the positive and negative signs in the preceding equation 5.1 (Al-Qahtani et al., 2023; Ayyubi et al., 2022).

$$\% \text{ removal} = -786.6535 - 11.8421A - 94.7399B + 0.5659C + 5.8444D - 1.2366A^2 - 26.6596B^2 - 0.0014C^2 - 0.0101D^2 + 1.2639AB - 0.0001AC + 0.0755AD - 0.0737BC + 0.4217BD - 0.0012CD \quad (5.1)$$

Table 5.1: Experimental and predicted values for adsorption of TC on MnO₂/PCBC obtained through CCD and RSM

Run No.	A	B (g/L)	C (mg/L)	D (K)	Experimental	Predicted	Residual
1	3	0.1	50	283	87.56	83.62	3.94
2	11	0.1	50	283	18.66	22.38	-3.72
3	3	0.5	50	283	89.36	87.11	2.25
4	11	0.5	50	283	23.25	29.91	-6.66
5	3	0.1	200	283	55.63	63.38	-7.75
6	11	0.1	200	283	8.64	1.99	6.65
7	3	0.5	200	283	55.90	62.44	-6.54
8	11	0.5	200	283	11.49	5.10	6.39
9	3	0.1	50	313	79.05	84.10	-5.05
10	11	0.1	50	313	46.09	40.99	5.11
11	3	0.5	50	313	84.57	92.65	-8.08
12	11	0.5	50	313	62.67	53.58	9.09
13	3	0.1	200	313	63.81	58.58	5.23
14	11	0.1	200	313	14.41	15.32	-0.91
15	3	0.5	200	313	67.76	62.71	5.06
16	11	0.5	200	313	18.12	23.49	-5.37
17	2	0.3	125	298	89.67	80.95	8.72
18	12	0.3	125	298	9.68	18.16	-8.48
19	7	0.05	125	298	72.34	75.16	-2.82
20	7	0.55	125	298	85.51	82.45	3.06
21	7	0.3	31.25	298	85.96	83.50	2.46
22	7	0.3	218.75	298	49.82	52.04	-2.22
23	7	0.3	125	279.25	75.33	71.01	4.32
24	7	0.3	125	316.75	78.73	82.81	-4.08
25	7	0.3	125	298	79.29	80.47	-1.18
26	7	0.3	125	298	80.43	80.47	-0.04
27	7	0.3	125	298	81.11	80.47	0.64

Analysis of variance (ANOVA) was used to evaluate the suggested model's efficacy. Table 5.2 shows the experimental design and expected results for the removal of TC on the basis of ANOVA. When the p value is < 0.05 , model terms are deemed significant. A, C, and A^2 are significant model terms in this case, and the strong F value of 23.34 indicates the significance of the model. Only 0.01% of cases might have an F-value this high due to noise. The quadratic model appears to be a viable option for forecasting the efficacy of DS removal, as evidenced by the close proximity of the adjacent R^2 of 0.92 to the predicted R^2 of 0.75.

Table 5.2: Analysis of variance for adsorption capacity of TC by using $MnO_2/PCBC$

Source	Sum of square	of DDL	Mean square	F-value	P-value
Model	20757.77	14	1482.7	23.34	< 0.0001
A-pH	12061.45	1	12061.45	189.9	< 0.0001
B- $MnO_2/PCBC$ dose	162.46	1	162.46	2.56	0.1357
C-TC initial concentration	3027.27	1	3027.27	47.66	< 0.0001
D-Temperature	425.59	1	425.59	6.7	0.0237
pH* $MnO_2/PCBC$ dose	16.36	1	16.36	0.2576	0.621
pH*TC initial concentration	0.0215	1	0.0215	0.0003	0.9856
pH*Temperature	328.76	1	328.76	5.18	0.0421
$MnO_2/PCBC$ dose*TC initial concentration	19.58	1	19.58	0.3083	0.5889
$MnO_2/PCBC$ dose*Temperature	25.61	1	25.61	0.4033	0.5373
TC initial concentration*Temperature	27.84	1	27.84	0.4384	0.5204
(pH) ²	2294.79	1	2294.79	36.13	< 0.0001
($MnO_2/PCBC$ dose) ²	6.67	1	6.67	0.1049	0.7516
(TC initial concentration) ²	387.34	1	387.34	6.1	0.0295
(Temperature) ²	30.46	1	30.46	0.4796	0.5018
Total Error	762.19	12			
Total (corr.)	21519.96	26			

The % removal of the TC shows a noticeable trend as the pH of the solution rises from 3 to 11. There is a high percentage removal at lower pH level (3- 5), indicating that the TC has been effectively removed from the solution. This implies that the TC might be eliminated more easily in an acidic environment.

The percentage removal, however, somewhat reduce when pH rises above 5, but it still stays very high until pH 7 or so. There is still a considerable percentage removal at pH 7 (neutral), but it starts to decrease more distinctly as the pH rises towards alkalinity. The percent removal decreases more sharply at pH values higher than 7, suggesting that TC is less successfully eliminated in an alkaline environment. This implies that removal efficiency declines with increasing solution pH.

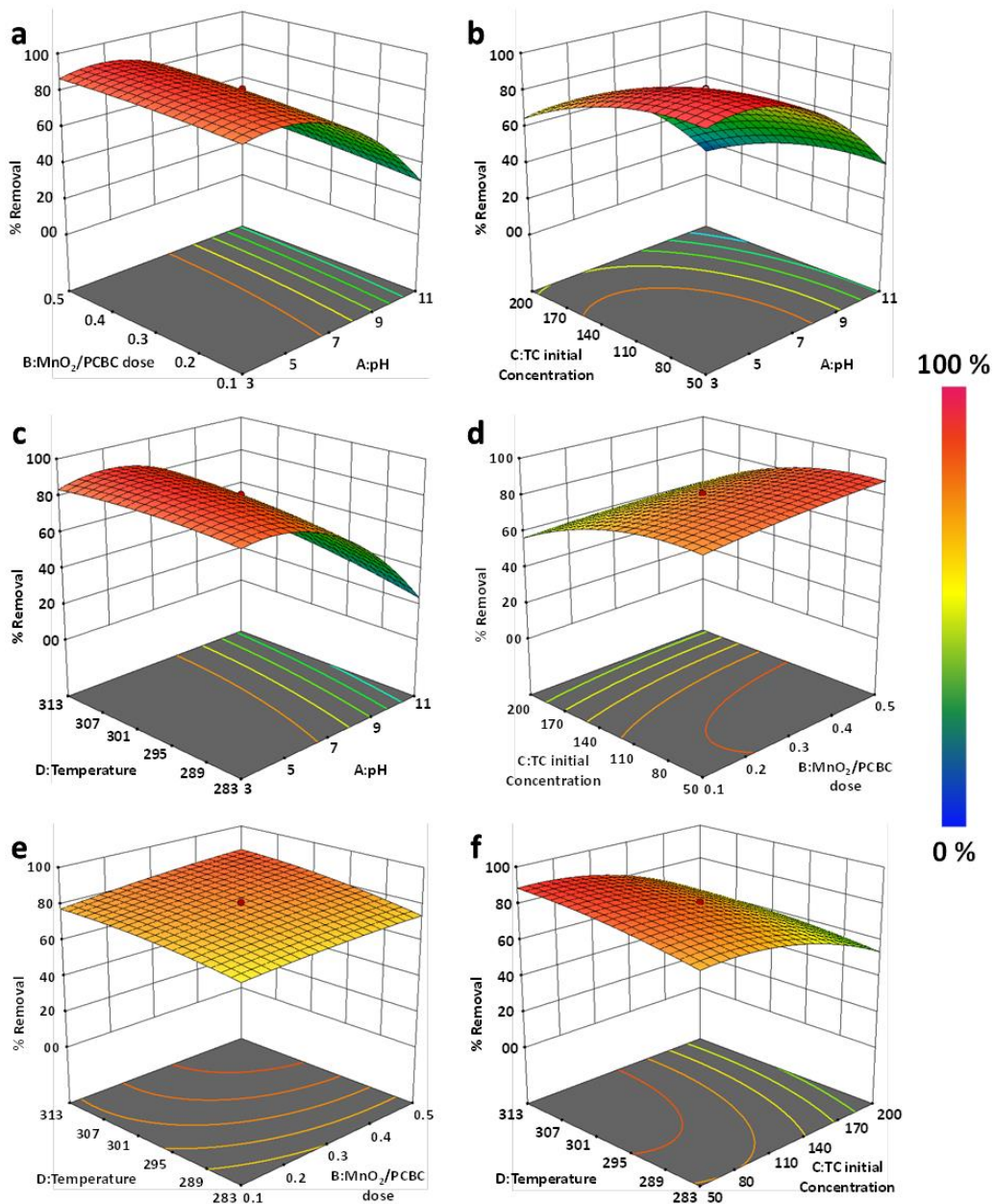


Figure 5.3: 3D surface graphs of percent removal efficiency of TC by using $MnO_2/PCBC$

The results show a strong positive association between the percentage of TC removed and the dose of $MnO_2/PCBC$ (Fig. 5.3). The removal effectiveness of TC consistently improves with incremental dosage in the range 0.1 to 0.5 g/L, as seen by the percentage removal rising from 89.8% to 96.4%. This pattern implies that TC removed from the system more successfully at larger $MnO_2/PCBC$

dosages. This could be explained by the fact that there are more active sites available for chemical reactions at greater doses, which enables complete adsorption and the subsequent removal of TC from the water (Althumayri et al., 2023).

Fig. 5.3 shows a substantial correlation between the percentage of TC removed and the initial concentration of TC. Interestingly, the percentage elimination gradually decreases from 96.2% to 69% when the initial TC concentration rises from 50 to 200 mg/L. This inverse relationship implies that removing TC across the course of treatment will be more difficult at higher initial doses. The tendency may be caused, in part, by the treatment system's available reactive sites being saturated as TC concentrations rise. Higher initial concentrations may overwhelm the treatment mechanism, reducing its efficacy and efficiency in reducing TC pollutants from the water sample (Al-Hazmi, Adam, et al., 2023; Althumayri et al., 2023). Higher initial concentrations may also cause more competition for reactive sites, which would slow down adsorption even further and produce a lower removal percentage overall.

The data demonstrates a strong positive association between temperature and percentage of TC elimination. The percentage removal rises steadily and significantly from 85.6% to 99.2% as the temperature rises from 278K to 313K. According to this pattern, increasing the temperature considerably improves the removal of TC from water. Higher temperatures may also increase the mobility of reactant molecules, which would allow for more contact between the TC and the MnO_2/PCBC and ultimately increase the removal efficiency (Al-Hazmi, Refat, et al., 2023; Althumayri et al., 2023; Hasan et al., 2023).

5.2.4. Optimization of the adsorption of TC

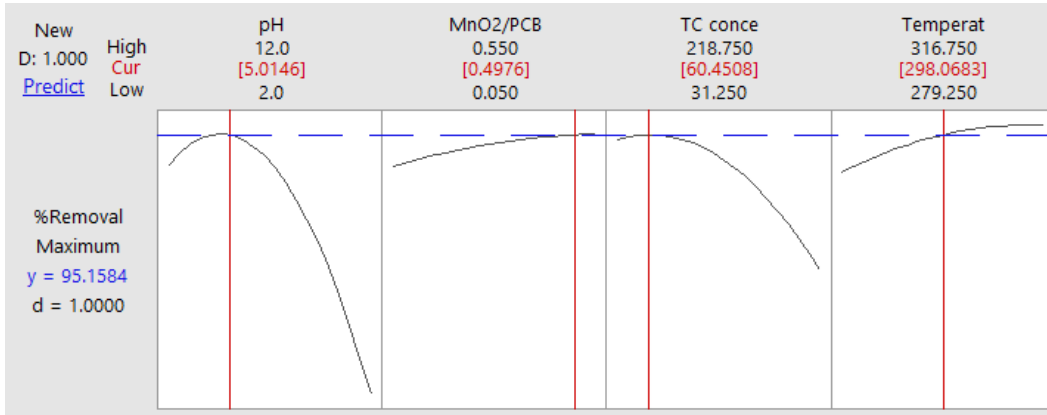


Figure 5.4: Optimization of adsorption process of TC onto MnO₂/PCBC

The optimal values for TC adsorption onto MnO₂/PCBC adsorbent are shown in the table 5.3. The expected percentage removal of TC is 95.16% at a pH of 5.00, an adsorbent dosage of 0.5 g/L, an initial TS (total solids) concentration of 60.45 mg/L, and a temperature of 298K (Fig. 5.4). A high degree of agreement between the expected and observed results is indicated by the fact that the expected percentage removal of TC closely matches the experimental result of 94.9%. This shows that MnO₂/PCBC exhibits effective adsorption capabilities for removing TC from the solution under these particular conditions.

Table 5.3: Optimum values for adsorption of TC onto MnO₂/PCBC

Adsorbent	A	B (g/L)	C (mg/L)	D (°K)	% Removal	
					Predicted	Experimental
PCBC	5.00	0.5	60.45	298	95.16	94.89

A-pH, B- MnO₂/PCBC dose, C-Initial TC concentration, and D-Temperature

5.2.5. Kinetic, isotherm and thermodynamic study

The kinetic parameters for the adsorption of TC onto MnO₂/PCBC are displayed in Table 5.4. These values, which explain the adsorption process, are obtained from different kinetic models. The equilibrium adsorption capacity, or q_e , is determined using PFO equation to be 319.89 mg/g, with a rate constant (K_1) of 0.0028 min⁻¹ and a R^2 value of 0.9797. A rate constant (K_2) of 8.33 x 10⁻⁶ g·mg⁻¹

$^1 \cdot \text{min}^{-1}$, a q_e value of 384.61 mg/g, and a R^2 value of 0.9909 are obtained from PSO equation. The R^2 value of the Elovich model is 0.9176, and its coefficients, α and β , are 5.2290 and 0.0168 accordingly. Finally, a R^2 value of 0.9826 is obtained from the intraparticle diffusion model, which yields a diffusion rate constant (K_i) of 9.3588 mg/g·min^{0.5} and a constant intercept (c) of -6.7256 (Fig. 5.5)

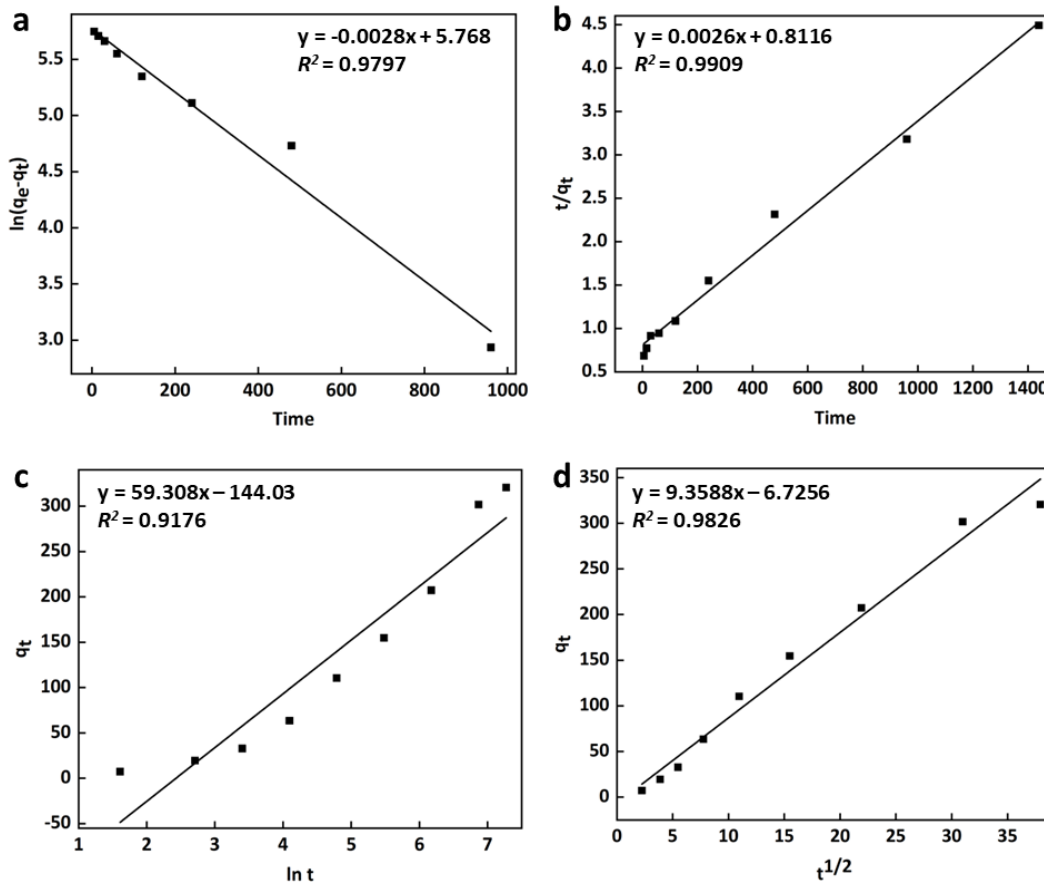


Figure 5.5: (a) PFO and (b) PSO (c) Elovich and (c) ID plots for the adsorption of TC on MnO₂/PCBC. Experimental conditions: MnO₂/PCBC dose = 0.5 g/L, Initial concentration of TS = 60 mg/L, Temperature = 298 K, pH = 5.

With the highest R^2 value (0.9909), which indicates a stronger correlation between the experimental and predicted values, the PSO kinetic model seems to be the best fit for explaining the adsorption of TC onto MnO₂/PCBC, according to the coefficient of determination (R^2) values. According to this model, the

adsorption process is most likely controlled by chemisorption mechanism, in which the adsorbent and TC molecules create chemical interactions that increase adsorption capacity and improve adsorption (Ho & McKay, 1999).

Table 5.4: Kinetic parameters for the adsorption of TC onto MnO₂/PCBC

	C_0 (mg/L)	200
	Theoretical q_e (mg/g)	320.66
PFO equation	q_e (mg/g)	319.89
	K_1 (min ⁻¹)	0.0028
	R^2	0.9797
PSO equation	q_e (mg/g)	384.61
	K_2 (g.mg ⁻¹ .min ⁻¹)	8.33 x 10 ⁻⁶
	R^2	0.9909
Elovich	α	5.2290
	β	0.0168
	R^2	0.9176
ID	K_i (mg/g.min ^{1/2})	9.3588
	c	-6.7256
	R^2	0.9826

Table 5.5 outlines the different isotherm parameters related to the adsorption of TC onto MnO₂/PCBC. The estimated K_L value of 90.090 L/g in the Langmuir isotherm model shows a high affinity between the MnO₂/PCBC and TC, however the a_L value of 0.3063 L/mg indicates a moderate adsorption capacity. Adsorbent efficiency in adsorbing TC molecules is indicated by the Q_0 value of 294.12 mg/g, which represents the highest monolayer adsorption capacity of the material. Since the R_L value of 0.0613 is between 0 and 1, it suggests favorable adsorption. The Langmuir model fits the experimental data quite well, exhibiting a very high coefficient of determination ($R_2 = 0.9997$). This indicates that the adsorption process is characterized by monolayer adsorption, where the active sites are distributed uniformly over the adsorbent surface (Langmuir, 1916) (Fig. 5.6).

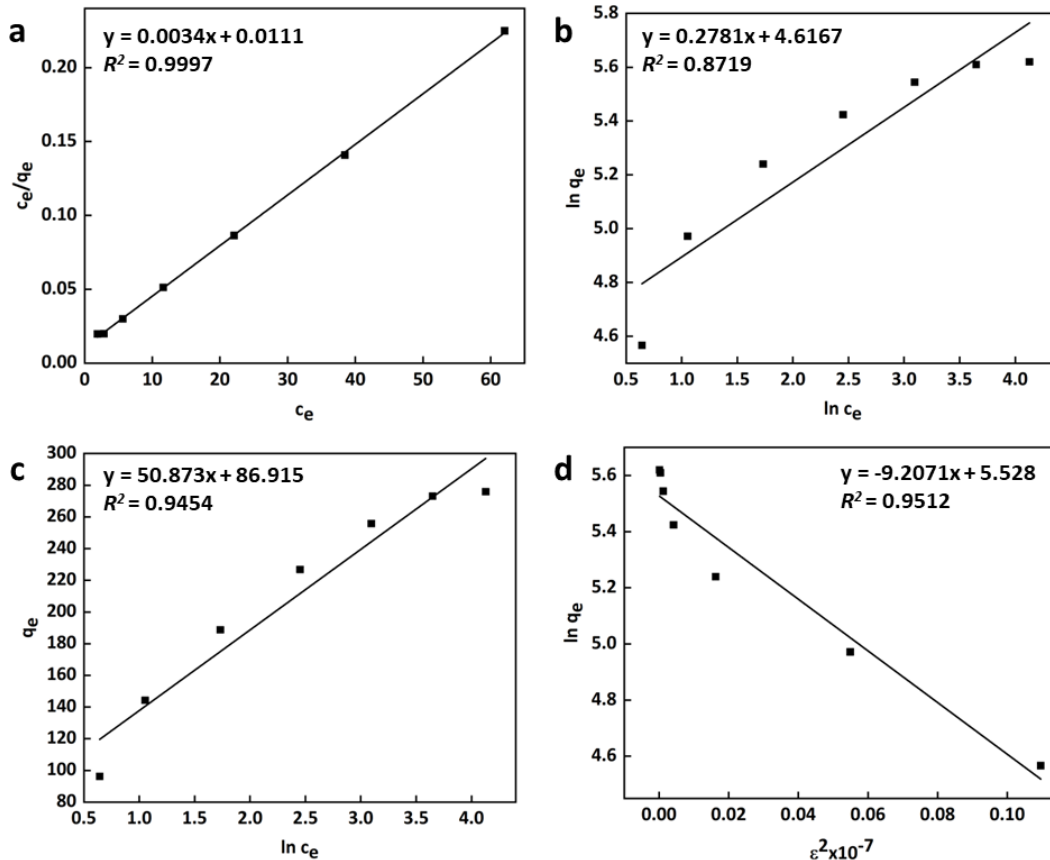


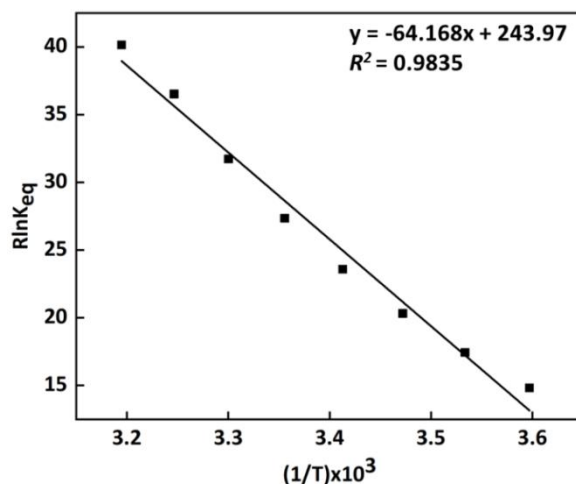
Figure 5.6: (a) Langmuir (b) Freundlich (c) Temkin and (d) Dubinin-Radushkevich plots for the adsorption of TC on MnO₂/PCBC. Experimental Conditions: MnO₂/PCBC dose= 0.5 g/L, shaking time = 1440 min., Temperature = 298 K, pH = 5

However, the Dubinin-Radushkevich, Temkin, and Freundlich isotherm models also offer important insights into the behavior of adsorption. A high adsorption capacity is indicated by the Freundlich model's K_f value of 101.16, and a favorable adsorption process is suggested by its n value of 3.5958. In contrast to the Langmuir model, it has a lower coefficient of determination ($R^2 = 0.8719$), suggesting a less precise fit to the experimental data. Similarly, the greatest binding energy in the Temkin model is indicated by an A value of 5.5205, while the B value of 50.873 indicates a moderate bonding energy between the TC and MnO₂/PCBC.

Table 5.5: Isotherm parameters for the adsorption of TC onto MnO₂/PCBC

Langmuir	K_L (L/g)	90.090
	a_L (L/mg)	0.3063
	Q_o (mg/g)	294.12
	R_L	0.0613
	R^2	0.9997
Freundlich	K_f	101.16
	n (g/L)	3.5958
	R^2	0.8719
Temkin	B	50.873
	A (L/g)	5.5205
	R^2	0.9454
Dubinin-Radushkevich	q_m (mg/g)	251.64
	β (mol ² k/J ²)	9.207×10^{-7}
	E (kJ/mol)	736.92
	R^2	0.9512

Despite showing a fair fit ($R^2 = 0.9454$), the Temkin model is not as excellent as the Langmuir model. The Dubinin-Radushkevich model, in comparison to the Langmuir model, suggests a lower theoretical monolayer adsorption capacity, as indicated by its q_m value of 251.64 mg/g. In terms of accuracy and fit to the experimental data, it still lags the Langmuir model, even with a comparatively high R^2 value (0.9512). Because of its better fit, the Langmuir isotherm model is thus the most appropriate one to describe the adsorption of TC onto MnO₂/PCBC.

**Figure 5.7:** Plot of $R \ln K_{eq}$ versus $(1/T) \times 10^3$ (K⁻¹) for estimation of thermodynamic parameters.

For the adsorption of TC onto MnO₂/PCBC at different temperatures, Figure 5.7 shows the plot of equilibrium constant of adsorption of TC versus 1/T and the thermodynamic parameters are shown in the table 5.6. As can be seen from the positive enthalpy change (ΔH°) of 64.168 kJ/mol, the process is endothermic and that energy is absorbed during adsorption. This finding is further supported by the positive entropy change (ΔS°) of 243.97 J/mol·K, which shows an increase in disorder or randomness throughout the adsorption process. It is also implied that the adsorption process is spontaneous and thermodynamically favorable indicated by the negative Gibbs free energy change (ΔG°) at each temperature. Hence, TC adsorption onto MnO₂/PCBC is influenced by both entropic and enthalpic forces, with rising temperatures favouring the spontaneity of the adsorption process (Al-Hazmi, Refat, et al., 2023; Althumayri et al., 2023; Hasan et al., 2023).

Table 5.6: Thermodynamic parameters for the adsorption of TC onto

MnO ₂ /PCBC		
	ΔH° (kJ/mol)	64.168
	ΔS° (J/mol)	243.97
	278 K	-2.436
	283 K	-4.876
	288 K	-6.095
ΔG° (kJ/mol)	293 K	-7.315
	298 K	-8.535
	303 K	-9.755
	308 K	-10.975
	313 K	-12.195

The table 5.7 provides a comparative analysis of the literature-reported TC adsorption onto various adsorbents. Based on factors including initial concentration of TC, adsorbent dosage, pH, temperature, time, removal efficiency, and adsorption capacity, several adsorbents are investigated. On the other hand, MnO₂/PCBC in this study shows an adsorption capacity of 294.12 mg/g and a removal efficiency of 94.89%. This indicates that MnO₂/PCBC

performs competitively with respect to the other adsorbents under investigation, providing notable adsorption capacity and efficient TC removal.

Table 5.7: Comparison of TC adsorption onto different adsorbents reported in literature.

Adsorbent	c_0 (mg/L)	Dosage (g/L)	pH	Temp (K)	Time (min.)	Removal (%)	q_e (mg/g)	Reference
MnFe ₂ O ₄ /Multi-Wall Carbon Nanotubes	20	0.012	5.43	288-318	120	99.16	-	(Zhao et al., 2023)
Chitosan-graft-poly(N-tert-butylacrylamide) Copolymer	100	0.03	-	-	52	-	104.81	(Tanyol & Torğut, 2022)
Biochar/Fe ₃ O ₄	100	0.3	4	298	1440	88.3	153.9	(Sun et al., 2021)
Aluminosilicate zeolite nanoparticle	-	-	6.7	-	20	97	454.55	(Al-Salihi et al., 2023)
Biomass-based material prepared by sulfuric acid reflux	50-500	0.02	-	-	1440	-	357.14	(Islam et al., 2018)
MnO ₂ modified pine cone bio-based adsorbent (MnO ₂ /PCBC)	60.45	0.5	5	298	1440	94.89	294.12	This study

5.2.6. Regeneration study

Regeneration study shows the average percentage of TC removed by MnO₂/PCBC over number of adsorption cycles. The average percentage removal gradually decreases from cycle 1 to cycle 5 of the adsorption process, from 95.25% to 91.25% by the fifth cycle. The decrease in TC removal efficiency of MnO₂/PCBC may be due to loss of adsorbent during washing to regenerate the adsorbent and as a result of changes in the adsorbent's characteristics brought about by frequent use or saturation of active sites on the adsorbent surface. However, marginal decrease in removal efficiency (~4% over 5 cycles) emphasizes that MnO₂/PCBC can be sustainably employed for TC removal from water.

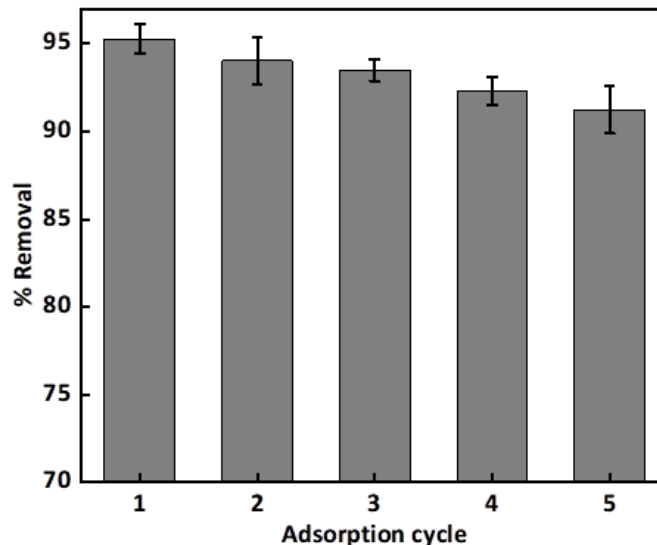


Figure 5.8: Regeneration of MnO₂/PCBC for TC adsorption

5.2.7. Adsorption mechanism

The addition of 1 mM EDTA-2Na to the solution was implemented to assess its impact on the adsorption efficiency of TC onto MnO₂/PCBC (Fig. 5.9a). Upon introduction of EDTA, there was a notable reduction in the removal rate of TC by approximately 22%. This decline suggests that surface complexation plays a significant role in the adsorption process. Specifically, manganese oxide within MnO₂/PCBC forms complexes with functional groups such as -NH₂ and reactive oxygen-containing moieties present in TC molecules. This complexation process facilitates efficient adsorption of TC (Xinyi Liao et al., 2023).

In Figure 5.9b, the FTIR spectra of MnO₂/PCBC before and after TC removal are compared. A discernible shift in the vibrational bands is observed, transitioning from 3426 cm⁻¹, 2920 cm⁻¹, 1616 cm⁻¹, 1383 cm⁻¹, and 524 cm⁻¹ in MnO₂/PCBC before TC adsorption to 3437 cm⁻¹, 2922 cm⁻¹, 1631 cm⁻¹, 1384 cm⁻¹, and 585 cm⁻¹ after TC adsorption. This shift in vibrational bands indicates alterations in the surface functional groups of MnO₂/PCBC as a result of TC adsorption. The FTIR study reveals the presence of various functional groups such as -OH, C-H groups in aromatic rings, and phenolic -OH bonds on the surface of MnO₂/PCBC, which likely contribute towards the TC adsorption process. further enhancing the adsorption mechanism (Jie Li et al., 2018). These findings underscore the intricate

interplay between surface functional groups and molecular interactions in facilitating the adsorption of TC onto MnO₂/PCBC.

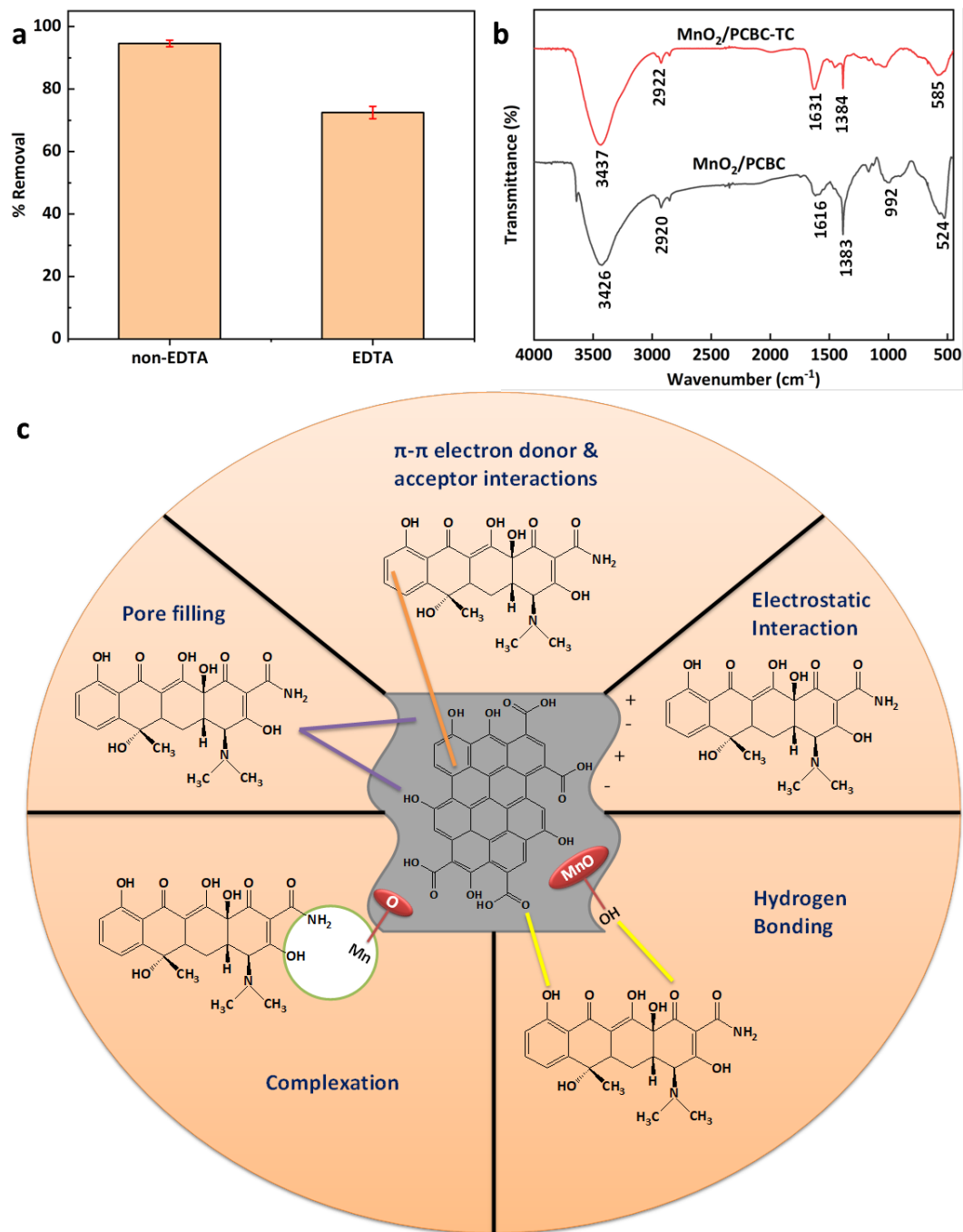


Figure 5.9: (a) Effect of EDTA on the adsorption of TC onto MnO₂/PCBC, (b) FTIR spectra of MnO₂/PCBC before and after adsorption of TC (MnO₂/PCBC - TC), (c) Proposed adsorption mechanism of TC adsorption on MnO₂/PCBC.

Additionally, the predominant aromatic composition of MnO₂/PCBC suggests potential π - π donor-acceptor interactions with electron-deficient TC molecules.

Table 5.8: Physicochemical properties of MnO₂/PCBC before and after TC adsorption

Adsorbent	Specific Surface Area (SSA) (m ² /g)	Total pore volume (cm ³ /g)	Average pore size (nm)
MnO ₂ /PCBC	50.83	0.1118	4.3967
MnO ₂ /PCBC after TC adsorption	17.38	0.0538	6.1909

In table 5.8, it is noted that the specific surface area (SSA), and overall pore volume of MnO₂/PCBC decreased after TC adsorption. This observation suggests that pore filling could be a significant factor influencing TC adsorption onto MnO₂/PCBC. According to Liang et al., the SSA and pore structure are crucial variables affecting the adsorption of organic pollutants on bio-based adsorbents through the pore-filling mechanism. This implies that changes in pore characteristics, such as reduced pore size and SSA, could impact the adsorption capacity and efficiency of MnO₂/PCBC for TC removal (H. Liang et al., 2022).

During the process of TC adsorption using MnO₂/PCBC (with a pH_{pzc} of 7.40) at acidic pH levels (below the first dissociation constant pK_{a1}=3.32 of TC), the surface functional and unsaturated groups of MnO₂/PCBC undergo protonation, resulting in minimal π electron interaction with TC. However, as the pH increases from 3.32 to 7.78 (pK_{a2}), TC adopts a zwitterionic form, acting both as a π donor and an acceptor, facilitating interactions with the MnO₂/PCBC surface (Atugoda et al., 2021). Additionally, the -OH and -COOH groups present on the MnO₂/PCBC surface may establish hydrogen bonds with N-containing moieties on TC molecules. Furthermore, the functional groups of TC and the benzene ring on the surface of MnO₂/PCBC may act as H-bond donors, potentially enhancing the sorption affinity of MnO₂/PCBC for TC (G. Liang et al., 2019; J. Luo et al.,

2018). This suggests that hydrogen bonding could play a crucial role in the adsorption mechanism of MnO₂/PCBC for TC, as illustrated in Figure 5.9c.

5.3. Conclusion

Using a number of tests and studies, the adsorption of tetracycline (TC) onto MnO₂/PCBC was carefully examined. MnO₂/PCBC shows promise for use in water treatment applications due to its efficient adsorption capabilities for TC removal, with an optimized removal effectiveness of 94.89% achieved under optimum conditions. The central composite design (CCD) analysis used to optimize TC removal showed that temperature, pH, MnO₂/PCBC dose, and initial TC concentration are important determinants of adsorption efficiency. With an adjusted R^2 of 0.9233, the quadratic model demonstrated a good association between the response (% elimination) and operational parameters. The PSO model fits the process, and the Langmuir isotherm model fits the experimental data remarkably well, suggesting monolayer adsorption. The adsorption process appears to be endothermic, spontaneous, and advantageous at elevated temperatures. Furthermore, using EDTA-2Na studies and FTIR spectroscopy, the effects of surface complexation and hydrogen bonding on adsorption efficiency are clarified. The importance of these mechanisms is demonstrated by the decrease in removal rate with EDTA addition and the observed alterations in vibrational bands. Moreover, the reduction in both specific surface area and total pore volume subsequent to TC adsorption implies that pore filling plays a crucial role in adsorption. In the end, it is concluded that MnO₂/PCBC is a sustainable adsorbent for the removal of TC wherein TC is adsorbed onto the adsorbent mainly by surface complexation, hydrogen bonding and pore filling mechanisms,

Chapter 6

ADSORPTION OF CIPROFLOXACIN BY LAYERED DOUBLE HYDROXIDE-MODIFIED PINE CONE BIOCHAR

Chapter 6

ADSORPTION OF CIPROFLOXACIN BY LAYERED DOUBLE HYDROXIDE-MODIFIED PINE CONE BIOCHAR

6.1. Introduction

Antibiotics are categorized as emerging contaminants as they are found in the environment at very low concentrations (Ashiq et al., 2019; J. R. de Andrade et al., 2020; Kiecak et al., 2019; Saxena et al., 2021) and are persistent. Antibiotics enter the environment through various pathways, including wastewater discharge and agricultural runoff (Prakash Bobde et al., 2021). Their presence in water bodies and soil has disrupted ecosystems, potentially contributed to antibiotic resistance in bacteria, and posed risks to aquatic and terrestrial organisms, including humans (Prakash Bobde et al., 2021). In wastewater, their concentrations typically vary in the range of ng/L to µg/L, while in industrial and hospital effluents, they can be found in mg/L (Kiecak et al., 2019; Maged et al., 2020).

Ciprofloxacin (CPF) is an antibiotic that is commonly utilized to manage bacterial infections in humans and animals. It belongs to the fluoroquinolone class of antibiotics and is known to have a broad spectrum of activity against a wide range of bacteria (Wakejo et al., 2022). However, the use and disposal of CPF can lead to its presence in the environment, including surface water bodies and groundwater (Jie Li et al., 2018). After administration, CPF and its metabolites are excreted in urine and feces. Approximately 15–50% of the administered dose is expelled unaffected in urine within 24 hours, while 10–15% is excreted as metabolites. In feces, around 20–40% of the dose is excreted unchanged or as metabolites over a period of 5 days (Antonelli et al., 2020).

The presence of CPF and other antibiotics in the environment raises concerns due to their potential impact on ecosystems and human health. Removing CPF from aqueous solutions is necessary to protect the environment and public health (Jie Li

et al., 2018). Their low concentration in water sources necessarily demands effective monitoring and removal strategies to mitigate their adverse effects. Various techniques exist in the literature demonstrating the elimination of CPF from aqueous solution, including adsorption (Alonso et al., 2018; Ezekoye et al., 2020; C. Liang et al., 2018), ozonation (Asif et al., 2021), photocatalytic degradation (X. X. Zhang et al., 2015), photochemical oxidation (Mahdi-Ahmed & Chiron, 2014), electro-coagulation (Parsa et al., 2016), biodegradation (Xiaobin Liao et al., 2016) and catalytic oxidation (Nemati Sani et al., 2019).

Adsorption is extensively employed for removing contaminants, including CPF, from aqueous solutions (Al-Musawi, Mahvi, et al., 2021; Guzel Kaya et al., 2021; Ji et al., 2021). It involves physical / chemical fixation of the contaminants onto the surface of the adsorbent, such as activated carbon, zeolite, or clay (Antonelli et al., 2020; Chandrasekaran et al., 2020; Zide et al., 2018). Adsorption is an effective technique for extracting CPF from aqueous solutions since it offers several advantages over other methods. Adsorption is considered to be very effective for CPF removal due to high removal efficiency, versatility, cost-effective, reusability, and non-toxicity (Y. Chen et al., 2015; Genç & Dogan, 2015; V. Shukla et al., 2023), and it is a widely accepted method for the elimination of CPF from water (Y. Chen et al., 2015; Genç & Dogan, 2015). However, the effectiveness of adsorption depends on different components, such as structural characteristics of the adsorbent, pH, temperature, and initial concentration of CPF in the water, among others. Biochar is one of the cost-effective adsorbents which can be mass produced by pyrolysis of an organic matter using food and agricultural waste as a source material. Among various sources for producing biochar, pine cone biochar (PCBC) is a highly porous carbon-rich material that is reported to have a high surface area and various surface functionalities, such as -OH, -COOH, and -NH₂, which can interact with adsorbate molecules through a number of chemical interactions (Prakash Bobde, Sharma, Kumar, Pandey, et al., 2023; H. Liang et al., 2022; L. Liang et al., 2021). PCBC can be obtained from Chir pine, a species of pine tree, which is widely

found in the Himalayan region of India (specifically Uttarakhand) and its neighboring countries. (Fulé et al., 2021). Chir pine trees are highly susceptible to forest fires due to the high resin content in their needles and twigs. To mitigate the impact of such natural disasters on forest cover, it is essential to utilize the vast biomass of pine trees in a sustainable manner (Neelima Shah , IFS Rajiv Dhiman, 2022). Researchers have explored the use of pine cones, pine needles, and pine bark as feedstock to develop bio-based adsorbents in their studies (Cela-Dablanca et al., 2022; Debnath et al., 2017; D. Pandey et al., 2022). By utilizing these organic resources, one can overcome the challenges posed by forest fires whilst deriving valuable products from the pine tree biomass. However, biochar on its own is not capable of adsorbing contaminants effectively (Prakash Bobde, Sharma, Kumar, Pal, et al., 2023; Kumar et al., 2023). This calls for the need to engineer its surface such that surface functionalities become competent enough to adsorb contaminant molecules with high efficiency. Layered double hydroxides (LDHs), on the other hand are known to have a high surface area and active sites (P. Bobde et al., 2022; Prakash Bobde et al., 2021), which can enhance the adsorption of contaminant molecules. Additionally, LDHs have a positively charged surface, which can attract and adsorb negatively charged molecules. When LDHs and PCBC are combined to form a composite, it is anticipated to act synergistically to enhance the adsorption of antibiotics (Y. Wang et al., 2020). Moreover, the combination of LDHs and PCBC creates a diverse range of functional groups on the surface (de Souza dos Santos et al., 2020), which increases the types of interactions that can occur with the adsorbate. Therefore, the LDH/PCBC is likely to be a better adsorbent than PCBC alone, encompassing the qualities of its constituents for the removal of CPF from water with high adsorption capacity, unique surface properties, and environmental friendliness (de Souza dos Santos et al., 2020). The composite has the potential to be cheap and competent method for the elimination of CPF from wastewater.

The intent of this work is to develop LDH/PCBC composite and to examine its adsorption efficacy for the elimination of CPF from its aqueous solution. The

adsorption process is optimized based on the design of experiment using central composite design. Adsorption isotherm, kinetics and thermodynamics of the process have also been investigated. Regeneration and reuse of the spent adsorbent upto several cycles have been investigated, and an adsorption mechanism is proposed. This is the first study of its kind that investigates the removal of CPF utilizing LDH/PCBC composite.

6.2. Results & Discussion

6.2.1. Selection of adsorbent

The removal efficiency of many adsorbents for the contaminant Ciprofloxacin (CPF) was shown in figure 6.1a. With an 85.94% Ciprofloxacin removal effectiveness, LDH/PCBC was the highest of all the adsorbents evaluated. As a result of its greater ability to remove ciprofloxacin, LDH/PCBC is the most effective adsorbent and need to be chosen for additional research.

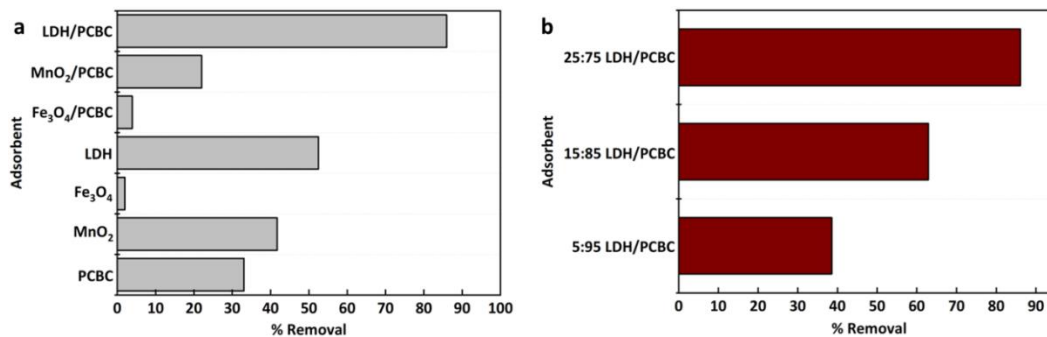


Figure 6.1: Comparison of different adsorbent for the removal of CPF (Prakash Bobde et al., 2024)

The removal efficiencies of several composite materials, namely 5:95 LDH/PCBC, 15:85 LDH/PCBC, and 25:75 LDH/PCBC, were given as percentages for the contaminant Ciprofloxacin in the figure 6.1b. With 86.09% Ciprofloxacin removal efficiency, the 25:75 LDH/PCBC composite outperformed the other adsorbent. Because of its better ability to remove ciprofloxacin, the 25:75 LDH/PCBC composite is the most promising adsorbent and ought to be the target of more research.

6.2.2. Adsorbent Characterization

The XRD pattern of PCBC and LDH/PCBC composite is shown in figure 6.2a. The diffraction peaks at 23.2° and 43.8° for PCBC were found to originate from the crystalline planes of C(002) amorphous carbon structures and C(100) in a graphite structure, respectively. The peaks correspond to the XRD pattern that has been previously identified (Yan et al., 2021). The formation of Mg-Al-LDH in LDH/PCBC was confirmed by the presence of the diffraction peaks at 11.3° , 22.5° , 34.1° , 60.0° , and 61.3° , which corresponds to (003), (006), (0 12), (110), and (113) reflections of LDHs comprising divalent and trivalent ions (Lee et al., 2019; Zubair et al., 2020). Thus, the XRD analysis of LDH/PCBC confirms its crystalline nature.

The FTIR spectra of a PCBC and LDH/PCBC composite are revealed in figure 6.2b. The spectra showed a vibrational band around 3432 cm^{-1} for PCBC and 3450 cm^{-1} for LDH/PCBC caused by stretching vibrations of O-H bonds in hydroxyl groups (Lee et al., 2019; Zubair et al., 2020), whereas Abdellaoui et al. (de Souza dos Santos et al., 2020) reported that a weak band around 1630 cm^{-1} mean intensity range is attributed to two factors: the bending mode of water molecules and the vibration of the anion within the lamella. Two peaks at around 1384 and 1096 cm^{-1} (in LDH/PCBC) or 1045 cm^{-1} (in PCBC) were found to correspond to the stretching vibration of nitrate and C-O functional groups respectively (Wakejo et al., 2022)(Zubair et al., 2020). The vibrational bands observed around 632 cm^{-1} are typically associated with the stretching vibrations of the Al-O or Mg-O bands, which are the cations responsible for forming LDH (de Souza dos Santos et al., 2020; Zubair et al., 2020). Thus FTIR spectra clearly confirm that the coupling of biochar into MgAl-LDH layers produced promising composites with a variety of functionalities (OH, C-O-C, C=O, C=C, NO_3 , metal

metal

oxide).

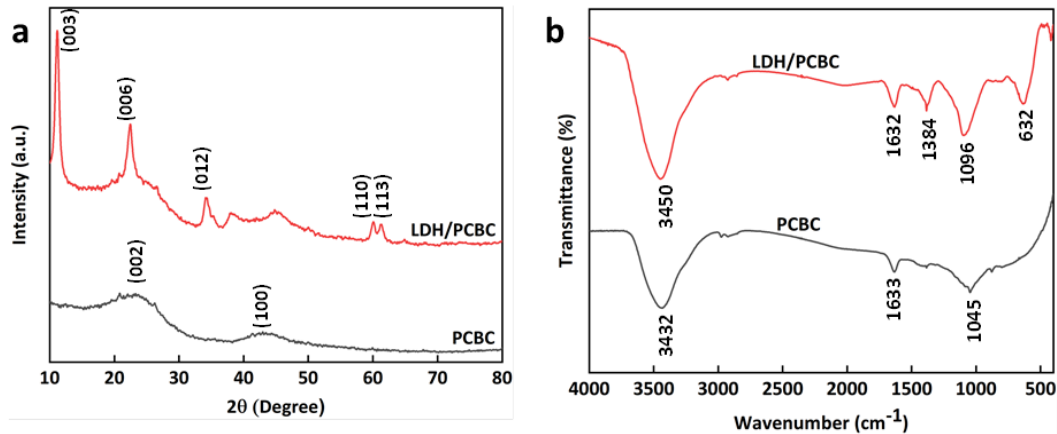


Figure 6.2: (a)XRD, (b)FTIR of PCBC and LDH/PCBC

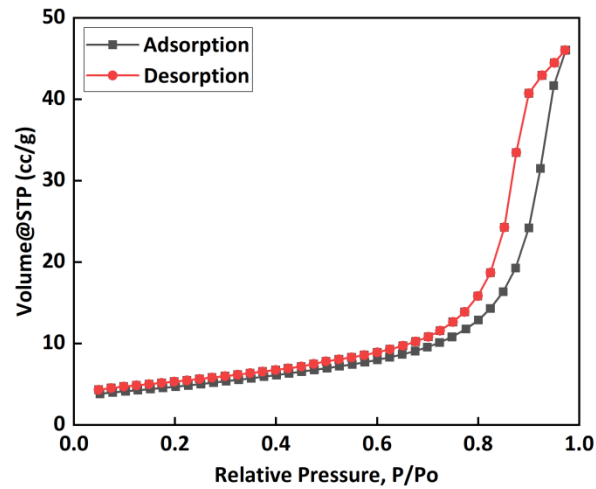


Figure 6.3: BET adsorption-desorption isotherm of LDH/PCBC (Prakash Bobde et al., 2024)

Figures 6.3, which show the N₂ adsorption-desorption isotherms of LDH/PCBC, was measured at 77.35 K. The volume of N₂ adsorbed increased dramatically at a low value of P/P₀, as seen in figure 6.3, showing the existence of micropores on the surface of LDH/PCBC. As the relative pressure increased, the adsorption capacity subsequently steadily increased. The specific surface area (SSA) was calculated using the BET equation. LDH/PCBC has a little less total pore volume but a greater average pore size than PCBC (Table 6.1). However, the SSA may be reduced by around one order of magnitude when LDH is combined with PCBC to form LDH/PCBC composite. This might be explained by the development of

surface-bonded species as a result of LDH's alteration of PCBC (Y. Wang et al., 2020). PCBC is classified as a Type I isotherm by the IUPAC, whereas LDH/PCBC is shown to have a Type III isotherm. Type III isotherm also suggests an unregulated layered growth process. Instead of direct interactions between the adsorbent surface and the adsorbate, Type III isotherms arise from strong lateral contacts among adsorbed molecules. The non-rigid agglomeration of the biochar particles prevents the LDH/PCBC's adsorption isotherm from flattening at the highest relative pressure yet observed.

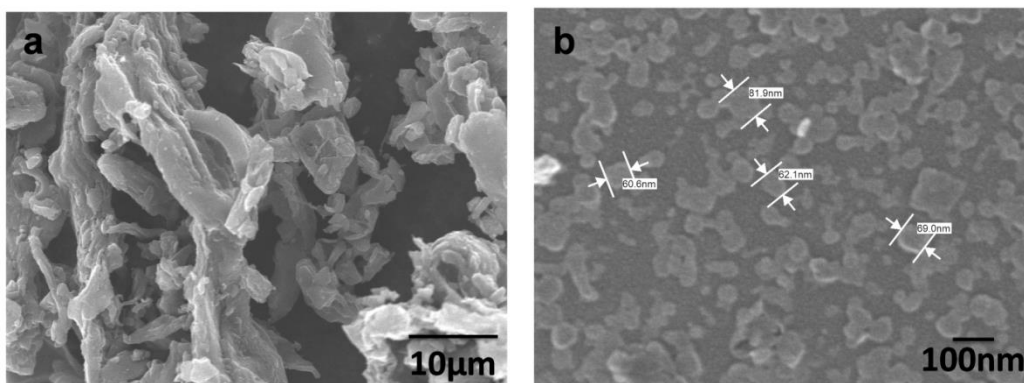


Figure 6.4: FESEM images of (a)PCBC (magnification x2000) and (b)LDH/PCBC (magnification x100000) (Prakash Bobde et al., 2024)

The PCBC surface is relatively loose, as noticeable in the FESEM images in figure 6.4a. The LDH/PCBC's (figure 6.4b) surface is covered with many protrusions that resemble thorns. As the material's surface becomes looser, the adsorption properties become more visible. Table 6.1 and 6.2 lists the microstructural characteristics and elemental composition, respectively. According to the elemental analysis, the addition of LDH results in MgAl-LDH emerging on the surface of LDH/PCBC as opposed to PCBC, which lowers the PCBC's carbon content while raising its oxygen content.

Table 6.1: Microstructural properties and elemental composition of the adsorbents

Adsorbent	SSA (m ² /g)	Total pore volume (cm ³ /g)	Average pore size (nm)
PCBC	172.19	0.1046	1.2144
LDH/PCBC	20.14	0.0712	8.6414
LDH/PCBC after CPF adsorption	16.48	0.065	6.43

Table 6.2: Elemental composition of PCBC and MnO₂/PCBC

Adsorbent	Elemental Composition (Weight %)					
	C	H	O	N	Mg	Al
PCBC	78.38	1.25	15.78	1.34	0.23	0.16
LDH/PCBC	61.76	1.66	23.59	1.22	6.41	1.95
LDH/PCBC after CPF adsorption	-	-	-	-	-	-

6.2.3. Influence of contact duration on the adsorption of CPF

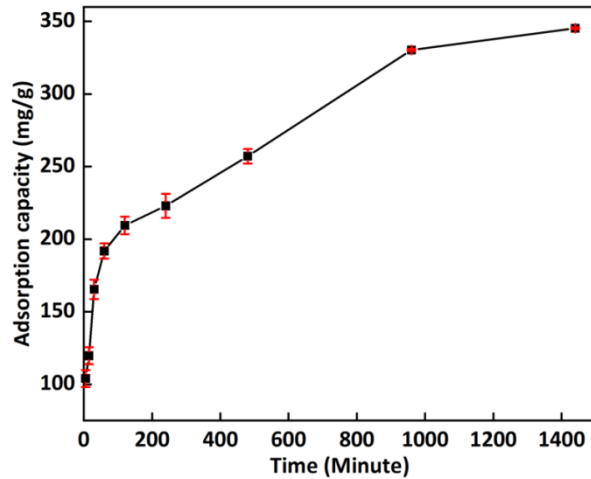


Figure 6.5: Influence of the quantity of CPF adsorbed (mg/g) versus contact duration onto the adsorbents (Prakash Bobde et al., 2024)

The study investigated the rate of CPF adsorption by LDH/PCBC at pH 7, by varying the contact time between 5 minutes and 1440 minutes. The experiments were conducted using 0.5 g/L LDH/PCBC and an initial CPF concentration of 200 mg/L, with contact times ranging between 5 minutes to 1440 minutes. Figure

6.5 illustrates that the adsorption capacity of CPF is enhanced sharply with shaking intervals up to 480 minutes for both the adsorbents, followed by a gradual increase up to a contact time 960 minutes. Adsorption capacity very slowly increased from 960 minutes to 1440 minutes. The equilibrium adsorption capacity was reached at 1440 minutes.

6.2.4. Model of fitting and Analysis of Variance (ANOVA) using CCD

The CPF adsorption process parameters were optimized employing the CCD, and the experimental data was mentioned in Table 6.3. A second-order polynomial model was employed to fit the data, which shows a good fit with an R^2 value of 0.95. A suggested quadratic model was also tested, and it has higher R^2 and adjusted R^2 values of 0.98 and 0.95, respectively. To access the model's validity and adequacy, ANOVA was used to identify the impact of key factors and interaction factors. The ANOVA results show that the proposed polynomial model is statistically significant.

Table 6.4 presents the outcome of the ANOVA analysis, which shows that the F-value and p-value of the model are 40.86 and <0.0001 , respectively. The small p-values indicate that the model is significant, and F-value suggests that there is only a 0.01% possibility that such a large F-value could happen owing to noise. Table 6.4 also shows that the independent variables, including initial CPF concentration, pH, LDH/PCBC dose and temperature have a remarkable impact on CPF removal. The terms B, C, D, BD, A^2 and B^2 are all significant in the model. These findings are consistent with similar studies by Najafpoor et al., Yousefi et al. and Wakejo et al., who used different adsorbents to remove CPF from aqueous solutions (Najafpoor et al., 2019; Wakejo et al., 2022; Yousefi et al., 2021).

Important model terms have p-values < 0.05 , while non-significant terms have p-values > 0.05 . The signal-to-noise ratio is calculated by Adeq precision, and a value > 4 is considered desirable. The ratio of 22.641 in this design stipulates an adequate signal. Therefore, this model can successfully steer the design space.

According to the statistical analysis using CCD, the predicted model equation that includes significant main and interaction factors can be expressed as equation 6.2. The coded value of the pH, LDH/PCBC dose, initial CPF concentration, and temperature are represented by A, B, C and D respectively in the equation. Additionally, the significant interaction parameters are represented by AB, AC, AD, BC, BD and CD.

$$\begin{aligned} \text{CPF removal} = & 84.43 - 0.79*A + 12.52*B - \\ & 5.13*C + 9.15*D + 0.19*A*B + 0.0085*A*C + 0.07*A*D - 0.29*B*C - \\ & 3.92*B*D + 0.04*C*D - 3.59*A^2 - 8.28*B^2 + 1.60*C^2 - 1.41*D^2 \end{aligned} \quad (6.1)$$

Based on the coefficients presented in equation 6.1, it is evident that factor C has a negative effect, while factors A, B and D have a positive effect on the removal of CPF. The order of impact of each parameter on CPF removal is $B > D > A > C$ as confirmed by the results in Table 6.4. It is noteworthy that the temperature and LDH/PCBC dose have the most significant impact on the removal of CPF. Equation 6.2 demonstrates the equation in terms of actual factors for the adsorption of CPF onto LDH/PCBC.

$$\begin{aligned} \text{CPF Removal} = & -799.72 + 2.54*A + 576.78*B - 0.14*C + 4.71*D - 0.23*A^2 - \\ & 207*B^2 + 0.0003*C^2 - 0.0063*D^2 + 0.2333*A*B + 0.000028*A*C + \\ & 0.0011*A*D - 0.0196*B*C - 1.30*B*D + 0.000036*C*D \end{aligned} \quad (6.2)$$

The coefficient of regression (R^2), adjusted coefficient of determination, and predicted determination coefficients, have model fit statistics of 0.98, 0.95, and 0.91, respectively. This suggests that the model accounts for 95% of the variation in the CPF removal response, indicating good fitness of the model (Table 6.4). In a study conducted by Wakejo et al., using CCD experimental design, similar model fit statistic values were reported ($R^2=0.98$) for CPF adsorption (Wakejo et al., 2022).

Table 6.3: Adsorption capacity values for the adsorption of CPF on LDH/PCBC obtained using CCD and RSM

Run No.	A	B (g/L)	C (mg/L)	D (K)	Experimental	Predicted	Residual
1	3	0.1	50	283	54.28	53.09	1.20
2	11	0.1	50	283	52.83	50.98	1.85
3	3	0.5	50	283	87.17	86.19	0.98
4	11	0.5	50	283	85.50	84.82	0.68
5	3	0.1	200	283	45.13	43.33	1.80
6	11	0.1	200	283	42.73	41.25	1.48
7	3	0.5	200	283	75.57	75.25	0.32
8	11	0.5	200	283	74.58	73.92	0.66
9	3	0.1	50	313	79.26	79.00	0.26
10	11	0.1	50	313	77.18	77.16	0.02
11	3	0.5	50	313	95.29	96.43	-1.15
12	11	0.5	50	313	94.45	95.34	-0.88
13	3	0.1	200	313	69.06	69.41	-0.35
14	11	0.1	200	313	67.53	67.60	-0.07
15	3	0.5	200	313	84.72	85.66	-0.93
16	11	0.5	200	313	83.74	84.60	-0.86
17	2	0.3	125	298	78.51	79.81	-1.30
18	12	0.3	125	298	75.93	77.83	-1.90
19	7	0.05	125	298	51.29	55.84	-4.55
20	7	0.55	125	298	88.50	87.15	1.35
21	7	0.3	31	298	91.37	93.33	-1.96
22	7	0.3	218	298	79.28	80.52	-1.24
23	7	0.3	125	279	64.03	70.80	-6.77
24	7	0.3	125	316	97.24	93.67	3.57
25	7	0.3	125	298	87.00	84.43	2.57
26	7	0.3	125	298	86.92	84.43	2.49
27	7	0.3	125	298	87.17	84.43	2.74

Table 6.4: ANOVA results for adsorption capacity of CPF by using LDH/PCBC

Source	Sum of square	DDL	Mean square	F-value	p-value
Model	6117.23	14	436.95	40.86	< 0.0001
A-pH	12.02	1	12.02	1.12	0.3099
B- LDH/PCBC dose	3000	1	3000	280.56	< 0.0001
C- CPF initial concentration	502.43	1	502.43	46.99	< 0.0001
D-Temperature	1600.72	1	1600.72	149.7	< 0.0001
pH* LDH/PCBC dose	0.5576	1	0.5576	0.0521	0.8232
pH* CPF initial concentration	0.0011	1	0.0011	0.0001	0.9919
pH*Temperature	0.0718	1	0.0718	0.0067	0.936
LDH/PCBC dose* CPF initial concentration	1.39	1	1.39	0.1299	0.7248
LDH/PCBC dose*Temperature	245.54	1	245.54	22.96	0.0004
CPF initial concentration*Temperature	0.0269	1	0.0269	0.0025	0.9609
(pH) ²	75.58	1	75.58	7.07	0.0208
(LDH/PCBC) ²	401.82	1	401.82	37.58	< 0.0001
(CPF initial concentration) ²	14.96	1	14.96	1.4	0.2599
(Temperature) ²	11.59	1	11.59	1.08	0.3183
Total Error	128.32	12			
Total (corr.)	6245.55	26			

6.2.5. Interaction effects of different experimental factors

The pH of a solution is a critical parameter as it impacts both the surface characteristics of the adsorbent and the interactions between the adsorbate and adsorbent (Asghar et al., 2019b). As can be shown in figure 6.6, the LDH/PCBC's pH point of zero charge (pH_{PZC}) is around 7.35. The surface of LDH/PCBC is positively charged at pH values below 7.35 and negatively charged at pH values over 7.35, according to the pH_{PZC} finding. CPF has two pK_a values, namely pK_{a1} (6.1) and pK_{a2} (8.7), which correspond to the protonation and deprotonation of the $-NH_2$ group in the piperazine moiety, respectively. At a pH lower than pK_{a1} , CPF exists in the form of CPF^+ due to protonation, while at a pH higher than pK_{a2} , it exists in the form of CPF^- due to deprotonation. Between pK_{a1} and pK_{a2} , CPF molecules exist in the zwitterionic form owing to the balance of charges between $-NH_2$ and $-COOH$ groups (Yousefi et al., 2021; B. Zhang et al., 2017).

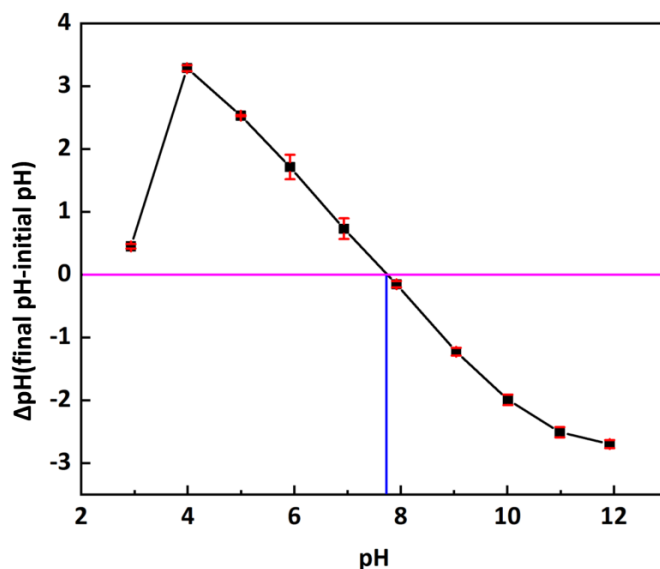


Figure 6.6: Plot of initial pH versus ΔpH for LDH/PCBC (Prakash Bobde et al., 2024)

Figure 6.7 represents 3D surface graphs of percentage removal of CPF onto LDH/PCBC. According to figure 6.7(a-c), the percentage removal of CPF by LDH/PCBC was found to increase as the pH of the solution was raised from 2 to 7 and then reduced upon further increase in the pH. The optimal pH for CPF adsorption onto LDH/PCBC was found to be 7.0. This pH level is significant because CPF forms zwitterions, leading to strong electrostatic attraction among CPF and positively charged LDH/PCBC, resulting in maximum adsorption at this pH level. Dehghan et al. (2019) reported a similar trend in CPF adsorption onto a metal organic framework (MOF) with increasing pH from 3 to 7.5, while CPF adsorption decreased at pH values above 7.5, attributed to protonation-deprotonation reactions of CPF groups (A. Dehghan et al., 2019).

The dose of LDH/PCBC used in an adsorption process is an important factor affecting the removal efficiency of CPF from its aqueous solution. Figure 6.7 shows that increasing the adsorbent dose from 0.1 g/L to 0.5 g/L (at pH 7.0, 200 mg/L initial CPF concentration, and temperature 298 K) results in an enhancement in the elimination of CPF. Gulen and Demircivi (2020) witnessed a comparable pattern in CPF adsorption using a dioctahedral clay structure. Shang et al. (2016) also reported similar pattern in an increase in CPF removal efficiency

with rise in the adsorbent dose from 0.025 to 0.5 g/L. This behaviour can be attributed to the increase in available active sites, which enhances the adsorption of CPF onto the adsorbent (Khoshnamvand et al., 2017; Najafpoor et al., 2019). The initial concentration of the pollutant is known to influence the efficiency of adsorption and therefore, the effect of initial concentration of CPF was examined, and the results are depicted in figure 6.7. At pH 7, an adsorbent dose of 0.5 g/L, and temperature 298 K, rise in the initial CPF concentration from 50 to 200 mg/L resulted in decrease in the removal efficiency. An increase in initial CPF concentration reduced the removal efficiency due to the inadequate availability of adsorbent sites for high CPF concentrations (El-Bendary et al., 2022). Similar findings were reported by Yousefi et al., who noted a decline in CPF removal efficiency from 83% to 59% when the CPF concentration is raised from 30 to 100 mg/L (Yousefi et al., 2021). The highly negative value of ΔG° for LDH/PCBC at all temperatures indicates spontaneous adsorption process (table 6.8). Further evidence to the spontaneity of the adsorption process at higher temperature comes from an increasingly negative free energy shift as temperature rises. The above stated thermodynamic characteristics of the adsorption process are suggested by the positive values of ΔH° and ΔS° (Q. Li et al., 2021; P. Zhang et al., 2019).

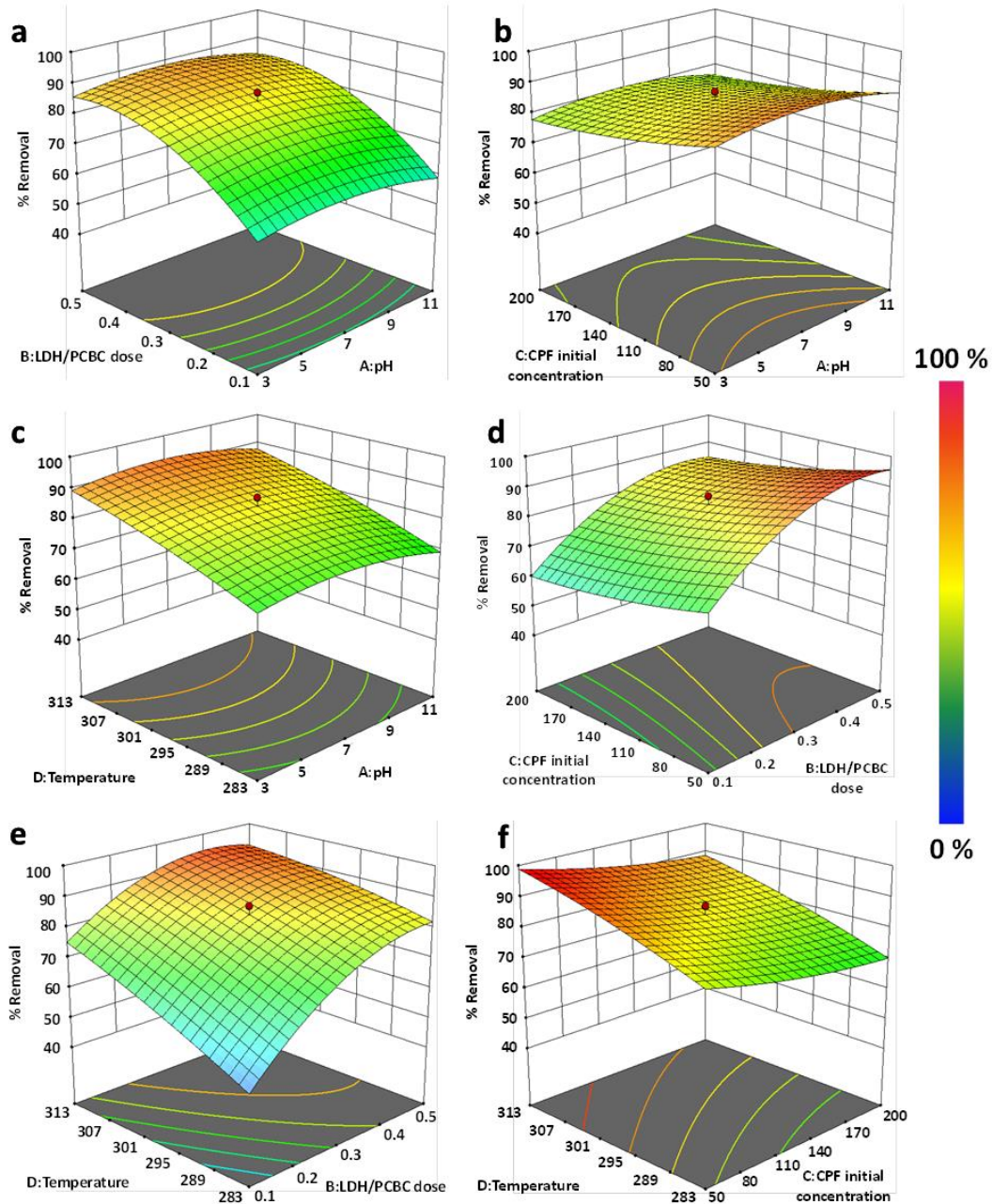


Figure 6.7: 3D surface graphs for % removal efficiency of CPF by LDH/PCBC (Prakash Bobde et al., 2024)

6.2.6. Process parameters optimization

Simulation of the adsorption mechanism was performed to determine ideal values for process variables like pH, primary concentration of CPF, adsorbent dosage and temperature for the reduction of CPF through LDH/PCBC using Minitab 16.

The optimum values of all the factors affecting adsorption of CPF on LDH/PCBC are given in table 6.5. For validation of the model, the experimental tests were performed under optimal conditions which clarify that the predicted and investigated adsorption capacity is near about same for the adsorbent LDH/BC.

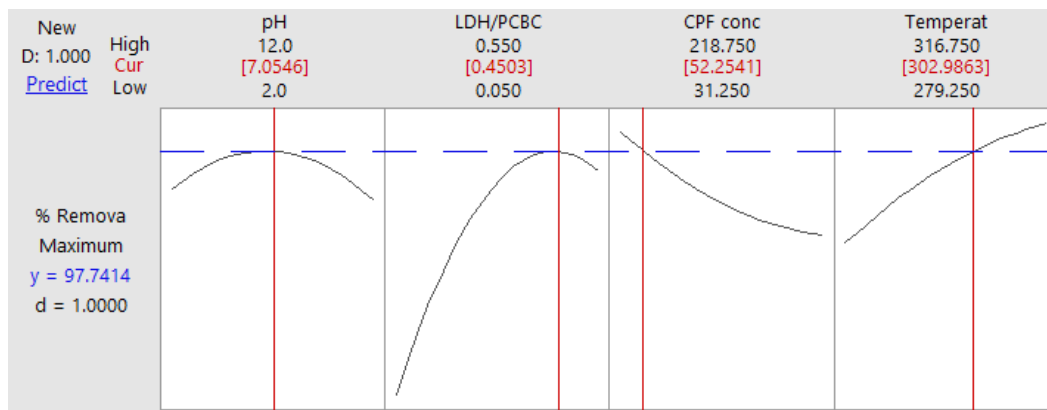


Figure 6.8: Optimization of adsorption process of CPF onto LDH/PCBC (Prakash Bobde et al., 2024)

Table 6.5: Optimum values for adsorption of CPF by LDH/PCBC

Adsorbent	A	B (g/L)	C (mg/L)	D (⁰ K)	Removal (%)	
					Experimental	Predicted
LDH/PCBC	7.05	0.45	52	303	97.6	97.74

A-pH, B-LDH/PCBC dose, C-Initial CPF concentration and D-Temperature

6.2.7. Adsorption kinetic, isotherm and thermodynamic study

The adherence of atoms, ions, or molecules from a liquid or solution to the adsorbent's surface is known as adsorption. The adsorption mechanism is a behaviour that occurs on the surface. The impact of temperature, pH, adsorbent dose, initial concentration, agitation time can be visualized in the adsorption process. PFO, PSO, Elovich and ID models were used to validate the adsorption kinetics of the experimental data. In this study, the transient action of the CPF sorption method was analysed utilizing the PSO, PFO, Elovich and ID model.

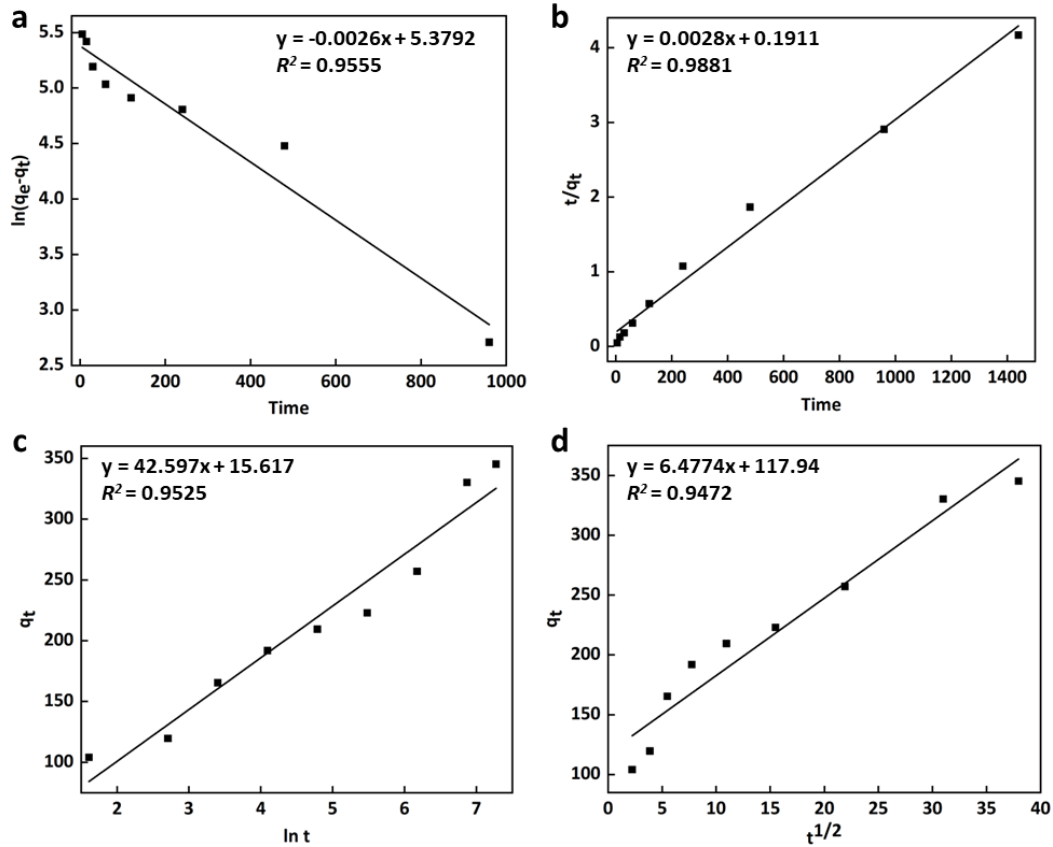


Figure 6.9: (a) PFO, (b) PSO (c) Elovich and (d) ID plots for the adsorption of CPF on LDH/PCBC. Experimental conditions: LDH/PCBC dose = 0.5 g/L, Initial concentration of CPF = 200 mg/L, Temperature = 298K, pH = 7. (Prakash Bobde et al., 2024)

The rate constant, K_1 (min^{-1}) was evaluated using the plot of $\ln(q_e - q_t)$ vs time t . The plot of $\ln(q_e - q_t)$ against time t is shown in figure 6.9a. Figure 6.9b reveals the plot between t/q_t against time t . As revealed in table 6.6, the R^2 value of PSO were observed to be higher than that of R^2 value of other kinetic models suggesting that the adsorption of CPF onto LDH/PCBC follows PSO kinetics [37]. Furthermore, the estimated q_e , which is derived from a PSO kinetic model, closely approximates the observed q_e . Overall, these findings imply that the rate of CPF adsorption, which entails covalent bonding via electron sharing between LDH/PCBC and the CPF molecule, was regulated by chemisorption (Wakejo et al., 2022)(Atugoda et al., 2021)(Balarak, Baniasadi, et al., 2021). More precisely,

the complexation reaction, hydrogen bonding, and π - π interaction could have contributed to the chemisorption process. Comparable results have been documented in the literature. Adsorption of CPF by modified bamboo biochar (Wakejo et al., 2022), thermally modified bentonite clay (Antonelli et al., 2020), γ -Al₂O₃ nanoparticles (Najafpoor et al., 2019) and functionalized multi-walled carbon nanotubes (Yousefi et al., 2021) obtained similar findings.

As shown in figure 6.9d, the plots had a multi-linear trend, suggesting that the CPF adsorption process included three phases. According to Balarak and McKay et al. (Balarak & McKay, 2021; Wakejo et al., 2022) the first stage, which lasted from 0 to 120 min., represented boundary layer mass transfer. The second linear segment, which depicts the intraparticle diffusion process, comprised the adsorption time of 120-960 min. In the third step, which lasted between 960 to 1440 min., CPF molecules were adsorbed on the LDH/PCBC's internal surface. Due to the drop in CPF concentrations (Wakejo et al., 2022; B. Zhang et al., 2017) and the number of accessible active sites (Wakejo et al., 2022), the last stage had a relatively low slope, indicating that the adsorption equilibrium had been attained. The quick removal of CPF in the first stage was shown by the rapid adsorption rate; however, when CPF concentrations and accessible active sites reduced in the succeeding phases, the adsorption process slowed down (Wakejo et al., 2022). Furthermore, it seemed that the intraparticle diffusion mechanism had less of an impact on the CPF adsorption kinetics, as seen by the modest linear dependence of CPF adsorption on $t^{0.5}$ (Emily Chelangat Ngeno et al., 2016; Wakejo et al., 2022). However, the high constant (c) parameter value indicated that the CPF adsorption onto LDH/PCBC was also caused by the boundary layer's influence. As a result, it was discovered that the large surface area of the MBC and the presence of many functional groups on the surface of biochar improved the adsorption of CPF onto LDH/PCBC (Atugoda et al., 2021; Wakejo et al., 2022). In general, liquid film diffusion, surface adsorption, and intraparticle diffusion worked together to regulate the CPF adsorption rate onto LDH/PCBC (W. Huang et al., 2020; Wakejo et al., 2022).

Various sorption isothermal models are commonly used to analyse the correlation among sorption and aqueous concentration of the adsorbate at equilibrium. Isotherm models play a crucial role in adsorption processes as they provide important information about the sorption capacity and the interactions among the adsorbent and adsorbate (Davoud Balarak et al., 2022).

Table 6.6: Kinetic parameters for the adsorption of CPF onto LDH/PCBC

C_0 (mg/L)		200
Theoretical q_e (mg/g)		345.35
PFO	q_e (mg/g)	216.84
	K_1 (min ⁻¹)	0.0026
	R^2	0.9555
PSO	q_e (mg/g)	357.14
	K_2 (g.mg ⁻¹ .min ⁻¹)	4.1 x 10 ⁻⁵
	R^2	0.9881
Elovich	α	61.461
	β	0.0234
	R^2	0.9525
ID	K_i (mg/g.min ^{1/2})	6.4774
	c	117.94
	R^2	0.9472

In this study, four isotherm models were used to understand the adsorption behaviour of CPF onto LDH/PCBC. The Langmuir, Freundlich, Temkin, and Dubinin-Radushkevich models were utilized to calculate the adsorption of CPF onto LDH/PCBC, and their parameters are presented in Table 6.7. The adsorption isotherm plots are shown in figure 6.10(a-d).

The Langmuir isotherm model was utilized to characterize the type and nature of the isotherm. The calculated value of the separation factor, R_L (0.0463), denoted that the CPF adsorption process onto LDH/PCBC is favorable (Jie Li et al., 2018; Stylianou et al., 2021). The regression coefficient of the Freundlich model was found to be greater than that of Langmuir, Temkin, and Dubinin-Radushkevich models, indicating a good fit of the former to the adsorption data. The value of the Freundlich constant, $1/n$, indicated that the LDH/PCBC surface is heterogeneous, with $n > 1$, indicating preferential adsorption. CPF was found to have monolayer

adsorption on a heterogeneous surface, consistent with previous studies (Jie Li et al., 2018). The results indicating heterogenous nature of LDH/PCBC surface conforms with the intraparticle kinetic study indicating multi-mechanistic nature of CPF adsorption onto LDH/PCBC.

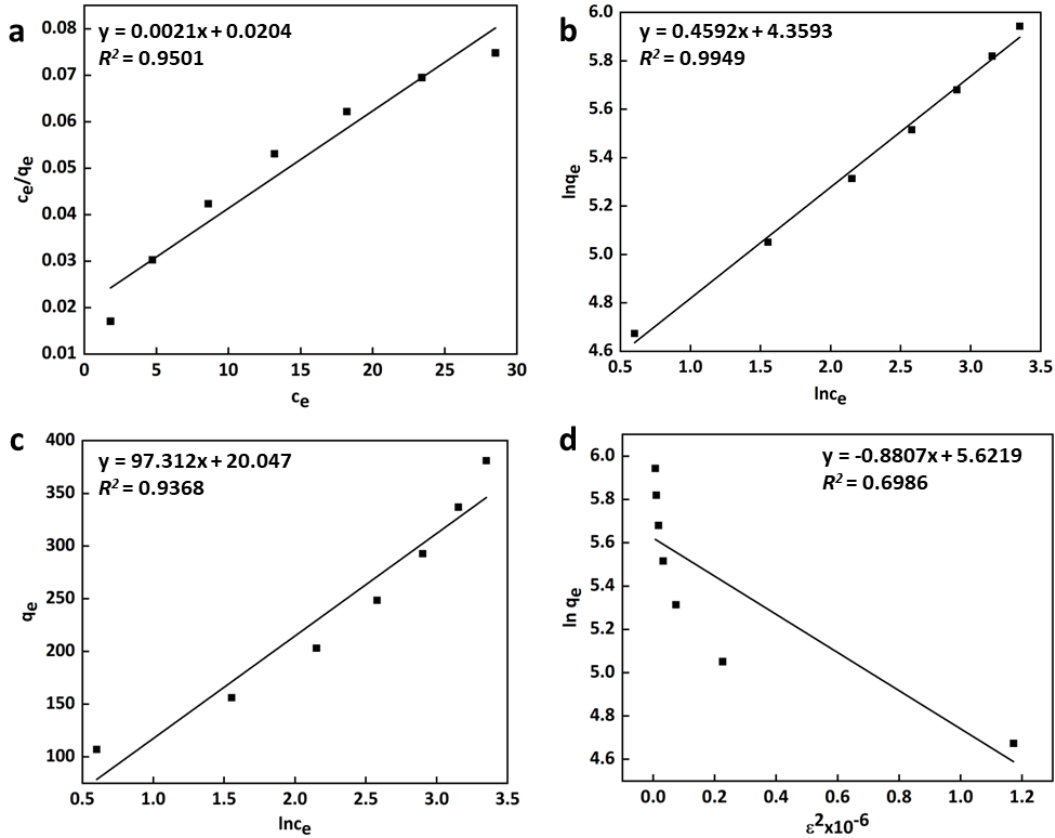


Figure 6.10: (a)Langmuir, (b)Freundlich, (c)Temkin and (d)Dubinin-Radushkevich plots for the adsorption of CPF on LDH/PCBC. Experimental Conditions: LDH/PCBC dose= 0.45 g/L, shaking time = 1440 min., initial CPF concentration = 52 mg/L, pH = 7.05, Temperature = 303 K. (Prakash Bobde et al., 2024)

The functional groups responsible for CPF adsorption onto LDH/PCBC were identified as OH, C-H, C-O, and C=O, which provided a heterogeneous surface for CPF adsorption (Wakejo et al., 2022). Overall, the isotherm models provided important information about the adsorption process and the nature of the

LDH/PCBC surface, which can be useful for optimizing the adsorption process in practical applications (Wakejo et al., 2022).

To investigate the adsorption of CPF onto LDH/PCBC, the influence of temperature was analysed with the optimized conditions, ranging from 278K to 313K (figure 6.11).

Table 6.7: Isotherm parameters for the adsorption of CPF onto LDH/PCBC

Langmuir	K_L (L/g)	49.019
	a_L (L/mg)	0.1029
	Q_o (mg/g)	476.19
	R_L	0.0463
	R^2	0.9501
Freundlich	K_f	78.202
	n (g/L)	2.1777
	R^2	0.9949
Temkin	B	97.312
	A (L/g)	1.2287
	R^2	0.9368
Dubinin-Radushkevich	q_m (mg/g)	276.41
	β (mol ² k/J ²)	8.807 x 10 ⁻⁷
	E (kJ/mol)	753.47
	R^2	0.6986

The negative values of ΔG^o for CPF adsorption on LDH/PCBC at a certain temperature revealed the spontaneous nature of the adsorption process and hence beneficial for adsorption of CPF. The positive values of ΔH^o also pointed that the adsorption process is endothermic. Positive values of ΔS^o stipulated an endothermic adsorption process that is aided by the enhanced randomness of CPF. Thermodynamic parameters for the adsorption of CPF onto LDH/PCBC are presented in table 6.8.

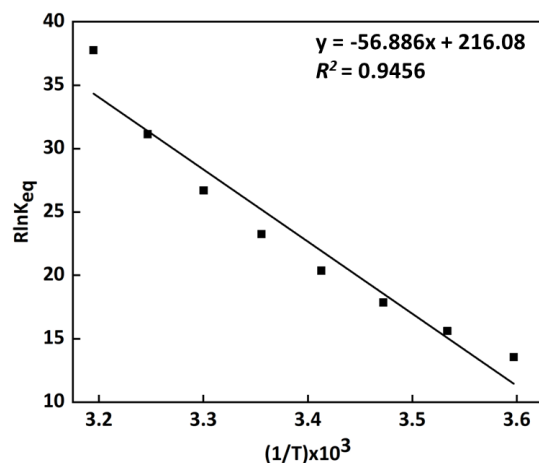


Figure 6.11: Plot of $R\ln K_{eq}$ versus $(1/T) \times 10^3 (K^{-1})$ for estimation of thermodynamic parameters. (Prakash Bobde et al., 2024)

Table 6.8: Thermodynamic parameters for the adsorption of OTC onto

MnO ₂ /PCBC		
ΔH° (kJ/mol)	56.886	
ΔS° (J/mol)	216.08	
ΔG° (kJ/mol)	278 K	-3.1842
	283 K	-4.2646
	288 K	-5.3450
	293 K	-6.4254
	298 K	-7.5058
	303 K	-8.5862
	308 K	-9.6666
	313 K	-10.7470

The maximum CPF adsorption capacity by LDH/PCBC in this study was 476.19 mg/g at pH 7.05 and at 303K temperature, which is comparable to higher CPF uptake than mostly reported adsorbents. Table 6.9 summarises the adsorption capacity of CPF on the reported adsorbents.

Table 6.9: Adsorption of CPF onto numerous adsorbents reported in literature.

Adsorbent	C_0 (mg/L)	Dosage (g/L)	pH	Temp. (K)	Time (min.)	Removal (%)	q_e (mg/g)	References
Modified bamboo biochar (MBC)	20	0.5	7.5	-	46	96.0	78.43	(Wakejo et al., 2022)
MWCNTs/Al ₂ O ₃	10	1.2	7	318	60	-	41.73	(Balarak & McKay, 2021)
Bentonite CVL clay	-	0.06	-	328	-	-	144.5	(Antonelli et al., 2020)
KMS-1/CYS/Fe ₃ O ₄	10-200	0.135	-	-	-	-	181.32	(Y. X. Wang et al., 2018)
Graphene	2-60	5	7	298	1440	-	322.60	(Zhu et al., 2015)
Siliceous hybrid shells of alginic acid	50-1200	1.5	5	298	1440	-	464	(Soares et al., 2019)
ZIF-67 derived hollow cobalt sulfide	3-100	40	7	303	720	-	471.7	(C. Liang et al., 2018)
LDH modified pine cone biochar (LDH/PCBC)	52	0.45	7.05	303	1440	97.6	476.19	This Study

6.2.8. Regeneration Study of LDH/PCBC

A feasibility study was carried out to evaluate if LDH/PCBC could be used effectively in the CPF adsorptive removal process. The study involved 5 cycles of adsorption and desorption, and the results revealed that the removal of CPF onto LDH/PCBC reduced from 97.6% to 91.6% as illustrated in figure 6.12. This suggests that the LDH/PCBC can be reused without remarkable loss in the percentage removal, with 91.6% of CPF still being removed in the fifth cycle, emphasizing that the LDH/PCBC is stable and sustainable adsorbent for CPF removal from its aqueous solution. This feature of LDH/PCBC makes it a valuable adsorbent considering environmental concerns and economic feasibility for practical applications.

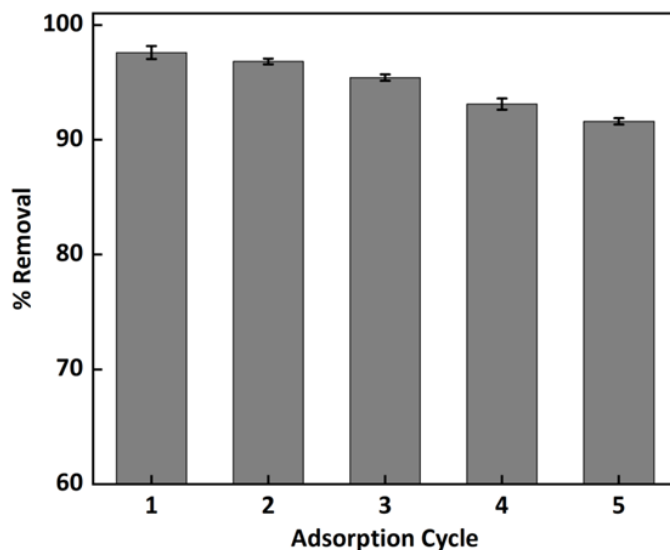


Figure 6.12: Adsorbent regeneration study (Prakash Bobde et al., 2024)

6.2.9. Adsorption Mechanism of CPF on LDH/PCBC

Surface adsorption likely occurred, with hydrogen bonding and metal-C π bonding potentially playing significant roles. The -NH groups from the CPF molecules and hydroxyl groups from LDH/PCBC likely formed hydrogen bonds between them. Additionally, metal-C π interactions, involving electrostatic interactions where positively charged cations interact with the negatively charged electron cloud of π -systems, were possible. Magnesium and aluminium likely engaged in these interactions with the π -electron cloud of CPF molecules. To confirm the impact of surface complexation on CPF adsorption, EDTA-2Na was introduced into the solution to observe its effect on adsorption efficiency (Fig. 6.13a). Upon the addition of 1 mM EDTA, the removal rate of CPF by LDH/PCBC decreased by approximately 14%, suggesting efficient CPF adsorption through complexation. Figure 6.13b demonstrates FTIR spectra of LDH/PCBC before and after CPF removal. A shift in the vibrational bands from 3450 cm^{-1} , 1096 cm^{-1} and 632 cm^{-1} in LDH/PCBC before CPF adsorption to 3457 cm^{-1} , 1029 cm^{-1} and 639 cm^{-1} , respectively after adsorption of CPF is observed. The surface of LDH/PCBC consists of numerous functional groups such as -OH, C-H groups in aromatic rings, and phenolic O-H bonds as evident from FTIR study, which may play a remarkable role in the CPF adsorption process. A new weak band at 1484 cm^{-1}

appeared in LDH/PCBC, indicating N-H bending vibration in CPF molecule (S. Pandey et al., 2012). The LDH/PCBC mainly comprises aromatics and may undergo π - π donor-acceptor interactions with the electron deficient CPF molecules (π -acceptor) during its adsorption (Jie Li et al., 2018), thereby enhancing the adsorption process. Average pore size, SSA, and overall pore volume were all observed to be relatively smaller in the LDH/PCBC after CPF adsorption (Table 6.1). This implies that pore filling may be one of the variables influencing CPF adsorption onto LDH/PCBC. The SSA and pore structure, according to Liang et al., are important factors that affect the adsorption of organic pollutants on bio-based adsorbents by pore-filling mechanism (H. Liang et al., 2022).

During CPF adsorption using LDH/PCBC ($\text{pH}_{\text{pzc}} = 7.7$) (figure 6.6), at low pH values (lower than $\text{pK}_{\text{a}1} = 6.1$), the surface functional and unsaturated groups of LDH/PCBC become protonated, leading to minimal π electron interaction with CPF. However, with increase in the pH from 6.1 to 8.7 ($\text{pK}_{\text{a}2}$), CPF becomes zwitterionic and acts as both as a π donor and an acceptor, thereby supporting interactions with the LDH/PCBC surface (Atugoda et al., 2021). Furthermore, the -OH and -COOH groups on the LDH/PCBC surface may form hydrogen bonds with -N and F-containing moieties on CPF molecules. In addition, the adsorption process may involve ion exchange.

The piperazine rings of CPF molecules carry a positive charge (NH_2^+) in neutral / slightly acidic solutions, and the resulting CPF^+ ions are attracted to the polar surface of the biochar, causing the release of H^+ ions (Jie Li et al., 2020). Considering above results, Figure 6.13c illustrates the possible mechanism for the adsorption of CPF onto LDH/PCBC.

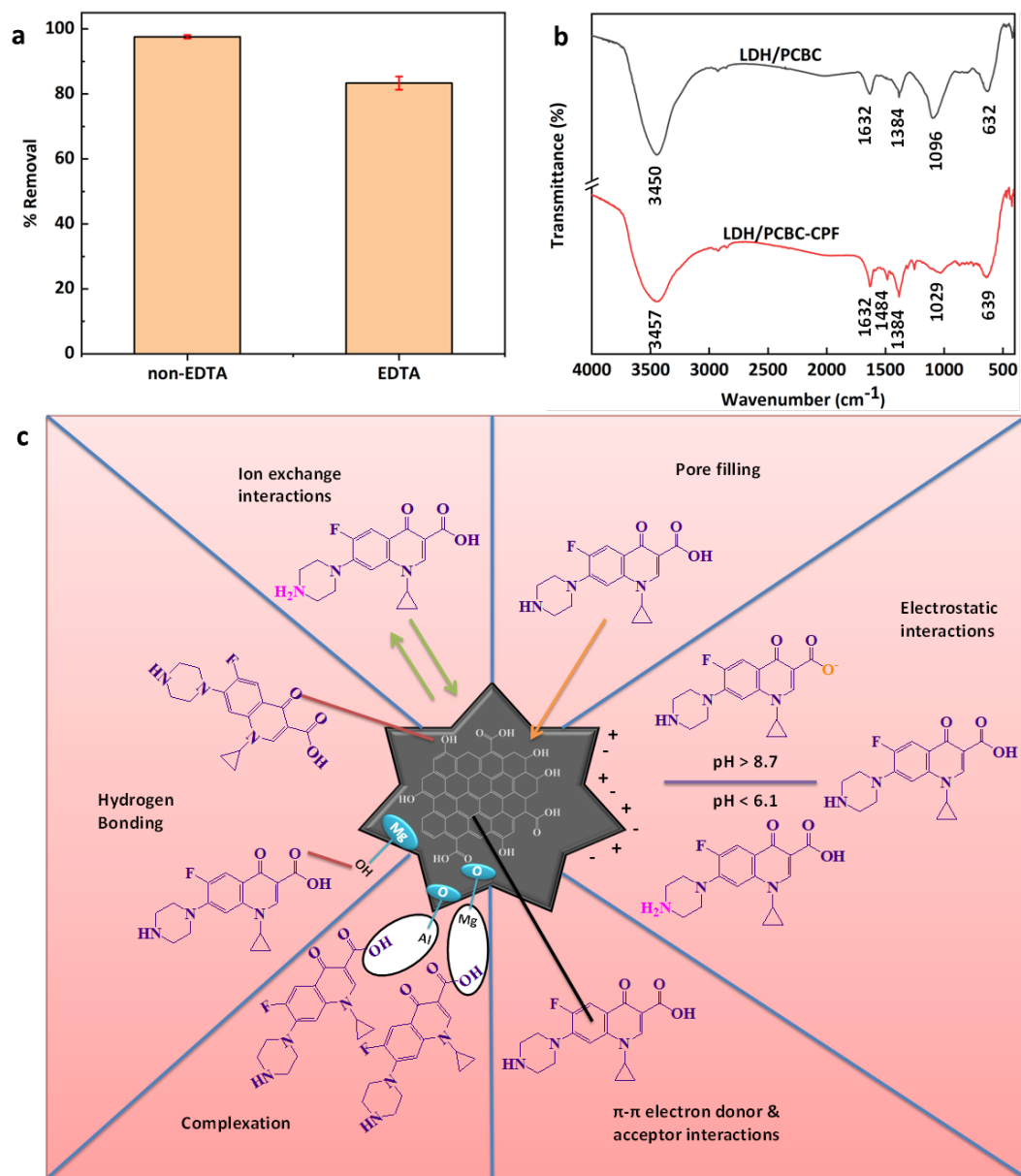


Figure 6.13: (a) Effect of EDTA on adsorption of CPF, (b) FTIR spectra of LDH/PCBC before and after adsorption of CPF (LDH/PCBC-CPF), (c) Proposed adsorption mechanism of CPF adsorption on LDH/PCBC. (Prakash Bobde et al., 2024)

6.3. Conclusion

In this study, the efficacy of LDH/PCBC composite is assessed for the adsorptive removal of CPF from its aqueous solution. The efficiency of LDH/PCBC in the elimination of CPF from aqueous solution is found to be 97.6% under optimised conditions (pH = 7.05, adsorbent dose = 0.45 g/L, initial CPF concentration = 52 mg/L and temperature = 303K). The findings show that the initial concentrations of CPF and temperature have a direct correlation with adsorption capacity, but the adsorbent dose has an adverse impact on the adsorption capacity of LDH/PCBC. The results of the statistical analysis show that the LDH/PCBC dose and the initial CPF concentration levels that were taken into consideration have the greatest impacts on CPF adsorption. The Freundlich isotherm and the Ho's PSO kinetics model provided the best descriptions. The pore-filling, π - π -EDA interactions, electrostatic interactions, ion exchange, and hydrogen bonding are implicated in the adsorption of CPF on LDH/PCBC composites. Additionally, it is noteworthy that LDH/PCBC is reusable as a competent adsorbent for the removal of antibiotics from water, indicating the possibility of its development into a sustainable and affordable method for CPF removal from water.

Chapter 7
ADSORPTION OF TRICLOSAN BY PINE CONE BIOCHAR

Chapter 7

ADSORPTION OF TRICLOSAN BY PINE CONE BIOCHAR

7.1. Introduction

In recent decades, the widespread use of antimicrobial agents in personal care products and household items has led to the increased presence of contaminants in water sources, drawing attention to the potential risks posed to both ecosystems and human health. Among these contaminants, triclosan, a commonly used antibacterial and antifungal agent, has gained particular scrutiny due to its widespread use and persistence in the environment. Triclosan, initially introduced for its antimicrobial properties, is commonly found in soaps, toothpaste, and various household items.

Triclosan has been extensively used in personal care products and medical settings due to its ability to inhibit bacterial and fungal growth. Its chemical structure and persistent nature makes it resistant to degradation, contributing to its accumulation in the environment (Yin et al., 2022). The need for effective removal strategies has become paramount to address the environmental and human health implications associated with its widespread use. The comprehensive understanding of triclosan's applications is crucial for assessing its potential impact on water quality.

The ecotoxicological effects of triclosan extend beyond its antibacterial properties. Research has highlighted its potential to disrupt endocrine systems in aquatic organisms, raising concerns about similar effects on humans through exposure from contaminated water sources (Cherednichenko et al., 2012). The urgency to remove triclosan from water arises from its persistence and the associated risks to ecosystems and human health. Triclosan has been detected in various environmental matrices, and its bioaccumulation potential emphasizes the need for proactive measures (Pycke et al., 2014). Long-term exposure to triclosan has been linked to adverse health effects, reinforcing the significance of water

remediation strategies. Investigations into triclosan's impact on human health emphasize the necessity of developing efficient removal methods.

Various methods have been explored for triclosan removal, including biological degradation, chemical oxidation, and physical processes. Some microorganisms have the ability to break down triclosan into less harmful substances. Microbes such as bacteria and fungi can metabolize triclosan, converting it into simpler compounds. This method is eco-friendly, but its efficiency may vary based on environmental conditions (Singer et al., 2002). Advanced Oxidation Processes (AOPs) like ozonation, UV irradiation, and Fenton's reagent involve generation of highly reactive oxygen species /free radicals that can oxidize triclosan molecules, breaking them down into less harmful byproducts. AOPs can be effective but may require careful control and monitoring (S. Khan et al., 2019). Various membrane processes, such as reverse osmosis and nanofiltration, can physically separate triclosan molecules from water based on their size and molecular weight (Y. L. Lin & Lee, 2014). These processes are effective but can be energy-intensive and may produce concentrated waste streams. While each method has its merits and demerits, adsorption has gained prominence due to its simplicity, efficiency, and versatility. Adsorption involves the attraction of triclosan molecules to a solid surface, effectively removing them from the water.

Activated carbon is widely used adsorbent for triclosan removal. Triclosan molecules are attracted to the porous surface of activated carbon, leading to their adsorption (Mohd Khori et al., 2018). This method is versatile, and activated carbon can be derived from various sources, including coconut shells and wood.

Adsorption involves the adherence of triclosan molecules to the surface of a solid material (adsorbent). This process occurs due to attractive forces, such as Van der Waals forces, hydrogen bonding, and electrostatic interactions between the triclosan molecules and the adsorbent.

Adsorption stands out as the preferred method for triclosan removal due to its selectivity, cost-effectiveness, and minimal environmental impact. Adsorbents, when properly chosen, can target specific contaminants, providing a tailored and

efficient solution for water treatment (Aljuboury et al., 2017). This method has shown success in removing a wide range of pollutants, making it a versatile and practical choice. Various adsorbents have been investigated for triclosan removal, including activated carbon, clay minerals, and biochar. Each material possesses unique characteristics that influence its adsorption capacity and efficiency. Activated carbon, for example, has been widely employed but may pose economic and sustainability challenges (Y. Li et al., 2020). Biochar, derived from biomass pyrolysis, offers a promising alternative with its abundant availability and environmental friendliness.

Biochar has gained attention as a superior adsorbent for triclosan due to its high surface area, porous structure, and carbon-rich composition. These properties enhance its adsorption capacity and provide an environmentally friendly alternative to conventional adsorbents (Mohan et al., 2014). Biochar's stability and potential for modification further contribute to its effectiveness in triclosan removal.

Among various biochar sources, pine cone biochar stands out for its abundance, cost-effectiveness, and unique properties. Pine cone biochar exhibits desirable characteristics, including high porosity and specific surface area, making it an effective adsorbent for triclosan. Additionally, utilizing pine cone waste for biochar production, especially in mountain region of Uttarakhand, contributes significantly in transforming 'trash to treasure', simultaneously addressing pine cone waste management. Thus, the work aligns with sustainability goals and contributes to waste reduction.

7.2. Results & Discussion

7.2.1. Selection of the best adsorbent

The % elimination of triclosan (TS) (200 mg/L) using different adsorbents (PCBC, MnO₂, Fe₃O₄, LDH, Fe₃O₄/PCBC, PCBC, and LDH/PCBC composite) (1 g/L) is shown in Figure 7.1. Out of all the adsorbents evaluated, the PCBC composite exhibited the highest TS removal efficacy (93%). For additional investigation, the PCBC composite is selected for TS removal.

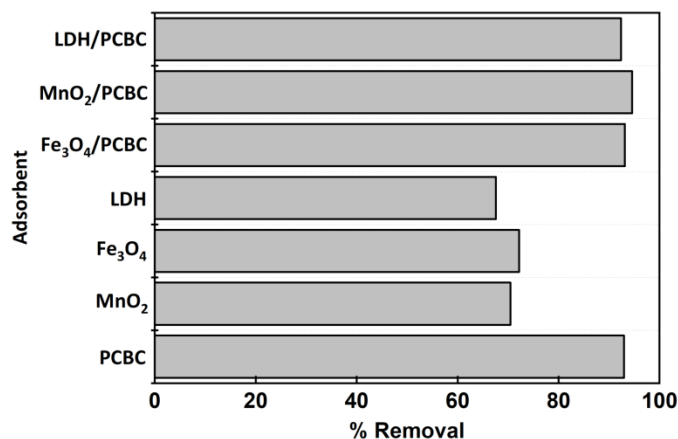


Figure 7.1: Comparison of different synthesized adsorbent (1 g/L) for the adsorptive removal of Triclosan (200 mg/L) from water.

7.2.2. Characterization of the adsorbent

The XRD pattern of the PCBC is shown in Fig. 7.2(a). Broad diffraction peaks at $2\theta = 20\text{--}30^\circ$ are recognised as originating from C (002) of amorphous carbon structures that comprise aromatic carbon sheets aligned randomly. At $2\theta = 40\text{--}50^\circ$, the broader and less strong peaks are associated with C (100) in a graphite structure.

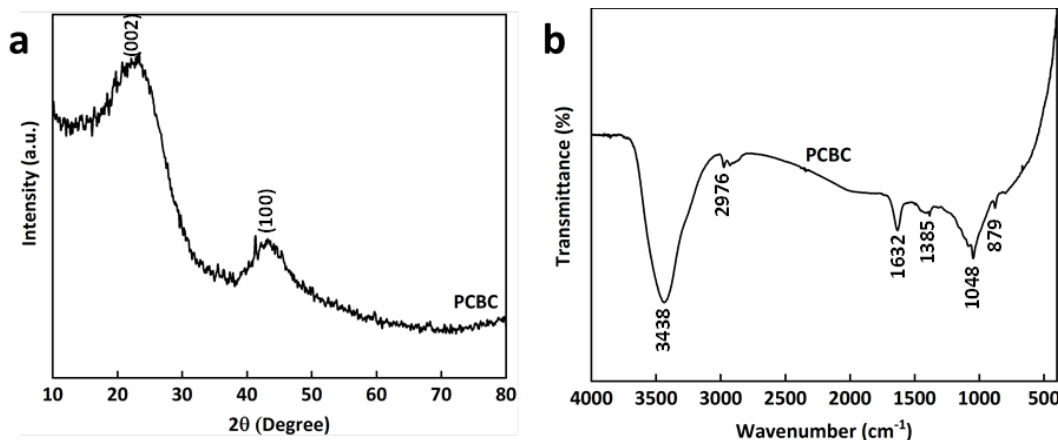


Fig. 7.2: (a) XRD pattern and (b) FTIR spectrum of PCBC

Figure 7.2(b) shows the FTIR spectra of a PCBC. The stretching vibration of O-H bonds in hydroxyl groups caused a notable peak in the spectra around 3438 cm^{-1} PCBC (P. Bobde et al., 2022; Prakash Bobde et al., 2021). In contrast, the C-H stretching and deformation vibrations are responsible for spectral band at 2976 cm^{-1} (B. Zhang et al., 2017). C=C bond stretching vibration was suggested by a

spectral line at roughly 1632 cm^{-1} (Al-Musawi, Rajiv, et al., 2021; Ramanayaka, Kumar, et al., 2020). It was discovered that two peaks, at approximately 1385 and 879 cm^{-1} , respectively, corresponded to the bending vibrations of C-H (Ramanayaka, Kumar, et al., 2020) and C=C bonds. The -OH bending and C-O-C bending in the cellulose and lignin structures of the PCBC are most likely the cause of the peaks at 1048 cm^{-1} (B. Zhang et al., 2017).

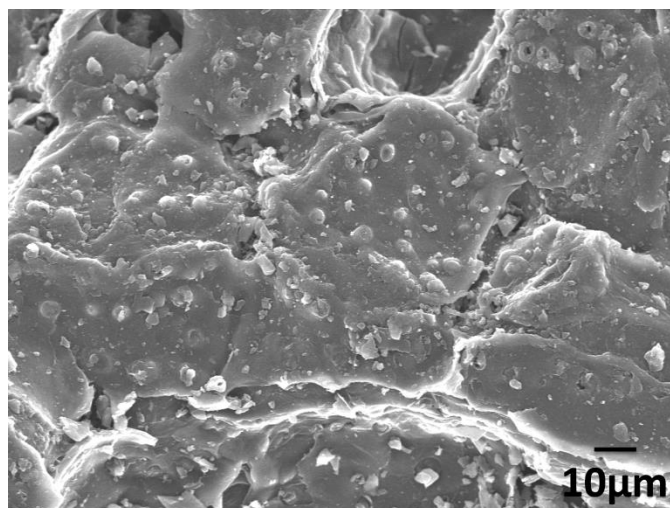


Figure 7.3: SEM images of PCBC

The PCBC morphology was investigated using SEM; the resulting image is shown in figure 7.3. The SEM of PCBC displayed an uneven surface on a porous structure. Table 7.1 lists the microporous structural characteristics and elemental composition of synthesised PCBC as obtained from BET surface area analysis and CHNS analysis.

Table 7.1: Physicochemical properties of PCBC

Adsorbent	Specific Surface Area (SSA) (m^2/g)	Total pore volume (cm^3/g)	Average pore size (nm)	Elemental Composition (Weight %)			
				C (%)	H (%)	O (%)	N (%)
PCBC	172.19	0.1046	1.2144	81.40	0.94	14.22	1.42
PCBC after TS adsorption	2.174	0.0051	4.7642	-	-	-	-

7.2.3. Effect of contact time on the adsorption of TS

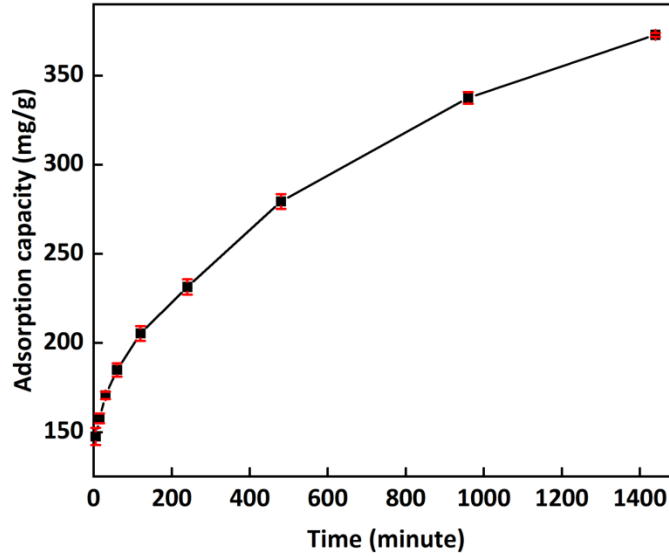


Figure 7.4: Effect of the amount of TS adsorbed (mg/g) onto adsorbent PCBC with contact time

The plot of the amount of TS adsorbed (mg/g) for 200 mg/L of TS onto the adsorbent PCBC as a function of contact time is shown in Figure 7.4. According to Figure 7.4, the amount of TS adsorption, q_e (mg/g), increases from 0 min to 1440 min with contact time. Initially the adsorption of TS grew from 147.51 to 279.39 mg/g for the first 480 min, and then rose to 372.84 mg/g until reaching equilibrium at 1440 min. Thus, in 480 minutes, the adsorption capacity grew rapidly, reaching equilibrium in 1440 minutes.

7.2.4. RSM Study

During the investigation, a multivariable method was used to examine the characteristics that had an impact on the removal process of TS by the PCBC. Using analysis of variance (ANOVA) and least squares analysis, the predictability and significance of the second-degree models were assessed. The factors that significantly affect the response variables under inquiry can be found using the ANOVA approach. The Fisher's F-Test is a statistical test that is used to achieve this. The software assessed the significance and magnitude of each variable's predicted coefficient as well as any potential interactions between them in relation to the response variables. Effects that had p-values more than 0.05 ($p > 0.05$), or

significance levels less than 95%, were regarded as errors and deleted (B. Wu et al., 2022). The p-value shows how much a coefficient lowers the degree of confidence in a result. Estimating the empirical error is aided by reproducing the central points in the experimental design. To identify the crucial elements and develop a model for optimisation, a second-degree model containing every term was utilised. Table 7.2 provides the actual values of the four variables as well as the percent removal values (both experimental and predicted) for the adsorption of TS on the adsorbent PCBC.

Table 7.2: Experimental and predicted values for adsorption of TS on adsorbent PCBC obtained through CCD and RSM

Run No.	A	B (g/L)	C (mg/L)	D (K)	Experimental	Predicted	Residual
1	3	0.1	50	283	26.90	26.11	0.78
2	11	0.1	50	283	25.28	23.76	1.51
3	3	0.5	50	283	63.55	63.01	0.54
4	11	0.5	50	283	61.70	61.49	0.21
5	3	0.1	200	283	16.69	14.06	2.63
6	11	0.1	200	283	14.02	11.75	2.28
7	3	0.5	200	283	50.62	49.64	0.98
8	11	0.5	200	283	49.52	48.16	1.36
9	3	0.1	50	313	54.74	54.22	0.52
10	11	0.1	50	313	52.42	52.16	0.25
11	3	0.5	50	313	72.60	73.64	-1.04
12	11	0.5	50	313	71.67	72.42	-0.75
13	3	0.1	200	313	43.37	42.34	1.03
14	11	0.1	200	313	41.67	40.33	1.34
15	3	0.5	200	313	60.83	60.46	0.37
16	11	0.5	200	313	59.73	59.28	0.45
17	2	0.3	125	298	29.39	33.05	-3.66
18	12	0.3	125	298	26.52	30.84	-4.32
19	7	0.05	125	298	48.06	55.34	-7.28
20	7	0.55	125	298	89.54	90.24	-0.70
21	7	0.3	31.25	298	92.75	93.37	-0.63
22	7	0.3	218.75	298	70.27	77.62	-7.35
23	7	0.3	125	279.25	62.27	69.51	-7.24
24	7	0.3	125	316.75	93.28	94.02	-0.74
25	7	0.3	125	298	87.87	81.43	6.45
26	7	0.3	125	298	87.78	81.43	6.36
27	7	0.3	125	298	88.06	81.43	6.63

Data with p-values greater than 0.05 ($p > 0.05$) should be excluded from the model to create a straightforward and valid model. A procedure of backward elimination is used to accomplish this. In statistical modelling, the adjusted R-squared (R^2 -adj), which accounts for the number of regression variables, is chosen since the coefficient of determination (R^2) drops as regression variables are eliminated. For the same reason as previously stated, the predictive R-squared (R^2 -pred), which represents the predictive power of the model, is also taken into consideration (Joshi & Acharya, 2018). As a result, when one of the variables is removed, R^2 , R^2 -adj, and R^2 -pred taken together can offer a quick and simple way to evaluate the model's fit and predictive ability. These three numbers should not differ much in a suitable model. The model equation's regression analysis reveals that the key parameters and their interactions have statistically significant p-values (less than 0.0001). The significance of each coefficient is determined by the F-value and p-value. Greater significance of the coefficients is indicated by greater F-values and smaller p-values. In this instance, significant model terms included the first-order effects, squared effects, and interaction effects of the variables. For TS, the model's F-values were found to be 36.64. Moreover, it was discovered that the p-value for each drug was less than 0.0001, demonstrating the importance of the models. Table 4.3 displays the average squares and total squares for each factor, along with the F and P values. Eq. (7.1) is used to forecast the process responses for the elimination of TS after non-significant factors are eliminated with a 95% confidence level.

$$\begin{aligned} \% \text{ removal} = & -265.9868 + 27.0355A + 587.3333B - 0.2055C + 0.5080D - 1.9792A^2 - \\ & 138.1320B^2 + 0.0004C^2 + 0.0009D^2 + 0.2600AB + 0.00003AC + 0.0012AD - \\ & 0.0218BC - 1.4555BD + 0.00004CD \end{aligned} \quad (7.1)$$

In these equations, A, B, C, and D were pH, PCBC dose, TS initial concentration, and temperature, respectively. A notable rise in percentage removal is observed (Fig. 7.5) when pH rises from 3 to 7, suggesting that the removal process becomes more successful as the solution becomes more alkaline. The removal process appears to be most effective at a neutral pH, as indicated by the peak in

percentage removal at pH 7. The percentage of removal gradually decreases beyond pH 7 as it rises towards alkaline levels (8–11). In contrast to acidic pH, the percentage removal is still rather high even at pH 11.

Table 7.3: Analysis of variance for adsorption capacity of TS by using PCBC

Source	Sum of square	DDL	Mean square	F-value	P-value
Model	14624.89	14	1044.63	36.64	< 0.0001
A-pH	14.91	1	14.91	0.5231	0.4834
B-PCBC dose	3727.13	1	3727.13	130.72	< 0.0001
C-TS initial concentration	759.34	1	759.34	26.63	0.0002
D-Temperature	1838.37	1	1838.37	64.48	< 0.0001
pH*PCBC dose	0.6927	1	0.6927	0.0243	0.8787
pH*TS initial concentration	0.0014	1	0.0014	0	0.9945
pH*Temperature	0.0892	1	0.0892	0.0031	0.9563
PCBC dose*TS initial concentration	1.73	1	1.73	0.0605	0.8098
PCBC dose*Temperature	305.06	1	305.06	10.7	0.0067
TS initial concentration*Temperature	0.0334	1	0.0334	0.0012	0.9733
(pH) ²	5877.87	1	5877.87	206.16	< 0.0001
(PCBC dose) ²	178.94	1	178.94	6.28	0.0277
(TS initial concentration) ²	39.77	1	39.77	1.39	0.2605
(Temperature) ²	0.2699	1	0.2699	0.0095	0.9241
Total Error	342.14	12			
Total (corr.)	14967.02	26			

The percentage removal of TS consistently rises as the PCBC dose is increased from 0.1 g/L to 0.5 g/L. There is a dose-response connection evident in the percentage of removal, which rises steadily with each PCBC dosage increment. The removal % increases significantly with each PCBC increment at lower dose range (0.1–0.2 g/L). The rate of increase in removal percentage decreases as the dose increases in the range 0.2–0.5 g/L, but there is still noticeable enhancement with each increase in dose. The whole process efficiency is increased by higher PCBC dosages because they offer more active sites for adsorption (Harja & Ciobanu, 2017; Q. Li et al., 2021). The removal percentage reaches saturation at very high dosages (about 0.5 g/L), after which any dose increases may have decreasing returns in terms of removal efficiency. This could explain the slowing rate of increase in removal percentage observed at higher doses.

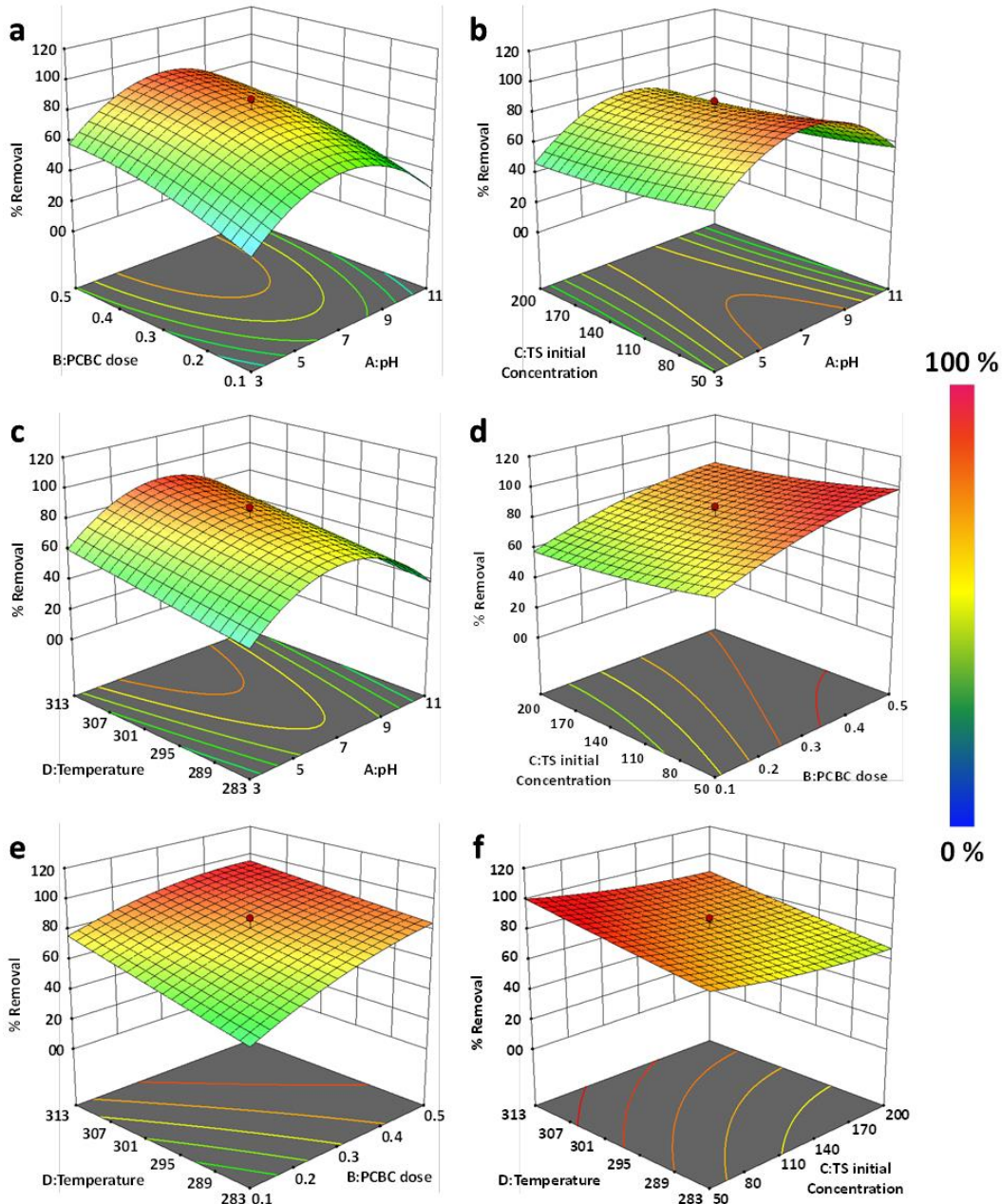


Figure 7.5: 3D surface graphs of percent removal efficiency of TS by using PCBC

The relationship between TS initial concentration and the corresponding removal percentage is shown in fig. 7.5. This indicates an inverse link between initial TS concentration and removal efficiency. The percentage of removal noticeably decreases as the initial concentration of TS increases from 50 mg/L to 200 mg/L. The removal percentage is remarkably high at lower initial concentrations, such

50 mg/L, reaching 99.2%, showing effective TS removal from the solution. However, the removal efficiency rapidly decreases with increasing initial concentration; at 200mg/L, the percentage of removal drops to 85.8%. This pattern indicates that higher starting TS concentrations can make the removal process more difficult, possibly as a result of saturation effects or more competition for adsorption sites on the adsorbent material (Harja & Ciobanu, 2017).

The correlation between temperature and the TS elimination percentage is shown in fig. 7.5. The percentage of TS removal clearly shows a rising trend as the temperature rises from 278K to 313K. The removal percentage is only 85.6% at lower temperatures, such 278 K, suggesting that TS is removed from the solution less effectively. On the other hand, removal efficiency increases with rising temperature; at 313 K, the percentage of removal increases to 98.0%. This pattern indicates that higher temperatures improve the removal process efficacy, most likely by speeding up adsorption of TS (G. Liang et al., 2019). Overall, the data emphasise how temperature has a major impact on the removal of TS and how crucial it is to control temperature as a critical component in order to optimise adsorption methods for effective TS removal.

7.2.5. Optimization of the adsorption of TS

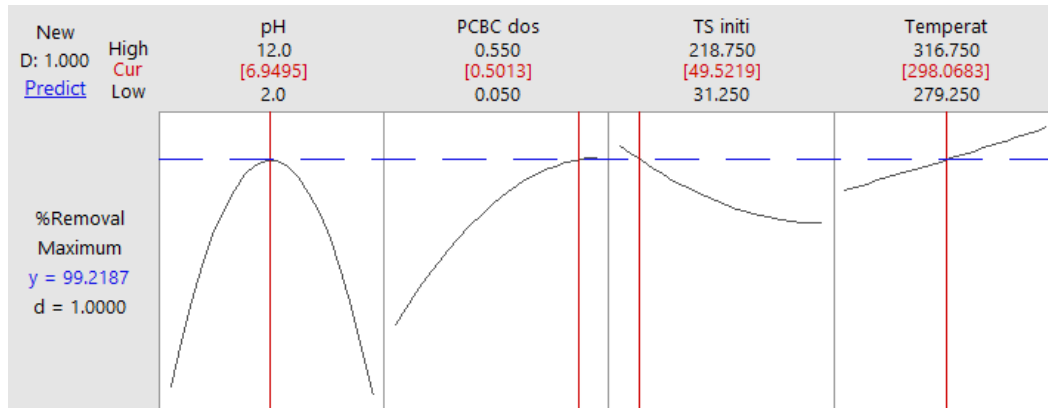


Figure 7.6: Optimization of adsorption process of TS onto PCBC

The optimum conditions for the TS adsorption onto PCBC are shown in Figure 7.6. The results show that TS may be effectively removed from a solution containing 50 mg/L initial concentration at pH at 6.95, PCBC dosage of 0.5 g/L,

and 298 Kelvin. The predicted and experimental percentage removal values nearly match, confirming the precision and dependability of the model's predictions. These optimized conditions provide efficient TS removal using PCBC as the adsorbent and provide insightful information for practical applications.

Table 7.4: Optimum values for adsorption of TS onto PCBC

Adsorbent	A	B (g/L)	C (mg/L)	D (^o K)	% Removal	
					Predicted	Experimental
PCBC	6.95	0.5	50	298	99.22	98.67

A-pH, B-PCBC dose, C-Initial TS concentration, and D-Temperature

7.2.6. Kinetic, isotherm and thermodynamic study

The table 7.5 gives the kinetic parameters and models that are used to explain how TS is adsorbed onto PCBC. It is determined that the theoretical equilibrium adsorption capacity (q_e) is 372.84 mg/g. This value serves as a benchmark for evaluating the accuracy of the kinetic models. The significant connection between the PFO equation and the experimental data is shown by the high coefficient of determination (R^2) of 0.9969. The PFO equation predicts a lower equilibrium adsorption capacity (q_e) of 218.42 mg/g with a rate constant (K_1) of 0.0019 min⁻¹. A better match to the experimental data is indicated by PSO equation, which produces a q_e value of 370.37 mg/g, which is close to the theoretical value. Its rate constant (K_2) is 3.79 x 10⁻⁵ g/mg.min, and its R^2 value is 0.9863.

The Elovich model offers valuable insights into the chemisorption process. Its R^2 value of 0.8854 indicates a decent match, and its parameters α and β are calculated to be 124.31 and 0.0252, respectively. The intraparticle diffusion model has the greatest coefficient of determination (R^2) of 0.9986 based on the available data, suggesting a very good match with the experimental results. Furthermore, the intercept (c) of 134.51 and the diffusion rate constant (K_i) of 6.4145 mg/g.min^{1/2} imply that intraparticle diffusion is important for the adsorption process. Overall, the intraparticle diffusion model seems to be the best fit for explaining the mechanism of adsorption due to its high R^2 value and the

physical relevance of the parameters, even if all models offer insightful information on the kinetics of the adsorption process. The curve fitting for the equations of PFO, PSO, Elovich, and ID is shown in fig.7.7.

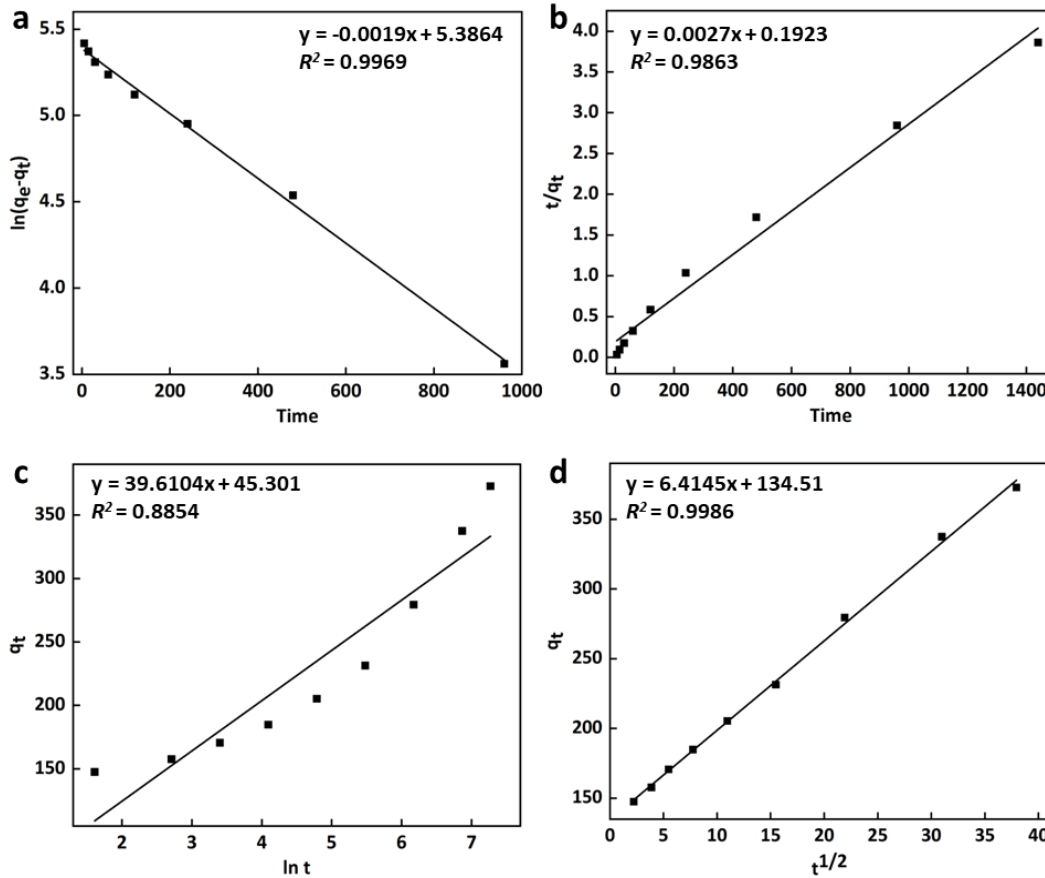


Figure 7.7: (a) PFO and (b) PSO (c) Elovich and (c) ID plots for the adsorption of TS on PCBC. Experimental conditions: PCBC dose = 0.5 g/L, Initial concentration of TS = 50 mg/L, Temperature = 298 K, pH = 6.95.

The isotherm parameters for the TS adsorption onto PCBC are given in table 7.6. A maximal monolayer adsorption capacity of 370.37 mg/g, is revealed by the Langmuir isotherm model. Furthermore, a favorable adsorption is indicated by the dimensionless separation factor (R_L), which is calculated to be 0.0958. With a coefficient of determination (R^2) of 0.9362, the Langmuir model appears to suit the experimental data quite well. With a R^2 value of 0.9449, the Freundlich isotherm model produces a Freundlich constant (K_f) of 114.46 and a Freundlich

exponent (n) of 3.4566, showing multilayer adsorption onto heterogeneous surfaces and a favorable fit.

Table 7.5: Kinetic parameters for the adsorption of TS onto PCBC

	C_0 (mg/L)	200
	Theoretical q_e (mg/g)	372.84
PFO	q_e (mg/g)	218.42
	K_1 (min ⁻¹)	0.0019
	R^2	0.9969
PSO	q_e (mg/g)	370.37
	K_2 (g/mg.min)	3.79×10^{-5}
	R^2	0.9863
Elovich	α	124.31
	β	0.0252
	R^2	0.8854
ID	K_i (mg/g.min ^{1/2})	6.4145
	c	134.51
	R^2	0.9986

Temkin constants (A and B) for the Temkin isotherm model are 7.9257 L/g and 54.229, respectively, and it has a R^2 value of 0.8405, which is reasonable but marginally less than that of the Langmuir and Freundlich models. The Dubinin-Radushkevich isotherm model, on the other hand, has a R^2 value of 0.5804 and shows a weaker fit to the experimental data than other isotherm models. Its maximum adsorption capacity is 236.89 mg/g, its mean free energy of adsorption (β) is 9.811×10^{-8} mol²k/J², and its energy of adsorption (E) is 2257.5 kJ/mol. The Freundlich isotherm seems to fit the best among the isotherm models examined to describe the adsorption of TS onto PCBC. The high coefficient of determination (R^2) value of 0.9449, which shows a significant correlation between the experimental and projected data points, serves as the foundation for this conclusion. Furthermore, this system's complex adsorption behavior can be explained using the Freundlich model since it can take into account multilayer adsorption on heterogeneous surfaces.

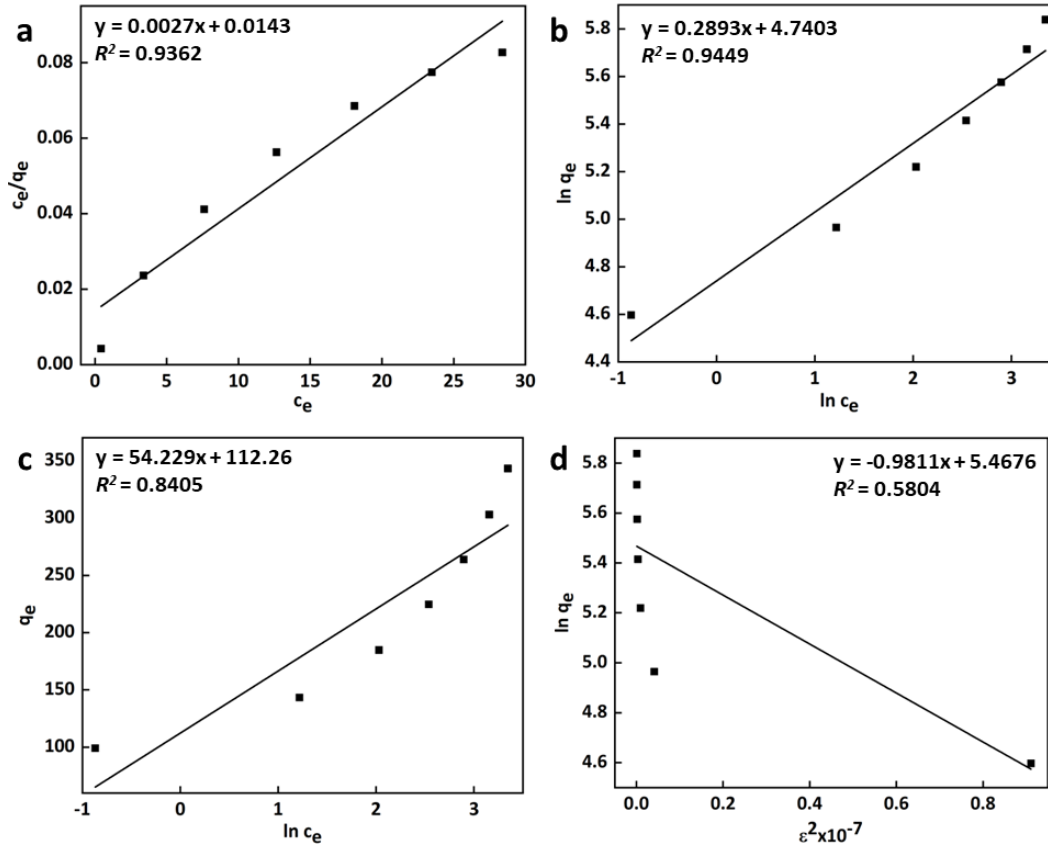


Figure 7.8: (a) Langmuir (b) Freundlich (c) Temkin and (d) Dubinin-Radushkevich plots for the adsorption of TS on PCBC. Experimental Conditions: PCBC dose= 0.5 g/L, shaking time = 1440 min., Temperature = 298 K, pH = 6.95

Table 7.6: Isotherm parameters for the adsorption of TS onto PCBC

Langmuir	K_L (L/g)	69.930
	a_L (L/mg)	0.1888
	Q_o (mg/g)	370.37
	R_L	0.0958
	R^2	0.9362
Freundlich	K_f	114.46
	n (g/L)	3.4566
	R^2	0.9449
Temkin	B	54.229
	A (L/g)	7.9257
	R^2	0.8405
Dubinin-Radushkevich	q_m (mg/g)	236.89
	β (mol ² k/J ²)	9.811×10^{-8}
	E (kJ/mol)	2257.5
	R^2	0.5804

TS adsorption thermodynamic characteristics are shown in table 7.7 for PCBC. The computed values for the in entropy (ΔS°), enthalpy (ΔH°), and Gibbs free energy (ΔG°) at various temperatures (278 K to 313 K) are given in table 7.7. At every temperature taken into consideration in the study, the adsorption process of TS onto PCBC is thermodynamically favourable, as indicated by the negative values of ΔG° . The magnitude of ΔG° decreases with temperature, suggesting that the adsorption process becomes more spontaneous. Furthermore, the fact that ΔH° (40.425 kJ/mol) is positive indicates that the adsorption process is endothermic, meaning that energy input is necessary for it to proceed. The adsorption process is expected to promote system disorder, as indicated by the positive value of ΔS° (158.26 J/mol·K).

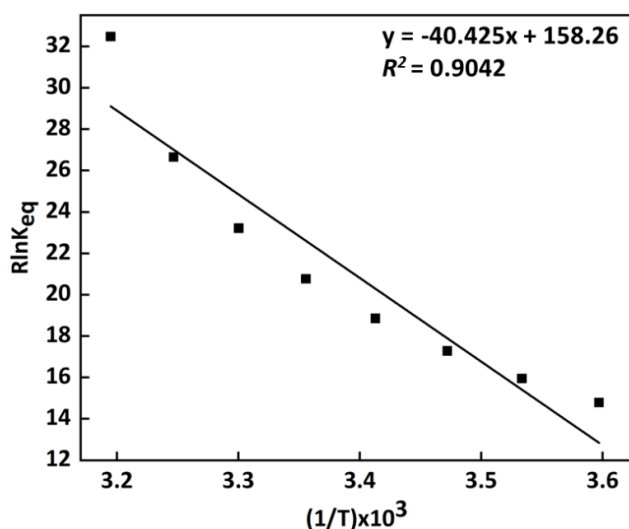


Figure 7.9: Plot of $R\ln K_{eq}$ versus $(1/T) \times 10^3 (K^{-1})$ for estimation of thermodynamic parameters.

Overall, the interpretation of Table 7.7 suggests that the adsorption of TS onto PCBC is favorable, spontaneous, and endothermic. The increasing negativity of ΔG° with temperature indicates that higher temperatures promote greater spontaneous process. The positive value of ΔS° suggests that the adsorption process increases the disorder of the system, contributing to its spontaneity.

Table 7.7: Thermodynamic parameters for the adsorption of TS onto PCBC

ΔH° (kJ/mol)	40.425	
ΔS° (J/mol)	158.26	
ΔG° (kJ/mol)	278 K	-3.571
	283 K	-4.363
	288 K	-5.154
	293 K	-5.945
	298 K	-6.736
	303 K	-7.528
	308 K	-8.319
	313 K	-9.110

Table 7.8 shows how this result compares to earlier studies that used a variety of adsorbents to extract TS from water. Of all the adsorbents that were taken into consideration, the PCBC composite showed the best adsorption performance. The PCBC showed a maximum adsorption capacity and satisfactory removal efficiency when compared to other adsorbents. As a result, PCBC shows promise as TS adsorbent, indicating that it can be used to effectively remove TS from water sources.

7.2.7. Regeneration Study

The regeneration study was carried out using the same amount of adsorbent (mention amount) after desorption of TS (concentration of TS) (explain the desorption methodology here) over a number of cycles (mention how many cycles). The average percentage removal of the target substance gradually decreases as the number of cycles rises. With an average percentage removal of 99.26% in the first cycle, suggested that the target pollutant was efficiently adsorbed onto the adsorbent. Nonetheless, the average percentage removal gradually declines with each succeeding cycle, indicating a progressive decline either in the concentration of adsorbent during washing steps or in the adsorption efficiency over time due to loss of active sites with time. The average percentage removal drops to 95.96% after the fifth cycle (Fig 7.10a), suggesting that the adsorption process is becoming less effective. Merely 3% decrease in removal efficiency of PCBC towards TS after 5 regeneration cycles emphasizes the effectiveness and sustainable recyclability of PCBC as an adsorbent for

pharmaceutical pollutant removal. This is an important inference drawn from the study of TS adsorptive removal using PCBC synthesized from waste pine cones.

Table 7.8: Comparison of TS adsorption onto different adsorbents reported in literature.

Adsorbent	C ₀ (mg/L)	Dosage (g/L)	pH	Temp. (K)	Time (min.)	Removal (%)	q _e (mg/g)	References
Inactivated dried sludge	200	2	5	308	180	-	7.36 μg/g	(Tohidi & Cai, 2016)
Biosolids derived biochar	200 μg/L	-	3	-	-	-	872 μg/g	(Tong et al., 2016)
Activated carbon derived from waste biomass	10-90	0.1	-	-	30	-	2.036	(Mohd Khori et al., 2018)
Kenaf derived biochar	-	4	5	-	180	90	77.4	(Cho et al., 2021)
MWCNT/P EG/b-CD	230	0.006	6.5	313	18	-	430	(Azqhandi et al., 2019)
Pine cone bio-based adsorbent (PCBC)	50-200	0.5	6.95	298	1440	98.67	370.37	This Study

7.2.8. Adsorption mechanism

The FTIR spectra of PCBC before and after TS adsorption are displayed in Figure 7.10b. With TS adsorbed PCBC, some vibrational bands show significant shift while many bands show only a little or no shift. This could be the result of the functional groups on PCBC interacting with TS during the adsorption process. The C-O stretching (1048 cm⁻¹) band shifts to 1100 cm⁻¹ indicating π-π interactions between adsorbed TS and PCBC. Functional groups on PCBC surfaces, such as -OH, C=C, and C=O, may act as π-electron donors. Accordingly, it is possible to control the adsorption of TS onto the PCBC surface through the π-π interaction. Furthermore, the free carboxylic acid groups present

on PCBC's surface interact with the functional groups of TS, which may act as H-bond donors, indicating that PCBC's sorption affinity for TS may have been enhanced by hydrogen bonding (G. Liang et al., 2019; J. Luo et al., 2018). The possible interactions of adsorbed TS on PCBC surface are schematized in Figure 7.10c.

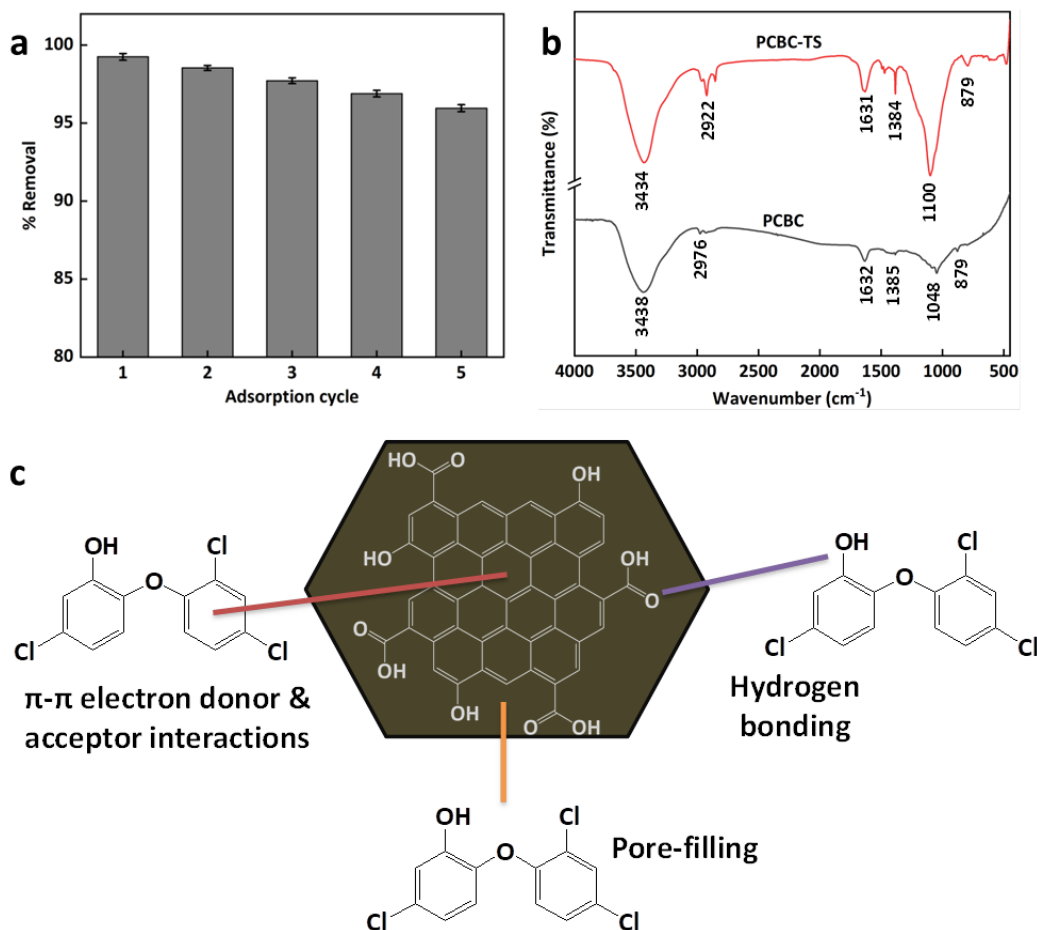


Figure 7.10: (a) Regeneration of PCBC for TS adsorption, over 5 cycles (b) FTIR spectra of PCBC before and after adsorption of TS (PCBC-TS), (c) Possible adsorption mechanism of TS over PCBC

Adsorbent total pore volume, and BET specific surface area were observed to be decreased during TS adsorption (Table 7.1). This implies that one of the elements influencing the TS adsorption onto PCBC may be pore filling. Liang et al. stated that pore structure and specific surface area are important factors that affect how

organic pollutants are adsorbed onto bio-based composites through a pore-filling mechanism (H. Liang et al., 2022).

7.3. Conclusion

The thorough analysis carried out on the TS adsorption onto PCBC provides important information about the adsorption mechanism and the possible uses of PCBC as an efficient and sustainable adsorbent (99% removal efficiency for Triclosan). PCBC's structural and chemical composition is revealed by XRD and FTIR investigations, which highlight the material's physical and surface characteristics. SEM images show the PCBC's morphology, which is advantageous to adsorption processes. The adsorption behavior of TS onto PCBC is determined by kinetic tests to be time-dependent, with the adsorption capacity reaching equilibrium in 1440 minutes. Additionally, TS removal is significantly influenced by pH, adsorbent dosage, starting concentration, and temperature, as revealed by RSM and kinetic modeling. The isotherm studies suggest that multilayer adsorption on heterogeneous surfaces occurs, and the Freundlich model best describes the adsorption behavior. Thermodynamic analysis verifies that the adsorption process is advantageous, spontaneous, and endothermic, and that temperature has a major effect on the removal efficiency. Furthermore, FTIR spectra obtained before and after adsorption indicated possible interactions between TS and PCBC, including hydrogen bonding, π - π interactions and pore-filling mechanisms playing key role. Merely 3% decrease in the removal efficiency from 99% to 96% emphasizes the potential of PCBC as an efficient and sustainable adsorbent generated from pine cone waste. Overall, these results show that PCBC has a promising future as an effective adsorbent for TS removal from water sources, opening the door to useful applications in environmental remediation and water treatment.

Chapter 8
CONCLUSION

Chapter 8

CONCLUSION

8.1. Summary

Firstly, the work highlights the effectiveness of biochar-based nanocomposites in removing contaminants of emerging concerns (CECs) from aqueous solutions. Through detailed adsorption studies, it is demonstrated that nanocomposites, such as manganese oxide-modified pine cone biochar and layered double hydroxide-modified pine cone biochar, exhibit high adsorption capacities for various CECs including oxytetracycline, tetracycline, ciprofloxacin, and triclosan.

Additionally, the role of response surface methodology study in experimental design and parameter optimization is reflected in all the results chapters. Furthermore, the adsorption mechanisms involved in the removal of CECs by biochar-based nanocomposites are discussed. It elucidates the role of surface functional groups, pore structures, and chemical interactions in facilitating adsorption processes. The understanding of these mechanisms is crucial for optimizing the design and synthesis of nanocomposites for enhanced CEC removal efficiency.

Moreover, the chapters emphasize the potential of biochar-based nanocomposites as cost-effective and sustainable adsorbents for the removal of CECs in water bodies, at the same time mitigating waste management of pine cones, which is one of the major waste generated in the forests of the Himalayan region. The findings of the study contribute to the development of innovative technologies for addressing emerging environmental challenges.

Lastly, the future research directions and areas for further investigation are elaborated. It identifies opportunities for optimizing the synthesis methods, exploring novel nanocomposite materials, and scaling up the production of biochar-based adsorbents for real-world applications. Additionally, the

importance of interdisciplinary collaboration and continued research efforts in advancing the field of environmental nanotechnology are emphasized.

8.2. Conclusion

Pine cone biochar based adsorbents have been designed for the removal of contaminants of emerging concerns from water. It became clear that the efficacy of the various adsorbents in removing particular contaminants varied in the range 79 – 95% for different CECs. With an 89.9% removal rate for OTC, MnO₂/PCBC proved to be the most effective adsorbent. This suggests that the MnO₂/PCBC is especially effective at adsorbing OTC from water sample. With a removal rate of 79.68%, MnO₂/PCBC is shown to be the most effective adsorbent for TC removal. This suggests that the removal of TC from the solution is especially well-suited for MnO₂/PCBC.

On the other hand, LDH/PCBC shows the best elimination efficiency of 85.94% for CPF. This implies that the most efficient method for eliminating CPF from the aqueous solution is LDH/PCBC. With removal rates ranging from 67.59% to 94.57%, it is clear from the data that all evaluated adsorbents had exceptionally high removal efficiency for TS. Owing to PCBC's outstanding performance and its inherent compatibility that doesn't require modification, it becomes the best option for additional research and possible use in water treatment procedures that remove TS. MnO₂/PCBC is ideal for removing OTC and TC, whereas LDH/PCBC is better for removing CPF and PCBC is good for the TS removal. PCBC, MnO₂/PCBC, and LDH/PCBC underwent thorough characterization using various analytical techniques including FTIR spectroscopy, XRD, FESEM, CHNS analyzer, ICP-OES, BET nitrogen adsorption analysis, and pH point of zero charge (pH_{PZC}) determination.

The adsorption processes of various contaminants onto different adsorbents, as evidenced by the experimental data and analyses, highlight the intricate mechanisms involved in pollutant removal. The reduction in removal rates observed upon the addition of EDTA-2Na suggests the significant role of surface complexation in the adsorption of contaminants such as OTC, TC, and CPF onto

MnO₂/PCBC and LDH/PCBC. Furthermore, the shifts in FTIR spectra and changes in physicochemical properties of the adsorbents before and after adsorption indicate alterations in surface functional groups and pore structures, which likely influence the adsorption capacities and mechanisms. Notably, interactions such as π - π bonding and hydrogen bonding between the adsorbates and adsorbents contribute to enhanced sorption affinity and efficient removal of contaminants. These findings underscore the importance of understanding the adsorption mechanisms and surface interactions for developing effective adsorbents and remediation strategies for water treatment applications.

The repeated cycles of adsorption-desorption studies provide valuable insights into the regeneration potential and sustainability of the synthesized adsorbents for pollutant removal. The gradual reduction in adsorption efficiency observed over multiple cycles suggests some loss of adsorbent material during washing steps or saturation of active sites on the adsorbent surface. However, the marginal decrease in removal efficiency (~4% to 8% over 5 cycles) for OTC, TC, CPF, and TS removal highlights the potential reusability and sustainability of MnO₂/PCBC, LDH/PCBC, and PCBC adsorbents. Despite the decline in removal efficiency, the adsorbents demonstrate stable performance over multiple cycles, with significant percentages of pollutants still being removed even after five regeneration cycles. This underscores the effectiveness and practical feasibility of these adsorbents for continuous and sustainable pollutant removal from aqueous solutions. Such findings are crucial for addressing environmental concerns and promoting the adoption of cost-effective and environmentally friendly adsorption techniques in water treatment applications. Table 8.1 summarizes the removal efficiencies of various adsorbates obtained by various bio-based adsorbents under various optimized conditions.

Table 8.1: Summary of removal efficiencies of various CECs from water using different biochar-based adsorbents

Sr. No.	Optimized conditions				Removal efficiency (%)
	pH	Adsorbent dose (g/L)	Adsorbate concentration (mg/L)	Temperature (K)	
1	8.00	MnO ₂ /PCBC – 0.44	OTC – 200	303	88.10
2	5.00	MnO ₂ /PCBC – 0.50	TC – 60.45	298	94.89
3	7.05	LDH/PCBC – 0.45	CPF – 52	303	97.60
4	6.95	PCBC – 0.5	TS – 50	298	98.67

8.3. Future prospects

- **Tailored Adsorbents for Specific Contaminants:** The study highlights the need for tailored adsorbents to address specific contaminants effectively. By identifying MnO₂/PCBC's superior efficacy for oxytetracycline (OTC) and tetracycline (TC) removal, and LDH/PCBC's efficiency for ciprofloxacin (CPF), future research can focus on designing adsorbents optimized for targeted contaminant removal.
- **Enhanced Adsorbent Regeneration Techniques:** Investigating enhanced regeneration techniques for adsorbents like MnO₂/PCBC and LDH/PCBC can further extend their lifespan and sustainability. Developing efficient regeneration methods can reduce operational costs and environmental impact, making these materials more viable for large-scale water treatment applications.
- **Exploring Novel Adsorbent Combinations:** Combining different adsorbent materials or modifying existing ones could lead to synergistic effects, improving overall contaminant removal efficiency. Investigating hybrid materials or composite structures may offer enhanced adsorption capacities and selectivity, opening avenues for innovative water treatment technologies.

- **Scale-Up and Real-World Application:** Scaling up the synthesized adsorbents and conducting pilot-scale studies in real-world settings will be crucial for validating their efficacy and feasibility for practical water treatment applications. Assessing factors such as cost-effectiveness, scalability, and long-term performance can pave the way for the widespread implementation of these advanced adsorption technologies.
- **Membrane development using bio-based adsorbents:** Further experimental work may involve the designing of membranes using bio-based adsorbents to be used for water filtration in rural areas where cost effective approach is required.

REFERENCES

- Abdel-Aziz, H. M., Farag, R. S., & Abdel-Gawad, S. A. (2020). Removal of caffeine from aqueous solution by green approach using Ficus Benjamina zero-valent iron/copper nanoparticles. *Adsorption Science and Technology*, 38(9-10), 325–343. <https://doi.org/10.1177/0263617420947495>
- Abdel-Raouf, M. E. S., Farag, R. K., Farag, A. A., Keshawy, M., Abdel-Aziz, A., & Hasan, A. (2023). Chitosan-Based Architectures as an Effective Approach for the Removal of Some Toxic Species from Aqueous Media. *ACS Omega*, 8(11), 10086–10099. <https://doi.org/10.1021/acsomega.2c07264>
- Abdoallahzadeh, H., Rashtbari, Y., Américo-Pinheiro, J. H. P., Azari, A., Afshin, S., Fazlzadeh, M., & Poureshgh, Y. (2023). Application of green and red local soils as a catalyst for catalytic ozonation of fulvic acid: experimental parameters and kinetic. *Biomass Conversion and Biorefinery*. <https://doi.org/10.1007/s13399-023-03895-6>
- Abo El Naga, A. O., El Saied, M., Shaban, S. A., & El Kady, F. Y. (2019). Fast removal of diclofenac sodium from aqueous solution using sugar cane bagasse-derived activated carbon. *Journal of Molecular Liquids*, 285, 9–19. <https://doi.org/10.1016/j.molliq.2019.04.062>
- Abu Rumman, G., Al-Musawi, T. J., Sillanpaa, M., & Balarak, D. (2021). Adsorption performance of an amine-functionalized MCM-41 mesoporous silica nanoparticle system for ciprofloxacin removal. *Environmental Nanotechnology, Monitoring and Management*, 16. <https://doi.org/10.1016/j.enmm.2021.100536>
- Adesina, M. O., Block, I., Günter, C., Unuabonah, E. I., & Taubert, A. (2023). Efficient Removal of Tetracycline and Bisphenol A from Water with a New Hybrid Clay/TiO₂ Composite. *ACS Omega*, 8(24), 21594–21604. <https://doi.org/10.1021/acsomega.3c00184>
- Ahmad, J., Naeem, S., Ahmad, M., Usman, A. R. A., & Al-Wabel, M. I. (2019). A critical review on organic micropollutants contamination in wastewater and removal through carbon nanotubes. *Journal of Environmental Management*, 246, 214–228. <https://doi.org/10.1016/j.jenvman.2019.05.152>
- Ahmaruzzaman, M. (2010). A review on the utilization of fly ash. In *Progress in Energy and Combustion Science* (Vol. 36, Issue 3, pp. 327–363). <https://doi.org/10.1016/j.pecs.2009.11.003>
- Ahmed, M. B., Zhou, J. L., Ngo, H. H., & Guo, W. (2015). Adsorptive removal of

- antibiotics from water and wastewater: Progress and challenges. In *Science of the Total Environment* (Vol. 532, pp. 112–126). <https://doi.org/10.1016/j.scitotenv.2015.05.130>
- Ahmed, M. B., Zhou, J. L., Ngo, H. H., Guo, W., & Chen, M. (2016). Progress in the preparation and application of modified biochar for improved contaminant removal from water and wastewater. In *Bioresour. Technol.* (Vol. 214, pp. 836–851). <https://doi.org/10.1016/j.biortech.2016.05.057>
- Aigbe, U. O., Ukhurebor, K. E., Onyancha, R. B., Osibote, O. A., Darmokoesoemo, H., & Kusuma, H. S. (2021). Fly ash-based adsorbent for adsorption of heavy metals and dyes from aqueous solution: a review. In *Journal of Materials Research and Technology* (Vol. 14, pp. 2751–2774). <https://doi.org/10.1016/j.jmrt.2021.07.140>
- Ajala, O. A., Akinnawo, S. O., Bamisaye, A., Adedipe, D. T., Adesina, M. O., Okon-Akan, O. A., Adebunsi, T. A., Ojedokun, A. T., Adegoke, K. A., & Bello, O. S. (2023). Adsorptive removal of antibiotic pollutants from wastewater using biomass/biochar-based adsorbents. In *RSC Advances* (Vol. 13, Issue 7, pp. 4678–4712). <https://doi.org/10.1039/d2ra06436g>
- Akhtar, J., Amin, N. A. S., & Shahzad, K. (2016). A review on removal of pharmaceuticals from water by adsorption. *Desalination and Water Treatment*, 57(27), 12842–12860. <https://doi.org/10.1080/19443994.2015.1051121>
- Akporomie, K. G., Ofomatah, A. C., Chukwuemeka-Okorie, H. O., Ani, J. U., Agbo, S. C., Odewole, O. A., Ojo, F. K., Alum, O. L., & Conradie, J. (2023). Equilibrium isotherm investigation on the sequestration of ciprofloxacin from solution via adsorption onto yam peel powder. *IOP Conference Series: Earth and Environmental Science*, 1178(1). <https://doi.org/10.1088/1755-1315/1178/1/012020>
- Albers, C. N., Feld, L., Ellegaard-Jensen, L., & Aamand, J. (2015). Degradation of trace concentrations of the persistent groundwater pollutant 2,6-dichlorobenzamide (BAM) in bioaugmented rapid sand filters. *Water Research*, 83, 61–70. <https://doi.org/10.1016/j.watres.2015.06.023>
- Alekseeva, T., Prevot, V., Sancelme, M., Forano, C., & Besse-Hoggan, P. (2011). Enhancing atrazine biodegradation by *Pseudomonas* sp. strain ADP adsorption to Layered Double Hydroxide bionanocomposites. *Journal of Hazardous Materials*, 191(1-3), 126–135. <https://doi.org/10.1016/j.jhazmat.2011.04.050>
- Al-Hazmi, G. H., Adam, A. M. A., El-Desouky, M. G., ElBindary, A. A., Alsuhaibani, A.

- M., & Refat, M. S. (2023). EFFICIENT ADSORPTION OF RHODAMINE B USING A COMPOSITE OF Fe₃O₄@ZIF-8: SYNTHESIS, CHARACTERIZATION, MODELING ANALYSIS, STATISTICAL PHYSICS AND MECHANISM OF INTERACTION. *Bulletin of the Chemical Society of Ethiopia*, 37(1), 211–229. <https://doi.org/10.4314/BCSE.V37I1.17>
- Al-Hazmi, G. H., Refat, M. S., Alshammari, K. F., Kubra, K. T., & Shahat, A. (2023). Efficient toxic doxorubicin hydrochloride removal from aqueous solutions using facial alumina nanorods. *Journal of Molecular Structure*, 1272. <https://doi.org/10.1016/j.molstruc.2022.134187>
- Ali, I. (2012). New generation adsorbents for water treatment. In *Chemical Reviews* (Vol. 112, Issue 10, pp. 5073–5091). <https://doi.org/10.1021/cr300133d>
- Aljuboury, D. A. D. A., Palaniandy, P., Abdul Aziz, H. B., & Feroz, S. (2017). Treatment of petroleum wastewater by conventional and new technologies - A review. In *Global Nest Journal* (Vol. 19, Issue 3, pp. 439–452). <https://doi.org/10.30955/gnj.002239>
- Almeida-Naranjo, C. E., Guerrero, V. H., & Villamar-Ayala, C. A. (2023). Emerging Contaminants and Their Removal from Aqueous Media Using Conventional/Non-Conventional Adsorbents: A Glance at the Relationship between Materials, Processes, and Technologies. In *Water (Switzerland)* (Vol. 15, Issue 8). <https://doi.org/10.3390/w15081626>
- AlMubaddal, F., AlRumaihi, K., & Ajbar, A. (2009). Performance optimization of coagulation/flocculation in the treatment of wastewater from a polyvinyl chloride plant. *Journal of Hazardous Materials*, 161(1), 431–438. <https://doi.org/10.1016/j.jhazmat.2008.03.121>
- Almufarij, R. S., Abdulkhair, B. Y., Salih, M., & Alhamdan, N. M. (2022). Sweep-Out of Tigecycline, Chlortetracycline, Oxytetracycline, and Doxycycline from Water by Carbon Nanoparticles Derived from Tissue Waste. *Nanomaterials*, 12(20). <https://doi.org/10.3390/nano12203617>
- Al-Musawi, T. J., Mahvi, A. H., Khatibi, A. D., & Balarak, D. (2021). Effective adsorption of ciprofloxacin antibiotic using powdered activated carbon magnetized by iron(III) oxide magnetic nanoparticles. *Journal of Porous Materials*, 28(3), 835–852. <https://doi.org/10.1007/s10934-021-01039-7>
- Al-Musawi, T. J., Rajiv, P., Mengelizadeh, N., Mohammed, I. A., & Balarak, D. (2021).

- Development of sonophotocatalytic process for degradation of acid orange 7 dye by using titanium dioxide nanoparticles/graphene oxide nanocomposite as a catalyst. *Journal of Environmental Management*, 292. <https://doi.org/10.1016/j.jenvman.2021.112777>
- Alonso, J. J. S., El Kori, N., Melián-Martel, N., & Del Río-Gamero, B. (2018). Removal of ciprofloxacin from seawater by reverse osmosis. *Journal of Environmental Management*, 217, 337–345. <https://doi.org/10.1016/j.jenvman.2018.03.108>
- Al-Qahtani, S. D., Ibarhiam, S., Sallam, S., Almotairy, A. R. Z., Al-Bonayan, A. M., Munshi, A. M., & El-Metwaly, N. M. (2023). Magnetic sodium alginate grafted with waste carbonaceous material for diclofenac sodium removal: optimization of operational parameters and process mechanism. *RSC Advances*, 13(10), 6466–6480. <https://doi.org/10.1039/d3ra00495c>
- Al-Salihi, S., Fidalgo, M. M., & Xing, Y. (2023). Fast Removal of Tetracycline from Aqueous Solution by Aluminosilicate Zeolite Nanoparticles with High Adsorption Capacity. *ACS ES and T Water*, 3(3), 838–847. <https://doi.org/10.1021/acsestwater.2c00600>
- Althumayri, K., Guesmi, A., El-Fattah, W. A., Houas, A., Hamadi, N. Ben, & Shahat, A. (2023). Enhanced Adsorption and Evaluation of Tetracycline Removal in an Aquatic System by Modified Silica Nanotubes. *ACS Omega*, 8(7), 6762–6777. <https://doi.org/10.1021/acsomega.2c07377>
- Ameen, H. M., Kunsági-Máté, S., Noveczky, P., Szente, L., & Lemli, B. (2020). Adsorption of sulfamethazine drug onto the modified derivatives of carbon nanotubes at different pH. *Molecules*, 25(11). <https://doi.org/10.3390/molecules25112489>
- Andrade, M. B., Santos, T. R. T., Guerra, A. C. S., Silva, M. F., Demiti, G. M. M., & Bergamasco, R. (2022). Evaluation of magnetic nano adsorbent produced from graphene oxide with iron and cobalt nanoparticles for caffeine removal from aqueous medium. *Chemical Engineering and Processing - Process Intensification*, 170. <https://doi.org/10.1016/j.cep.2021.108694>
- Anfar, Z., Zbair, M., Ait Ahsiane, H., Jada, A., & El Alem, N. (2020). Microwave assisted green synthesis of Fe₂O₃/biochar for ultrasonic removal of nonsteroidal anti-inflammatory pharmaceuticals. *RSC Advances*, 10(19), 11371–11380. <https://doi.org/10.1039/d0ra00617c>

- Antonelli, R., Malpass, G. R. P., Da Silva, M. G. C., & Vieira, M. G. A. (2020). Adsorption of ciprofloxacin onto thermally modified bentonite clay: Experimental design, characterization, and adsorbent regeneration. *Journal of Environmental Chemical Engineering*, 8(6). <https://doi.org/10.1016/j.jece.2020.104553>
- Asgharian, M., Mehdipourghazi, M., Khoshandam, B., & Keramati, N. (2020). Experimental design and rsm modeling of tetracycline photocatalytic degradation using rgo/zno/cu. *Desalination and Water Treatment*, 195, 177–185. <https://doi.org/10.5004/dwt.2020.25878>
- Ashiq, A., Adassooriya, N. M., Sarkar, B., Rajapaksha, A. U., Ok, Y. S., & Vithanage, M. (2019). Municipal solid waste biochar-bentonite composite for the removal of antibiotic ciprofloxacin from aqueous media. *Journal of Environmental Management*, 236, 428–435. <https://doi.org/10.1016/j.jenvman.2019.02.006>
- Ashiq, A., Walpita, J., & Vithanage, M. (2021). Functionalizing non-smectic clay via methoxy-modification for enhanced removal and recovery of oxytetracycline from aqueous media. *Chemosphere*, 276. <https://doi.org/10.1016/j.chemosphere.2021.130079>
- Asif, M. B., Li, C., Ren, B., Maqbool, T., Zhang, X., & Zhang, Z. (2021). Elucidating the impacts of intermittent in-situ ozonation in a ceramic membrane bioreactor: Micropollutant removal, microbial community evolution and fouling mechanisms. *Journal of Hazardous Materials*, 402. <https://doi.org/10.1016/j.jhazmat.2020.123730>
- Atugoda, T., Gunawardane, C., Ahmad, M., & Vithanage, M. (2021). Mechanistic interaction of ciprofloxacin on zeolite modified seaweed (*Sargassum crassifolium*) derived biochar: Kinetics, isotherm and thermodynamics. *Chemosphere*, 281. <https://doi.org/10.1016/j.chemosphere.2021.130676>
- aus der Beek, T., Weber, F. A., Bergmann, A., Hickmann, S., Ebert, I., Hein, A., & Küster, A. (2016). Pharmaceuticals in the environment-Global occurrences and perspectives. *Environmental Toxicology and Chemistry*, 35(4), 823–835. <https://doi.org/10.1002/etc.3339>
- Aydin, S., Aydin, M. E., Beduk, F., & Ulvi, A. (2019). Removal of antibiotics from aqueous solution by using magnetic Fe₃O₄/red mud-nanoparticles. *Science of the Total Environment*, 670, 539–546. <https://doi.org/10.1016/j.scitotenv.2019.03.205>
- Ayyubi, S. N., Purbasari, A., & Kusmiyati. (2022). The effect of composition on

- mechanical properties of biodegradable plastic based on chitosan/cassava starch/PVA/crude glycerol: Optimization of the composition using Box Behnken Design. *Materials Today: Proceedings*, 63, S78–S83. <https://doi.org/10.1016/j.matpr.2022.01.294>
- Azari, A., Nabizadeh, R., Mahvi, A. H., & Nasser, S. (2020). Integrated Fuzzy AHP-TOPSIS for selecting the best color removal process using carbon-based adsorbent materials: multi-criteria decision making vs . systematic review approaches and modeling of textile wastewater treatment in real conditions Integrated F. *International Journal of Environmental Analytical Chemistry*, 00(00), 1–16. <https://doi.org/10.1080/03067319.2020.1828395>
- Azizian, S. (2004). Kinetic models of sorption: A theoretical analysis. *Journal of Colloid and Interface Science*, 276(1), 47–52. <https://doi.org/10.1016/j.jcis.2004.03.048>
- Azqhandi, M. H. A., Foroughi, M., & Yazdankish, E. (2019). A highly effective, recyclable, and novel host-guest nanocomposite for Triclosan removal: A comprehensive modeling and optimization-based adsorption study. *Journal of Colloid and Interface Science*, 551, 195–207. <https://doi.org/10.1016/j.jcis.2019.05.007>
- Baharum, N. A., Nasir, H. M., Ishak, M. Y., Isa, N. M., Hassan, M. A., & Aris, A. Z. (2020). Highly efficient removal of diazinon pesticide from aqueous solutions by using coconut shell-modified biochar. *Arabian Journal of Chemistry*, 13(7), 6106–6121. <https://doi.org/10.1016/j.arabjc.2020.05.011>
- Bai, Y., Chang, Y., Liang, J., Chen, C., & Qu, J. (2016). Treatment of groundwater containing Mn(II), Fe(II), As(III) and Sb(III) by bioaugmented quartz-sand filters. *Water Research*, 106, 126–134. <https://doi.org/10.1016/j.watres.2016.09.040>
- Balarak, D., Baniasadi, M., Lee, S. M., & Shim, M. J. (2021). Ciprofloxacin adsorption onto azolla filiculoides activated carbon from aqueous solutions. *Desalination and Water Treatment*, 218, 444–453. <https://doi.org/10.5004/dwt.2021.26986>
- Balarak, D., & McKay, G. (2021). Utilization of MWCNTs/Al₂O₃ as adsorbent for ciprofloxacin removal: equilibrium, kinetics and thermodynamic studies. *Journal of Environmental Science and Health - Part A Toxic/Hazardous Substances and Environmental Engineering*, 56(3), 324–333. <https://doi.org/10.1080/10934529.2021.1873674>
- Balarak, D., Zafariyan, M., Igwegbe, C. A., Onyechi, K. K., & Ighalo, J. O. (2021).

- Adsorption of Acid Blue 92 Dye from Aqueous Solutions by Single-Walled Carbon Nanotubes: Isothermal, Kinetic, and Thermodynamic Studies. *Environmental Processes*, 8(2), 869–888. <https://doi.org/10.1007/s40710-021-00505-3>
- Barjasteh-Askari, F., Davoudi, M., Dolatabadi, M., & Ahmadzadeh, S. (2021). Iron-modified activated carbon derived from agro-waste for enhanced dye removal from aqueous solutions. *Heliyon*, 7(6). <https://doi.org/10.1016/j.heliyon.2021.e07191>
- Başkan, G., Açıkel, Ü., & Levent, M. (2022). Investigation of adsorption properties of oxytetracycline hydrochloride on magnetic zeolite/Fe₃O₄ particles. *Advanced Powder Technology*, 33(6). <https://doi.org/10.1016/j.appt.2022.103600>
- Beyer, F., Rietman, B. M., Zwijnenburg, A., van den Brink, P., Vrouwenvelder, J. S., Jarzembowska, M., Laurinonyte, J., Stams, A. J. M., & Plugge, C. M. (2014). Long-term performance and fouling analysis of full-scale direct nanofiltration (NF) installations treating anoxic groundwater. *Journal of Membrane Science*, 468, 339–348. <https://doi.org/10.1016/j.memsci.2014.06.004>
- Bidel, F., Di Poi, C., Budzinski, H., Pardon, P., Callewaert, W., Arini, A., Basu, N., Dickel, L., Bellanger, C., & Jozet-Alves, C. (2016). The antidepressant venlafaxine may act as a neurodevelopmental toxicant in cuttlefish (*Sepia officinalis*). *NeuroToxicology*, 55, 142–153. <https://doi.org/10.1016/j.neuro.2016.05.023>
- Bisaria, K., Wadhwa, S., Mathur, A., Roy, S., Dixit, A., & Singh, R. (2022). New bismuth oxyiodide/chitosan nanocomposite for ultrasonic waves expedited adsorptive removal of amoxicillin from aqueous medium: kinetic, isotherm and thermodynamic investigations. *Environmental Science and Pollution Research*. <https://doi.org/10.1007/s11356-021-17546-8>
- Bobde, P., Pandey, J. K., Kumar, R., Sharma, A. K., Pal, S., & Wadhwa, S. (2024). Sustainable Layered Double Hydroxide-Pine Cone Biochar (LDH/PCBC) composite for Enhanced Removal of Ciprofloxacin from Water. *New Journal of Chemistry*. <https://doi.org/10.1039/d4nj02064b>
- Bobde, P., Patel, R. K., Panchal, D., Sharma, A., Sharma, A. K., Dhodapkar, R. S., & Pal, S. (2021). Utilization of layered double hydroxides (LDHs) and their derivatives as photocatalysts for degradation of organic pollutants. *Environmental Science and Pollution Research*, 28(42), 59551–59569. <https://doi.org/10.1007/s11356-021-16296-x>
- Bobde, P., Sharma, A. K., Kumar, R., Pal, S., Pandey, J. K., & Wadhwa, S. (2023).

- Adsorptive removal of oxytetracycline using - MnO₂ - engineered pine - cone biochar: thermodynamic and kinetic investigation and process optimization. *Environmental Monitoring and Assessment*. <https://doi.org/10.1007/s10661-023-11932-0>
- Bobde, P., Sharma, A. K., Kumar, R., Pandey, J. K., & Wadhwa, S. (2023). Recent Advances for Sustainable Removal of Emerging Contaminants from Water by Bio-based Adsorbent. *New Journal of Chemistry*. <https://doi.org/10.1039/d3nj03731b>
- Bobde, P., Sharma, A. K., Panchal, D., Sharma, A., Patel, R. K., Dhodapkar, R. S., & Pal, S. (2022). Layered double hydroxides (LDHs)-based photocatalysts for dye degradation: a review. In *International Journal of Environmental Science and Technology*. <https://doi.org/10.1007/s13762-022-04007-z>
- Borrego, B., Lorenzo, G., Mota-Morales, J. D., Almanza-Reyes, H., Mateos, F., López-Gil, E., de la Losa, N., Burmistrov, V. A., Pestryakov, A. N., Brun, A., & Bogdanchikova, N. (2016). Potential application of silver nanoparticles to control the infectivity of Rift Valley fever virus in vitro and in vivo. *Nanomedicine: Nanotechnology, Biology, and Medicine*, *12*(5), 1185–1192. <https://doi.org/10.1016/j.nano.2016.01.021>
- Brodin, T., Fick, J., Jonsson, M., & Klaminder, J. (2013). Dilute concentrations of a psychiatric drug alter behavior of fish from natural populations. *Science*, *339*(6121), 814–815. <https://doi.org/10.1126/science.1226850>
- Cardona, Y., Korili, S. A., & Gil, A. (2023). Use of response surface methodology to optimize triclosan adsorption on alumina pillared clays in a fixed-bed column for applications in solid-phase extraction. *Applied Clay Science*, *235*. <https://doi.org/10.1016/j.clay.2023.106879>
- Cela-Dablanca, R., Barreiro, A., López, L. R., Santás-Miguel, V., Arias-Estévez, M., Núñez-Delgado, A., Álvarez-Rodríguez, E., & Fernández-Sanjurjo, M. J. (2022). Potential of low-cost bio-adsorbents to retain amoxicillin in contaminated water. *Environmental Research*, *213*. <https://doi.org/10.1016/j.envres.2022.113621>
- Chandrasekaran, A., Patra, C., Narayanasamy, S., & Subbiah, S. (2020). Adsorptive removal of Ciprofloxacin and Amoxicillin from single and binary aqueous systems using acid-activated carbon from *Prosopis juliflora*. *Environmental Research*, *188*. <https://doi.org/10.1016/j.envres.2020.109825>
- Chen, H., Gao, B., Yang, L. Y., & Ma, L. Q. (2015). Montmorillonite enhanced

- ciprofloxacin transport in saturated porous media with sorbed ciprofloxacin showing antibiotic activity. *Journal of Contaminant Hydrology*, 173, 1–7. <https://doi.org/10.1016/j.jconhyd.2014.11.010>
- Chen, L., Zhou, C. H., Fiore, S., Tong, D. S., Zhang, H., Li, C. S., Ji, S. F., & Yu, W. H. (2016). Functional magnetic nanoparticle/clay mineral nanocomposites: Preparation, magnetism and versatile applications. In *Applied Clay Science* (Vols. 127–128, pp. 143–163). <https://doi.org/10.1016/j.clay.2016.04.009>
- Chen, Y., Lan, T., Duan, L., Wang, F., Zhao, B., Zhang, S., & Wei, W. (2015). Adsorptive removal and adsorption kinetics of fluoroquinolone by nano-hydroxyapatite. *PLoS ONE*, 10(12). <https://doi.org/10.1371/journal.pone.0145025>
- Cherednichenko, G., Zhang, R., Bannister, R. A., Timofeyev, V., Li, N., Fritsch, E. B., Feng, W., Barrientos, G. C., Schebb, N. H., Hammock, B. D., Beam, K. G., Chiamvimonvat, N., & Pessah, I. N. (2012). Triclosan impairs excitation-contraction coupling and Ca²⁺ dynamics in striated muscle. *Proceedings of the National Academy of Sciences of the United States of America*, 109(35), 14158–14163. <https://doi.org/10.1073/pnas.1211314109>
- Cho, E. J., Kang, J. K., Moon, J. K., Um, B. H., Lee, C. G., Jeong, S., & Park, S. J. (2021). Removal of triclosan from aqueous solution via adsorption by kenaf-derived biochar: Its adsorption mechanism study via spectroscopic and experimental approaches. *Journal of Environmental Chemical Engineering*, 9(6). <https://doi.org/10.1016/j.jece.2021.106343>
- Choudhary, V., & Philip, L. (2022). Sustainability assessment of acid-modified biochar as adsorbent for the removal of pharmaceuticals and personal care products from secondary treated wastewater. *Journal of Environmental Chemical Engineering*, 10(3). <https://doi.org/10.1016/j.jece.2022.107592>
- Clara, M., Windhofer, G., Hartl, W., Braun, K., Simon, M., Gans, O., Scheffknecht, C., & Chovanec, A. (2010). Occurrence of phthalates in surface runoff, untreated and treated wastewater and fate during wastewater treatment. *Chemosphere*, 78(9), 1078–1084. <https://doi.org/10.1016/j.chemosphere.2009.12.052>
- Clarke, B. O., & Smith, S. R. (2011). Review of “emerging” organic contaminants in biosolids and assessment of international research priorities for the agricultural use of biosolids. In *Environment International* (Vol. 37, Issue 1, pp. 226–247). <https://doi.org/10.1016/j.envint.2010.06.004>

- Crini, G. (2005). Recent developments in polysaccharide-based materials used as adsorbents in wastewater treatment. In *Progress in Polymer Science (Oxford)* (Vol. 30, Issue 1, pp. 38–70). <https://doi.org/10.1016/j.progpolymsci.2004.11.002>
- da Silva Bruckmann, F., Schnorr, C. E., da Rosa Salles, T., Nunes, F. B., Baumann, L., Müller, E. I., Silva, L. F. O., Dotto, G. L., & Bohn Rhoden, C. R. (2022). Highly Efficient Adsorption of Tetracycline Using Chitosan-Based Magnetic Adsorbent. *Polymers*, *14*(22). <https://doi.org/10.3390/polym14224854>
- Dąbrowski, A. (2001). Adsorption - From theory to practice. In *Advances in Colloid and Interface Science* (Vol. 93, Issues 1-3, pp. 135–224). [https://doi.org/10.1016/S0001-8686\(00\)00082-8](https://doi.org/10.1016/S0001-8686(00)00082-8)
- Dai, Z., Zhao, L., Peng, S., Yue, Z., Zhan, X., & Wang, J. (2022). Removal of oxytetracycline promoted by manganese-doped biochar based on density functional theory calculations: Comprehensive evaluation of the effect of transition metal doping. *Science of The Total Environment*, *806*, 150268. <https://doi.org/10.1016/j.scitotenv.2021.150268>
- Das, R., & Panda, S. N. (2022). Preparation and applications of biochar based nanocomposite: A review. *Journal of Analytical and Applied Pyrolysis*, *167*, 105691. <https://doi.org/10.1016/j.jaap.2022.105691>
- Daughton, C. G. (2002). Environmental stewardship and drugs as pollutants. In *Lancet* (Vol. 360, Issue 9339, pp. 1035–1036). [https://doi.org/10.1016/S0140-6736\(02\)11176-7](https://doi.org/10.1016/S0140-6736(02)11176-7)
- Davoud Balarak, Mohadeseh Zafariyan, & Shaziya Siddiqui. (2022). Investigation of Adsorptive Properties of Surfactant Modified Sepiolite for Removal of Ciprofloxacin. *International Journal of Life Science and Pharma Research*. <https://doi.org/10.22376/ijpbs/lpr.2020.10.3.p12-19>
- Dawson, A. H., Eddleston, M., Senarathna, L., Mohamed, F., Gawarammana, I., Bowe, S. J., Manuweera, G., & Buckley, N. A. (2010). Acute human lethal toxicity of agricultural pesticides: A prospective cohort study. *PLoS Medicine*, *7*(10). <https://doi.org/10.1371/journal.pmed.1000357>
- de Andrade, J. R., Oliveira, M. F., Canevesi, R. L. S., Landers, R., da Silva, M. G. C., & Vieira, M. G. A. (2020). Comparative adsorption of diclofenac sodium and losartan potassium in organophilic clay-packed fixed-bed: X-ray photoelectron spectroscopy characterization, experimental tests and theoretical study on DFT-based chemical

- descriptors. *Journal of Molecular Liquids*, 312. <https://doi.org/10.1016/j.molliq.2020.113427>
- de Azevedo, C. F., Machado, F. M., de Souza, N. F., Silveira, L. L., Lima, E. C., Andrezza, R., & Bergamnn, C. P. (2023). Comprehensive adsorption and spectroscopic studies on the interaction of carbon nanotubes with diclofenac anti-inflammatory. *Chemical Engineering Journal*, 454. <https://doi.org/10.1016/j.cej.2022.140102>
- de Ilurdoz, M. S., Sadhwani, J. J., & Reboso, J. V. (2022). Antibiotic removal processes from water & wastewater for the protection of the aquatic environment - a review. *Journal of Water Process Engineering*, 45, 102474. <https://doi.org/10.1016/j.jwpe.2021.102474>
- de Sousa, D. N. R., Insa, S., Mozeto, A. A., Petrovic, M., Chaves, T. F., & Fadini, P. S. (2018). Equilibrium and kinetic studies of the adsorption of antibiotics from aqueous solutions onto powdered zeolites. *Chemosphere*, 205, 137–146. <https://doi.org/10.1016/j.chemosphere.2018.04.085>
- de Souza dos Santos, G. E., Ide, A. H., Duarte, J. L. S., McKay, G., Silva, A. O. S., & Meili, L. (2020). Adsorption of anti-inflammatory drug diclofenac by MgAl/layered double hydroxide supported on Syagrus coronata biochar. *Powder Technology*, 364, 229–240. <https://doi.org/10.1016/j.powtec.2020.01.083>
- Deblonde, T., Cossu-Leguille, C., & Hartemann, P. (2011). Emerging pollutants in wastewater: A review of the literature. *International Journal of Hygiene and Environmental Health*, 214(6), 442–448. <https://doi.org/10.1016/j.ijheh.2011.08.002>
- Debnath, S., Ballav, N., Maity, A., & Pillay, K. (2017). Competitive adsorption of ternary dye mixture using pine cone powder modified with β -cyclodextrin. *Journal of Molecular Liquids*, 225, 679–688. <https://doi.org/10.1016/j.molliq.2016.10.109>
- Dehghan, A., Mohammadi, A. A., Yousefi, M., Najafpoor, A. A., Shams, M., & Rezanian, S. (2019). Enhanced kinetic removal of ciprofloxacin onto metal-organic frameworks by sonication, process optimization and metal leaching study. *Nanomaterials*, 9(10). <https://doi.org/10.3390/nano9101422>
- Dehghan, S., Azari, A., & Kalantary, R. R. (2018). *Reductive degradation of high concentration nitrobenzene using nanoscale zero-valent iron particles immobilized on Polyaniline*. *Reductive degradation of high concentration nitrobenzene using nanoscale zero-valent iron particles immobilized on Polyaniline*. December.

<https://doi.org/10.5004/dwt.2018.22536>

- Dehghan, S., Kalantary, R. R., & Azari, A. (2017). *Nitrobenzene degradation from aqueous solutions using zerovalent iron nanoparticles / polyaniline composite Nitrobenzene Degradation from Aqueous Solutions Using Zero-valent Iron Nanoparticles / Polyaniline Composite*. January.
- Deng, Y., & Zhao, R. (2015). Advanced Oxidation Processes (AOPs) in Wastewater Treatment. In *Current Pollution Reports* (Vol. 1, Issue 3, pp. 167–176). <https://doi.org/10.1007/s40726-015-0015-z>
- Dey, S., Bano, F., & Malik, A. (2019). Pharmaceuticals and personal care product (PPCP) contamination-a global discharge inventory. In *Pharmaceuticals and Personal Care Products: Waste Management and Treatment Technology Emerging Contaminants and Micro Pollutants* (pp. 1–26). <https://doi.org/10.1016/B978-0-12-816189-0.00001-9>
- Dionísio, J., Gonçalves, C., Guedes, P., Ribeiro, A. B., & Couto, N. (2021). Electrochemical treatment of effluent for the removal of contaminants of emergent concern and culturable microorganisms. *Water (Switzerland)*, 13(4). <https://doi.org/10.3390/w13040520>
- Dolatabadi, M., Ghorbanian, A., & Ahmadzadeh, S. (2021). Mg-Al-layered Double Hydroxide as Promising Sustainable Nanoadsorbent for Application in Water/Wastewater Treatment Processes; Diethyl Phthalate Removal. *Journal of Environmental Health and Sustainable Development*, 6(3), 1367–1375. <https://doi.org/10.18502/JEHS.D.V6I3.7244>
- Dolatabadi, M., Kheirieh, A., Yoosefian, M., & Ahmadzadeh, S. (2022). Hydroxyzine removal from the polluted aqueous solution using the hybrid treatment process of electrocoagulation and adsorption; optimization, and modeling. *Applied Water Science*, 12(11). <https://doi.org/10.1007/s13201-022-01780-7>
- Dolatabadi, M., Meftahizade, H., Ahmadzadeh, S., Abbasi, F., Falakian, M., & Ghorbanpour, M. (2023). Efficiency of modified plant guar gum as aid coagulant for removal of diazinon from aqueous solution: optimization by response surface methodology. *Chemical Papers*, 77(3), 1339–1349. <https://doi.org/10.1007/s11696-022-02555-9>
- Dolatabadi, M., Naidu, H., & Ahmadzadeh, S. (2021). A green approach to remove acetamiprid insecticide using pistachio shell-based modified activated carbon;

- economical groundwater treatment. *Journal of Cleaner Production*, 316. <https://doi.org/10.1016/j.jclepro.2021.128226>
- Dolatabadi, M., Naidu, H., & Ahmadzadeh, S. (2022). Adsorption characteristics in the removal of chlorpyrifos from groundwater using magnetic graphene oxide and carboxy methyl cellulose composite. *Separation and Purification Technology*, 300. <https://doi.org/10.1016/j.seppur.2022.121919>
- Donkadokula, N. Y., Kola, A. K., Naz, I., & Saroj, D. (2020). A review on advanced physico-chemical and biological textile dye wastewater treatment techniques. In *Reviews in Environmental Science and Biotechnology* (Vol. 19, Issue 3, pp. 543–560). <https://doi.org/10.1007/s11157-020-09543-z>
- Dotto, G. L., Vieira, M. L. G., Esquerdo, V. M., & Pinto, L. A. A. (2013). Equilibrium and thermodynamics of azo dyes biosorption onto *Spirulina platensis*. *Brazilian Journal of Chemical Engineering*, 30(1), 13–21. <https://doi.org/10.1590/S0104-66322013000100003>
- Du, L., & Liu, W. (2012). Occurrence, fate, and ecotoxicity of antibiotics in agro-ecosystems. A review. In *Agronomy for Sustainable Development* (Vol. 32, Issue 2, pp. 309–327). <https://doi.org/10.1007/s13593-011-0062-9>
- El Hadki, A., Ulucan-Altuntas, K., El Hadki, H., Ustundag, C. B., Kabbaj, O. K., Dahchour, A., Komiha, N., Zrineh, A., & Debik, E. (2021). Removal of oxytetracycline by graphene oxide and Boron-doped reduced graphene oxide: A combined density function Theory, molecular dynamics simulation and experimental study. *FlatChem*, 27. <https://doi.org/10.1016/j.flatc.2021.100238>
- Elamin, M. R., Abdulkhair, B. Y., & Elzupir, A. O. (2022). Removal of ciprofloxacin and indigo carmine from water by carbon nanotubes fabricated from a low-cost precursor: Solution parameters and recyclability. *Ain Shams Engineering Journal*. <https://doi.org/10.1016/j.asej.2022.101844>
- El-Bendary, N., El-Etriby, H. K., & Mahanna, H. (2022). Reuse of adsorption residuals for enhancing removal of ciprofloxacin from wastewater. *Environmental Technology (United Kingdom)*, 43(28), 4438–4454. <https://doi.org/10.1080/09593330.2021.1952310>
- El-Sheikh, A. H., Qawariq, R. F., & Abdelghani, J. I. (2019). Adsorption and magnetic solid-phase extraction of NSAIDs from pharmaceutical wastewater using magnetic carbon nanotubes: Effect of sorbent dimensions, magnetite loading and competitive

- adsorption study. *Environmental Technology and Innovation*, 16. <https://doi.org/10.1016/j.eti.2019.100496>
- Emily Chelangat Ngeno, Francis Orata, Lilechi Danstone Baraza, Victor Odhiambo Shikuku, & Selly Jemutai Kimosop. (2016). Adsorption of Caffeine and Ciprofloxacin onto Pyrolytically Derived Water Hyacinth Biochar: Isothermal, Kinetic and Thermodynamic Studies. *Journal of Chemistry and Chemical Engineering*, 10(4). <https://doi.org/10.17265/1934-7375/2016.04.006>
- Ewis, D., Ba-Abbad, M. M., Benamor, A., & El-Naas, M. H. (2022). Adsorption of organic water pollutants by clays and clay minerals composites: A comprehensive review. In *Applied Clay Science* (Vol. 229). <https://doi.org/10.1016/j.clay.2022.106686>
- Ewis, D., & Hameed, B. H. (2021). A review on microwave-assisted synthesis of adsorbents and its application in the removal of water pollutants. In *Journal of Water Process Engineering* (Vol. 41). <https://doi.org/10.1016/j.jwpe.2021.102006>
- Eze, S. I., Akpomie, K. G., Ezekoye, O. M., Chukwujindu, C. N., Ojo, F. K., Ani, J. U., & Ujam, O. T. (2021). Antibiotic Adsorption by Acid Enhanced Dialium guineense Seed Waste. *Arabian Journal for Science and Engineering*, 46(1), 309–324. <https://doi.org/10.1007/s13369-020-04771-5>
- Ezekoye, O. M., Akpomie, K. G., Eze, S. I., Chukwujindu, C. N., Ani, J. U., & Ujam, O. T. (2020). Biosorptive interaction of alkaline modified Dialium guineense seed powders with ciprofloxacin in contaminated solution: central composite, kinetics, isotherm, thermodynamics, and desorption. *International Journal of Phytoremediation*, 22(10), 1028–1037. <https://doi.org/10.1080/15226514.2020.1725869>
- Fan, Y., Su, J., Xu, L., Liu, S., Hou, C., Liu, Y., & Cao, S. (2023). Removal of oxytetracycline from wastewater by biochar modified with biosynthesized iron oxide nanoparticles and carbon nanotubes: Modification performance and adsorption mechanism. *Environmental Research*, 231. <https://doi.org/10.1016/j.envres.2023.116307>
- Fan, Z., Fang, J., Zhang, G., Qin, L., Fang, Z., & Jin, L. (2022). Improved Adsorption of Tetracycline in Water by a Modified Caulis spatholobi Residue Biochar. *ACS Omega*, 7(34), 30543–30553. <https://doi.org/10.1021/acsomega.2c04033>
- Farias, K. C. S., Guimarães, R. C. A., Oliveira, K. R. W., Nazário, C. E. D., Ferencz, J.

- A. P., & Wender, H. (2023). Banana Peel Powder Biosorbent for Removal of Hazardous Organic Pollutants from Wastewater. *Toxics*, *11*(8). <https://doi.org/10.3390/toxics11080664>
- Feng, L., Yuan, G., Xiao, L., Wei, J., & Bi, D. (2021a). Biochar Modified by Nanomanganese Dioxide as Adsorbent and Oxidant for Oxytetracycline. *Bulletin of Environmental Contamination and Toxicology*, *107*(2), 269–275. <https://doi.org/10.1007/s00128-020-02813-0>
- Feng, L., Yuan, G., Xiao, L., Wei, J., & Bi, D. (2021b). Biochar Modified by Nanomanganese Dioxide as Adsorbent and Oxidant for Oxytetracycline. *Bulletin of Environmental Contamination and Toxicology*, *107*(2), 269–275. <https://doi.org/10.1007/s00128-020-02813-0>
- Fernando, J. C., Peiris, C., Navarathna, C. M., Gunatilake, S. R., Welikala, U., Wanasinghe, S. T., Madduri, S. B., Jayasinghe, S., Mlsna, T. E., Hassan, E. B., & Ferez, F. (2021). Nitric acid surface pre-modification of novel *Lasia spinosa* biochar for enhanced methylene blue remediation. *Groundwater for Sustainable Development*, *14*. <https://doi.org/10.1016/j.gsd.2021.100603>
- Ferreira, A. R., Couto, N., Guedes, P., Pinto, J., Mateus, E. P., & Ribeiro, A. B. (2018). Electrolytic 2-compartment cells for emerging organic contaminants removal from effluent. *Journal of Hazardous Materials*, *358*, 467–474. <https://doi.org/10.1016/j.jhazmat.2018.04.066>
- Forouzes, M., Ebadi, A., & Aghaeinejad-Meybodi, A. (2019). Degradation of metronidazole antibiotic in aqueous medium using activated carbon as a persulfate activator. *Separation and Purification Technology*, *210*, 145–151. <https://doi.org/10.1016/j.seppur.2018.07.066>
- Fountain, M. T., Brown, V. K., Gange, A. C., Symondson, W. O. C., & Murray, P. J. (2007). The effects of the insecticide chlorpyrifos on spider and Collembola communities. *Pedobiologia*, *51*(2), 147–158. <https://doi.org/10.1016/j.pedobi.2007.03.001>
- Fujioka, T., Khan, S. J., Poussade, Y., Drewes, J. E., & Nghiem, L. D. (2012). Nitrosamine removal by reverse osmosis for indirect potable water reuse - A critical review based on observations from laboratory-, pilot- and full-scale studies. In *Separation and Purification Technology* (Vol. 98, pp. 503–515). <https://doi.org/10.1016/j.seppur.2012.07.025>

- Fulé, P. Z., Garkoti, S. C., & Semwal, R. L. (2021). Frequent burning in chir pine forests, Uttarakhand, India. *Fire Ecology*, *17*(1). <https://doi.org/10.1186/s42408-021-00106-3>
- Furlong, E. T., Batt, A. L., Glassmeyer, S. T., Noriega, M. C., Kolpin, D. W., Mash, H., & Schenck, K. M. (2017). Nationwide reconnaissance of contaminants of emerging concern in source and treated drinking waters of the United States: Pharmaceuticals. *Science of the Total Environment*, *579*, 1629–1642. <https://doi.org/10.1016/j.scitotenv.2016.03.128>
- Gabet, A., Guy, C., Fazli, A., Métivier, H., de Brauer, C., Brigante, M., & Mailhot, G. (2023). The ability of recycled magnetite nanoparticles to degrade carbamazepine in water through photo-Fenton oxidation at neutral pH. *Separation and Purification Technology*, *317*. <https://doi.org/10.1016/j.seppur.2023.123877>
- Gadipelly, C., Pérez-González, A., Yadav, G. D., Ortiz, I., Ibáñez, R., Rathod, V. K., & Marathe, K. V. (2014). Pharmaceutical industry wastewater: Review of the technologies for water treatment and reuse. In *Industrial and Engineering Chemistry Research* (Vol. 53, Issue 29, pp. 11571–11592). <https://doi.org/10.1021/ie501210j>
- Gámiz, B., Velarde, P., Spokas, K. A., & Cox, L. (2022). The Role of Nanoengineered Biochar Activated with Fe for Sulfanilamide Removal from Soils and Water. *Molecules*, *27*(21). <https://doi.org/10.3390/molecules27217418>
- Gao, M., Zhang, Y., Gong, X., Song, Z., & Guo, Z. (2018). Removal mechanism of di-n-butyl phthalate and oxytetracycline from aqueous solutions by nano-manganese dioxide modified biochar. *Environmental Science and Pollution Research*, *25*(8), 7796–7807. <https://doi.org/10.1007/s11356-017-1089-5>
- Gao, Y., Li, Y., Zhang, L., Huang, H., Hu, J., Shah, S. M., & Su, X. (2012). Adsorption and removal of tetracycline antibiotics from aqueous solution by graphene oxide. *Journal of Colloid and Interface Science*, *368*(1), 540–546. <https://doi.org/10.1016/j.jcis.2011.11.015>
- García-Mateos, F. J., Ruiz-Rosas, R., Marqués, M. D., Cotoruelo, L. M., Rodríguez-Mirasol, J., & Cordero, T. (2015). Removal of paracetamol on biomass-derived activated carbon: Modeling the fixed bed breakthrough curves using batch adsorption experiments. *Chemical Engineering Journal*, *279*, 18–30. <https://doi.org/10.1016/j.cej.2015.04.144>

- Geissen, V., Mol, H., Klumpp, E., Umlauf, G., Nadal, M., van der Ploeg, M., van de Zee, S. E. A. T. M., & Ritsema, C. J. (2015). Emerging pollutants in the environment: A challenge for water resource management. *International Soil and Water Conservation Research*, 3(1), 57–65. <https://doi.org/10.1016/j.iswcr.2015.03.002>
- Genç, N., & Dogan, E. C. (2015). Adsorption kinetics of the antibiotic ciprofloxacin on bentonite, activated carbon, zeolite, and pumice. *Desalination and Water Treatment*, 53(3), 785–793. <https://doi.org/10.1080/19443994.2013.842504>
- Gerente, C., Lee, V. K. C., Le Cloirec, P., & McKay, G. (2007). Application of chitosan for the removal of metals from wastewaters by adsorption - Mechanisms and models review. In *Critical Reviews in Environmental Science and Technology* (Vol. 37, Issue 1, pp. 41–127). <https://doi.org/10.1080/10643380600729089>
- Giglio, A., Giulianini, P. G., Zetto, T., & Talarico, F. (2011). Effects of the pesticide dimethoate on a non-target generalist carabid, *Pterostichus melas italicus* (Dejean, 1828) (Coleoptera: Carabidae). In *Italian Journal of Zoology* (Vol. 78, Issue 4, pp. 471–477). <https://doi.org/10.1080/11250003.2011.571222>
- Gil, A., Santamaría, L., & Korili, S. A. (2018). Removal of Caffeine and Diclofenac from Aqueous Solution by Adsorption on Multiwalled Carbon Nanotubes. *Colloids and Interface Science Communications*, 22, 25–28. <https://doi.org/10.1016/j.colcom.2017.11.007>
- Girardi, C., Greve, J., Lamshöft, M., Fetzer, I., Miltner, A., Schäffer, A., & Kästner, M. (2011). Biodegradation of ciprofloxacin in water and soil and its effects on the microbial communities. *Journal of Hazardous Materials*, 198, 22–30. <https://doi.org/10.1016/j.jhazmat.2011.10.004>
- Giulivo, M., Lopez de Alda, M., Capri, E., & Barceló, D. (2016). Human exposure to endocrine disrupting compounds: Their role in reproductive systems, metabolic syndrome and breast cancer. A review. In *Environmental Research* (Vol. 151, pp. 251–264). <https://doi.org/10.1016/j.envres.2016.07.011>
- Gräfe, M., Power, G., & Klauber, C. (2011). Bauxite residue issues: III. Alkalinity and associated chemistry. *Hydrometallurgy*, 108(1-2), 60–79. <https://doi.org/10.1016/j.hydromet.2011.02.004>
- Grassi, M., Kaykioglu, G., Belgiorno, V., & Lofrano, G. (2012). *Removal of Emerging Contaminants from Water and Wastewater by Adsorption Process* (pp. 15–37). https://doi.org/10.1007/978-94-007-3916-1_2

- Gu, Y., Xue, Y., & Zhang, D. (2021). Preparation of magnetic biochar with different magnetization sequences for efficient removal of oxytetracycline from aqueous solution. *Colloids and Surfaces A: Physicochemical and Engineering Aspects*, 626. <https://doi.org/10.1016/j.colsurfa.2021.126987>
- Guo, J., Wang, R., Tjiu, W. W., Pan, J., & Liu, T. (2012). Synthesis of Fe nanoparticles@graphene composites for environmental applications. *Journal of Hazardous Materials*, 225-226, 63–73. <https://doi.org/10.1016/j.jhazmat.2012.04.065>
- Gupta, V. K., Agarwal, S., & Saleh, T. A. (2011). Chromium removal by combining the magnetic properties of iron oxide with adsorption properties of carbon nanotubes. *Water Research*, 45(6), 2207–2212. <https://doi.org/10.1016/j.watres.2011.01.012>
- Gupta, V. K., & Ali, I. (2001). Removal of DDD and DDE from wastewater using bagasse fly ash, a sugar industry waste. *Water Research*, 35(1), 33–40. [https://doi.org/10.1016/S0043-1354\(00\)00232-3](https://doi.org/10.1016/S0043-1354(00)00232-3)
- Gupta, V. K., Jain, C. K., Ali, I., Chandra, S., & Agarwal, S. (2002). Removal of lindane and malathion from wastewater using bagasse fly ash - A sugar industry waste. *Water Research*, 36(10), 2483–2490. [https://doi.org/10.1016/S0043-1354\(01\)00474-2](https://doi.org/10.1016/S0043-1354(01)00474-2)
- Guzel Kaya, G., Aznar, E., Deveci, H., & Martínez-Máñez, R. (2021). Low-cost silica xerogels as potential adsorbents for ciprofloxacin removal. *Sustainable Chemistry and Pharmacy*, 22. <https://doi.org/10.1016/j.scp.2021.100483>
- Hamadeen, H. M., & Elkhatib, E. A. (2022). New nanostructured activated biochar for effective removal of antibiotic ciprofloxacin from wastewater: Adsorption dynamics and mechanisms. *Environmental Research*, 210. <https://doi.org/10.1016/j.envres.2022.112929>
- Han, Y., Zheng, J., Jiang, C., Zhang, F., Wei, L., & Zhu, L. (2022). Hydrochloric acid-modified algal biochar for the removal of *Microcystis aeruginosa*: Coagulation performance and mechanism. *Journal of Environmental Chemical Engineering*, 10(6). <https://doi.org/10.1016/j.jece.2022.108903>
- Hao, M., Qiu, M., Yang, H., Hu, B., & Wang, X. (2021). Recent advances on preparation and environmental applications of MOF-derived carbons in catalysis. In *Science of the Total Environment* (Vol. 760). <https://doi.org/10.1016/j.scitotenv.2020.143333>
- Harja, M., & Ciobanu, G. (2017). Removal of oxytetracycline from aqueous solutions by

- hydroxyapatite as a low-cost adsorbent. *E3S Web of Conferences*, 22. <https://doi.org/10.1051/e3sconf/20172200062>
- Hasan, M. N., Salman, M. S., Hasan, M. M., Kubra, K. T., Sheikh, M. C., Rehan, A. I., Rasee, A. I., Awual, M. E., Waliullah, R. M., Hossain, M. S., Islam, A., Khandaker, S., Alsukaibi, A. K. D., Alshammari, H. M., & Awual, M. R. (2023). Assessing sustainable Lutetium(III) ions adsorption and recovery using novel composite hybrid nanomaterials. *Journal of Molecular Structure*, 1276. <https://doi.org/10.1016/j.molstruc.2022.134795>
- Hashemi, S. Y., Yegane Badi, M., Pasalari, H., Azari, A., Arfaeinia, H., & Kiani, A. (2022). Degradation of Ceftriaxone from aquatic solution using a heterogeneous and reusable O₃/UV/ Fe₃O₄@TiO₂ systems: operational factors, kinetics and mineralisation. *International Journal of Environmental Analytical Chemistry*, 102(18), 6904–6920. <https://doi.org/10.1080/03067319.2020.1817909>
- Hiew, B. Y. Z., Lee, L. Y., Lee, X. J., Gan, S., Thangalazhy-Gopakumar, S., Lim, S. S., Pan, G. T., & Yang, T. C. K. (2019). Adsorptive removal of diclofenac by graphene oxide: Optimization, equilibrium, kinetic and thermodynamic studies. *Journal of the Taiwan Institute of Chemical Engineers*, 98, 150–162. <https://doi.org/10.1016/j.jtice.2018.07.034>
- Ho, Y. S., & McKay, G. (1999). Pseudo-second order model for sorption processes. *Process Biochemistry*, 34(5), 451–465. [https://doi.org/10.1016/S0032-9592\(98\)00112-5](https://doi.org/10.1016/S0032-9592(98)00112-5)
- Ho, Y. S., & McKay, G. (2000). The kinetics of sorption of divalent metal ions onto sphagnum moss peat. *Water Research*, 34(3), 735–742. [https://doi.org/10.1016/S0043-1354\(99\)00232-8](https://doi.org/10.1016/S0043-1354(99)00232-8)
- Hongsawat, P., & Prarat, P. (2022). Comparative adsorption performance of oxytetracycline and sulfamethoxazole antibiotic on powder activated carbon and graphene oxide. *Chemical Papers*, 76(4), 2293–2305. <https://doi.org/10.1007/s11696-021-02024-9>
- Hoslett, J., Ghazal, H., Katsou, E., & Jouhara, H. (2021). The removal of tetracycline from water using biochar produced from agricultural discarded material. *Science of the Total Environment*, 751. <https://doi.org/10.1016/j.scitotenv.2020.141755>
- Houtman, C. J. (2010). Emerging contaminants in surface waters and their relevance for the production of drinking water in Europe. In *Journal of Integrative Environmental*

- Sciences* (Vol. 7, Issue 4, pp. 271–295).
<https://doi.org/10.1080/1943815X.2010.511648>
- Hristovski, K. D., & Markovski, J. (2017). Engineering metal (hydr)oxide sorbents for removal of arsenate and similar weak-acid oxyanion contaminants: A critical review with emphasis on factors governing sorption processes. *Science of the Total Environment*, 598, 258–271. <https://doi.org/10.1016/j.scitotenv.2017.04.108>
- Huang, R., Zhu, Q., Wang, W., & Hu, Y. (2023). Adsorptive removal of ciprofloxacin by a chitosan modified Fe pretreatment biochar composite from aqueous solution. *New Journal of Chemistry*, 47(16), 7910–7921. <https://doi.org/10.1039/d3nj00403a>
- Huang, W., Chen, J., & Zhang, J. (2020). Removal of ciprofloxacin from aqueous solution by rabbit manure biochar. *Environmental Technology (United Kingdom)*, 41(11), 1380–1390. <https://doi.org/10.1080/09593330.2018.1535628>
- Huo, X., Yi, H., Almatrafi, E., Ma, D., Fu, Y., Qin, L., Xia, W., Xiang, L., Xu, F., Yan, H., Zhou, C., Zeng, G., & Lai, C. (2023). Insights into Fenton-like oxidation of oxytetracycline mediated by Fe-doped porous g-C₃N₄ nanomaterials: synthesis, performance and mechanism. *Environmental Science: Nano*. <https://doi.org/10.1039/d3en00108c>
- Islam, M. T., Saenz-Arana, R., Hernandez, C., Guinto, T., Ahsan, M. A., Kim, H., Lin, Y., Alvarado-Tenorio, B., & Noveron, J. C. (2018). Adsorption of methylene blue and tetracycline onto biomass-based material prepared by sulfuric acid reflux. *RSC Advances*, 8(57), 32545–32557. <https://doi.org/10.1039/c8ra05395b>
- James-Todd, T. M., Chiu, Y.-H., & Zota, A. R. (2016). Racial/Ethnic Disparities in Environmental Endocrine Disrupting Chemicals and Women's Reproductive Health Outcomes: Epidemiological Examples Across the Life Course. *Current Epidemiology Reports*, 3(2), 161–180. <https://doi.org/10.1007/s40471-016-0073-9>
- Jang, H. M., Yoo, S., Choi, Y. K., Park, S., & Kan, E. (2018). Adsorption isotherm, kinetic modeling and mechanism of tetracycline on Pinus taeda-derived activated biochar. *Bioresource Technology*, 259, 24–31. <https://doi.org/10.1016/j.biortech.2018.03.013>
- Jha, S., Gaur, R., Shahabuddin, S., & Tyagi, I. (2023). Biochar as Sustainable Alternative and Green Adsorbent for the Remediation of Noxious Pollutants: A Comprehensive Review. In *Toxics* (Vol. 11, Issue 2). <https://doi.org/10.3390/toxics11020117>
- Ji, H., Wang, T., Huang, T., Lai, B., & Liu, W. (2021). Adsorptive removal of

- ciprofloxacin with different dissociated species onto titanate nanotubes. *Journal of Cleaner Production*, 278. <https://doi.org/10.1016/j.jclepro.2020.123924>
- Jiang, N., Erdős, M., Moulτος, O. A., Shang, R., Vlugt, T. J. H., Heijman, S. G. J., & Rietveld, L. C. (2020). The adsorption mechanisms of organic micropollutants on high-silica zeolites causing S-shaped adsorption isotherms: An experimental and Monte Carlo simulation study. *Chemical Engineering Journal*, 389. <https://doi.org/10.1016/j.cej.2019.123968>
- Jiang, N., Shang, R., Heijman, S. G. J., & Rietveld, L. C. (2018). High-silica zeolites for adsorption of organic micro-pollutants in water treatment: A review. In *Water Research* (Vol. 144, pp. 145–161). <https://doi.org/10.1016/j.watres.2018.07.017>
- Jiang, Q., Han, Z., Li, W., Ji, T., Yuan, Y., Zhang, J., Zhao, C., Cheng, Z., & Wang, S. (2022). Adsorption properties of heavy metals and antibiotics by chitosan from larvae and adult *Trypoxylus dichotomus*. *Carbohydrate Polymers*, 276. <https://doi.org/10.1016/j.carbpol.2021.118735>
- Jiao, S., Zheng, S., Yin, D., Wang, L., & Chen, L. (2008). Aqueous photolysis of tetracycline and toxicity of photolytic products to luminescent bacteria. *Chemosphere*, 73(3), 377–382. <https://doi.org/10.1016/j.chemosphere.2008.05.042>
- Jin, J., Kang, M., Sun, K., Pan, Z., Wu, F., & Xing, B. (2016). Properties of biochar-amended soils and their sorption of imidacloprid, isoproturon, and atrazine. *Science of the Total Environment*, 550, 504–513. <https://doi.org/10.1016/j.scitotenv.2016.01.117>
- Jobb, D. B., Anderson, W. B., Lecraw, R. A., & Collins, M. R. (2007). *Removal of Emerging Contaminants and Pathogens Using Modified Slow Sand Filtration: An Overview. November 2007.*
- Jokandan, S. F., Badi, M. Y., Esrafilı, A., Azari, A., Ahmadi, E., Tarhandeh, H., & Kermani, M. (2019). Investigation of the efficiency of powder activated carbon magnetized with Fe₃O₄ nanoparticles in the removal of catechol from aqueous solutions by response surface methodology. *Iranian Journal of Health and Environment*, 12(2), 289–306.
- Joshi, H. I., & Acharya, G. D. (2018). Numerical investigation of design parameters influence on stress distributions in horizontal multi-saddle cylindrical pressure vessel. *Materials Today: Proceedings*, 5(9), 19480–19489. <https://doi.org/10.1016/j.matpr.2018.06.309>

- Juengchareonpoon, K., Boonamnuyvitaya, V., & Wanichpongpan, P. (2019). Kinetics and isotherms of oxytetracycline adsorption on β -cyclodextrin/carboxymethylcellulose hydrogel films. *Aquaculture Research*, *50*(11), 3412–3419. <https://doi.org/10.1111/are.14299>
- Jurado, A., Vázquez-Suñé, E., Carrera, J., López de Alda, M., Pujades, E., & Barceló, D. (2012). Emerging organic contaminants in groundwater in Spain: A review of sources, recent occurrence and fate in a European context. In *Science of the Total Environment* (Vol. 440, pp. 82–94). <https://doi.org/10.1016/j.scitotenv.2012.08.029>
- Kashyap, A., Nishil, B., & Thatikonda, S. (2023). Experimental and numerical elucidation of the fate and transport of antibiotics in aquatic environment: A review. In *Environmental monitoring and assessment* (Vol. 195, Issue 8, p. 942). <https://doi.org/10.1007/s10661-023-11482-5>
- Katibi, K. K., Yunos, K. F., Man, H. C., Aris, A. Z., Nor, M. Z. M., & Azis, R. S. (2021). An insight into a sustainable removal of bisphenol a from aqueous solution by novel palm kernel shell magnetically induced biochar: Synthesis, characterization, kinetic, and thermodynamic studies. *Polymers*, *13*(21). <https://doi.org/10.3390/polym13213781>
- Kayal, A., & Mandal, S. (2022). Microbial degradation of antibiotic: future possibility of mitigating antibiotic pollution. In *Environmental Monitoring and Assessment* (Vol. 194, Issue 9). <https://doi.org/10.1007/s10661-022-10314-2>
- Kevan, P. G. (1999). Pollinators as bioindicators of the state of the environment: Species, activity and diversity. *Agriculture, Ecosystems and Environment*, *74*(1-3), 373–393. [https://doi.org/10.1016/S0167-8809\(99\)00044-4](https://doi.org/10.1016/S0167-8809(99)00044-4)
- Khan, A. D., & Alam, M. N. (2019). COSMETICS AND THEIR ASSOCIATED ADVERSE EFFECTS: A REVIEW. *Journal of Applied Pharmaceutical Sciences and Research*, 1–6. <https://doi.org/10.31069/japsr.v2i1.1>
- Khan, M. H., Bae, H., & Jung, J. Y. (2010). Tetracycline degradation by ozonation in the aqueous phase: Proposed degradation intermediates and pathway. *Journal of Hazardous Materials*, *181*(1-3), 659–665. <https://doi.org/10.1016/j.jhazmat.2010.05.063>
- Khan, S., Raja, M. A., Sayed, M., Shah, L. A., & Sohail, M. (2019). Advanced Oxidation and Reduction Processes. In *Advances in Water Purification Techniques: Meeting the Needs of Developed and Developing Countries* (pp. 135–164).

<https://doi.org/10.1016/B978-0-12-814790-0.00006-5>

- Khatibi, A. D., Mahvi, A. H., Mengelizadeh, N., & Balarak, D. (2021). Adsorption–desorption of tetracycline onto molecularly imprinted polymer: Isotherm, kinetics, and thermodynamics studies. *Desalination and Water Treatment*, 230, 240–251. <https://doi.org/10.5004/dwt.2021.27396>
- Khoshnamvand, N., Ahmadi, S., & Mostafapour, F. K. (2017). Kinetic and isotherm studies on ciprofloxacin an adsorption using magnesium oxide nanoparticles. *Journal of Applied Pharmaceutical Science*, 7(11), 79–83. <https://doi.org/10.7324/JAPS.2017.71112>
- Kiani, A., Ahmadloo, M., Moazzen, M., Shariatifar, N., Shahsavari, S., Arabameri, M., Hasani, M. M., Azari, A., & Abdel-Wahhab, M. A. (2021). Monitoring of polycyclic aromatic hydrocarbons and probabilistic health risk assessment in yogurt and butter in Iran. *Food Science and Nutrition*, 9(4), 2114–2128. <https://doi.org/10.1002/fsn3.2180>
- Kiecak, A., Sassine, L., Boy-Roura, M., Elsner, M., Mas-Pla, J., Le Gal La Salle, C., & Stumpp, C. (2019). Sorption properties and behaviour at laboratory scale of selected pharmaceuticals using batch experiments. *Journal of Contaminant Hydrology*, 225(April), 103500. <https://doi.org/10.1016/j.jconhyd.2019.103500>
- Kiezyk, P. R., & Mackay, D. (1971). Waste water treatment by solvent extraction. *The Canadian Journal of Chemical Engineering*, 49(6), 747–752. <https://doi.org/10.1002/cjce.5450490607>
- Kim, J. D., Yun, H., Kim, G. C., Lee, C. W., & Choi, H. C. (2013). Antibacterial activity and reusability of CNT-Ag and GO-Ag nanocomposites. *Applied Surface Science*, 283, 227–233. <https://doi.org/10.1016/j.apsusc.2013.06.086>
- Kim, S., Chu, K. H., Al-Hamadani, Y. A. J., Park, C. M., Jang, M., Kim, D. H., Yu, M., Heo, J., & Yoon, Y. (2018). Removal of contaminants of emerging concern by membranes in water and wastewater: A review. In *Chemical Engineering Journal* (Vol. 335, pp. 896–914). <https://doi.org/10.1016/j.cej.2017.11.044>
- Košutić, K., Dolar, D., Ašperger, D., & Kunst, B. (2007). Removal of antibiotics from a model wastewater by RO/NF membranes. *Separation and Purification Technology*, 53(3), 244–249. <https://doi.org/10.1016/j.seppur.2006.07.015>
- Kumar, A., Kumar, P., Goyal, N., Bobde, P., Kwon, E. E., Lin, K. A., & Chen, W. (2023). A critical review on biochar production from pine wastes , upgradation

- techniques , environmental sustainability , and challenges. *Bioresource Technology*, 387(July), 129632. <https://doi.org/10.1016/j.biortech.2023.129632>
- Kunduru, K. R., Nazarkovsky, M., Farah, S., Pawar, R. P., Basu, A., & Domb, A. J. (2017). Nanotechnology for water purification: applications of nanotechnology methods in wastewater treatment. In *Water Purification* (pp. 33–74). <https://doi.org/10.1016/B978-0-12-804300-4.00002-2>
- Kyzas, G. Z., Koltsakidou, A., Nanaki, S. G., Bikiaris, D. N., & Lambropoulou, D. A. (2015). Removal of beta-blockers from aqueous media by adsorption onto graphene oxide. *Science of the Total Environment*, 537, 411–420. <https://doi.org/10.1016/j.scitotenv.2015.07.144>
- Lagadic, L., Katsiadaki, I., Bieber, R., Guiney, P. D., Karouna-Renier, N., Schwarz, T., & Meador, J. P. (2018). Tributyltin: Advancing the science on assessing endocrine disruption with an unconventional endocrine-disrupting compound. In *Reviews of Environmental Contamination and Toxicology* (Vol. 245, pp. 65–127). https://doi.org/10.1007/398_2017_8
- Langmuir, I. (1916). The constitution and fundamental properties of solids and liquids. Part I. Solids. *Journal of the American Chemical Society*, 38(11), 2221–2295. <https://doi.org/10.1021/ja02268a002>
- Lapworth, D. J., Baran, N., Stuart, M. E., & Ward, R. S. (2012). Emerging organic contaminants in groundwater: A review of sources, fate and occurrence. In *Environmental Pollution* (Vol. 163, pp. 287–303). <https://doi.org/10.1016/j.envpol.2011.12.034>
- Lazaratou, C. V., Vayenas, D. V., & Papoulis, D. (2020). The role of clays, clay minerals and clay-based materials for nitrate removal from water systems: A review. In *Applied Clay Science* (Vol. 185). <https://doi.org/10.1016/j.clay.2019.105377>
- Lee, S. Y., Choi, J. W., Song, K. G., Choi, K., Lee, Y. J., & Jung, K. W. (2019). Adsorption and mechanistic study for phosphate removal by rice husk-derived biochar functionalized with Mg/Al-calcined layered double hydroxides via co-pyrolysis. *Composites Part B: Engineering*, 176. <https://doi.org/10.1016/j.compositesb.2019.107209>
- Lei, Y., Chen, F., Luo, Y., & Zhang, L. (2014). Three-dimensional magnetic graphene oxide foam/Fe₃O₄ nanocomposite as an efficient absorbent for Cr(VI) removal. *Journal of Materials Science*, 49(12), 4236–4245. <https://doi.org/10.1007/s10853->

- Li, A. J., Schmitz, O. J., Stephan, S., Lenzen, C., Yue, P. Y. K., Li, K., Li, H., & Leung, K. S. Y. (2016). Photocatalytic transformation of acesulfame: Transformation products identification and embryotoxicity study. *Water Research*, *89*, 68–75. <https://doi.org/10.1016/j.watres.2015.11.035>
- Li, C., Wang, D., Li, N., Luo, Q., Xu, X., & Wang, Z. (2016). Identifying unknown by-products in drinking water using comprehensive two-dimensional gas chromatography–quadrupole mass spectrometry and in silico toxicity assessment. *Chemosphere*, *163*, 535–543. <https://doi.org/10.1016/j.chemosphere.2016.08.053>
- Li, D., Zeng, S., He, M., & Gu, A. Z. (2016). Water Disinfection Byproducts Induce Antibiotic Resistance-Role of Environmental Pollutants in Resistance Phenomena. *Environmental Science and Technology*, *50*(6), 3193–3201. <https://doi.org/10.1021/acs.est.5b05113>
- Li, H., Wu, W., Hao, X., Wang, S., You, M., Han, X., Zhao, Q., & Xing, B. (2018). Removal of ciprofloxacin from aqueous solutions by ionic surfactant-modified carbon nanotubes. *Environmental Pollution*, *243*, 206–217. <https://doi.org/10.1016/j.envpol.2018.08.059>
- Li, J., Cai, X., Liu, Y., Gu, Y., Wang, H., Liu, S., Liu, S., Yin, Y., & Liu, S. (2020). Design and Synthesis of a Biochar-Supported Nano Manganese Dioxide Composite for Antibiotics Removal From Aqueous Solution. *Frontiers in Environmental Science*, *8*(May), 1–12. <https://doi.org/10.3389/fenvs.2020.00062>
- Li, J., Yu, G., Pan, L., Li, C., You, F., & Wang, Y. (2020). Ciprofloxacin adsorption by biochar derived from co-pyrolysis of sewage sludge and bamboo waste. *Environmental Science and Pollution Research*, *27*(18), 22806–22817. <https://doi.org/10.1007/s11356-020-08333-y>
- Li, J., Yu, G., Pan, L., Li, C., You, F., Xie, S., Wang, Y., Ma, J., & Shang, X. (2018). Study of ciprofloxacin removal by biochar obtained from used tea leaves. *Journal of Environmental Sciences (China)*, *73*, 20–30. <https://doi.org/10.1016/j.jes.2017.12.024>
- Li, Q., Zhao, S., & Wang, Y. (2021). Mechanism of oxytetracycline removal by coconut shell biochar loaded with nano-zero-valent iron. *International Journal of Environmental Research and Public Health*, *18*(24). <https://doi.org/10.3390/ijerph182413107>

- Li, R., Zhang, Y., Deng, H., Zhang, Z., Wang, J. J., Shaheen, S. M., Xiao, R., Rinklebe, J., Xi, B., He, X., & Du, J. (2020). Removing tetracycline and Hg(II) with ball-milled magnetic nanobiochar and its potential on polluted irrigation water reclamation. *Journal of Hazardous Materials*, 384(August 2019). <https://doi.org/10.1016/j.jhazmat.2019.121095>
- Li, X., Gan, T., Zhang, J., Shi, Z., Liu, Z., & Xiao, Z. (2022). High-capacity removal of oxytetracycline hydrochloride from wastewater via Mikania micrantha Kunth-derived biochar modified by Zn/Fe-layered double hydroxide. *Bioresource Technology*, 361, 127646. <https://doi.org/10.1016/j.biortech.2022.127646>
- Li, Y., Liu, S., Wang, C., Ying, Z., Huo, M., & Yang, W. (2020). Effective column adsorption of triclosan from pure water and wastewater treatment plant effluent by using magnetic porous reduced graphene oxide. *Journal of Hazardous Materials*, 386. <https://doi.org/10.1016/j.jhazmat.2019.121942>
- Liang, C., Zhang, X., Feng, P., Chai, H., & Huang, Y. (2018). ZIF-67 derived hollow cobalt sulfide as superior adsorbent for effective adsorption removal of ciprofloxacin antibiotics. *Chemical Engineering Journal*, 344, 95–104. <https://doi.org/10.1016/j.cej.2018.03.064>
- Liang, G., Wang, Z., Yang, X., Qin, T., Xie, X., Zhao, J., & Li, S. (2019). Efficient removal of oxytetracycline from aqueous solution using magnetic montmorillonite-biochar composite prepared by one step pyrolysis. *Science of the Total Environment*, 695. <https://doi.org/10.1016/j.scitotenv.2019.133800>
- Liang, H., Zhu, C., Ji, S., Kannan, P., & Chen, F. (2022). Magnetic Fe₂O₃/biochar composite prepared in a molten salt medium for antibiotic removal in water. *Biochar*, 4(1). <https://doi.org/10.1007/s42773-021-00130-1>
- Liang, L., Xi, F., Tan, W., Meng, X., Hu, B., & Wang, X. (2021). Review of organic and inorganic pollutants removal by biochar and biochar-based composites. *Biochar*, 3(3), 255–281. <https://doi.org/10.1007/s42773-021-00101-6>
- Liao, X., Chen, C., Liang, Z., Zhao, Z., & Cui, F. (2023). Selective adsorption of antibiotics on manganese oxide-loaded biochar and mechanism based on quantitative structure–property relationship model. *Bioresource Technology*, 367. <https://doi.org/10.1016/j.biortech.2022.128262>
- Liao, X., Li, B., Zou, R., Dai, Y., Xie, S., & Yuan, B. (2016). Biodegradation of antibiotic ciprofloxacin: pathways, influential factors, and bacterial community

- structure. *Environmental Science and Pollution Research*, 23(8), 7911–7918. <https://doi.org/10.1007/s11356-016-6054-1>
- Lima Morais, R., Ferreira Garcia, L., Kussmaul Gonçalves Moreno, E., Vieira Thomaz, D., De Brito Rodrigues, L., Barroso Brito, L., Sanz Lobón, G., Augusto Rodrigues de Oliveira, G., Ferreira Rodrigues, M., Gontijo Vaz, B., & Gil, E. D. S. (2019). Electrochemical remediation of industrial pharmaceutical wastewater containing hormones in a pilot scale treatment system. *Eclética Química Journal*, 44(1), 40. <https://doi.org/10.26850/1678-4618eq.v44.1.2019.p40-52>
- Lin, S. H., & Juang, R. S. (2009). Adsorption of phenol and its derivatives from water using synthetic resins and low-cost natural adsorbents: A review. In *Journal of Environmental Management* (Vol. 90, Issue 3, pp. 1336–1349). <https://doi.org/10.1016/j.jenvman.2008.09.003>
- Lin, Y. L., & Lee, C. H. (2014). Elucidating the rejection mechanisms of PPCPs by nanofiltration and reverse osmosis membranes. *Industrial and Engineering Chemistry Research*, 53(16), 6798–6806. <https://doi.org/10.1021/ie500114r>
- Lins, P. V. S., Henrique, D. C., Ide, A. H., Duarte, J. L. da Silva, Dotto, G. L., Yazidi, A., Sellaoui, L., Erto, A., Zanta, C. L. de P. e. S., & Meili, L. (2020). Adsorption of a non-steroidal anti-inflammatory drug onto MgAl/LDH-activated carbon composite – Experimental investigation and statistical physics modeling. *Colloids and Surfaces A: Physicochemical and Engineering Aspects*, 586(November 2019). <https://doi.org/10.1016/j.colsurfa.2019.124217>
- Liu, Y., Cao, S., Xi, C., Su, H., & Chen, Z. (2021). A new nanocomposite assembled with metal organic framework and magnetic biochar derived from pomelo peels: A highly efficient adsorbent for ketamine in wastewater. *Journal of Environmental Chemical Engineering*, 9(5). <https://doi.org/10.1016/j.jece.2021.106207>
- Lonappan, L., Rouissi, T., Kaur Brar, S., Verma, M., & Surampalli, R. Y. (2018). An insight into the adsorption of diclofenac on different biochars: Mechanisms, surface chemistry, and thermodynamics. *Bioresource Technology*, 249, 386–394. <https://doi.org/10.1016/j.biortech.2017.10.039>
- Lu, H., Wang, J., Stoller, M., Wang, T., Bao, Y., & Hao, H. (2016). An Overview of Nanomaterials for Water and Wastewater Treatment. In *Advances in Materials Science and Engineering* (Vol. 2016). <https://doi.org/10.1155/2016/4964828>
- Lu, Z., He, Z., Parisi, V. A., Kang, S., Deng, Y., Van Nostrand, J. D., Masoner, J. R.,

- Cozzarelli, I. M., Suflita, J. M., & Zhou, J. (2012). GeoChip-based analysis of microbial functional gene diversity in a landfill leachate-contaminated aquifer. *Environmental Science and Technology*, 46(11), 5824–5833. <https://doi.org/10.1021/es300478j>
- Luo, J., Li, X., Ge, C., Müller, K., Yu, H., Huang, P., Li, J., Tsang, D. C. W., Bolan, N. S., Rinklebe, J., & Wang, H. (2018). Sorption of norfloxacin, sulfamerazine and oxytetracycline by KOH-modified biochar under single and ternary systems. *Bioresource Technology*, 263(May), 385–392. <https://doi.org/10.1016/j.biortech.2018.05.022>
- Luo, S., Qin, J., Wu, Y., & Feng, F. (2022). Tetracycline adsorption on magnetic sludge biochar: Size effect of the Fe₃O₄nanoparticles. *Royal Society Open Science*, 9(1). <https://doi.org/10.1098/rsos.210805>
- Lye, J. W. P., Saman, N., Sharuddin, S. S. N., Othman, N. S., Mohtar, S. S., Md Noor, A. M., Buhari, J., Cheu, S. C., Kong, H., & Mat, H. (2017). Removal Performance of Tetracycline and Oxytetracycline From Aqueous Solution Via Natural Zeolites: An Equilibrium and Kinetic Study. *Clean - Soil, Air, Water*, 45(10). <https://doi.org/10.1002/clen.201600260>
- Ma, Y., Liu, W. J., Zhang, N., Li, Y. S., Jiang, H., & Sheng, G. P. (2014). Polyethylenimine modified biochar adsorbent for hexavalent chromium removal from the aqueous solution. *Bioresource Technology*, 169, 403–408. <https://doi.org/10.1016/j.biortech.2014.07.014>
- Machado, F. M., Bergmann, C. P., Fernandes, T. H. M., Lima, E. C., Royer, B., Calvete, T., & Fagan, S. B. (2011). Adsorption of Reactive Red M-2BE dye from water solutions by multi-walled carbon nanotubes and activated carbon. *Journal of Hazardous Materials*, 192(3), 1122–1131. <https://doi.org/10.1016/j.jhazmat.2011.06.020>
- Maged, A., Iqbal, J., Kharbish, S., Ismael, I. S., & Bhatnagar, A. (2020). Tuning tetracycline removal from aqueous solution onto activated 2:1 layered clay mineral: Characterization, sorption and mechanistic studies. *Journal of Hazardous Materials*, 384. <https://doi.org/10.1016/j.jhazmat.2019.121320>
- Magro, C., Mateus, E. P., Paz-Garcia, J. M., & Ribeiro, A. B. (2020). Emerging organic contaminants in wastewater: Understanding electrochemical reactors for triclosan and its by-products degradation. *Chemosphere*, 247.

<https://doi.org/10.1016/j.chemosphere.2019.125758>

- Mahdi, Z., El Hanandeh, A., & Yu, Q. J. (2019). Preparation, characterization and application of surface modified biochar from date seed for improved lead, copper, and nickel removal from aqueous solutions. *Journal of Environmental Chemical Engineering*, 7(5). <https://doi.org/10.1016/j.jece.2019.103379>
- Mahdi-Ahmed, M., & Chiron, S. (2014). Ciprofloxacin oxidation by UV-C activated peroxymonosulfate in wastewater. *Journal of Hazardous Materials*, 265, 41–46. <https://doi.org/10.1016/j.jhazmat.2013.11.034>
- Mahmood, T., Momin, S., Ali, R., Naeem, A., & Khan, A. (2022). Technologies for Removal of Emerging Contaminants from Wastewater. In *Wastewater Treatment*. <https://doi.org/10.5772/intechopen.104466>
- Mahmoodi, H., Fattahi, M., & Motevassel, M. (2021). Graphene oxide-chitosan hydrogel for adsorptive removal of diclofenac from aqueous solution: Preparation, characterization, kinetic and thermodynamic modelling. *RSC Advances*, 11(57), 36289–36304. <https://doi.org/10.1039/d1ra06069d>
- Mahmoud, M. E., El-Ghanam, A. M., Saad, S. R., & Mohamed, R. H. A. (2020). Promoted removal of metformin hydrochloride anti-diabetic drug from water by fabricated and modified nanobiochar from artichoke leaves. *Sustainable Chemistry and Pharmacy*, 18(October). <https://doi.org/10.1016/j.scp.2020.100336>
- Mansouri, T., Alimohammadi, M., Nodehi, R. N., Yaghmaeian, K., & Azari, A. (2018). Risk assessment of sari fatemeh zahra hospital using failure mode effect analysis, individualized rapid assessment tool, and preliminary hazard analysis. *Journal of Mazandaran University of Medical Sciences*, 28(161), 89–107.
- Mashile, G. P., Mpupa, A., Nqombolo, A., Dimpe, K. M., & Nomngongo, P. N. (2020). Recyclable magnetic waste tyre activated carbon-chitosan composite as an effective adsorbent rapid and simultaneous removal of methylparaben and propylparaben from aqueous solution and wastewater. *Journal of Water Process Engineering*, 33. <https://doi.org/10.1016/j.jwpe.2019.101011>
- Masoner, J. R., Kolpin, D. W., Furlong, E. T., Cozzarelli, I. M., Gray, J. L., & Schwab, E. A. (2014). Contaminants of emerging concern in fresh leachate from landfills in the conterminous United States. *Environmental Science: Processes and Impacts*, 16(10), 2335–2354. <https://doi.org/10.1039/c4em00124a>
- Matolia, J., Shukla, S. P., Kumar, S., Kumar, K., & Singh, A. R. (2019). Physical

- entrapment of chitosan in fixed-down-flow column bed enhances triclosan removal from water. *Water Science and Technology*, 80(7), 1374–1383. <https://doi.org/10.2166/wst.2019.386>
- Mohan, D., Sarswat, A., Ok, Y. S., & Pittman, C. U. (2014). Organic and inorganic contaminants removal from water with biochar, a renewable, low cost and sustainable adsorbent - A critical review. *Bioresource Technology*, 160, 191–202. <https://doi.org/10.1016/j.biortech.2014.01.120>
- Mohd Khori, N. K. E., Hadibarata, T., Elshikh, M. S., Al-Ghamdi, A. A., Salmiati, & Yusop, Z. (2018). Triclosan removal by adsorption using activated carbon derived from waste biomass: Isotherms and kinetic studies. *Journal of the Chinese Chemical Society*, 65(8), 951–959. <https://doi.org/10.1002/jccs.201700427>
- Mostafapour, F. K., Yilmaz, M., Mahvi, A. H., Younesi, A., Ganji, F., & Balarak, D. (2022). Adsorptive removal of tetracycline from aqueous solution by surfactant-modified zeolite: equilibrium, kinetics and thermodynamics. *Desalination and Water Treatment*, 247, 216–228. <https://doi.org/10.5004/dwt.2022.27943>
- Mouser, P. J., Rizzo, D. M., Röling, W. F. M., & Van Breukelen, B. M. (2005). A multivariate statistical approach to spatial representation of groundwater contamination using hydrochemistry and microbial community profiles. *Environmental Science and Technology*, 39(19), 7551–7559. <https://doi.org/10.1021/es0502627>
- Muhamad, M. S., Salim, M. R., Lau, W. J., & Yusop, Z. (2016). A review on bisphenol A occurrences, health effects and treatment process via membrane technology for drinking water. *Environmental Science and Pollution Research*, 23(12), 11549–11567. <https://doi.org/10.1007/s11356-016-6357-2>
- N, M., Renita A, A., Kumar P, S., & Abraham L, S. (2022). Adsorption of ciprofloxacin from aqueous solution using surface improved tamarind shell as an economical and effective adsorbent. *International Journal of Phytoremediation*, 24(3), 224–234. <https://doi.org/10.1080/15226514.2021.1932730>
- Nagarajan, V., & Chandiramouli, R. (2022). Sorption studies and removal of chlortetracycline and oxytetracycline using theta phosphorene nanoribbon – A DFT outlook. *Journal of Molecular Liquids*, 346, 117070. <https://doi.org/10.1016/j.molliq.2021.117070>
- Najafpoor, A. A., Nemati Sani, O., Alidadi, H., Yazdani, M., Navaei Fezabady, A. A., &

- Taghavi, M. (2019). Optimization of ciprofloxacin adsorption from synthetic wastewaters using γ -Al₂O₃ nanoparticles: An experimental design based on response surface methodology. *Colloids and Interface Science Communications*, 33. <https://doi.org/10.1016/j.colcom.2019.100212>
- Nawaz, T., & Sengupta, S. (2019). Contaminants of Emerging Concern: Occurrence, Fate, and Remediation. In *Advances in Water Purification Techniques: Meeting the Needs of Developed and Developing Countries* (pp. 67–114). <https://doi.org/10.1016/B978-0-12-814790-0.00004-1>
- Ncibi, M. C., & Sillanpää, M. (2015). Optimized removal of antibiotic drugs from aqueous solutions using single, double and multi-walled carbon nanotubes. *Journal of Hazardous Materials*, 298, 102–110. <https://doi.org/10.1016/j.jhazmat.2015.05.025>
- Neelima Shah , IFS Rajiv Dhiman, I. R. V. (2022). *Utilisation of Pine needles (Pinus roxburghii) to reduce the forest fire in Nowshera Forest Division , J & K Neelima Shah , IFS Rajiv Dhiman , IFS Rakesh Verma*. 8(12), 11–18.
- Nemati Sani, O., Navaei fezabady, A. A., Yazdani, M., & Taghavi, M. (2019). Catalytic ozonation of ciprofloxacin using γ -Al₂O₃ nanoparticles in synthetic and real wastewaters. *Journal of Water Process Engineering*, 32. <https://doi.org/10.1016/j.jwpe.2019.100894>
- Nghiem, L. D., & Fujioka, T. (2016). Removal of Emerging Contaminants for Water Reuse by Membrane Technology. In *Emerging Membrane Technology for Sustainable Water Treatment* (pp. 217–247). <https://doi.org/10.1016/B978-0-444-63312-5.00009-7>
- Ngomsik, A. F., Bee, A., Talbot, D., & Cote, G. (2012). Magnetic solid-liquid extraction of Eu(III), La(III), Ni(II) and Co(II) with maghemite nanoparticles. *Separation and Purification Technology*, 86, 1–8. <https://doi.org/10.1016/j.seppur.2011.10.013>
- Nguyen, V. T., Nguyen, T. M. T., Liu, Y. G., & Cai, Q. Y. (2021). Fabrication of Partially Graphitic Biochar for the Removal of Diclofenac and Ibuprofen from Aqueous Solution: Laboratory Conditions and Real Sample Applications. *Environmental Engineering Science*, 38(10), 974–989. <https://doi.org/10.1089/ees.2020.0202>
- Noudeh, G. D., Asdaghi, M., Noudeh, N. D., Dolatabadi, M., & Ahmadzadeh, S. (2023). Response surface modeling of ceftriaxone removal from hospital wastewater.

- Environmental Monitoring and Assessment*, 195(1). <https://doi.org/10.1007/s10661-022-10808-z>
- Ohale, P. E., Igwegbe, C. A., Iwuozor, K. O., Emenike, E. C., Obi, C. C., & Białowiec, A. (2023). A review of the adsorption method for norfloxacin reduction from aqueous media. In *MethodsX* (Vol. 10). <https://doi.org/10.1016/j.mex.2023.102180>
- Oladipo, A. A., Ifebajo, A. O., & Vaziri, R. (2018). *Green Adsorbents for Removal of Antibiotics, Pesticides and Endocrine Disruptors* (pp. 327–351). https://doi.org/10.1007/978-3-319-92162-4_10
- Özacar, M. (2003). Equilibrium and kinetic modelling of adsorption of phosphorus on calcined alunite. *Adsorption*, 9(2), 125–132. <https://doi.org/10.1023/A:1024289209583>
- Özacar, M., & Şengil, I. A. (2003). Adsorption of reactive dyes on calcined alunite from aqueous solutions. *Journal of Hazardous Materials*, 98(1-3), 211–224. [https://doi.org/10.1016/S0304-3894\(02\)00358-8](https://doi.org/10.1016/S0304-3894(02)00358-8)
- Özacar, M., & Şengil, I. A. (2004). Equilibrium data and process design for adsorption of disperse dyes onto Alunite. *Environmental Geology*, 45(6), 762–768. <https://doi.org/10.1007/s00254-003-0936-5>
- Özer, Ç., & İmamoğlu, M. (2022). Removal of ciprofloxacin from aqueous solutions by pumpkin peel biochar prepared using phosphoric acid. *Biomass Conversion and Biorefinery*. <https://doi.org/10.1007/s13399-022-02832-3>
- Ozin, G. A., Kuperman, A., & Stein, A. (1989). Advanced zeolite materials science. *Advanced Materials*, 1(3), 69–86. <https://doi.org/10.1002/adma.19890010303>
- Pallarés, J., González-Cencerrado, A., & Arauzo, I. (2018). Production and characterization of activated carbon from barley straw by physical activation with carbon dioxide and steam. *Biomass and Bioenergy*, 115, 64–73. <https://doi.org/10.1016/j.biombioe.2018.04.015>
- Pan, B., Pan, B., Zhang, W., Lv, L., Zhang, Q., & Zheng, S. (2009). Development of polymeric and polymer-based hybrid adsorbents for pollutants removal from waters. In *Chemical Engineering Journal* (Vol. 151, Issues 1-3, pp. 19–29). <https://doi.org/10.1016/j.cej.2009.02.036>
- Pandey, D., Daverey, A., Dutta, K., Yata, V. K., & Arunachalam, K. (2022). Valorization of waste pine needle biomass into biosorbents for the removal of methylene blue dye from water: Kinetics, equilibrium and thermodynamics study. *Environmental*

- Technology and Innovation*, 25. <https://doi.org/10.1016/j.eti.2021.102200>
- Pandey, S., Pandey, P., Tiwari, G., Tiwari, R., & Rai, A. K. (2012). FTIR spectroscopy: A tool for quantitative analysis of ciprofloxacin in tablets. *Indian Journal of Pharmaceutical Sciences*, 74(1), 86–90. <https://doi.org/10.4103/0250-474X.102551>
- Parsa, J. B., Panah, T. M., & Chianeh, F. N. (2016). Removal of ciprofloxacin from aqueous solution by a continuous flow electro-coagulation process. *Korean Journal of Chemical Engineering*, 33(3), 893–901. <https://doi.org/10.1007/s11814-015-0196-6>
- Parsons, S. A., & Jefferson, B. (2009). Introduction to Potable Water Treatment Processes. In *Introduction to Potable Water Treatment Processes*. <https://doi.org/10.1002/9781444305470>
- Pavón-Silva, T., Pacheco-Salazar, V., Carlos Sánchez-Meza, J., Roa-Morales, G., & Colín-Cruz, A. (2009). Physicochemical and biological combined treatment applied to a food industry wastewater for reuse. *Journal of Environmental Science and Health - Part A Toxic/Hazardous Substances and Environmental Engineering*, 44(1), 108–115. <https://doi.org/10.1080/10934520802515467>
- Piccin, J. S., Cadaval, T. R. S., de Pinto, L. A. A., & Dotto, G. L. (2017). Adsorption Isotherms in Liquid Phase: Experimental, Modeling, and Interpretations BT - Adsorption Processes for Water Treatment and Purification. In *Adsorption Processes for Water Treatment and Purification* (pp. 19–51).
- Pignatello, J. J., Oliveros, E., & MacKay, A. (2006). Advanced oxidation processes for organic contaminant destruction based on the fenton reaction and related chemistry. In *Critical Reviews in Environmental Science and Technology* (Vol. 36, Issue 1, pp. 1–84). <https://doi.org/10.1080/10643380500326564>
- Pires, B. C., do Nascimento, T. A., Dutra, F. V. A., & Borges, K. B. (2019). Removal of a non-steroidal anti-inflammatory by adsorption on polypyrrole/multiwalled carbon nanotube composite—Study of kinetics and equilibrium in aqueous medium. *Colloids and Surfaces A: Physicochemical and Engineering Aspects*, 578. <https://doi.org/10.1016/j.colsurfa.2019.123583>
- Premarathna, K. S. D., Rajapaksha, A. U., Adassoriya, N., Sarkar, B., Sirimuthu, N. M. S., Cooray, A., Ok, Y. S., & Vithanage, M. (2019). Clay-biochar composites for sorptive removal of tetracycline antibiotic in aqueous media. *Journal of Environmental Management*, 238(February), 315–322.

<https://doi.org/10.1016/j.jenvman.2019.02.069>

- Priya, S. S., & Radha, K. V. (2017). A Review on the Adsorption Studies of Tetracycline onto Various Types of Adsorbents. In *Chemical Engineering Communications* (Vol. 204, Issue 8, pp. 821–839). <https://doi.org/10.1080/00986445.2015.1065820>
- Pukcothanung, Y., Siritanon, T., & Rangswatananon, K. (2018). The efficiency of zeolite Y and surfactant-modified zeolite Y for removal of 2,4-dichlorophenoxyacetic acid and 1,1"-dimethyl-4,4"-bipyridinium ion. *Microporous and Mesoporous Materials*, 258, 131–140. <https://doi.org/10.1016/j.micromeso.2017.08.035>
- Pycke, B. F. G., Geer, L. A., Dalloul, M., Abulafia, O., Jenck, A. M., & Halden, R. U. (2014). Human fetal exposure to triclosan and triclocarban in an urban population from Brooklyn, New York. *Environmental Science and Technology*, 48(15), 8831–8838. <https://doi.org/10.1021/es501100w>
- Pyrzyńska, K., & Bystrzejewski, M. (2010). Comparative study of heavy metal ions sorption onto activated carbon, carbon nanotubes, and carbon-encapsulated magnetic nanoparticles. *Colloids and Surfaces A: Physicochemical and Engineering Aspects*, 362(1-3), 102–109. <https://doi.org/10.1016/j.colsurfa.2010.03.047>
- Quesada, H. B., Baptista, A. T. A., Cusioli, L. F., Seibert, D., de Oliveira Bezerra, C., & Bergamasco, R. (2019). Surface water pollution by pharmaceuticals and an alternative of removal by low-cost adsorbents: A review. In *Chemosphere* (Vol. 222, pp. 766–780). <https://doi.org/10.1016/j.chemosphere.2019.02.009>
- Quintero-Jaramillo, J. A., Carrero-Mantilla, J. I., & Sanabria-Gonzalez, N. R. (2021). A review of caffeine adsorption studies onto various types of adsorbents. In *Scientific World Journal* (Vol. 2021). <https://doi.org/10.1155/2021/9998924>
- Qureshi, U. A., Hameed, B. H., & Ahmed, M. J. (2020). Adsorption of endocrine disrupting compounds and other emerging contaminants using lignocellulosic biomass-derived porous carbons: A review. *Journal of Water Process Engineering*, 38. <https://doi.org/10.1016/j.jwpe.2020.101380>
- Rahman, F., Langford, K. H., Scrimshaw, M. D., & Lester, J. N. (2001). Polybrominated diphenyl ether (PBDE) flame retardants. In *Science of the Total Environment* (Vol. 275, Issues 1-3, pp. 1–17). [https://doi.org/10.1016/S0048-9697\(01\)00852-X](https://doi.org/10.1016/S0048-9697(01)00852-X)
- Rajan, A., Sreedharan, S., & V, B. (2016). Solvent Extraction and Adsorption Technique for the Treatment of Pesticide Effluent. *Civil Engineering and Urban Planning: An*

International Journal (CiVEJ), 3(2), 155–165.
<https://doi.org/10.5121/civej.2016.3214>

- Rakshit, S., Sarkar, D., Elzinga, E. J., Punamiya, P., & Datta, R. (2013). Mechanisms of ciprofloxacin removal by nano-sized magnetite. *Journal of Hazardous Materials*, 246-247, 221–226. <https://doi.org/10.1016/j.jhazmat.2012.12.032>
- Ramanayaka, S., Kumar, M., Etampawala, T., & Vithanage, M. (2020). Macro, colloidal and nanobiochar for oxytetracycline removal in synthetic hydrolyzed human urine. *Environmental Pollution*, 267. <https://doi.org/10.1016/j.envpol.2020.115683>
- Ramanayaka, S., Sarkar, B., Cooray, A. T., Ok, Y. S., & Vithanage, M. (2020). Halloysite nanoclay supported adsorptive removal of oxytetracycline antibiotic from aqueous media. *Journal of Hazardous Materials*, 384. <https://doi.org/10.1016/j.jhazmat.2019.121301>
- Ramanayaka, S., Tsang, D. C. W., Hou, D., Ok, Y. S., & Vithanage, M. (2020). Green synthesis of graphitic nanobiochar for the removal of emerging contaminants in aqueous media. *Science of the Total Environment*, 706(November), 135725. <https://doi.org/10.1016/j.scitotenv.2019.135725>
- Rao, M. M., Reddy, D. H. K. K., Venkateswarlu, P., & Seshaiiah, K. (2009). Removal of mercury from aqueous solutions using activated carbon prepared from agricultural by-product/waste. *Journal of Environmental Management*, 90(1), 634–643. <https://doi.org/10.1016/j.jenvman.2007.12.019>
- Rashed, M. N. (2013). Adsorption Technique for the Removal of Organic Pollutants from Water and Wastewater. *Organic Pollutants - Monitoring, Risk and Treatment*, 167–194.
- Rasheed, T., Bilal, M., & Iqbal, H. M. N. (2022). Toxicological impact and adsorptive removal of triclosan from water bodies using chitosan and carbon-based nano-architectures. In *Nano-biosorbents for Decontamination of Water, Air, and Soil Pollution* (pp. 437–452). <https://doi.org/10.1016/B978-0-323-90912-9.00019-8>
- Raupp, Í. N., Filho, A. V., Arim, A. L., Muniz, A. R. C., & da Rosa, G. S. (2021). Development and characterization of activated carbon from olive pomace: experimental design, kinetic and equilibrium studies in nimesulide adsorption. *Materials*, 14(22). <https://doi.org/10.3390/ma14226820>
- Regulska, E., Brezcko, J., Basa, A., Niemirowicz-Laskowska, K., & Kiszkiel-Taudul, I. (2022). Photocatalytic degradation of oxytetracycline with the REMs (Er, Tm, Yb)-

- doped nickel and copper aluminates. *Materials Science and Engineering B: Solid-State Materials for Advanced Technology*, 285. <https://doi.org/10.1016/j.mseb.2022.115959>
- Richardson, S. D., & Ternes, T. A. (2018). Water Analysis: Emerging Contaminants and Current Issues. In *Analytical Chemistry* (Vol. 90, Issue 1, pp. 398–428). <https://doi.org/10.1021/acs.analchem.7b04577>
- Rizzi, V., Lacalamita, D., Gubitosa, J., Fini, P., Petrella, A., Romita, R., Agostiano, A., Gabaldón, J. A., Fortea Gorbe, M. I., Gómez-Morte, T., & Cosma, P. (2019). Removal of tetracycline from polluted water by chitosan-olive pomace adsorbing films. *Science of the Total Environment*, 693. <https://doi.org/10.1016/j.scitotenv.2019.133620>
- Rodrigues, A. C., Boroski, M., Shimada, N. S., Garcia, J. C., Nozaki, J., & Hioka, N. (2008). Treatment of paper pulp and paper mill wastewater by coagulation-flocculation followed by heterogeneous photocatalysis. *Journal of Photochemistry and Photobiology A: Chemistry*, 194(1), 1–10. <https://doi.org/10.1016/j.jphotochem.2007.07.007>
- Rodriguez-Narvaez, O. M., Peralta-Hernandez, J. M., Goonetilleke, A., & Bandala, E. R. (2017). Treatment technologies for emerging contaminants in water: A review. In *Chemical Engineering Journal* (Vol. 323, pp. 361–380). <https://doi.org/10.1016/j.cej.2017.04.106>
- Rout, P. R., Zhang, T. C., Bhunia, P., & Surampalli, R. Y. (2021). Treatment technologies for emerging contaminants in wastewater treatment plants: A review. *Science of the Total Environment*, 753. <https://doi.org/10.1016/j.scitotenv.2020.141990>
- Saadati, F., Keramati, N., & Ghazi, M. M. (2016). Influence of parameters on the photocatalytic degradation of tetracycline in wastewater: A review. In *Critical Reviews in Environmental Science and Technology* (Vol. 46, Issue 8, pp. 757–782). <https://doi.org/10.1080/10643389.2016.1159093>
- Saadi, R., Saadi, Z., Fazaeli, R., & Fard, N. E. (2015). Monolayer and multilayer adsorption isotherm models for sorption from aqueous media. In *Korean Journal of Chemical Engineering* (Vol. 32, Issue 5, pp. 787–799). <https://doi.org/10.1007/s11814-015-0053-7>
- Sacher, F., Lange, F. T., Brauch, H. J., & Blankenhorn, I. (2001). Pharmaceuticals in

- groundwaters: Analytical methods and results of a monitoring program in Baden-Württemberg, Germany. *Journal of Chromatography A*, 938(1-2), 199–210. [https://doi.org/10.1016/S0021-9673\(01\)01266-3](https://doi.org/10.1016/S0021-9673(01)01266-3)
- Sadegh, H., Ali, G. A. M., Gupta, V. K., Makhlof, A. S. H., Shahryari-ghoshekandi, R., Nadagouda, M. N., Sillanpää, M., & Megiel, E. (2017). The role of nanomaterials as effective adsorbents and their applications in wastewater treatment. In *Journal of Nanostructure in Chemistry* (Vol. 7, Issue 1, pp. 1–14). <https://doi.org/10.1007/s40097-017-0219-4>
- Sahoo, T. R., & Prelot, B. (2020). Adsorption processes for the removal of contaminants from wastewater: The perspective role of nanomaterials and nanotechnology. In *Nanomaterials for the Detection and Removal of Wastewater Pollutants* (pp. 161–222). <https://doi.org/10.1016/B978-0-12-818489-9.00007-4>
- Santos, L. C., da Silva, A. F., dos Santos Lins, P. V., da Silva Duarte, J. L., Ide, A. H., & Meili, L. (2020). Mg-Fe layered double hydroxide with chloride intercalated: synthesis, characterization and application for efficient nitrate removal. *Environmental Science and Pollution Research*, 27(6), 5890–5900. <https://doi.org/10.1007/s11356-019-07364-4>
- Saucedo-Vence, K., Elizalde-Velázquez, A., Dublán-García, O., Galar-Martínez, M., Islas-Flores, H., SanJuan-Reyes, N., García-Medina, S., Hernández-Navarro, M. D., & Gómez-Oliván, L. M. (2017). Toxicological hazard induced by sucralose to environmentally relevant concentrations in common carp (*Cyprinus carpio*). *Science of the Total Environment*, 575, 347–357. <https://doi.org/10.1016/j.scitotenv.2016.09.230>
- Saxena, P., Hiwrale, I., Das, S., Shukla, V., Tyagi, L., Pal, S., Dafale, N., & Dhodapkar, R. (2021). Profiling of emerging contaminants and antibiotic resistance in sewage treatment plants: An Indian perspective. *Journal of Hazardous Materials*, 408. <https://doi.org/10.1016/j.jhazmat.2020.124877>
- Sayin, F., Akar, S. T., & Akar, T. (2021). From green biowaste to water treatment applications: Utilization of modified new biochar for the efficient removal of ciprofloxacin. *Sustainable Chemistry and Pharmacy*, 24. <https://doi.org/10.1016/j.scp.2021.100522>
- Scholz, M. (2016). Activated Sludge Processes. *Wetlands for Water Pollution Control*, 91–105. <https://doi.org/10.1016/b978-0-444-63607-2.00015-0>

- Schulz, M., Löffler, D., Wagner, M., & Ternes, T. A. (2008). Transformation of the X-ray contrast medium iopromide in soil and biological wastewater treatment. *Environmental Science and Technology*, 42(19), 7207–7217. <https://doi.org/10.1021/es800789r>
- Shaari, N., Tan, S. H., & Mohamed, A. R. (2012). Synthesis and characterization of CNT/Ce-TiO₂ nanocomposite for phenol degradation. *Journal of Rare Earths*, 30(7), 651–658. [https://doi.org/10.1016/S1002-0721\(12\)60107-0](https://doi.org/10.1016/S1002-0721(12)60107-0)
- Shahwan, T., & Erten, H. N. (2004). Temperature effects in barium sorption on natural kaolinite and chlorite-illite clays. *Journal of Radioanalytical and Nuclear Chemistry*, 260(1), 43–48. <https://doi.org/10.1023/B:JRNC.0000027059.66424.b4>
- Shao, S., Hu, Y., Cheng, C., Cheng, J., & Chen, Y. (2018). Simultaneous degradation of tetracycline and denitrification by a novel bacterium, *Klebsiella* sp. SQY5. *Chemosphere*, 209, 35–43. <https://doi.org/10.1016/j.chemosphere.2018.06.093>
- Sheha, R. R., & Metwally, E. (2007). Equilibrium isotherm modeling of cesium adsorption onto magnetic materials. *Journal of Hazardous Materials*, 143(1-2), 354–361. <https://doi.org/10.1016/j.jhazmat.2006.09.041>
- Shukla, P., Giri, B. S., Mishra, R. K., Pandey, A., & Chaturvedi, P. (2021). Lignocellulosic biomass-based engineered biochar composites: A facile strategy for abatement of emerging pollutants and utilization in industrial applications. *Renewable and Sustainable Energy Reviews*, 152. <https://doi.org/10.1016/j.rser.2021.111643>
- Shukla, V., Panchal, D., Prakash, O., Mondal, P., Hiwrale, I., Dhodapkar, R. S., & Pal, S. (2023). Magnetically engineered sulfurized peat-based activated carbon for remediation of emerging pharmaceutical contaminants. *Bioresource Technology*, 369(November 2022), 128399. <https://doi.org/10.1016/j.biortech.2022.128399>
- Singer, H., Müller, S., Tixier, C., & Pillonel, L. (2002). Triclosan: Occurrence and fate of a widely used biocide in the aquatic environment: Field measurements in wastewater treatment plants, surface waters, and lake sediments. *Environmental Science and Technology*, 36(23), 4998–5004. <https://doi.org/10.1021/es025750i>
- Singh, P. K., Bhattacharjya, R., Lakshmi, N. J., Thakur, I. S., & Tiwari, A. (2023). Evaluation of the antioxidative response of diatoms grown on emerging steroidal contaminants. *Environmental Monitoring and Assessment*, 195(7). <https://doi.org/10.1007/s10661-023-11336-0>

- Smith, S. C., & Rodrigues, D. F. (2015). Carbon-based nanomaterials for removal of chemical and biological contaminants from water: A review of mechanisms and applications. In *Carbon* (Vol. 91, pp. 122–143). <https://doi.org/10.1016/j.carbon.2015.04.043>
- So, H. L., Lin, K. Y., & Chu, W. (2019). Triclosan removal by heterogeneous Fenton-like process: Studying the kinetics and surface chemistry of Fe₃O₄ as catalyst. *Journal of Environmental Chemical Engineering*, 7(5). <https://doi.org/10.1016/j.jece.2019.103432>
- Soares, S. F., Rocha, M. J., Ferro, M., Amorim, C. O., Amaral, J. S., Trindade, T., & Daniel-da-Silva, A. L. (2019). Magnetic nanosorbents with siliceous hybrid shells of alginic acid and carrageenan for removal of ciprofloxacin. *International Journal of Biological Macromolecules*, 139, 827–841. <https://doi.org/10.1016/j.ijbiomac.2019.08.030>
- Solińska, A., & Bajda, T. (2022). Modified zeolite as a sorbent for removal of contaminants from wet flue gas desulphurization wastewater. *Chemosphere*, 286. <https://doi.org/10.1016/j.chemosphere.2021.131772>
- Solmaz, A., Karta, M., Depci, T., Turna, T., & Sari, Z. A. (2023). Preparation and characterization of activated carbons from Lemon Pulp for oxytetracycline removal. *Environmental Monitoring and Assessment*, 195(7), 0–18. <https://doi.org/10.1007/s10661-023-11421-4>
- Song, Y., Zeng, Y., Liao, J., Chen, J., & Du, Q. (2021). Efficient removal of sulfamethoxazole by resin-supported zero-valent iron composites with tunable structure: Performance, mechanisms, and degradation pathways. *Chemosphere*, 269. <https://doi.org/10.1016/j.chemosphere.2020.128684>
- Sophia A., C., & Lima, E. C. (2018). Removal of emerging contaminants from the environment by adsorption. *Ecotoxicology and Environmental Safety*, 150, 1–17. <https://doi.org/10.1016/j.ecoenv.2017.12.026>
- Spellman, F. R. (2023). Mathematics Manual for Water and Wastewater Treatment Plant Operators: Wastewater Treatment Operations: Math Concepts and Calculations, Third Edition. In *Mathematics Manual for Water and Wastewater Treatment Plant Operators: Wastewater Treatment Operations: Math Concepts and Calculations, Third Edition*. <https://doi.org/10.1201/9781003354314>
- Starling, M. C. V. M., Amorim, C. C., & Leão, M. M. D. (2019). Occurrence, control and

- fate of contaminants of emerging concern in environmental compartments in Brazil. *Journal of Hazardous Materials*, 17–36. <https://doi.org/10.1016/j.jhazmat.2018.04.043>
- Stefanakis, A. I., & Becker, J. A. (2019). A review of emerging contaminants in water: Classification, sources, and potential risks. In *Waste Management: Concepts, Methodologies, Tools, and Applications* (pp. 177–202). <https://doi.org/10.4018/978-1-7998-1210-4.ch008>
- Stuart, M., Lapworth, D., Crane, E., & Hart, A. (2012). Review of risk from potential emerging contaminants in UK groundwater. In *Science of the Total Environment* (Vol. 416, pp. 1–21). <https://doi.org/10.1016/j.scitotenv.2011.11.072>
- Stylianou, M., Christou, A., Michael, C., Agapiou, A., Papanastasiou, P., & Fattakassinou, D. (2021). Adsorption and removal of seven antibiotic compounds present in water with the use of biochar derived from the pyrolysis of organic waste feedstocks. *Journal of Environmental Chemical Engineering*, 9(5), 105868. <https://doi.org/10.1016/j.jece.2021.105868>
- Sun, H., Yang, J., Wang, Y., Liu, Y., Cai, C., & Davarpanah, A. (2021). Study on the removal efficiency and mechanism of tetracycline in water using biochar and magnetic biochar. *Coatings*, 11(11). <https://doi.org/10.3390/coatings11111354>
- Suriyanon, N., Punyapalakul, P., & Ngamcharussrivichai, C. (2013). Mechanistic study of diclofenac and carbamazepine adsorption on functionalized silica-based porous materials. *Chemical Engineering Journal*, 214, 208–218. <https://doi.org/10.1016/j.cej.2012.10.052>
- Tan, L., Xu, J., Xue, X., Lou, Z., Zhu, J., Baig, S. A., & Xu, X. (2014). Multifunctional nanocomposite Fe₃O₄@SiO₂-mPD/SP for selective removal of Pb(II) and Cr(VI) from aqueous solutions. *RSC Advances*, 4(86), 45920–45929. <https://doi.org/10.1039/c4ra08040h>
- Tanyol, M., & Torğut, G. (2022). Chitosan-graft-poly(N-tert-butylacrylamide) Copolymer: Synthesis, Characterization and Optimization of Tetracycline Removal Using RSM. *Journal of Polymers and the Environment*, 30(2), 752–764. <https://doi.org/10.1007/s10924-021-02236-w>
- Teh, C. Y., Budiman, P. M., Shak, K. P. Y., & Wu, T. Y. (2016). Recent Advancement of Coagulation-Flocculation and Its Application in Wastewater Treatment. In *Industrial and Engineering Chemistry Research* (Vol. 55, Issue 16, pp. 4363–4389).

<https://doi.org/10.1021/acs.iecr.5b04703>

- Ternes, T. A., & Hirsch, R. (2000). Occurrence and behavior of X-ray contrast media in sewage facilities and the aquatic environment. *Environmental Science and Technology*, *34*(13), 2741–2748. <https://doi.org/10.1021/es991118m>
- Tian, Y., Gao, B., Morales, V. L., Chen, H., Wang, Y., & Li, H. (2013). Removal of sulfamethoxazole and sulfapyridine by carbon nanotubes in fixed-bed columns. *Chemosphere*, *90*(10), 2597–2605. <https://doi.org/10.1016/j.chemosphere.2012.11.010>
- Tohidi, F., & Cai, Z. (2016). Adsorption isotherms and kinetics for the removal of triclosan and methyl triclosan from wastewater using inactivated dried sludge. *Process Biochemistry*, *51*(8), 1069–1077. <https://doi.org/10.1016/j.procbio.2016.04.018>
- Toles, C. A., Marshall, W. E., & Johns, M. M. (1997). Granular activated carbons from nutshells for the uptake of metals and organic compounds. *Carbon*, *35*(9), 1407–1414. [https://doi.org/10.1016/S0008-6223\(97\)00073-0](https://doi.org/10.1016/S0008-6223(97)00073-0)
- Tong, Y., Mayer, B. K., & McNamara, P. J. (2016). Triclosan adsorption using wastewater biosolids-derived biochar. *Environmental Science: Water Research and Technology*, *2*(4), 761–768. <https://doi.org/10.1039/c6ew00127k>
- Torres, L. G., Belloc, C., Vaca, M., Iturbe, R., & Bandala, E. R. (2009). Coagulation-flocculation process applied to wastewaters generated in hydrocarbon-contaminated soil washing: Interactions among coagulant and flocculant concentrations and pH value. *Journal of Environmental Science and Health - Part A Toxic/Hazardous Substances and Environmental Engineering*, *44*(13), 1449–1456. <https://doi.org/10.1080/10934520903217716>
- Triwiswara, M., Kang, J. K., Moon, J. K., Lee, C. G., & Park, S. J. (2020). Removal of triclosan from aqueous solution using thermally treated rice husks. *Desalination and Water Treatment*, *202*, 317–326. <https://doi.org/10.5004/dwt.2020.26161>
- Varjani, S., Joshi, R., Srivastava, V. K., Ngo, H. H., & Guo, W. (2020). Treatment of wastewater from petroleum industry: current practices and perspectives. *Environmental Science and Pollution Research*, *27*(22), 27172–27180. <https://doi.org/10.1007/s11356-019-04725-x>
- Ventresque, C., Gisclon, V., Bablon, G., & Chagneau, G. (2000). Outstanding feat of modern technology: the Mery-sur-Oise nanofiltration treatment plant (340,000

- m3/d). *Desalination*, 131(1-3), 1–16. [https://doi.org/10.1016/S0011-9164\(00\)90001-8](https://doi.org/10.1016/S0011-9164(00)90001-8)
- Verslycke, T., Mayfield, D. B., Tabony, J. A., Capdevielle, M., & Slezak, B. (2016). Human health risk assessment of triclosan in land-applied biosolids. *Environmental Toxicology and Chemistry*, 35(9), 2358–2367. <https://doi.org/10.1002/etc.3370>
- Vievard, J., Alem, A., Pantet, A., Ahfir, N. D., Arellano-Sánchez, M. G., Devouge-Boyer, C., & Mignot, M. (2023). Bio-Based Adsorption as Ecofriendly Method for Wastewater Decontamination: A Review. In *Toxics* (Vol. 11, Issue 5). <https://doi.org/10.3390/toxics11050404>
- Wakejo, W. K., Meshasha, B. T., Kang, J. W., & Chebude, Y. (2022). Enhanced Ciprofloxacin Removal from Aqueous Solution Using a Chemically Modified Biochar Derived from Bamboo Sawdust: Adsorption Process Optimization with Response Surface Methodology. *Adsorption Science and Technology*, 2022. <https://doi.org/10.1155/2022/2699530>
- Wang, B., Lin, J., Hu, Q., Huang, F., Huang, Y., Tu, W., Chen, Q., & Li, S. (2023). Adsorption of oxytetracycline on subalpine meadow soil from Zoige Plateau, China: Effects of the coexisting Cu²⁺. *Environmental Research*, 231. <https://doi.org/10.1016/j.envres.2023.116221>
- Wang, C. J., Li, Z., & Jiang, W. T. (2011). Adsorption of ciprofloxacin on 2:1 dioctahedral clay minerals. *Applied Clay Science*, 53(4), 723–728. <https://doi.org/10.1016/j.clay.2011.06.014>
- Wang, F., Yang, B., Wang, H., Song, Q., Tan, F., & Cao, Y. (2016). Removal of ciprofloxacin from aqueous solution by a magnetic chitosan grafted graphene oxide composite. *Journal of Molecular Liquids*, 222, 188–194. <https://doi.org/10.1016/j.molliq.2016.07.037>
- Wang, H., Gao, B., Wang, S., Fang, J., Xue, Y., & Yang, K. (2015). Removal of Pb(II), Cu(II), and Cd(II) from aqueous solutions by biochar derived from KMnO₄ treated hickory wood. *Bioresource Technology*, 197, 356–362. <https://doi.org/10.1016/j.biortech.2015.08.132>
- Wang, H., Li, Z., Chen, H., Jin, J., Zhang, P., Shen, L., Hu, S., & Liu, H. (2023). Metabolomic analysis reveals the impact of ketoprofen on carbon and nitrogen metabolism in rice (*Oryza sativa* L.) seedling leaves. *Environmental Science and Pollution Research*, 30(8), 21825–21837. <https://doi.org/10.1007/s11356-022->

- Wang, H., Luan, W., Sun, L., Zeng, Z., Xue, W., & Bai, Y. (2022). Study on polyvinyl butyral purification process based on Box-Behnken design and artificial neural network. *Chemical Engineering Research and Design*, *184*, 291–302. <https://doi.org/10.1016/j.cherd.2022.05.050>
- Wang, J., de Ridder, D., van der Wal, A., & Sutton, N. B. (2021). Harnessing biodegradation potential of rapid sand filtration for organic micropollutant removal from drinking water: A review. *Critical Reviews in Environmental Science and Technology*, *51*(18), 2086–2118. <https://doi.org/10.1080/10643389.2020.1771888>
- Wang, J., & Wang, S. (2019). Preparation, modification and environmental application of biochar: A review. In *Journal of Cleaner Production* (Vol. 227, pp. 1002–1022). <https://doi.org/10.1016/j.jclepro.2019.04.282>
- Wang, J., & Zhang, M. (2020). Adsorption characteristics and mechanism of bisphenol a by magnetic biochar. *International Journal of Environmental Research and Public Health*, *17*(3). <https://doi.org/10.3390/ijerph17031075>
- Wang, J., Zhi, D., Zhou, H., He, X., & Zhang, D. (2018). Evaluating tetracycline degradation pathway and intermediate toxicity during the electrochemical oxidation over a Ti/Ti4O7 anode. *Water Research*, *137*, 324–334. <https://doi.org/10.1016/j.watres.2018.03.030>
- Wang, Q., Yue, Y., Liu, W., Liu, Q., Song, Y., Ge, C., & Ma, H. (2023). Removal Performance of KOH-Modified Biochar from Tropical Biomass on Tetracycline and Cr(VI). *Materials*, *16*(11). <https://doi.org/10.3390/ma16113994>
- Wang, W., & Wang, J. (2018). Comparative evaluation of sorption kinetics and isotherms of pyrene onto microplastics. *Chemosphere*, *193*, 567–573. <https://doi.org/10.1016/j.chemosphere.2017.11.078>
- Wang, X., Bi, W., Zhai, P., Wang, X., Li, H., Mailhot, G., & Dong, W. (2016). Adsorption and photocatalytic degradation of pharmaceuticals by BiOCl_xI_y nanospheres in aqueous solution. *Applied Surface Science*, *360*, 240–251. <https://doi.org/10.1016/j.apsusc.2015.10.229>
- Wang, X., Wang, X., Lynch, I., & Ma, J. (2023). High-efficiency removal of tetracycline from water by electrolysis-assisted NZVI: mechanism of electron transfer and redox of iron. *RSC Advances*, *13*(23), 15881–15891. <https://doi.org/10.1039/d3ra00954h>
- Wang, X., Zhang, H., Wei, Y., Bao, L., Liu, S., Yuan, S., & Yuan, S. (2022). Effect of

- pH on caffeine removal from aqueous media by graphene/graphene oxide adsorption. *Colloids and Surfaces A: Physicochemical and Engineering Aspects*, 644. <https://doi.org/10.1016/j.colsurfa.2022.128864>
- Wang, Y., Kang, J., Jiang, S., Li, H., Ren, Z., Xu, Q., Jiang, Q., Liu, W., Li, R., & Zhang, Y. (2020). A composite of Ni–Fe–Zn layered double hydroxides/biochar for atrazine removal from aqueous solution. *Biochar*, 2(4), 455–464. <https://doi.org/10.1007/s42773-020-00066-y>
- Wang, Y. X., Gupta, K., Li, J. R., Yuan, B., Yang, J. C. E., & Fu, M. L. (2018). Novel chalcogenide based magnetic adsorbent KMS-1/L-Cystein/Fe₃O₄ for the facile removal of ciprofloxacin from aqueous solution. *Colloids and Surfaces A: Physicochemical and Engineering Aspects*, 538, 378–386. <https://doi.org/10.1016/j.colsurfa.2017.11.016>
- Wang, Z., Yang, X., Qin, T., Liang, G., Li, Y., & Xie, X. (2019). Efficient removal of oxytetracycline from aqueous solution by a novel magnetic clay–biochar composite using natural attapulgite and cauliflower leaves. *Environmental Science and Pollution Research*, 26(8), 7463–7475. <https://doi.org/10.1007/s11356-019-04172-8>
- Weerasooriyagedara, M., Ashiq, A., Gunatilake, S. R., Giannakoudakis, D. A., & Vithanage, M. (2022). Surface interactions of oxytetracycline on municipal solid waste-derived biochar–montmorillonite composite. *Sustainable Environment*, 8(1). <https://doi.org/10.1080/27658511.2022.2046324>
- Wei, X., Xu, X., Yang, X., Liu, Z., Naraginti, S., Sen, L., Weidi, S., & Buwei, L. (2022). Novel assembly of BiVO₄@N-Biochar nanocomposite for efficient detoxification of triclosan. *Chemosphere*, 298, 134292. <https://doi.org/10.1016/j.chemosphere.2022.134292>
- Wei, Z., Hou, C., Gao, Z., Wang, L., Yang, C., Li, Y., Liu, K., & Sun, Y. (2023). Preparation of Biochar with Developed Mesoporous Structure from Poplar Leaf Activated by KHCO₃ and Its Efficient Adsorption of Oxytetracycline Hydrochloride. *Molecules (Basel, Switzerland)*, 28(7). <https://doi.org/10.3390/molecules28073188>
- Witek-Krowiak, A., Chojnacka, K., Podstawczyk, D., Dawiec, A., & Pokomeda, K. (2014). Application of response surface methodology and artificial neural network methods in modelling and optimization of biosorption process. *Bioresource Technology*, 160, 150–160. <https://doi.org/10.1016/j.biortech.2014.01.021>

- Wu, B., An, X., Wang, C., & Shin, H. Y. (2022). Extending UTAUT with national identity and fairness to understand user adoption of DCEP in China. *Scientific Reports*, 12(1). <https://doi.org/10.1038/s41598-022-10927-0>
- Wu, X., Dodgen, L. K., Conkle, J. L., & Gan, J. (2015). Plant uptake of pharmaceutical and personal care products from recycled water and biosolids: A review. In *Science of the Total Environment* (Vol. 536, pp. 655–666). <https://doi.org/10.1016/j.scitotenv.2015.07.129>
- Wu, Y., Lin, L., Suanon, F., Hu, A., Sun, Y. N., Yu, Z. M., Yu, C. P., & Sun, Q. (2018). Effect of a weak magnetic field on triclosan removal using zero-valent iron under aerobic and anaerobic conditions. *Chemical Engineering Journal*, 346, 24–33. <https://doi.org/10.1016/j.cej.2018.03.134>
- Xiao, L., Feng, L., Yuan, G., & Wei, J. (2020). Low-cost field production of biochars and their properties. *Environmental Geochemistry and Health*, 42(6), 1569–1578. <https://doi.org/10.1007/s10653-019-00458-5>
- Xu, Z., Zhang, Q., & Fang, H. H. P. (2003). Applications of Porous Resin Sorbents in Industrial Wastewater Treatment and Resource Recovery. In *Critical Reviews in Environmental Science and Technology* (Vol. 33, Issue 4, pp. 363–389). <https://doi.org/10.1080/10643380390249512>
- Yaashikaa, P. R., Senthil Kumar, P., Varjani, S. J., & Saravanan, A. (2019). Advances in production and application of biochar from lignocellulosic feedstocks for remediation of environmental pollutants. In *Bioresource Technology* (Vol. 292). <https://doi.org/10.1016/j.biortech.2019.122030>
- Yan, Y., Manickam, S., Lester, E., Wu, T., & Pang, C. H. (2021). Synthesis of graphene oxide and graphene quantum dots from miscanthus via ultrasound-assisted mechano-chemical cracking method. *Ultrasonics Sonochemistry*, 73. <https://doi.org/10.1016/j.ultsonch.2021.105519>
- Yang, W., Zheng, F., Lu, Y., Xue, X., & Li, N. (2011). Adsorption interaction of tetracyclines with porous synthetic resins. *Industrial and Engineering Chemistry Research*, 50(24), 13892–13898. <https://doi.org/10.1021/ie202166g>
- Yang, Z., Xing, R., Zhou, W., & Zhu, L. (2020). Adsorption characteristics of ciprofloxacin onto g-MoS₂ coated biochar nanocomposites. *Frontiers of Environmental Science and Engineering*, 14(3). <https://doi.org/10.1007/s11783-019-1218-0>

- Yao, J., Deng, Y., Li, D. S., Li, H., & Yang, H. Y. (2023). Role of magnetic substances in adsorption removal of ciprofloxacin by gamma ferric oxide and ferrites co-modified carbon nanotubes. *Journal of Colloid and Interface Science*, 638, 872–881. <https://doi.org/10.1016/j.jcis.2023.02.036>
- Yao, L., Yang, H., Chen, Z., Qiu, M., Hu, B., & Wang, X. (2021). Bismuth oxychloride-based materials for the removal of organic pollutants in wastewater. In *Chemosphere* (Vol. 273). <https://doi.org/10.1016/j.chemosphere.2020.128576>
- Yin, Y., Wu, H., Jiang, Z., Jiang, J., & Lu, Z. (2022). Degradation of Triclosan in the Water Environment by Microorganisms: A Review. In *Microorganisms* (Vol. 10, Issue 9). <https://doi.org/10.3390/microorganisms10091713>
- Yousefi, M., Gholami, M., Oskoei, V., Mohammadi, A. A., Baziar, M., & Esrafil, A. (2021). Comparison of LSSVM and RSM in simulating the removal of ciprofloxacin from aqueous solutions using magnetization of functionalized multi-walled carbon nanotubes: Process optimization using GA and RSM techniques. *Journal of Environmental Chemical Engineering*, 9(4). <https://doi.org/10.1016/j.jece.2021.105677>
- Yu, H., Gu, L., Chen, L., Wen, H., Zhang, D., & Tao, H. (2020). Activation of grapefruit derived biochar by its peel extracts and its performance for tetracycline removal. *Bioresource Technology*, 316. <https://doi.org/10.1016/j.biortech.2020.123971>
- Yue, T., Cao, X., Liu, Q., Bai, S., Zhang, F., & Liu, L. (2023). Enhancement on removal of oxytetracycline in aqueous solution by corn stover biochar: Comparison of KOH and KMnO₄ modifications. *Chemical Engineering Research and Design*, 190, 353–365. <https://doi.org/10.1016/j.cherd.2022.12.049>
- Zaied, B. K., Rashid, M., Nasrullah, M., Zularisam, A. W., Pant, D., & Singh, L. (2020). A comprehensive review on contaminants removal from pharmaceutical wastewater by electrocoagulation process. In *Science of the Total Environment* (Vol. 726). <https://doi.org/10.1016/j.scitotenv.2020.138095>
- Zeng, Z., Ye, S., Wu, H., Xiao, R., Zeng, G., Liang, J., Zhang, C., Yu, J., Fang, Y., & Song, B. (2019). Research on the sustainable efficacy of g-MoS₂ decorated biochar nanocomposites for removing tetracycline hydrochloride from antibiotic-polluted aqueous solution. *Science of the Total Environment*, 648, 206–217. <https://doi.org/10.1016/j.scitotenv.2018.08.108>
- Zhang, B., Han, X., Gu, P., Fang, S., & Bai, J. (2017). Response surface methodology

- approach for optimization of ciprofloxacin adsorption using activated carbon derived from the residue of desilicated rice husk. *Journal of Molecular Liquids*, 238, 316–325. <https://doi.org/10.1016/j.molliq.2017.04.022>
- Zhang, H., Song, X., Zhang, J., Liu, Y., Zhao, H., Hu, J., & Zhao, J. (2022). Performance and mechanism of sycamore flock based biochar in removing oxytetracycline hydrochloride. *Bioresource Technology*, 350, 126884. <https://doi.org/10.1016/j.biortech.2022.126884>
- Zhang, H., Xu, F., Xue, J., Chen, S., Wang, J., & Yang, Y. (2020). Enhanced removal of heavy metal ions from aqueous solution using manganese dioxide-loaded biochar: Behavior and mechanism. *Scientific Reports*, 10(1). <https://doi.org/10.1038/s41598-020-63000-z>
- Zhang, P., Li, Y., Cao, Y., & Han, L. (2019). Characteristics of tetracycline adsorption by cow manure biochar prepared at different pyrolysis temperatures. *Bioresource Technology*, 285. <https://doi.org/10.1016/j.biortech.2019.121348>
- Zhang, W., Ding, Y., Boyd, S. A., Teppen, B. J., & Li, H. (2010). Sorption and desorption of carbamazepine from water by smectite clays. *Chemosphere*, 81(7), 954–960. <https://doi.org/10.1016/j.chemosphere.2010.07.053>
- Zhang, X., Sühling, R., Serodio, D., Bonnell, M., Sundin, N., & Diamond, M. L. (2016). Novel flame retardants: Estimating the physical-chemical properties and environmental fate of 94 halogenated and organophosphate PBDE replacements. *Chemosphere*, 144, 2401–2407. <https://doi.org/10.1016/j.chemosphere.2015.11.017>
- Zhang, X. X., Li, R., Jia, M., Wang, S., Huang, Y., & Chen, C. (2015). Degradation of ciprofloxacin in aqueous bismuth oxybromide (BiOBr) suspensions under visible light irradiation: A direct hole oxidation pathway. *Chemical Engineering Journal*, 274, 290–297. <https://doi.org/10.1016/j.cej.2015.03.077>
- Zhang, Y. L., Liu, Y. J., Dai, C. M., Zhou, X. F., & Liu, S. G. (2014). Adsorption of clofibric acid from aqueous solution by graphene oxide and the effect of environmental factors. *Water, Air, and Soil Pollution*, 225(8). <https://doi.org/10.1007/s11270-014-2064-0>
- Zhang, Y. N., Chen, J., Xie, Q., Li, Y., & Zhou, C. (2016). Photochemical transformation of five novel brominated flame retardants: Kinetics and photoproducts. *Chemosphere*, 150, 453–460. <https://doi.org/10.1016/j.chemosphere.2015.12.125>
- Zhao, W., Hao, C., Guo, Y., Shao, W., Tian, Y., & Zhao, P. (2023). Optimization of

- Adsorption Conditions Using Response Surface Methodology for Tetracycline Removal by MnFe₂O₄/Multi-Wall Carbon Nanotubes. *Water (Switzerland)*, 15(13). <https://doi.org/10.3390/w15132392>
- Zhou, S., Shao, Y., Gao, N., Deng, J., & Tan, C. (2013). Equilibrium, Kinetic, and Thermodynamic Studies on the Adsorption of Triclosan onto Multi-Walled Carbon Nanotubes. *Clean - Soil, Air, Water*, 41(6), 539–547. <https://doi.org/10.1002/clen.201200082>
- Zhou, Y., Cao, S., Xi, C., Li, X., Zhang, L., Wang, G., & Chen, Z. (2019). A novel Fe₃O₄/graphene oxide/citrus peel-derived bio-char based nanocomposite with enhanced adsorption affinity and sensitivity of ciprofloxacin and sparfloxacin. *Bioresource Technology*, 292. <https://doi.org/10.1016/j.biortech.2019.121951>
- Zhou, Y., Liu, X., Xiang, Y., Wang, P., Zhang, J., Zhang, F., Wei, J., Luo, L., Lei, M., & Tang, L. (2017). Modification of biochar derived from sawdust and its application in removal of tetracycline and copper from aqueous solution: Adsorption mechanism and modelling. *Bioresource Technology*, 245, 266–273. <https://doi.org/10.1016/j.biortech.2017.08.178>
- Zhou, Y., Xue, C., Gan, L., Owens, G., & Chen, Z. (2023). Simultaneous removal of triclosan and Cd(II) by bio-reduced graphene oxide and its mechanism. *Chemosphere*, 311. <https://doi.org/10.1016/j.chemosphere.2022.137021>
- Zhu, X., Tsang, D. C. W., Chen, F., Li, S., & Yang, X. (2015). Ciprofloxacin adsorption on graphene and granular activated carbon: Kinetics, isotherms, and effects of solution chemistry. *Environmental Technology (United Kingdom)*, 36(24), 3094–3102. <https://doi.org/10.1080/09593330.2015.1054316>
- Zide, D., Fatoki, O., Oputu, O., Opeolu, B., Nelana, S., & Olatunji, O. (2018). Zeolite “adsorption” capacities in aqueous acidic media; The role of acid choice and quantification method on ciprofloxacin removal. *Microporous and Mesoporous Materials*, 255, 226–241. <https://doi.org/10.1016/j.micromeso.2017.07.033>
- Zubair, M., Manzar, M. S., Mu’azu, N. D., Anil, I., Blaisi, N. I., & Al-Harhi, M. A. (2020). Functionalized MgAl-layered hydroxide intercalated date-palm biochar for Enhanced Uptake of Cationic dye: Kinetics, isotherm and thermodynamic studies. *Applied Clay Science*, 190. <https://doi.org/10.1016/j.clay.2020.105587>

Outcome

Research Papers

1. **Prakash Bobde**, Amit Kumar Sharma, Ranjit Kumar, Jitendra K Pandey, Shikha Wadhwa; Recent Advances on Sustainable Removal of Emerging Contaminants From Water by Bio-based Adsorbent; RSC New Journal of Chemistry; (2023) (**Published**)
2. **Prakash Bobde**, Amit Kumar Sharma, Ranjit Kumar, Sukdeb Pal, Jitendra K Pandey, Shikha Wadhwa; Adsorptive Removal of Oxytetracycline using MnO₂-engineered Pine-Cone Biochar: Thermodynamic and Kinetic Investigation and Process Optimization; Environmental Monitoring and Assessment; (2023) 195, 1291 (**Published**)
3. **Prakash Bobde**, Jitendra K Pandey, Ranjit Kumar, Amit Kumar Sharma, Sukdeb Pal, Shikha Wadhwa; A Sustainable Layered Double Hydroxide-Pine Cone Biochar Composite for Enhanced Removal of Ciprofloxacin from Water; RSC New Journal of Chemistry; (2024) 48, 14444-14459 (**Published**)
4. Arnab Mondal; Ritu Jangid; Rahul Arya; Lokesh Yadav; Sakshi Ahlawat; Pooja Yadav; Paramjeet Singh Paliyal; **Prakash Bobde**; Paulami Ghosh; Surajit Mondal; Akansha Rai; Rubiya Banoo; Nikki Chaudhary; Martina Rani; Garima Kotnala; Eiko Nemitz; Sudhir Kumar Sharma; A simple model for mitigation of solid residential fuels by clean Liquefied Petroleum Gas over National Capital Territory of India (**Communicated**)
5. Vishal Kumar Singh, Mukul Kumar, **Prakash Bobde**, Muthusamy Govarthan, Suvendu Manna; Removal of Arsenic from Jarosite using Hydrometallurgical Treatment; Environmental Geochem Health; (2024), 46-67 (**Published**)
6. Amit Kumar Sharma, Praveen Kumar Ghodke, Nishu Goyal, **Prakash Bobde**, Eilhann E. Kwon, Kun-Yi Andrew Lin, Wei-Hsin Chen; A Critical Review on Biochar Production from Pine Wastes, Upgradation Techniques, Environmental Sustainability, and Challenges; Bioresource Technology; (2023) 387, 129632 (**Published**)
7. Wei-Hsin Chen, Naveen C, Praveen Kumar Ghodke, Amit Kumar Sharma, **Prakash Bobde**; Co-pyrolysis of lignocellulosic biomass with other carbonaceous materials: A review on advance technologies, synergistic effect, and future prospectus; Fuel; (2023) 345, 128177 (**Published**)
8. Khushboo Bhurat, Tushar Banarjee, **Prakash Bobde**, Swapnil Bhurat; Effect of Chemical, Physical and Biological Pretreatment of Food Wastes on Bio-hydrogen Production by Dark Anaerobic Fermentation Under Mesophilic Conditions; (2023) 45:1017-1029 (**Published**)
9. Pallavi Bhardwaj, Rajesh Kumar Sharma, Abhishek Chauhar, Anuj Ranjan, Vishnu D. Rajput, Saglara S. Mandzhieva, Tatiana Minkina, Usha Mina,

- Shikha Wadhwa, **Prakash Bobde**, Ashutosh Tripathi; Assessment of Heavy Metal Distribution and Health Risk of Vegetable Crops Grown on Soils Amended with Municipal Solid Waste Compost for Sustainable Urban Agriculture Water; (2023) 15, 228 (**Published**)
10. **Prakash Bobde**, Amit Kumar Sharma, Deepak Panchal, Abhishek Sharma, Ravi Kumar Patel, Rita S. Dhodapkar, Sukdeb Pal; Layered double hydroxides (LDHs)-based photocatalysts for dye degradation: a review; International Journal of Environmental Science & Technology; (2022) (**Published**)
 11. **Prakash Bobde**, Amit Kumar Sharma, Deepak Panchal, Abhishek Sharma, Ravi Kumar Patel, Rita S. Dhodapkar, Sukdeb Pal; Utilization of layered double hydroxides (LDHs) and their derivatives as photocatalysts for degradation of organic pollutants; Environmental Science and Pollution Research; (2021) 28:59551–59569 (**Published**)
 12. Deepak Panchal, Om Prakash, **Prakash Bobde**, Sukdeb Pal; SARS-CoV-2: sewage surveillance as an early warning system and challenges in developing countries; Environmental Science and Pollution Research (2021) 28:22221–22240 (**Published**)
 13. Suvendu Manna, **Prakash Bobde**, Debasis Roy, Amit Kumar Sharma, Surajit Mondal; Separation of iodine using neem oil-cashew nut shell liquid based-phenol formaldehyde resin modified lignocellulosic biomatrices: Batch and column study; Journal of the Taiwan Institute of Chemical Engineers (2021)122:98-105 (**Published**)
 14. Kameni Ngounou M. Bernard; **Prakash Bobde**, Ndi K. Sylvere, Kofa G. Patrice, Kayem G. Joseph, Sukdeb Pal; Effect of Grewia spp. biopolymer on floc properties of coagulated laterite Suspension; Desalination and Water Treatment (2020)185:132-144 (**Published**)

Patents:

1. **Mr. Prakash Bobde**, Dr. Ranjit Kumar; Method for Synthesis of Alpha-Manganese Oxide Nanoparticles; Application Number 202211061290 A; The Patent Office Journal No. 44/2022; 69946 (**Granted**)
2. **Mr. Prakash Bobde**, Dr. Ranjit Kumar; Method for Synthesis of Manganese Phosphate ($MnPO_4 \cdot H_2O$) Nanoparticles; Application No. 202211056376 A; The Patent Office Journal No. 41/2022; 65206 (**Published**)

Book

1. **Mr. Prakash Bobde**, Dr. Jitendra Kumar Pandey, Dr. Suvendu Manna, Dr. Ravi Kumar Patel; Disposal & Recycling Strategies for Nano-engineered Materials (**Published**)

Book Chapters

1. **Prakash Bobde**, Ajaya Kumar Behera, Ravi Kumar Patel; Oil Spill Treatment Using Porous Materials; Advances in Oil-Water Separation; (2022) 157-173 (**Published**)
2. Abhishek Sharma, Deepak Panchal, Om Prakash, Purusottam Tripathy, **Prakash Bobde**, Sukdeb Pal; Fabrication of Nanomaterials for Biomedical Imaging; Advanced Nanomaterials for Point Care Dignosis & Therapy; (2022) 81-100 (**Published**)
3. Ravi Kumar Patel, **Prakash Bobde**, Vishal Kumar Singh, Deepak Panchal, Sukdeb Pal; Synthesis & Applications of Nanomaterials-based Sensors; Advanced Nanomaterials for Point Care Dignosis & Therapy; (2022) 451-476 (**Published**)
4. **Prakash Bobde**, Ravi Kumar Patel, Lalit Nagpurkar; Fabrication of microchannel for water treatment using 3D printing; 3D Printing Technology for Water Treatment Applications; (2022) 39-53 (**Published**)

PhD Thesis-Prakash Bobde

ORIGINALITY REPORT

10% SIMILARITY INDEX	7% INTERNET SOURCES	10% PUBLICATIONS	1% STUDENT PAPERS
--------------------------------	-------------------------------	----------------------------	-----------------------------

PRIMARY SOURCES

1	coek.info Internet Source	<1%
2	www.science.gov Internet Source	<1%
3	www.unboundmedicine.com Internet Source	<1%
4	Huma Khan, Chirag R. Sharma, Saroj Sharma. "Fabrication of sustainable organometallic polymeric adsorbents for remediation of fluoride from water: A novel approach", Journal of Water Process Engineering, 2017 Publication	<1%
5	Xinyi Liao, Chen Chen, Zhijie Liang, Zhiwei Zhao, Fuyi Cui. "Selective adsorption of antibiotics on manganese oxide-loaded biochar and mechanism based on quantitative structure-property relationship model", Bioresource Technology, 2022 Publication	<1%
6	www.mdpi.com Internet Source	<1%